Studies on the Synthesis and Characterization of Encapsulated Organogels for Controlled Drug Delivery Applications

Thesis submitted by

SAI SATEESH SAGIRI (509BM103)

In partial fulfillment for the award of the Degree of

DOCTOR OF PHILOSOPHY

IN

BIOTECHNOLOGY AND MEDICAL ENGINEERING

Under the guidance of

Supervisor

Dr. KUNAL PAL

Co-supervisor

Dr. PIYALI BASAK

Department of Biotechnology and Medical Engineering

NATIONAL INSTITUTE OF TECHNOLOGY

Rourkela 769008, Odisha, India

August-2014

NATIONAL
INSTITUTE OF
TECHNOLOGY
ROURKELA - 769 008, ORISSA

Dr. Kunal Pal
Assistant Professor
Department of Biotechnology and Medical Engineering
E-mail: pal.kunal@yahoo.com
Tel: +91-876-3366085

CERTIFICATE

This to certify that the thesis entitled "**Studies on the synthesis and characterization of encapsulated organogels for controlled drug delivery applications"** being submitted by **Mr. Sai Sateesh Sagiri** for the award of the degree of Doctor of Philosophy in Biotechnology and Medical Engineering at NIT Rourkela, is a record of bonafide research work carried out by him under my supervision. Mr. Sai Sateeesh Sagiri has worked for four and half years on the above problem in the Department of Biotechnology & Medical Engineering, National Institute of Technology, Rourkela and his work has reached the standard for fulfilling the requirements and the regulation relating to the degree. The contents of this thesis, in full or part, has not been submitted to any other University or Institution for the award of any degree or diploma.

Place: Rourkela

Date: 25-03-2015.

(Dr. Kunal Pal)
Assistant professor
Dept. of Biotechnology & Medical Engineering,
NIT Rourkela.

JADAVPUR UNIVERSITY
SCHOOL OF BIOSCIENCE & ENGINEERING
Kolkata-700032, India

CERTIFICATE

This to certify that the thesis entitled "**Studies on the synthesis and characterization of encapsulated organogels for controlled delivery applications**" being submitted by **Mr. Sai Sateesh Sagiri** for the award of the degree of Doctor of Philosophy in Biotechnology and Medical Engineering, NIT Rourkela, is a record of bonafide research work carried out by him under the joint supervision of the undersigned and Dr. Kunal Pal, Department of Biotechnology & Medical Engineering, National Institute of Technology, Rourkela. The contents of this thesis, in full or part, has not been submitted to any other University or Institution for the award of any degree or diploma.

Piyali Basak
26th Aug 2019

(Dr. Piyali Basak)
Assistant professor
School of Bioscience and Engineering,
Jadavpur University

DR. PIYALI BASAK
ASSISTANT PROFESSOR
SCHOOL OF BIOSCIENCE & ENGG.
JADAVPUR UNIVERSITY,
KOLKATA - 700032

Acknowledgements

At this moment of accomplishment, it is easy to recognize that many people have helped me to achieve such an important stage of my life. Herein I express my deep gratitude to all of you who supported me throughout these years.

Foremost, I would like to express my sincere gratitude to my supervisor, Dr. Kunal Pal, for his relentless encouragement, constructive guidance and words of motivation throughout the duration of my research and moreover for the inspiration he provided to ensure the completion of this work. His expertise, availability to discuss ideas and willingness to give his knowledge were instrumental.

I gratefully thank Doctoral Research Committee (DSC) members, Prof. K. Pramanik, Prof.Indraneel Banerjee and Prof. Amit Biswas from the Department of Biotechnolgy and Medical Engineering, Prof. B. K Pal from the Department of Mining Engineering, for their constructive comments to improve the quality of this thesis. Many thanks go in particular to Prof. S. Paul, Prof. Sirsendu Ray, Prof. B.P.Nayak, Prof. Mukesh Gupta, Prof. Thirugnanam, and Prof. Devendra Varma for giving me such a pleasant time since I knew them in NIT Rourkela.

Collective and individual acknowledgments also owe to my research group members; Beauty Behera, Vinay K. Singh, Biswajeet Champaty, other Ph.D scholars of the department and institute whose presence somehow perpetually refreshed, helpful, and memorable..

Finally I would like to convey my heartiest thanks to my parents and brother for their support and love during my stay in Rourkela.

Sai Sateesh Sagiri

Abstract

Over the years, biopolymeric microparticles have been associated with the leaching of the internal phase. The present work was aimed at developing a new strategy in negotiating the problem of leaching from the microparticles. We hypothesized that gelation of the internal phase as organogels (core) and their encapsulation within the alginate microparticles may prevent leaching. Organogels were prepared using natural fatty acyl sources and synthetic source. Natural sources include vegetable fats (cocoa butter, mango butter), animal fat (lanolin) and fatty acid having both plant and animal origin (stearic acid), whereas, synthetic source include the mixture of Span 80 and Tween 80. Prior to encapsulation, the physicochemical, thermal and mechanical properties of the organogels were characterized in depth. The gelation mechanism and crystallization phenomenon during the formation of vegetable fat and stearic acid based organogels were critically evaluated. The predicted gelation mechanism in vegetable fat based organogels is instantaneous nucleation coupled with one or two dimensional growth of the fat crystals. On the other hand, stearate molecules followed heterogeneous nucleation coupled with one-dimensional growth during the formation of stearate organogels. The aforementioned organogels were encapsulated within the alginate microparticles by ionotropic gelation method. Microscopic, XRD and DSC studies confirmed the successful encapsulation of organogels as the core material of the developed microparticles. The organogel encapsulated microparticles prevented the leaching of the internal phase and improved the drug encapsulation efficiency. Presence of semi-solid organogels as the core material facilitated the controlled release of the drugs (model drugs: metronidazole and ciprofloxacin in stearate formulations) from the microparticles. The developed formulations showed good antimicrobial properties against *Escherichia coli*. The microparticles were found to be biocompatible and mucoadhesive in nature when checked against mammalian L929 fibroblast cells and goat's small intestine, respectively. Based on the results, it was concluded that the developed formulations (organogels and microparticles) may be used as the controlled drug delivery vehicles for *in vivo* applications.

CONTENTS

List of Figures

List of Tables

Chapter 1

Introduction

Biopharmaceutics Classification System reports that more than 35 % of the bioactive agents are poorly aqueous soluble and/or have technical problems in developing formulations [1-2]. To improve the solubility and/or bioavailability, a number of technologies are being adopted. Of these, lipid-based formulations have shown promising results in enhancing the bioavailability of active ingredients. Encapsulation has been extensively used either to immobilize or carry drugs [3], vaccines [4], proteins [5], antigens [6], microbial cells [7], animal cells [8], and food flavorants [9]. In cosmetics and pharmaceutical industries, encapsulation technology is one of the widely used methods for improving the stability, bioavailability and to enhance the loading capacity of the active ingredients. These bioactive ingredients can be directly encapsulated or encapsulated via lipid vehicle. In general, vegetable oils are being used as the lipid vehicles.

Encapsulation of the vegetable oils has been carried out using polymers of either synthetic or natural origin. The synthetic polymers include poly-α-cyanoacrylate alkyl esters, polyglycolic acid, polylactic acid, polylactic glycolic acid and polyvinyl alcohol. Polymers of natural origin may be obtained either from plant or animal sources. Plant-derived polymers are largely being used. The commonly used plant-derived polymers include alginate, arabic gum, carrageenan, cellulose and its derivatives, pectin and starch derivatives. Animal-derived polysaccharides include chitosan and pectin, whereas, protein-based polymers include albumin, casein, gelatin, silk fibroin, soy proteins and whey protein isolate.

Vegetable oils have been categorized as essential oils and non-essential oils. In general, essential oils are volatile and unstable at room-temperature (25 ^{o}C), whereas, non-essential oils are non-volatile and stable at room-temperature. Some of the essential and non-essential oils inherently possess antibacterial, antifungal and antiviral properties. These properties tend to change if the oils get oxidized and become rancid. These properties of the oils can be preserved by designing different formulations. These formulations can also be used for controlled release applications. The formulations may either be liquid, semi-solid or solid dosage forms. The oil-based liquid, semisolid and solid dosage forms are emulsions, organogels and microparticles, respectively.

Organogels entrap apolar liquid within a three-dimensional and thermo-reversible gel network. The apolar liquid can be either an organic solvent or vegetable oil. Over the last two decades, organogels have been explored as drug delivery matrices in pharmaceutical applications and saturated/*trans* fat replacers in food applications. The use of organogel based formulations has been increasing, which may be attributed to the easy method of preparation, cost effectiveness, inherent long-term stability of these products. The organogels have the capability to carry both hydrophilic and lipophilic constituents [10]. In the present study, organogels are prepared using non-essential oils such as sunflower oil, sesame oil and soy bean oil. Further, the stable semi-solid organogels are encapsulated within the alginate microparticles and convert to solid dosage forms.

In general, microparticles are the first choice of dosage forms for the encapsulation of vegetable oils. Encapsulation strategies help in converting oils into solid dosage forms and enables retention of their activity for longer periods of time. The role of polymers is very important in improving the encapsulation efficiency of the vegetable oils. Coating of the microparticles with another polymer (complex and composite microparticles) has been mainly used to improve the encapsulation efficiency. Better encapsulation efficiency is possible if the wall materials of microparticles possess both hydrophilic and hydrophobic nature [11]. But, in general, biopolymers are hydrophilic in nature. Hydrophobicity of the biopolymers may be improved by complexing the biopolymers with synthetic polymers [11]. But, the process is a tedious and time consuming process. Keeping this in mind, we hypothesized that instead of coating/complexing, the encapsulation efficiency can be improved by immobilizing the internal phase. Hence, attempts were made to encapsulate organogels (immobilized vegetable oils) within the microparticles. Alginate was chosen as the representative polymer, as alginate forms porous matrix in the microparticles and hence allows the leaching of the internal phase.

Chapter 2

Review of Literature

2.1. Organogels

Organogels are defined as the semi-solid formulations; which comprises a 3 dimensional (3-D) network structure of gelator molecules, and an immobilized apolar liquid [12]. Organogels have been synthesized using diverse group of gelators (e.g. low molecular weight organogelators (LMOGs) and polymeric organogelators) and organic apolar solvents. During the formation of organogels, the gelator molecules form a 3-D architecture either by chemical cross-linking (covalent or ionic bonds) or physical entanglement (hydrogen bonds, Van der Waal forces, π-π interactions) to immobilize the apolar phase. The formation of organogels *via* chemical reactions are referred as chemical gels [13]. On the other hand, formation of organogels *via* physical entanglement are referred as physical gels [13]. Organogel formation occurs due to the interaction of structures that develop due to the 3-D assembly of organogelators. Such organogelator structures may be either solid (formed during precipitation of the organogelators from the solution in an apolar solvent) or fluid-filled (resulting from the entrapment of the aqueous phase within the gelator structures) [13]. The properties of organogels mainly depend on the structuring ability of the organogelators and the properties of the incorporated compounds (e.g. drugs or bioactives). The structure of the organogel depends on a number of factors, namely, the method of gel preparation, the nature of the solvent, gelator and co-gelator, and the interactions between the components involved. These structures include, but are not limited to, reverse worm-like micelles [14], reverse spherical micelles [15-16], microemulsions [17], nanotubes [18], twisted or helical nanofibers [18], fibers [19], gel strands in lamellar form [20], and crystal networks [21]. The size and shape of the 3-D structures is dependent on the gelator-solvent interactions. A comprehensive list of the organogelators used in pharmaceutical applications is tabulated in Table 2.1.

Table 2.1: List of organogelators used in pharmaceutical applications

S. No.	Class	Example	Reference
1.	**Low molecular weight organogelators**		
	i. Anthryl and anthraquinone derivative organogelators	2,3-didecycloxytetracene	[22]
	Sterol organogelators		
	a. ALS organogelators	Cholesteryl 4-(2-anthryloxy) butanoate	[10]
	b. $A(LS)_2$ organogelators	Diacid monoamides of cholesteryl glycinate ammonium salts	[23]
	c. Organometallic cholesterol-based organogelators	Palladium pincer bis (carbene) complex	[24]
	d. Aminoacid-sterol based organogelators	Cholesteryl L-phenyl alaninate	[25]
	e. Bile acid-steroid organogelators	Cholic acid amino-alkylamides	[26]
	ii. Gemini organogelators	Bis (N-lauroyl-L-lysine ethyl ester) oxyl amide	[27]
	iii. Amino acid type organogelators	Phenylalanine derivatives of N-protected phthaloylhydrazide amino acids	[28]
	iv. Fatty acid organogelators	Lecithin, Spans, Tweens phytosterols+oryzanol compounds, Stearic acid and its derivatives	[29-30]
	v. Sugar-based organogelators	derivatives of methyl glycosides of 4,6-O-benzylidine	[31]
2.	Polymeric organogelators	Poly(ethylene)	[32]

Amongst the organogelators tabulated in Table 2.1, fatty acyl organogelators have been mostly used to immobilize vegetable oils [14, 16, 21].

2.1.1. Mechanism of organogel formation

In general, three mechanisms of organogel formation have been proposed. The first mechanism explains the formation of networked structures with fluid-filled fibers, while the second mechanism describes those formed by solid fibers. These two mechanisms involve non-covalent intermolecular physical interactions. Most LMOGs form organogels by either of these two mechanisms. The significant difference between the fluid-filled matrix and solid matrix organogels lies in their kinetic behavior. The fluid matrix-type organogels form a transient, dynamic gel structure (worm-like or polymer-like) which undergoes constant remodeling. On the other hand, solid matrix organogels are robust and exhibit a stable gel network over the gel's lifetime [13]. Schematic representation of the fluid-filled matrix and solid fiber mechanisms have been shown in Figure 2.1. The third mechanism describes the formation of 3-D network of crosslinked polymers by covalent and ionic interactions. The process of immobilization of apolar solvents within these networked structures has been attributed to surface activity present amongst the gelator and solvent molecules. The stability of the organogels is significantly affected by composition, properties of the bioactive compounds incorporated and functionality.

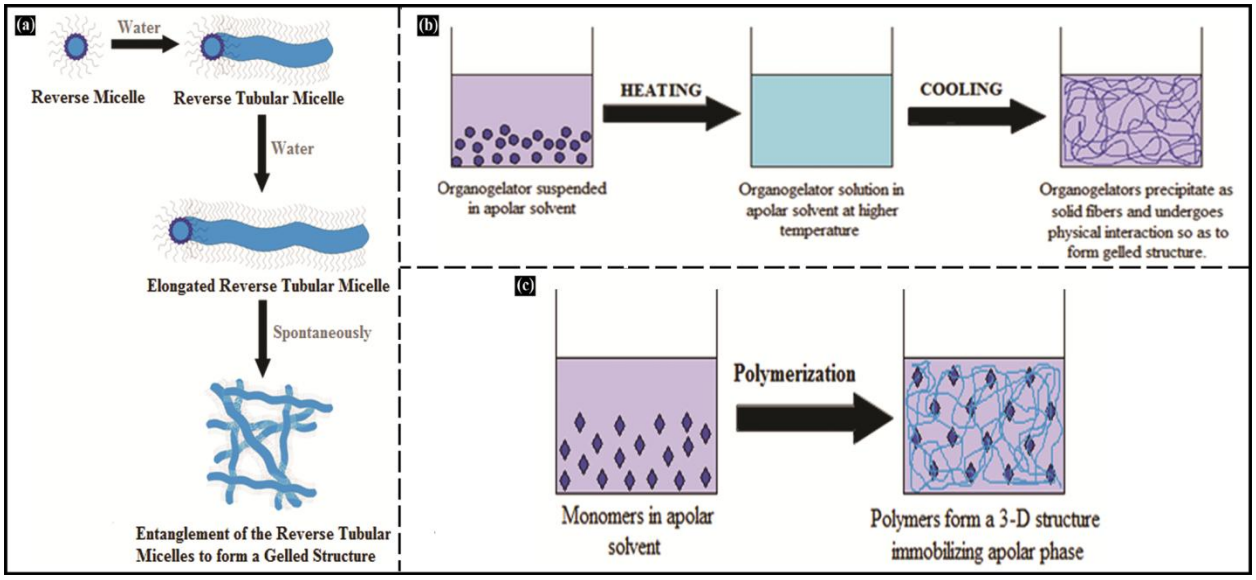

Figure 2.1: Schematic representation of: (a) Fluid fiber, (b) Solid fiber, and (c) Polymerization mechanism.

2.2. Types of vegetable oil-based formulations

Vegetable oils have been encapsulated by different routes. Figure 2.2 illustrates the different strategies being adopted to encapsulate the vegetable oils. The current section is devoted to discuss, in brief, the different strategies adopted to encapsulate vegetable oils.

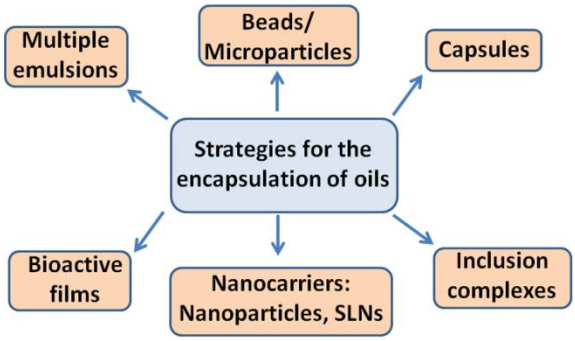

Figure 2.2: Schematic illustration of the encapsulation strategies of the vegetable oils

2.2.2. Multiple emulsions

Multiple emulsions have been developed since 1965, for pharmaceutical, cosmetic and food applications [33]. Multiple emulsions are three-phase systems, which can be either W/O/W or O/W/O-type emulsions (W: water; O: oil) (Figure 2.3a). As compared to O/W/O emulsions, W/O/W emulsions have been largely employed for the delivery of bioactive ingredients (Figure 2.3). In general, W/O/W emulsions are being prepared by phase inversion method either by one-step emulsification or two-step emulsification [34]. Cournarie *et al.* (2004) reported that two-step emulsification method exhibits higher encapsulation efficiencies as compared to one-step emulsification method [35]. The advantages and problems associated with the multiple emulsions have been tabulated in Table 2.2. Insulin-loaded W/O/W multiple emulsions showed a decrease in the blood glucose level in diabetic rats [36]. The oil phase was either medium-chain triglycerides or long-chain triglycerides (fish oil). In an another study, insulin loaded multiple emulsions were prepared using soy bean oil or medium-chain triglycerides [37]. Under *in vitro* conditions, the multiple emulsions were found to protect insulin from protease action. The release of insulin was found to be swelling-break down mediated. Multiple emulsions have also been synthesized using different non-essential oils, *viz.*, canola oil, sesame oil, peanut oil and safflower oil [38-40].

Table 2.2: The advantages and problems associated with multiple emulsions.

Advantages		Problems and remedies	
Ability to carry both hydrophilic and hydrophobic bioactive ingredients.	[2, 41]	The inherent thermodynamic stability is the major hurdle of the multiple emulsions. The stability of the emulsions can be improved by adding complex forming or gelling agents to the internal phase.	[42]
Prolonged drug release systems.	[43]		
W/O/W-type emulsions can be used for drug delivery, drug targeting and particularly as lymphotropic agents.	[44]		
Protects the bioactive ingredient from gastrointestinal harsh (pH, enzymatic degradation) conditions.	[41]		
Taste/smell masking	[45]		

Purity of the vegetable oils alters the stability of the multiple emulsions. W/O/W emulsions may be stabilized using low fluidity lipids. Low fluidity lipids possess low melting points and prevent the leaching/flow of the internal phase during storage, which in turn, improves the stability of the formulations. Multiple emulsions with low fluidity lipids are called as multiple lipid carriers [34]. In general, low fluidity lipids are semi-solid at room-temperature. The absorption of microcrystalline lipid particles at the W/O interface provides stability to the emulsion system [46]. Lee *et al.* (2011) synthesized multiple lipid carriers using coconut oil (melting point: 28 ºC) as the lipid phase [34]. Low fluidity lipid was prepared by adding PEG-30 dipolyhydroxy stearate to the molten coconut oil (40 ºC). The external water phase of the multiple emulsions was also thickened using either xanthan gum or carbomer or polyvinyl alcohol. The decrease in fluid flow and amorphous state of the lipid contributed to the high-drug loading capacity of the multiple lipid carriers [43].

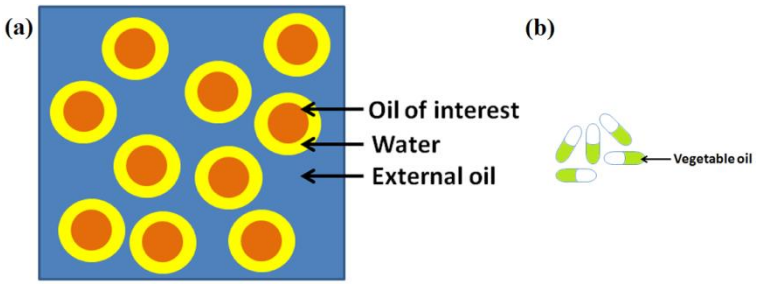

Figure 2.3: Schematic representation of: (a) Multiple emulsion, and (b) Capsules.

2.2.3. Capsules

Capsules are unit dosage containers to carry bioactive agents in the form of either soft capsules or hard capsules (Figure 2.3b). Conventionally, soft capsules have been used to carry liquids, whereas, hard capsules are used for the delivery of solids (powders and pellets). In general, gelatin is the most frequently used polymer to prepare capsules. During preparation of the hard capsules, water is used as the plasticizer, whereas, for soft capsules glycerin is used as the plasticizer. Presence of glycerin enhances the oxygen permeability and relative humidity in the soft capsules [47]. Due to this reason, hard capsules posses lower oxygen permeability over soft capsules. Since lipid oxidation is one of the main problems associated with oils, soft capsules are not suitable for the encapsulation of the oils. Hence, hard capsules are the preferred choice. To improve the oral bioavailability of the poorly water-soluble active ingredients, hard gelatin capsules are developed as lipophilic liquid vehicles and semi-solid lipophilic vehicles. Encapsulation of the bioactive agents as liquid or semi-solid formulations provides opportunity for delivering water insoluble bioactive agents with reproducible absorption and acceptable bioavailability. Non-essential oils are being used as excipients during the synthesis of either lipophilic liquid vehicles or semi-solid lipophilic vehicles. Non-essential oils are biocompatible and have the ability to carry lipophilic drugs. The commonly used non-essential oils are arachis oil, castor oil, corn oil, cotton seed oil, olive oil, sesame oil, soy bean oil and sunflower oil [48]. But, the encapsulation of the essential oils in the capsules is limited. This may be due to the higher lipid oxidation of the essential oils over non-essential oils. As capsules do not provide sufficient barrier for the oxygen transfer, essential oils may get rancid after the encapsulation. The replacement of gelatin was expected to solve the problem. Gelatin-gum arabic capsules showed a protective effect against the oxidation of flax seed oil during storage (25 days) at room-temperature [49]. Alginate complex capsules containing eucalyptus oil were prepared by interfacial insolubilization reaction [50]. The capsules showed 90-92 % of the oil encapsulation efficiency. To improve the stabilization of the essential oils, complex capsules and nanocapsules have been designed. Alginate nanocapsules were prepared to encapsulate the turmeric oil [51].

2.2.4. Nanoparticles

Nanoscale biopolymeric particles have attracted much attention for the development of new formulations for the controlled release systems and to enhance the stability of the essential oils. Polymer-based nanoparticles are classified as nanocapsules and nanospheres. They differ from

each other in terms of their structure. Nanocapsules possess a polymeric wall encapsulating the oil core, whereas, the oil may be conjugated with the polymeric wall or matrix in nanospheres (Figure 2.4) [52].

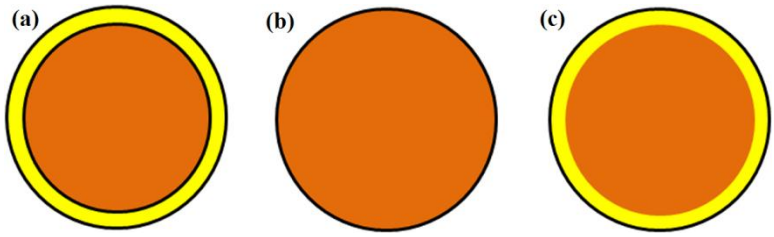

Figure 2.4: Schematic representation of: (a) Nanocapsules, (b) Nanospheres, and (c) SLNs.

Turmeric oil has been used in the pharmaceutical formulations for its antibacterial, antifungal, anticarcinogenic, antioxidant and antimutagenic properties. But the oil is volatile and insoluble in water. Alginate nanocapsules containing turmeric oil prevented the vapourization and enhanced the water solubilization potential of the oil [51]. Chitosan nanoparticles (40-80 nm) containing oregano oil were synthesized. After encapsulation, the antioxidant and antimicrobial activities of the oil were retained. The encapsulation efficiency of the developed nanoparticles was found to be 21-47 % at different oil loading ratios [53]. Blends of chitosan/angico gum (10-60 nm) and alginate/cashew gum (223–399 nm) were used to encapsulate *Lippia sidoides* essential oil. 16 to 77 % of encapsulation efficiency of *Lippia sidoides* essential oil was achieved when chitosan/angico gum nanoparticles were prepared [54]. But these nanoparticles showed poor stability and low oil release profiles. These properties (stability and oil release profiles) were improved by encapsulating the essential oil within alginate/cashew gum nanoparticles [55]. But the encapsulation efficiency of the oil was reduced to 21 to 48 %. Chitosan/angico gum naoparticles showed 80 % oil release after 60 h, whereas, alginate/cashew gum nanoparticles released 90 % of the encapsulated oil after 45 h. The higher and faster release of the oil from alginate/cashew gum was due to the increased hydrophilicity of the nanoparticles as compared to the chitosan/angico gum nanoparticles.

2.2.5. Solid lipid nanoparticles

Solid lipid nanoparticles (SLNs) are nanoscale sized particles prepared using lipids that are solid at room-temperature. The lipid component of the SLNs may be constituted by triacylglycerols or waxes. Vegetable oils are encapsulated within the lipid matrix of the nanoparticles (Figure 2.4c).

The size range of SLNs varies from 50 nm to 1 µm. SLNs carry the active ingredients either in the core or on their wall. They are highly advantageous in carrying lipophilic active components. They offer good protection, less leakage, and sustained release of the bioactive agents. AlHaj *et al.* (2010) developed SLNs using hydrogenated palm oil (Softisan 154) and *Nigella sativa* essential oil as the lipid matrix [56]. These SLNs were found to be stable at different storage temperatures during the three month study. *Artemisia arborescens* essential oil was encapsulated in SLNs (~223 nm) using Compritol 888 ATO as the lipid [57]. The SLNs were physically stable. They have retained the antiviral properties of the oil even after 2 years of storage. SLNs (~113 nm) of Compritol 888 ATO were also used to encapsulate the frankincense and myrrh essential oil [58]. SLNs containing *Zataria multiflora* essential oil showed only 38.66 % encapsulation efficiency [59]. The physicochemical characterization studies revealed that the oil interacted with the lipid matrix of the SLNs.

2.2.6. Beads and microcapsules/microparticles

Beads and microparticles have been synthesized to prepare food, pharmaceutical, nutraceutical and cosmetic products with high oil content in a reduced product volume. These formulations are mainly employed to encapsulate essential oils. Essential oils have been encapsulated for many reasons, *viz.*, to prevent oxidation, nutrition, therapeutics, flavoring or aroma (Table 2.3) [60].

Though beads and microparticles can carry high amounts of vegetable oils, they suffer with oxidation and leaching of oils during synthesis, storage and transportation. In general, vegetable oils with either unsaturated or polyunsaturated fatty acids are susceptible to oxidation. Lipid oxidation causes rancidity and affects the nutritional and health benefits of the vegetable oils. Lipid oxidation is governed by oxygen, heat or light. Storage of wheat bran oil containing alginate beads in the dark at 4 ºC proved to be very effective as compared to their storage in the presence of light at 25 ºC [61]. Storage of beads under these conditions prevented the oxidative degradation of nutritionally important compounds (vitamin E, lutein, zeaxanthin and β-carotene). Microparticles made of gum arabic and its ternary mixtures with maltodextrin and whey protein isolate presented high protection from oxidation to linseed oil (tested by accelerated Rancimat test) [62]. These microparticles showed very high encapsulation efficiencies (> 90 %) of linseed oil. To prevent the lipid oxidation and to improve the release parameters of flax seed oil, the oil was encapsulated in the wall materials of either chickpea or lentil protein isolate and

maltodextrin [63]. As compared to the unencapsulated oil, the encapsulated flax seed oil did not undergo oxidation over a period of 25 days, when stored at room-temperature. Apart from protection against lipid oxidation, the developed microcapsules showed high encapsulation efficiencies of flax seed oil. Flax seed oil encapsulation efficiency was higher in lentil protein isolate-maltodextrin microcapsules (~ 88 %) relative to the chickpea isolate-maltodextrin microcapsules (~ 86.3 %).

In addition to the lipid oxidation, leaching of the encapsulated oils is another major concern associated with the beads and microparticles. In general, leaching is due to the porous nature of the formulations. The oil loading capacity can be enhanced by coating the microparticles with another polymer, increasing the polymer concentration and curing time of polymer crosslinking. Calcium alginate beads with high palm oil content were achieved by varying the alginate concentration, type of alginate and drying properties. Palm oil encapsulation efficiency was highest (85 to 90 %) when the beads were prepared using alginate (25 g/L) having high guluronic acid (M/G ratio = 0.59, molecular weight ~ 97,000) at 50 % oil loading [60]. Calcium alginate beads lost 7 to 10 % of the encapsulated oil when the beads were oven-dried at 70 ºC. In contrast to the oven-drying, beads did not lose the encapsulated oil when they were freeze-dried at -55 ºC. This shows that the encapsulation of oils was influenced by the process parameters, such as, type and concentration of the polymer, amount of oil loading and drying conditions. Encapsulation of the oils does not always increase when the polymeric microparticles/beads are coated with another polymer. Chitosan-cashew gum beads (2.4 %) showed lower encapsulation efficiency of the essential oil (from the leaves of *Lippia sidoides*) as compared to chitosan beads (4.4 %) [64]. During the preparation of chitosan-cashew gum beads, the essential oil was leached out of the chitosan beads when they were incubated (30 min) in cashew gum solution. In another independent study, encapsulation efficiency of linanlool (monoterpene found in the essential oils of plants) was found to be 71 to 75 % in calcium alginate microparticles [65]. Impregnation of the alginate layer with modified starch resulted in the reduction of the encapsulation efficiency to 69 %. However, when linalool was encapsulated along with glycerol and modified starch, the encapsulation efficiency was enhanced to 86 %. Glycerol improved the viscosity and emulsion stability, which in turn, enhanced the encapsulation efficiency. Blending of modified starch with maltodextrin improved the encapsulation efficiency of rosemary essential oil (60.22 %) as compared to the modified starch microcapsules (56.79 %) [66]. The efficiency was 45.45 %

when modified starch and inulin blend was used. In the same study, it was found that the encapsulation efficiency of rosemary oil was lower in the blends of gum arabic: maltodextrin (45.45 %) and gum arabic: inulin (29.53 %) microcapsules as compared to gum arabic microcapsules (56.83 %). These studies signify that it is important to carefully choose the polymer solutions and other components for the encapsulation of oils.

Effective and efficient encapsulation is possible if the wall materials possess both hydrophilic and hydrophobic groups [11]. Such polymers enable the emulsification and stabilization of the formulations. In this regard, Sarkar *et al.* (2013) enhanced the hydrophobicity of gum arabic by mixing octenyl succinate derivative for the encapsulation of mint oil [11]. The microcapsules with gum arabic and octenyl succinate derivative (encapsulation efficiency: 84.19 %) were better than gum arabic microcapsules (encapsulation efficiency: 80.66 %). In another study, gum arabic and whey protein mixture was successfully used to encapsulate three different oils, namely, sunflower oil, lemon oil and orange oil. The oil encapsulation efficiency was > 80 % for each formulation. Microencapsulation of *l*-menthol was studied in gum arabic and gum arabic: modified starch mixture (Commercially available modified starches are CAPSUL and HI-CAP 100). Higher encapsulation efficiency was achieved when HI-CAP 100 (85 %) was used as compared to CAPSUL (79 %) and gum arabic (68 %) [67]. Presence of oil as the internal phase helps in enhancing the hydrophobicity of the formulation. This, in turn, helps increasing the encapsulation efficiency.

With the advancement in drug delivery technology, an alternative approach to improve the hydrophobicity of the biopolymeric microparticles has been designed. In this approach, the drug molecules are dissolved/dispersed in the vegetable oil and the oil is subsequently gellified using a gelating agent to form semi-solid organogels. The organogels are dispersed in an aqueous solution of biopolymer. Crosslinking of the biopolymer resulted in the formation of organogel containing microparticles. Using this approach, vegetable fat-based organogels, animal fat-based organogels and polysorbate fatty acyl organogels were encapsulated within alginate microparticles [68-70]. The aforementioned approach was independently developed by another group of researchers with modification. In this approach, the organogels were dispersed and stabilized in an aqueous medium using a stabilizer so as to form gelled oil particles [71].

Table 2.3: Advantages and problems associated with beads and microparticles.

Advantages		**Problems**	
Protection from evaporation, leaching and/or oxidation of vegetable oils	[60-61]	Involvement of multiple steps in the method of preparation. Sometimes, this may leads to lower the encapsulation efficiency	[72]
Controlled-release applications	[67]		
Easy handling	[73]		
Taste/smell masking	[73]		

2.3. Preparation methods of microparticles

The techniques used for the encapsulation of oils are spray drying [67], coacervation [74], emulsion extrusion [75], solvent evaporation [76], ionotropic gelation [77], co-axial electrospray [78] and supercritical fluid impregnation method [79].

2.3.1. Spray drying

Spray drying is a widely used technique for the encapsulation of oils in microparticles. Spray drying involves rapid atomization of the bioactive agent containing solution/emulsion to drying medium at high temperature (Figure 2.5a). Temperature is maintained by pumping hot air in the direction opposite to the spraying direction of the emulsion. The sudden change in temperature leads to the quick evaporation of water and subsequent formation of solid microparticles with the entrapment of the core material [80]. The advantages of this method include, easy availability of machinery and easy regulation of the microparticle size. The disadvantage associated with this method is the use of high temperature for the drying process. Spray drying technology requires fine tuned operating conditions and sufficient amount of solution with active ingredient. The operating conditions include air inlet temperature, atomization air flow, liquid flow rate, aspirator suction velocity and solid concentration [81].

Encapsulation efficiency of the microparticles in spray drying is dependent on some key steps *viz.*, preparation of the stable oil-in-water emulsion and spraying of the emulsion into small droplets on to the drying bed [9]. Spraying of the emulsion to the requisite droplet size and drying of the droplets depends on the emulsion properties. Hence, the weight ratio of hydrophilic and lipophilic phases, oil droplet size distribution in the emulsion, the dry matter content in the emulsion and the viscosity of the emulsion needs to be optimized prior to spray drying. The success of spray drying is mainly influenced by the oil droplet size distribution in the emulsion

[82]. The choice of polymer is also important as it constitutes the dry matter of the microparticles [83]. For spray drying, the carriers should possess emulsion forming abilities with reasonable viscosity so as to be pumped and sprayed. The emulsions should not be sticky and hygroscopic after drying. Otherwise, it will affect the stability of the microparticles during storage. The main carriers for spray drying in food and pharmaceutical industries are polysaccharides, starches, gums, celluloses and proteins. These have been used in either alone or in combination.

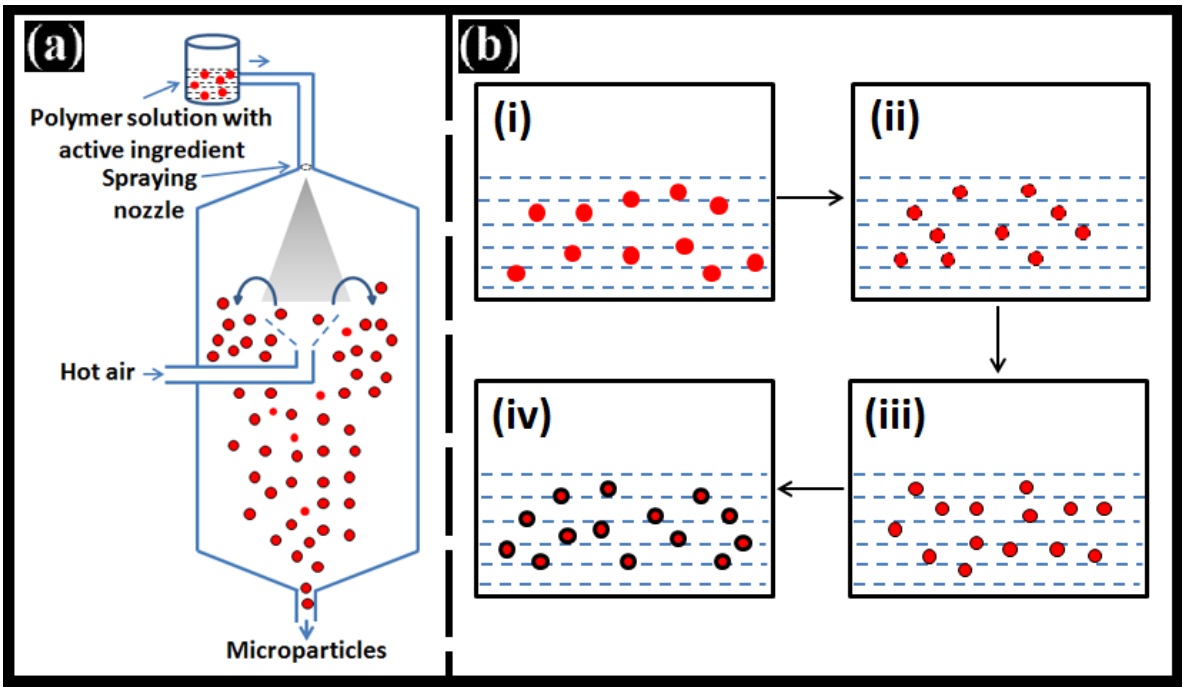

Figure 2.5: Schematic representation of: (a) Spray drying, and (b) Coacervation methods.

2.3.2. Coacervation

Coacervation is a technique that involves the partial desolvation of a homogeneous polymer solution into a polymer rich phase (coacervate) and polymer poor phase (coacervation medium) by the addition of a desolvating or coacervating agent (Figure 2.5b). During the process of encapsulation, the bioactive agent will be encapsulated within the polymer rich phase. Coacervation can be achieved in two ways: simple coacervation and complex coacervation. Both the techniques are identical to each other, differing only in the phase separation process.

In simple coacervation, water soluble desolvating agent is added to the polymer solution. Desolvating agent separates the aqueous phase from the polymer molecules, which in turn, affects the solubility of the polymer molecules. The polymer rich phase gets precipitated as spherical droplets. Crosslinking of these spherical droplets results in the formation of stable

microparticles. Choice of crosslinking agents depends on the type of biopolymer used. In general, glutaraldehyde, genipin and calcium salts have been widely used as the crosslinking agents. The polymers used in the coacervation process are alginate, chitosan, gelatin, cellulose derivatives and proteins [84-90]. Generally used desolvating agents include alcohols (ethanol, propanol, isopropanol, tertiary butyl alcohol), acetone and sodium sulfate [91-92].

On the other hand, the complex coacervation technique involves complexation between two oppositely charged polymers. Complex coacervation involves three basic steps. First step involves the formation of three immiscible phases; liquid vehicle, core material and coating material. The core material is dispersed in a solution of coating polymeric material. The coating material is made immiscible either by adding desolvating agent or salt or incompatible polymer or by inducing polymer-polymer interactions or by changing the temperature of the polymer solution. The second step involves the deposition of the liquid polymer on the core material. Finally, the third step involves the stabilization of the microcapsules by crosslinking, desolvation or thermal treatment. In general, protein-polysaccharide complexes (gelatin-pectin, whey protein-gum arabic, gelatin-acacia gum, β-lactoglobulin-acacia gum, gelatin-heparin, gelatin-carboxymethyl guar gum and albumin-alginic acid) are being used in complex coacervation [93-100].

2.3.3. Coaxial electrospray method

In general, encapsulation of oils and/or bioactive agents is mainly fabricated by emulsification processes, spray drying coacervation and solvent extraction methods. These processes involve the application of mechanical forces, chemical reagents and thermal treatment which may lead to polymer degradation or denaturation or aggregation [101]. These problems are more pronounced in protein-based polymers. In most of the cases, the microparticles/nanoparticles synthesized by these methods possess broad size distribution. Presence of multiple steps in each process results in the decrease in the encapsulation efficiency. Considering the limitations associated with the emulsification and other related processes, electrospray method was proposed.

Single-axial electrospray method was designed initially. The technical advancements lead to the transformation of single-axial electrospray method to coaxial electrospray method. Coaxial electrospray differs from the single-axial electrospray in the use of a coaxial capillary needle to deliver two liquids independently [101]. Coaxial electrospray allows preparation of multilayered

particles having sizes ranging from tens of nanometers to hundreds of micrometers. This process introduces high electric field between the coaxial capillary needle and the ground (Figure 2.6a). The resultant electrical shear stress elongates the shell (polymer) liquid and core (oil) liquid at the needle outlet so as to form an inverted triangle shape or "Taylor cone" [102]. At the end of the cone, the liquid propels out and breaks into multilayer droplets. It is possible to achieve 100 % encapsulation efficiency (using this method) due to the precise control over the core-shell geometry. This process protects the fragile therapeutic molecules from denaturation and aggregation [103]. Coaxial electrospray method was successfully used to encapsulate peppermint oil in alginate-pectin microcapsules [78].

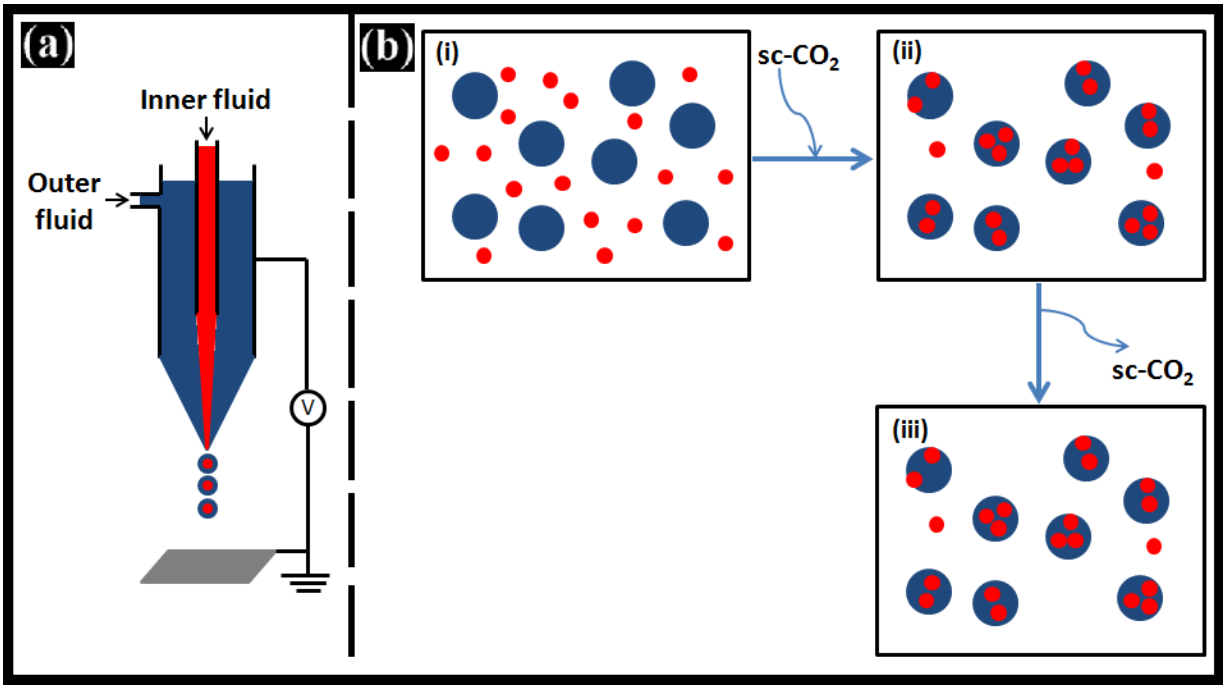

Figure 2.6: Schematic representation of: (a) Co-axial electrospray, and (b) Supercritical fluid technology.

2.3.4. Supercritical fluid technology

Supercritical fluid technology was developed to minimize the drawbacks associated with the traditional encapsulation methods. It is generally preferred for the essential oils which are sensitive to high temperature, oxygen and chemicals. For example, oregano oil degrades at ~80 ^{o}C, so supercritical fluid technology was employed instead of spray drying [79]. Supercritical fluid technology is an eco-friendly approach, where, supercritical carbon dioxide (sc-CO_2) is

used as the green solvent. sc-CO_2 possess the properties which are ideal for the encapsulation of bioactive agents. The characteristic properties of sc-CO_2 are lower viscosity, higher diffusivity, lower surface tension, faster process and high solubility of the active compound [79]. This technology is also termed as supercritical solvent impregnation. This process has been successful in the encapsulation of oil, fragrances and pharmaceutical ingredients etc.

Schematic sketch of the principle of this technology was shown in Figure 2.6b. The supercritical impregnation apparatus consist of a high pressure stainless steel impregnation cell, a magnetic stirrer plate, a temperature controlled water bath, a high pressure CO_2 pump and a pressure transducer. The impregnation cell contains two chambers separated by a mesh. Lower chamber is loaded with the essential oil and the upper chamber is loaded with microparticles or matrices in which the oil needs to be impregnated. During the assay, the cell is immersed in the water bath (40 to 50 ^{o}C) and CO_2 is pumped (10-12 kPa) into the cell after achieving the desired temperature. For better impregnation, homogenization is done by using magnetic stirrer. After impregnation time (~2 h), the system is depressurized after reducing the temperature of the water bath (~10 ^{o}C). At lower temperature, dissolution of the oil in sc-CO_2 is minimized. Slow depressurization (0.07‑0.15 MPa/min) is preferred over the fast depressurization. Thereafter, depressurizing, the oil impregnated microparticles are collected [104]. Heat sensitive lavandin (*Lavandula hybrida*) essential oil and oregano oil were encapsulated in modified starches by this method [79, 104].

In this study, ionotropic gelation method was chosen to encapsulate vegetable oils and organogels. Rationality behind the selection of the method is:

- Spray drying involves high temperature, which may destabilize the organogels.
- Coacervation, emulsion extrusion and solvent evaporation methods use organic solvents, which are usually non-biocompatible.
- Co-axial electrospray and supercritical fluid impregnation methods are advanced techniques and are not cost-effective.

2.3.5. Ionotropic gelation/ internal gelation method

In general, ionotropic gelation method has been extensively employed to prepare alginate microparticles [77]. This method is schematically shown in Figure 2.7. The polymer solution is mixed with vegetable oil and/or bioactive agent so as to form a primary emulsion. The primary

emulsion is slowly added to the bulk oil (may be different from the encapsulated oil) at 4 ^{o}C, under continuous stirring. Under these conditions, the primary emulsion droplets get dispersed in the bulk oil phase by forming oil-in-water-in-oil multiple emulsion. Addition of the crosslinker to the emulsion facilitates the formation of microparticles by inducing gelation of the polymeric layer. The microparticles are collected, washed and dried. After collecting, the microparticles can be hardened by incubating in the crosslinker solution. Internal gelation method has been employed to encapsulate organogels within alginate microparticles [68-70].

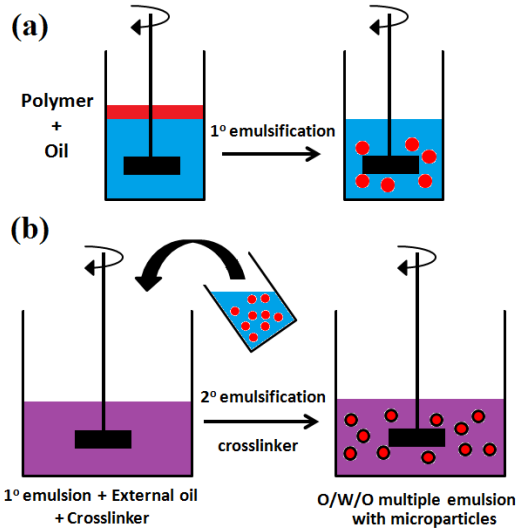

Figure 2.7: Schematic representation of the ionotroic gelation method.

Though alginate has been extensively reported in the literature, the main problem associated with the alginate microparticles is their porous nature which in turn leads to the leaching of the encapsulating agent [105]. This problem was tried to be solved by incorporating the semi-solid organogels as the core material of the microparticles.

2.4. Research objectives

To negate the leaching of the internal phase, we propose that the gelation of the internal apolar phase may prevent its leaching from the porous alginate microparticles. Based on this hypothesis, following objectives were made.

1. Encapsulation of cocoa butter and mango butter based organogels in alginate microparticles
2. Encapsulation of lanolin based organogels in alginate microparticles
3. Encapsulation of stearate organogels in alginate microparticles
4. Encapsulation of Span 80-Tween 80 based organogels in alginate microparticles

Chapter 3

Materials and methods

3.1. Materials

Sodium alginate, stearic acid, calcium carbonate, calcium chloride (fused), potassium dihydrogen phosphate, rhodamine B, Span 80, Tween 80 and dialysis tubing (MW cut-off 12 kDa) were purchased from Himedia, Mumbai, India. Cocoa butter and mango butter were procured from NV Organics (P) Ltd, New Delhi, India. Anhydrous lanolin was procured from Loba Chemie, Mumbai, India. Fluoral yellow 088 was purchased from Sigma-Aldrich, Mumbai, India. Glacial acetic acid was purchased from MERCK, Mumbai, India. Refined palm oil (Purti Vanaspati Pvt. Ltd. West Bengal, India), Refined sesame oil (Tilsona®, Recon oil industries Pvt. Ltd., Mumbai, India), soy bean oil (Saffola®, Marico Pvt. Ltd., Jalgaon, India) and sunflower oil (Fortune sunlite®, Adani Wilmar Ltd. Gujarat, India) were purchased from the local market. Metronidazole (MZ) was a kind gift from Aarthi drugs, Mumbai, India. Fresh goat's small intestine was procured from the local butcher shop. MG63 cell line was procured from NCCS, Pune, India. Double distilled water was used throughout the study. All the experiments were performed in duplicates.

3.2. Preparation of formulations

3.2.1. Preparation of cocoa butter and mango butter-based organogels

Emulsions of cocoa butter and mango butter were prepared by hot emulsification method [12]. Accurately weighed cocoa butter and span 80 were melted at 45 °C using a temperature controlled water-bath. The above mixture was homogenized for 5 min at 1200 rpm (45 °C) using an overhead stirrer (RQ-126/D, Remi Motors Ltd, India). Gelatin solution (20% w/w, 45 °C) was added drop-by-drop to the mixture and homogenized for another 15 min at the same temperature. The hot homogenized emulsion was put into culture bottles (10 ml) and incubated at room-temperature (25 ^{o}C) for 30 min to induce gelation. Similarly, mango butter based formulations were also made. Drug loaded organogels were prepared by dissolving 0.5 % (w/w) metronidazole in the emulsion. The stable organogels were stored at 4 °C for further analysis.

3.2.2. Preparation of lanolin-based organogels

Ten grams of lanolin was liquified at 55 °C. 0.1 g of SMO (1% w/w) was added to the molten lanolin and was homogenized at 1500 rpm using an over-head stirrer. This was followed by the drop-wise addition of double distilled water to the above mixture with continuous homogenization. The homogenization was continued till 15 min after the addition of water. The amount of double distilled water was varied so as to obtain semi-solid formulations having various proportions of lanolin and water. Metronidazole was used as the model drug. Drug containing formulations were prepared by dispersing drug (1 % (w/w)) in lanolin. The rest of the procedure was same.

3.2.3 Preparation of stearate organogels

Sesame oil and soy bean oil organogels were prepared using stearic acid as the organogelator [106]. Stearic acid was dissolved in either sesame oil or soy bean oil at 70 ºC in 15 ml vials. The hot stearic acid solution was cooled down to room–temperature (25 ^{o}C). This resulted in the formation of either cloudy suspension or organogel. To determine the critical gelation concentration (CGC) of stearic acid, the concentration of stearic acid was varied from 1 % (w/w) to 25 % (w/w). Drug containing organogels were prepared by dispersing ciprofloxacin (0.5 % w/w) in the hot stearic acid solution.

3.2.4. Preparation of Span 80-Tween 80 organogels

5.25 g of the surfactant mixture (Span 80: Tween 80 ratio of 1:2 w/w) and 1.25 g of sunflower oil were mixed to form a homogenous solution at room-temperature. To this, 3.25 g of water was added drop-by-drop with continuous mixing at 500 rpm. The homogeneous mixture was allowed to settle at room-temperature to form organogel. The prepared organogel was labeled as ‘OG’ and used for further studies. To prepare the drug containing organogels, 1 % (w/w) metronidazole was dispersed in water and the drug containing water was used for the preparation of the organogels. The metronidazole containing organogels were labeled as OGMZ.

3.2.5. Preparation of microparticles

The microparticles were synthesized by modified double emulsion method or internal gelation method [107]. Briefly, 0.5 g of sodium alginate was dissolved in 20 g of water, kept on stirring at 250 rpm at room-temperature. After complete dissolution of the sodium alginate, 0.4 g calcium carbonate was added and homogenized at 250 rpm. Then, a mixture of 0.5 g of span 80 and 5 g

of internal phase was added and further homogenized for 15 min to form an oil-in-water emulsion. The internal phase was either vegetable oil or organogel. The emulsion was further homogenized in an ice-bath for 10 min to form a thick emulsion. The thick emulsion, so obtained, was transferred to 60 ml of ice-cold sunflower oil (external phase) and homogenized for 5 min at 250 rpm to form a double emulsion. After the homogenization, 5 ml of acidified oil (4.5 ml sunflower oil + 0.5 ml glacial acetic acid) was added to the external phase of the double emulsion (which is under stirring) to induce ionic crosslinking and gelation of the alginate layer to form microparticles. The microparticles were washed with 0.5M calcium chloride solution containing 1 % (v/v) Tween 80, followed by washing with water. The microparticles without any internal phase (i.e. organogel or vegetable oil) were labeled as blank microparticles. Drug containing microparticles were also prepared as described above, but the internal phases of microparticles were changed with drug containing internal phases.

3.3. Characterization of the formulations

3.3.1. Microscopic studies

Microstructure of the formulations was observed using an upright bright-field microscope (Leica DM750 equipped with ICC50 HD camera, Germany), phase contrast microscope (Primo vert Carl Zeiss GMBH, Germany), fluorescence microscope (FM) (Carl-zeiss-HBO 50) with ProgRes capture 2.8 software, polarized light microscope (Leica DMLP attached with Leica DFC 295 camera) and confocal laser scanning microscope (FV1000 confocal microscope, Olympus, USA). For fluorescence microscopy, rhodamine dye solution in water was used as the aqueous phase for the preparation of samples. The microparticles for confocal laser scanning microscopy were prepared by dissolving fluoral yellow 088 (0.1 % w/w) dye in either organogels or palm oil. The dye containing organogels and palm oil were used for the preparation of the microparticles. The chromophore (fluoral yellow 088) containing microparticles were excited at 405 nm and the fluorescence was observed at 515 nm [108]. The microparticles were sputter coated with platinum before the study. Size distribution of the emulsion droplets was analyzed using National instrument vision assistant (NI vision assistant-2010, US) software [12]. The near circular particles were chosen for the particle size analysis (Heywood circularity factor= 0.9 to 1.1). On an average, 1000 microparticles were considered for the size distribution analysis.

3.3.2. Gelation kinetics of stearate organogels

The gelation kinetics was studied by visible spectroscopy. Absorbance of the molten gels was measured at 550 and 575 nm for sesame oil and soy bean oil based organogels, respectively. The chosen wavelengths were the absorption maxima of the pure sesame oil and soy bean oil. The absorbance of the molten organogels was recorded for 15 min at an interval of 15 sec during the cooling process. The weight of organogels was kept constant (3 g) for all the gels.

3.3.3. Molecular characterization studies

The physico-chemical nature of the formulations was studied by X-ray diffraction (XRD) and Fourier transform infrared (FTIR) spectroscopic studies. X-ray diffractometer (Pananalytical, X-Pert Pro; Almelo, Netharlands) was used to study the morphology of the formulations in their native state. Formulations were spread evenly over a glass plate and then subjected to X-ray analysis. X-rays of 1.54 Å were generated by a CuKα source. The diffraction was measured in the 2θ range of 5º to 50º.

FTIR spectra of the formulations were obtained using FTIR spectroscope (Alpha-E, Bruker, Germany), operated in the attenuated total reflectance (ATR) mode. Spectral analysis was performed in the range of 4,000 to 500 cm^{-1} at a resolution of 4 cm^{-1}.

3.3.4. DSC studies

The thermal properties of the formulations were examined using differential scanning calorimeter (DSC-200 F3 MAIA, Netzsch, Germany). Accurately weighed formulations were taken in aluminum crucibles with pierced aluminium lids. The experiment was performed at a scanning rate of 2 K/min under inert atmosphere, created using N_2 gas. The results were analyzed using the Netzsch-proteus software.

3.3.4. Mechanical analysis

Mechanical properties of the formulations were determined using a static mechanical tester (Stable Microsystems, TA-HD plus, U.K.). In order to determine the strength, visco-elastic nature and spreadability of the formulations, different experiments were conducted. Table 3.1 summarizes the details of the texture studies.

Table 3.1: Details of texture analysis studies.

Type of study	Type of fixture	Testing conditions			Mode of study
		Pre test speed (mm/sec)	Test speed (mm/sec)	Post test speed (mm/sec)	
Cyclic compression	P/3, 30mm diameter cylindrical probe	1.0	1.0	1.0	Button mode (30 mm)
Stress relaxation	HDP/SR spreadabilityrig with 45° conical perspex probe	1.0	1.0	1.0	Auto force (5 g, 5 mm)
Spreadability	HDP/SR spreadability rig with 45° conical perspex probe	10	1.0	1.0	Auto force (5 g, 20 mm)

Based on the compression results, following parameters were predicted: (i) Hardness or firmness (N) – The maximum peak force during the 1st penetration cycle, (ii) Cohesiveness – The ratio of force area during the 2nd cycle to that of the 1st cycle, (iii) Adhesiveness – The negative force area during the 1st cycle and (iv) Springiness - The ratio of time of 2nd cycle to the 1st cycle. Gumminess is the multiplication of hardness and cohesiveness.

3.3.5. Viscosity studies

Rheological behavior of the prepared formulations were analyzed using a rotational cone (angle= 5.4°; diameter= 30 mm) and plate viscometer (BOHLIN VISCO-88, Malvern, U.K.). A gap of 0.15 mm was maintained between the cone and the plate throughout the study. Viscosity of all the formulations was measured under variable shear rates ranging from 13 sec^{-1} to 95 sec^{-1} at room-temperature (25 ^{o}C) [109-110].

3.3.6. Leaching and swelling studies of the microparticles

Leaching studies were conducted both qualitatively and quantitatively. The qualitative measurement was done by placing 0.5 g of the microparticles on Whatmann filter paper (#1, Sartorius) and subsequently incubating the samples at room-temperature for 1 h [68, 111]. In another study, the leachate was quantified by soaking 0.1 g (W_1) of microparticles in 1.0 g (W_2) of water for 1.0 h at room-temperature in microcentrifuge tubes [112]. After incubation, the tubes were centrifuged at 10,000 rpm for 2 min (MC-02, SPINWIN, Tarsons). The pellet (W_3) and the supernatant (W_4) were weighed separately and dried at 55 ºC for 48 h. Subsequently, the dried pellet (W_5) and supernatant (W_6) were weighed again. Swelling power (equation 1) and % leaching (equation 2) of the microparticles were calculated using the following equations.

$$\text{Swelling power} = \frac{W_3}{W_5} \qquad (1)$$

$$\%\ \text{leaching} = \frac{W_6}{W_1} \times 100 \qquad (2)$$

3.3.7. Drug encapsulation efficiency of the microparticles

The microparticles (1.0 g) were triturated in 10 ml of acetone for 15 min at room-temperature. The mixture was transferred to a volumetric flask and incubated for 6.0 h (37 ºC) to achieve drug equilibration. Thereafter, the mixture was filtered using Whatmann (#1) filter paper and the filtrate was analyzed at 321 nm using UV-visible spectrophotometer (UV-3200, LabIndia, India). The drug encapsulation efficiency was represented as % drug encapsulation efficiency (% DEE) (equation 3).

$$\%\ \text{DEE} = \frac{\text{Practical loading}}{\text{Theoritical loading}} \times 100 \qquad (3)$$

3.3.8. *In vitro* biocompatibility studies

Biocompatibility of the formulations was carried out using L929 fibroblast cell line by “test on extract method” as per the reported literature [113]. In gist, leachant of 1 g of the formulation in 50 ml of phosphate buffer saline (pH 7.2) was used for the study. The formulations were put in the dialysis bags, dipped in the phosphate buffer and subsequently incubated at 37 °C for 24 h. The leachate was sterilized using syringe filter. 1×10^4 cells were seeded in each well of the 96

well plate containing DMEM and 10 % FBS. 10 µl and 20 µl of the filtered leachate was then added to the wells and was incubated in CO_2 incubator (5 % CO_2) and maintained at 37 °C for 24 h. Thereafter, the viability of the cells was determined by MTT (3-(4,5-dimethylthiazol-2-yl)-2,5-diphenyltetrazolium bromide) assay. The complete medium was used as negative control.

3.3.9. Mucoadhesivity studies

Mucoadhesivity studies were conducted using freshly excised goat intestine (ileum). The intestine (2 cm x 2 cm) was cut and adhered to a glass slide using acrylate adhesive such that the inner lumen was exposed. The dried microparticles were placed gently on the exposed mucosal surface for 5 min. The glass slides were subsequently kept vertically in the USP (United States Pharmacopeia) disintegration baskets (EI tablet disintegration apparatus, India) containing 900 ml of phosphate buffer (pH 7.4). The retention time of the microparticles on the mucosal surface was checked over a period of 36 h.

3.3.10. *In vitro* drug release studies

For drug release study, two-compartment modified Franz diffusion cell (receptor and donor) was used [12]. Precisely weighed 2 g of the emulsion gels were placed in the donor and the compartments were separated by a pre-activated dialysis membrane. On the other hand, donor chamber for the microparticles consists of dialysis bag loaded with 1 g of microparticles. Receptor compartment contained 50 ml receptor fluid. Donor chamber/dialysis bag was kept in contact with the receptor fluid, and it was kept on stirring at 100 rpm (37 °C). The receptor fluid was replaced every 15 min in the first 1 h and subsequently every 30 min up to 9 h. The replaced fluid spectrophotometrically analyzed at 321 nm using UV-visible spectrophotometer [12]. Attempts were also made to predict the drug release pattern by fitting the data in different drug kinetic models.

The antimicrobial activity of the formulated gels was tested against *Escherichia coli* (NCIM 5051) by well diffusion method. 100 µl of $2x10^5$ CFU/ml bacterial cells was spread over the autoclaved nutrient agar plates. In each plate, uniform sized wells were made using 9.0 mm borer. The formulations were placed gently in the wells and incubated at 37 ºC for overnight (12 h). The antimicrobial activity of the formulations was compared with Metrogyl® (metronidazole containing marketed formulation). After incubation, the zone of inhibition against bacteria was measured using a ruler.

3.3.11. Statistical analysis

Statistical analysis of the results was performed by one way ANOVA using Microsoft excel® 2007 software.

Chapter 4

Encapsulation of cocoa butter and mango butter based organogels in alginate microparticles

Abstract

Water-in-oil (fat) type cocoa butter (CB) and mango butter (MB) gels were prepared using gelatin solution (20 % (w/w)) by hot emulsification method. Stable CB and MB gels were formed until the aqueous proportion has reached to 70 % (w/w) and 35 % (w/w), respectively. Amongst the stable CB and MB formulations, gels with 10 % (w/w) and 35 % (w/w) aqueous fraction were chosen for further studies. The gels were characterized by microscopy, X-ray diffraction (XRD), differential scanning calorimetric (DSC) and mechanical studies. Drug (metronidazole) release kinetics indicated that the drug was released from planar matrices in either Fickian (mango butter organogels) or non-Fickian diffusion (cocoa butter organogels). The drug loaded gels showed good antimicrobial activity against *E. coli*. Amongst the characterized gels, formulations with 35 % (w/w) aqueous fraction were encapsulated within the alginate microparticles by ionotropic gelation method. Palm oil (cocoa butter equivalent) containing alginate microparticles were synthesized for comparative studies. The difference in the microstructure of the palm oil and organogel containing microparticles was elucidated by confocal microscopy. Encapsulation of the organogels was confirmed by XRD and DSC studies. Leaching of palm oil was noticed in palm oil containing microparticles but leaching of fats was less from the organogel containing microparticles. Difference in leaching properties has affected the drug encapsulation efficiency and in vitro drug release behavior. Super case II mode of drug delivery was shown by the microparticles with good antimicrobial action against *E. coli*. The developed formulations showed good biocompatibility and mucoadhesive nature. Based on the results, the developed formulations may be used as controlled delivery vehicles.

Graphical abstract

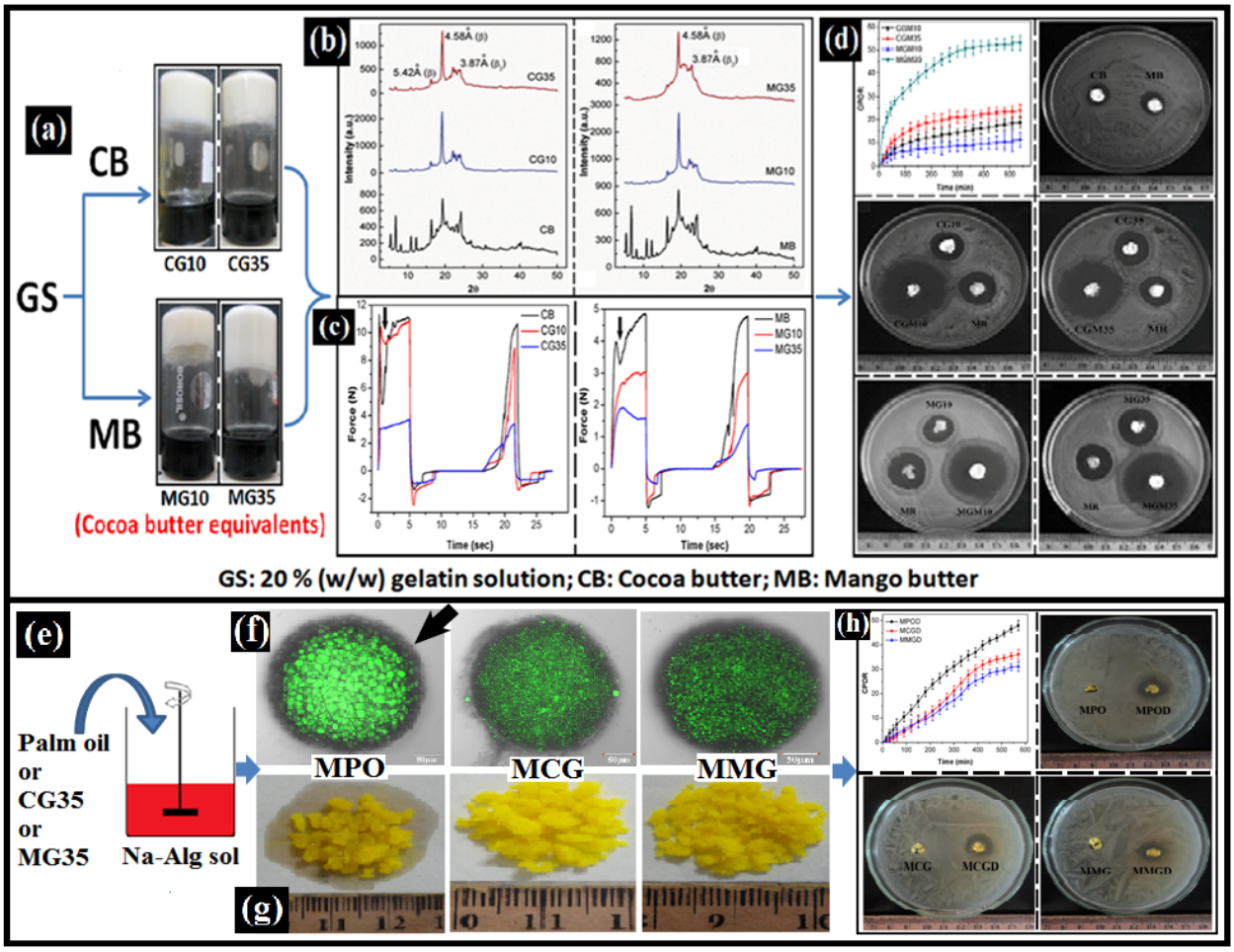

Part A: Preparation and characterization of cocoa butter and mango butter based organogels

Overview

Aqueous gelatin solution (20 % w/w) containing water-in-oil (fat) type cocoa butter (CB) and mango butter (MB) gels were prepared by hot emulsification method. Stable CB and MB gels were formed until the aqueous proportion has reached to 70 % (w/w) and 35 % (w/w), respectively. Amongst the stable CB and MB formulations, gels with 10 % (w/w) and 35 % (w/w) aqueous fraction were chosen for further studies. The results were analyzed in comparison with pure CB and MB. XRD and DSC melting profiles suggested the formation of unstable polymorphic forms (α and β`) of fats in the gels. The crystal size and solid fat content analyses suggested that the aqueous phase might have hindered the transformation of unstable polymorphic forms to stable polymorphic form (β) in the gels. This has improved the softness of the gels. As per Avrami analysis of the DSC thermograms, fat crystals were formed by instantaneous nucleation and have either uni- or bi-dimensional growth. Drug release kinetics suggested that the drug was released from planar matrices in either Fickian (mango butter organogels) or non-Fickian diffusion (cocoa butter organogels). Pure CB and MB also showed antimicrobial activity due to the presence of polyphenols. Metronidazole loaded gels showed better antimicrobial activity as compared to Metrogyl® (marketed formulation).

4.1. Introduction

The development of new materials and/or new technological approaches has grown in importance against the use of traditional materials. Agroindustrial residues are unconventional and alternative sources towards food, pharmaceutical and cosmetic industries. The fat sources that have been used in such industries include sesame oil, soy bean oil, olive oil, cocoa butter, shea butter etc. Among these, cocoa butter stands out as one of the best material because of its peculiar physico-chemical characteristics.

Theobroma oil or cocoa butter is extracted from the beans of *Theobroma cacao L*. It is a pale yellow vegetable fat rich in stearic and palmitic acids. Unsaturated fatty acids constitute about 40 % of the total fatty acid content. The polyphenols present in cocoa butter confers health benefits due to the presence of phyto-antioxidants [114]. Cocoa butter remains as solid at room temperature and melts at body temperature. This property makes it a special material and has been extensively explored in food (as chocolates), pharmaceuticals (as suppository bases and topical bases) and cosmetics (because of excellent emollient properties) applications [115]. Because of its wide range of applications, the availability of cocoa butter in large quantities has become a great concern at the industrial level. To cater the needs of the world, *Theobroma cacao L* (the only commercial producer of cocoa butter) has been cultivated in countries such as Ivory Coast, Ghana, Nigeria, Cameroon, Brazil, Ecuador, Indonesia and Malaysia [116]. Hence, much of the work has been carried out to find alternatives for cocoa butter.

Cocoa butter alternatives are identified as cocoa butter equivalents (palm oil, shea butter, kukum butter, illipe butter, mango butter), cocoa butter replacers (soy bean oil, rape seed oil, cotton seed oil, ground nut oil) and cocoa butter substitutes (coconut oil, palm kernel oil) [117]. The physico-chemical nature of the cocoa butter equivalents is similar to cocoa butter and can be used without altering the properties of cocoa butter. In this regard, mango butter (MB) was chosen as the cocoa butter equivalent because of its similar fatty acid profile as that of cocoa butter [1]. Fatty acid profile of mango butter in comparison with cocoa butter has been provided in Table 4.1. The fatty acids in cocoa butter and mango butter exist in 4 to 6 polymorphic states [1]. Mango (*Mangifera indica L.*) trees are grown naturally or cultivated in tropical and subtropical countries, mainly for the fruit pulp. In general, mango seeds are discarded as the agroindustrial waste. But, mango seed kernel is rich source of fat and can be used to extract mango butter [118]. The fatty acid content

of mango butter is similar to cocoa butter but contains higher amount of unsaturated fatty acids [1]. Just like cocoa butter, mango butter is also solid at room temperature and melts at body temperature.

Table 4.1: Fatty acid profile of cocoa butter and mango butter [1].

Fatty acid	**Cocoa butter (% w/w)**	**Mango butter (% w/w)**
Saturated fatty acids[*]		
Palmitic acid	24.0	9.0
Stearic acid	35.0	39.0
Arachidic acid	1.0	2.5
Behenic acid	--	1.0
Lignoceric acid	--	0.5
Unsaturated fatty acids[*]		
Oleic acid	36.0	41.0
Linoleic acid	3.0	6.0
Linolenic acid	1.0	1.0

* Approximate values

Often gelatin is used to improve the processing of the emulsion when low fat or during high aqueous phase volume is needed [119]. Gelatin improves the stability of the emulsions by preventing coalescence of the dispersed aqueous phase. In addition to these properties, gelatin gel has a melting point of ~32 ºC which results in the fat-like behavior [119]. Cocoa butter and gelatin have been used for preparing bases. In general, cocoa butter is insoluble in water/body fluids due to its high fatty acid content. To improve the compatibility and to reduce the high calorie content, researchers have been trying to develop water-in-oil (cocoa butter) organogels [120]. These organogels can be used as suppositories or chocolates. In this chapter, cocoa butter organogels were prepared using 20 % (w/w) aqueous gelatin solution. To check whether mango butter formulations can behave similar to that of cocoa butter formulations or not, mango butter organogels were prepared and their properties were compared with cocoa butter organogels.

4.2. Materials and methods

Experimental details for the preparation and characterization of the organogels are explained in the chapter 3.2.1. Organogels were characterized (chapter 3.3) by bright field microscopy, polar microscopy, XRD, DSC and mechanical studies. *In vitro* drug delivery and antimicrobial studies were also performed.

4.3. Results and discussion

4.3.1. Preparation of the organogels

The molten fats appeared as pale yellow translucent liquids. Addition of gelatin solution resulted in the formation of milky white emulsions. Appearance of milky white color without any phase separation is an indication to the formation of emulsions [121]. After incubation at room-temperature, the emulsions which failed to flow under gravity, upon inversion of the vials, were regarded as organogels [122]. The stability of the organogels was dependent on the type of the vegetable fat used. During preparation, cocoa butter organogels were able to accommodate 70 % (w/w) aqueous gelatin solution. On the other hand, only 35 % (w/w) gelatin solution was accommodated within the mango butter based organogels. An increase in the aqueous proportion beyond 70 % and 35 % for cocoa butter and mango butter formulations, respectively, resulted in the phase separation. The pictographs of the cocoa butter and mango butter organogels have been shown in Figure 4.1 and 4.2, respectively. The difference in the gelation properties of the vegetable fats can be attributed to the variation in the fatty acid compositions. The total unsaturated fatty acid content in cocoa butter is in the range of 36 to 43 %, whereas, in mango butter it is in the range of 43 to 59 % [1]. Literature suggests that the crystallization efficiency of the fats depends on the proportion of the unsaturated fatty acids present [123]. This may be associated with molecular geometry of the fatty acids. The tetrahedran bond angles of carbon enable the saturated fatty acids to arrange in linear and stack-wise fashion. On the other hand, presence of double bonds (unsaturation) in carbon linkages lead to the bending of the fatty acyl molecules [123]. These molecules do not stack well and lead to weak intermolecular interactions, which, in turn, affect the crystallization process. As mango butter possess higher amount of unsaturated fatty acids than cocoa butter, the crystallization efficiency was found to be lower. The organogels were stored at 4 ºC and were stable for more than 12 months. Since mango butter formed stable organogels up to MG35; CG10, MG10, CG35 and MG35 were chosen as the representative formulations for further characterization.

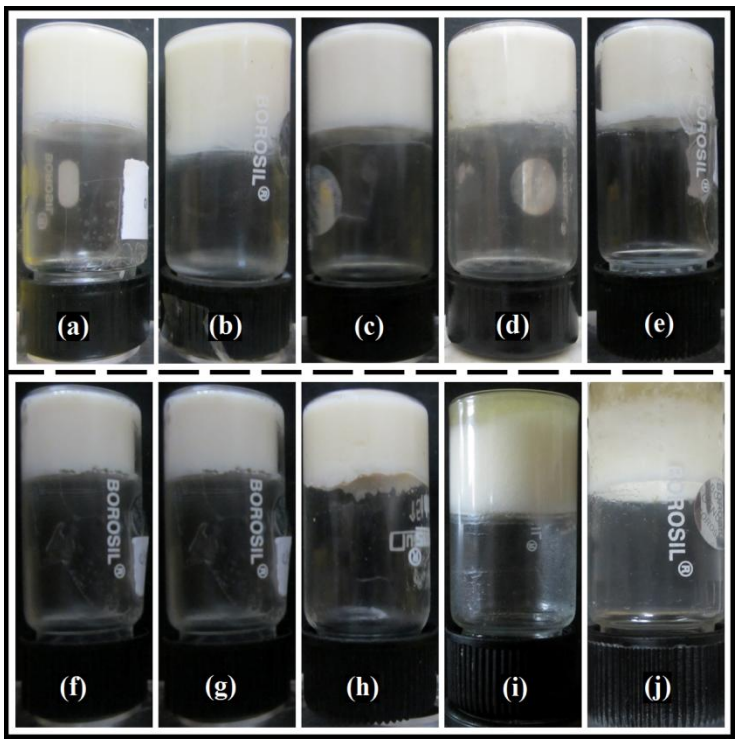

Figure 4.1: Cocoa butter based emulsion gels: (a) CG10, (b) CG20, (c) CG30, (d) CG35, (e) CG40, (f) CG50, (g) CB60, (h) CG70, (i) CG80, and (j) CG90.

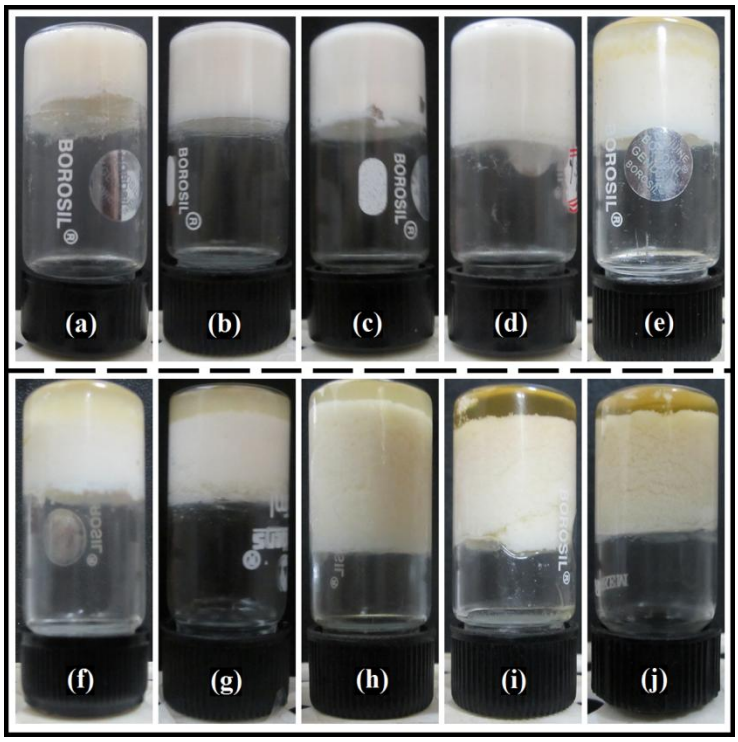

Figure 4.2: Mango butter based emulsion gels: (a) MG10, (b) MG20, (c) MG30, (d) MG35, (e) MG40 (f) MG50, (g) MG60, (h) MG70, (i) MG80, and (j) MG90.

4.3.2. Microscopic studies

The microstructure of the organogels showed evenly dispersed circular droplets of aqueous phase in the fat matrix (Figure 4.3). An increase in the droplet size was noticed with increase in the aqueous phase. Prevention of the droplets coalescence was responsible for the formation of such spatially arranged distinct droplets. Similar kinds of microstructures have been previously reported [124-125]. At higher water to fat ratio in cocoa butter organogels (> 70 % (w/w) aqueous phase) and mango butter organogels (> 35 % (w/w) aqueous phase), crystallization of fats was not sufficient to prevent droplet coalescence. Hence, larger and non-uniform droplets were observed in the unstable organogels (Figure 4.4). Formation of water-in-oil emulsion was confirmed by dilution test [126]. Both kinds of organogels showed uniform dispersion within the oil phase and showed phase separation in water (Figure 4.5). This indicated the formation of water-in-oil type of emulsions.

Polarized light micrographs of the organogels showed the presence of continuous crystalline network (Figure 4.6). Aqueous phase was dispersed as dark circles in the bright colored fat matrices of CG10 and MG10 (representative organogels). The continuous crystalline network stabilized the emulsion by physically locking the dispersed phase [126]. Bright field micrographs of the molten organogels showed dispersed water droplets within the fat continuous phase (Figure 4.3). Light micrographs of cocoa butter emulsions showed by Norton *et al.* (2012) also contained similar kind of microstructure [119]. Presence of fat around the water droplets imparts microbiological and physical stability to the organogels. The probability of microbial growth within the water droplets is minimized by completely isolating the aqueous phase from the environment. This helps in imparting microbial stability to the organogels. The presence of emulsifiers affects the network crystallization. Hence, high percentage of gelatin (20 % (w/w)) solution was used in the study. High gelatin concentration enhances the rate of adsorption of the gelatin at the newly formed fat-droplet interface. Rapid gelatin adsorption enhances the gelatin membrane formation thereby resulting in the decrease of the interfacial tension [120]. Lower interfacial tension prevented the coalescence of the droplets during homogenization process and resulted in the formation of smaller droplets. In general, a narrow size distribution was observed in the formulations with lower aqueous proportion as compared to the formulations with higher proportions of the aqueous phase (Figure 4.3e). CG10 and MG10 were having a narrow size

distribution as compared to CG35 and MG35, respectively. The mean size of the droplets (d_{32}) was calculated using the following equation:

$$d_{32} = \sum n_i d_i^3 / \sum n_i d_i^2 \qquad (4.1)$$

where, n_i is the number of droplets with diameter d_i.

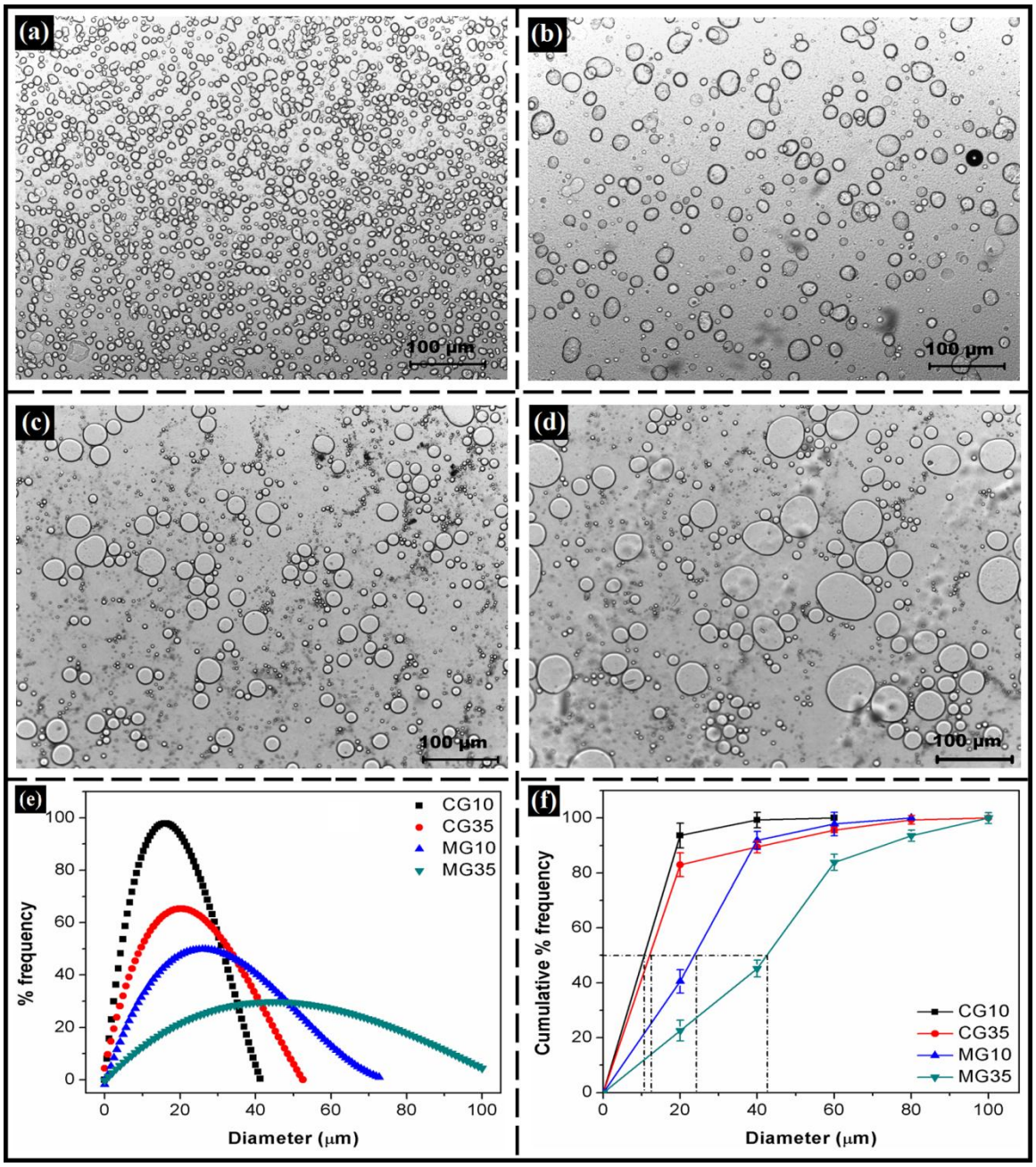

Figure 4.3: Pictographs of: (a) CG10, (b) CG35, (c) MG10, and (d) MG35; Dispersed size distribution analysis: (e) % frequency, and (f) Cumulative % frequency.

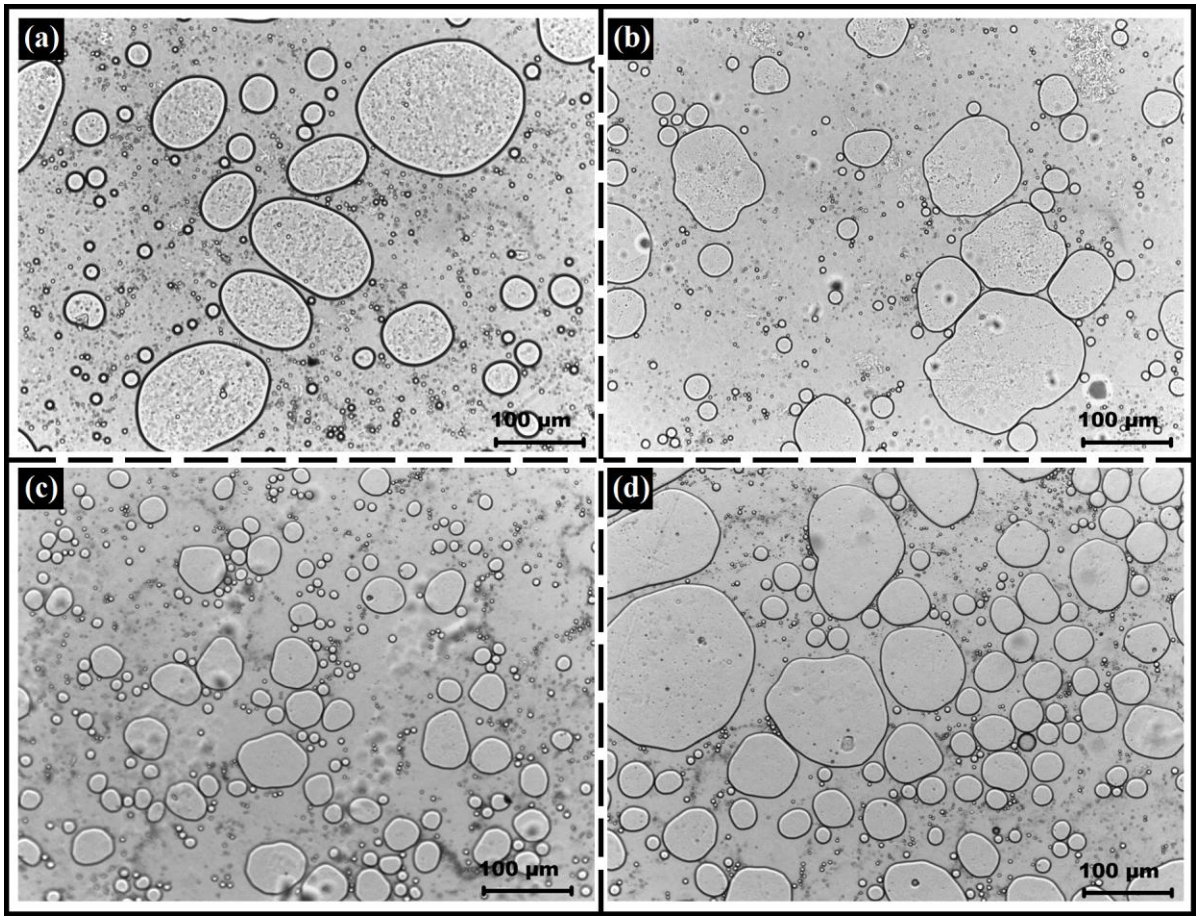

Figure 4.4: Micrographs of the unstable emulsion gels: (a) CG80, (b) CG90, (c) MG40, and (d) MG50.

The mean size of the droplets varied in the order of CG10 (15.2 µm) < CG35 (17.5 µm) < MG10 (19.63 µm) < MG35 (41.05 µm). The differences in the mean droplet size of the organogels with same water to fat ratio can be explained by the differences in the fatty acid composition of cocoa butter and mango butter. In general, long chain saturated fatty acids behave as solid at the fat-droplet interface and the unsaturated fatty acids behave as liquid. Since, the rate of crystallization of the unsaturated fatty acids at the fat-droplet interface is slower compared to the rate of crystallization of the saturated fatty acids [127], coalescence of the droplets might have lead to the formation of the larger droplets in mango butter based organogels. Stearic hindrances associated with the unsaturated fatty acids slows down the crystallization rate [127]. The average diameter (d_{avg}) of the droplets was calculated from Figure 4.3f (shown as dotted lines). The diameter of the 50 % population of the droplets was considered as $d_{avg.}$ The d_{avg} values were in close proximity of the d_{32} values.

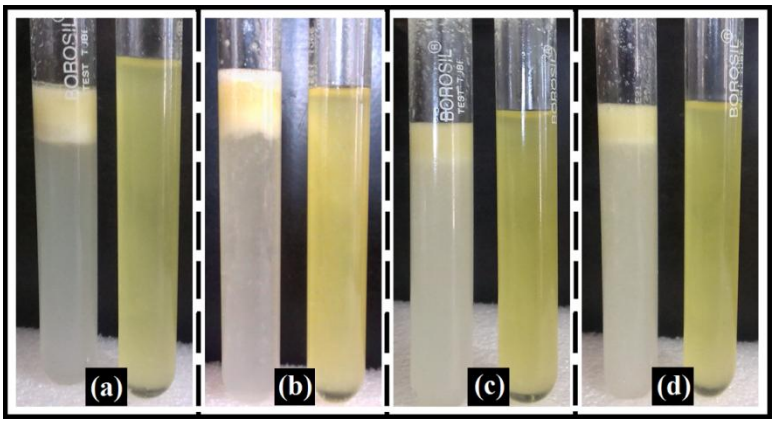

Figure 4.5: Dilution test: (a) CG10 in water (left), and oil (right); (b) CG35 in water (left), and oil (right); (c) MG10 in water (left), and oil (right); and MG35 in (left), and oil (right).

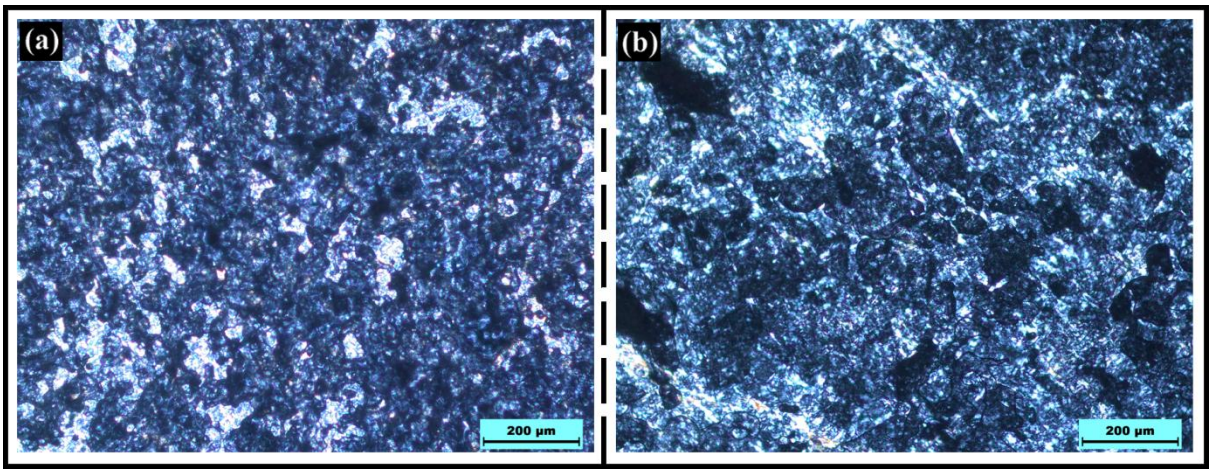

Figure 4.6: Polarized micrographs of: (a) CG10, and (b) MG10.

4.3.3. Molecular interaction studies

The XRD profiles of the organogels and the vegetable fats have been shown in Figure 4.7. Literature suggests that cocoa butter and mango butter exist in four to six polymorphic forms [1, 128]. The characteristic peaks (*d*-values: 3.79Å, 4.2Å) corresponding to α polymeric state were not found in the XRD profiles of the vegetable fats and their corresponding organogels [129]. Four characteristic *d*-values (3.7Å, 3.94Å, 4.58Å and 5.42Å), corresponding to the β polymorphic state of the fatty acids, were observed both in the vegetable fats and their organogels [129]. Peaks at 19.3º and 16.3º 2θ corresponded to the *d*-values of 4.58Å and 5.42Å, respectively [129-130]. These peaks were conserved in both kind of organogels. This indicated that the stable polymorphic state (β) was retained by the organogels. But their peak intensity was lowered as

compared to the peaks of pure cocoa butter and mango butter. This suggested that the number of fatty acids present in β polymorphic state might have been reduced and transformed to the other polymorphic states. The presence of peak at 2θ 23.2º (*d*-value: 3.83Å) indicated the presence of $\beta`_2$ and $\beta`_1$ polymorphic forms [129]. These peaks were retained in all the organogels and their intensity was not significantly changed. In general, $\beta`_2$ and $\beta`_1$ polymorphic states are intermediary polymorphic states during the conversion of α polymorphic fatty acids to the stable β polymorphic fatty acids [131-132]. Since wide angle X-ray scattering was performed, the peaks below 5^o 2θ were not observed. Hence, confirmation for the existence of α polymorphic state could not be estabilished. In general, tempering of the fats at high temperature leads to the polymorphic transition [133]. Keeping this in mind, organogels were prepared by melting the fats at 45 ºC, so as to minimize the tempering effects. As a result, minimal changes in the polymorphic state of the organogels were observed.

Though the position of the peaks and the *d*-value of the β polymorphic state were not significantly changed, the full width half maximum (FWHM) values of the organogels were altered (Table 4.2). The change in the FWHM values can be correlated to the change in the crystallinity of the organogels. The change in the crystallinity was determined by calculating the crystal size (D) using Debey-Scherrer equation [134].

$$D = \frac{K\lambda}{\beta \cos\theta} \qquad (4.2)$$

where, K is the Scherrer constant or shape factor, 0.89 (as shape of the crystallite is unknown); λ is the CuKα wavelength i.e., 1.54 Å; β is the full width at half maximum (FWHM) of the diffraction peak in radians and θ is the Braggs diffraction angle.

The crystal size was determined using the β polymorphic peak (19.3º 2θ), since it had the maximum intensity. The crystal size of cocoa butter was reduced with the incorporation of gelatin solution within the organogels (Table 4.2). The decrease in the crystal size can be attributed to the presence of heterogeneous system (fat and water mixture) within the organogels [135]. During crystallization, the crystal growth of cocoa butter might have been hindered by the presence of heterogeneous system [135]. This lead to the formation of smaller crystal sizes in the organogels. The changes in crystal size suggested that the crystallinity of the organogels was also changed. XRD patterns of the cocoa butter, mango butter and their corresponding organogels (hump-like structures at ~20º) suggested predominantly amorphous nature. Amorphousity of the organogels

was dependent on the proportion of the aqueous gelatin solution and liquid triacylglycerols. Change in crystal size of the fats can be correlated to the amorphousity of the gels [136]. Crystallinity of the cocoa butter and the mango butter gels was found to be in the order of cocoa butter > CG10 > CG35 and mango butter > MG10 > MG35, respectively. Higher crystallinity of the cocoa butter based organogels was due to the presence of higher amount of saturated fatty acids in cocoa butter as compared to mango butter.

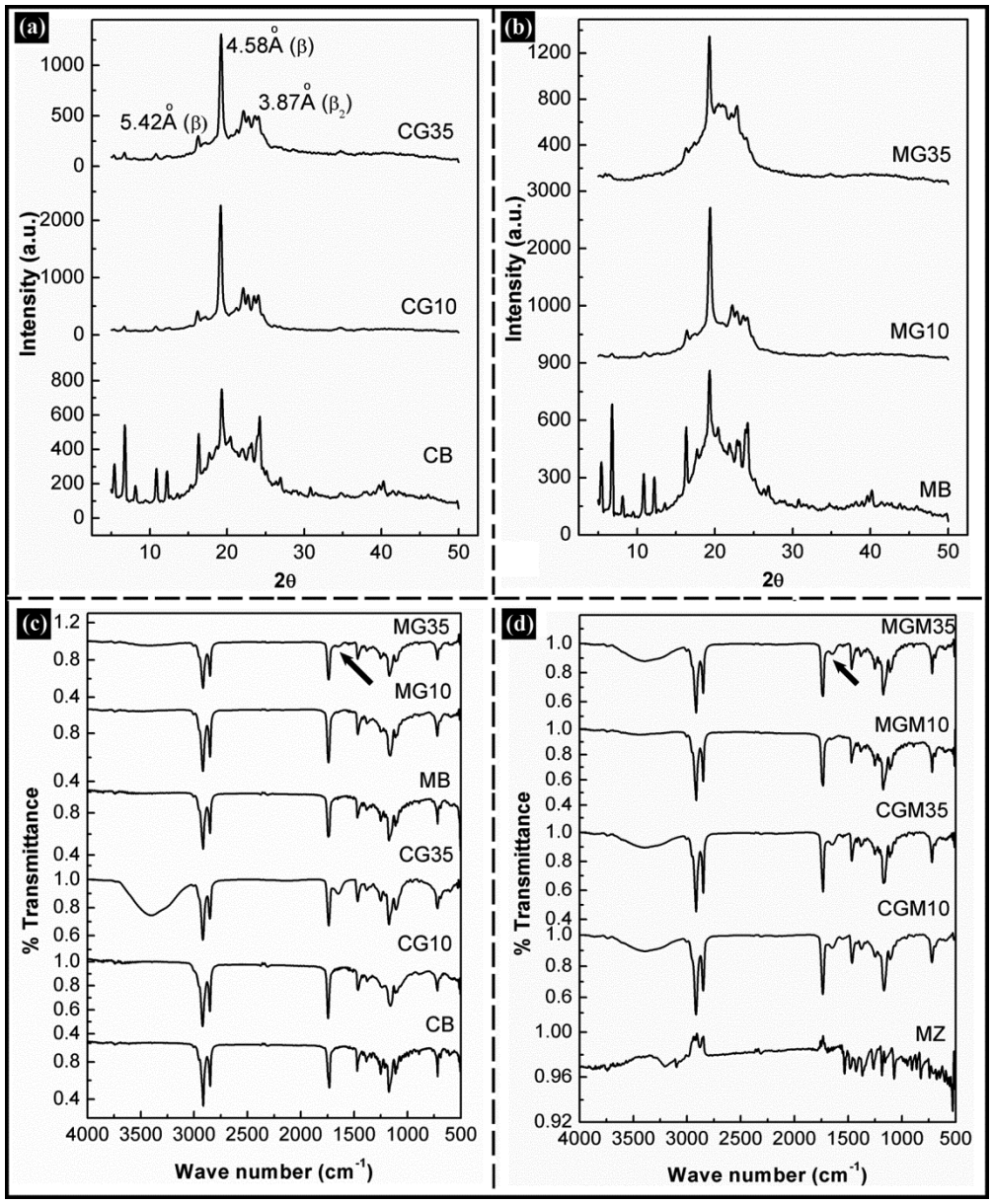

Figure 4.7: XRD profiles of: (a) cocoa butter based gels, and (b) mango butter based gels; and FTIR spectra of: (c) Gels, and (d) Gels with drug (metronidazole).

Table 4.2: XRD parameters of the cocoa butter, mango butter and organogels.

Sample	FWHM of peak at 19.3º 2θ	Crystal size (D), nm
Cocoa butter	0.14	61.11
CG10	0.22	38.9
CG35	0.25	33.68
Mango butter	0.16	53.5
MG10	0.22	38.9
MG35	0.26	32.71

Figure 4.7c and 4.7d shows the FTIR spectra of the organogels and the organogels with metronidazole, respectively. The vegetable fats and the organogels had very similar spectra with minor variations. This may be explained by the presence of similar fatty acid profile in cocoa butter and mango butter. Very strong stretching peaks of C-H or C=H bonds at ~2800 to 3000 cm^{-1}, ~725 cm^{-1} and ~1450 cm^{-1} were observed, indicating the presence of the saturated and the unsaturated fatty acyl chains (tails) of triacylglycerides [137]. The head of the triacylglyceride molecules is generally identified by ester linkages. Vibrations of O-C=O ester bond was observed at 1150 and 1750 cm^{-1} [137]. Position of these peaks was not altered with the addition of the aqueous gelatin solution. The characteristic amide (N-H) bands of gelatin at 1650 cm^{-1} and 1542 cm^{-1} was seen in CG35 and MG35 gels (indicated by arrows) [138]. These peaks were absent in pure cocoa butter and mango butter. CG10 and MG10 also did not show the N-H peaks which may be attributed to the presence of the aqueous portion at lower concentration in these formulations. The peak corresponding to O-H stretching vibration of water molecules at ~3500 cm^{-1} was stronger in CG35 and MG35 as compared to CG10 and MG10 indicating an increase in the hydrogen bonding as the proportion of the aqueous phase was increased [139]. Metronidazole spectrum was characterized by the presence of OH stretching vibrations at 3219 cm^{-1}, C=CH stretching vibrations at 3101 cm^{-1}, NO_2 and NO stretching vibrations at 1535 cm^{-1} and C-OH and C-O stretching vibrations at 1074 cm^{-1} [140]. Since metronidazole was completely dissolved in the gelatin solution, the peaks corresponding to the drug were not observed in the organogels. Absence of new peaks and shift in the peaks of the formulations indicated that there were no interactions amongst the drug and the formulation components.

4.3.4. DSC studies

Heating DSC curves showed four and five endotherms in cocoa butter and mango butter based organogels over the temperature range of 10 ºC to 40 ºC, respectively (Figure 4.8a and 4.8b). Presence of more than one endotherm indicated the existence of the fats in different polymorphic states. Pure cocoa butter and mango butter yielded a sharp endotherm at 36.7 ºC and 38.4 ºC, respectively, corresponding to the β polymorphic state [141]. The peak intensity of the β state's endotherm was decreased with the addition of aqueous phase. Simultaneously, considerable enhancement in the peak intensities of the other polymorphic forms (α and β`) was noticed. Presence of peaks at ~20 ºC indicated the existence of α polymorphic state of triacylglycerols in the organogels [141]. Next to the α-polymorphic peaks, peak corresponding to the β` polymorphism was observed. Pure fats showed a broad endotherm of β` polymorphic triacylglycerols with two overlapping endothermic peaks ($\beta`_2$ and $\beta`_1$ states) (indicated by arrows in Figure 4.8a and 4.8b) [129]. Incorporation of water showed distinct endothermic $\beta`_2$ and $\beta`_1$ polymorphic peaks in the organogels. This indicated that the presence of water might have slowed down the polymorphic transformation (from α to β) of fats. The extent of overlapping of $\beta`_2$ and $\beta`_1$ states was higher in cocoa butter based organogels, whereas, separate endotherms were noticed in mango butter based organogels. Thermal profiles of CG10 and CG35 showed overlapping endotherms of $\beta`_2$ and $\beta`_1$ (as that of cocoa butter) and an extra peak of α polymorphic state (unlike cocoa butter). On the contrary, MG10 and MG35 showed separate endotherms of α, $\beta`_2$ and $\beta`_1$ polymorphic states (unlike mango butter). The melting endotherm of β was not prominent in the organogels as compared to the pure fats. In addition to the aforementioned peaks (corresponding to α, β` and β polymorphic states), an additional peak at very low temperatures (< 15 ºC) was noticed in pure mango butter and its corresponding organogels. This peak was due to the sub- α or γ polymorphic triacylglycerols [129]. The cocoa butter based organogels did not show any such a peak. This may be explained by the merging of the endotherms of γ and α polymorphic triacylglycerols.

Since different polymorphic states were existing, the amount of fat (cocoa butter and mango butter) present in those forms was calculated as solid fat content (SFC) in the organogels [1].

$$\%SFC = \frac{\Delta H_t}{\Delta H_m} * 100 \qquad (4.3)$$

where, ΔH_t is the change in enthalpy at time t and ΔH_m is the change in enthalpy during total melting.

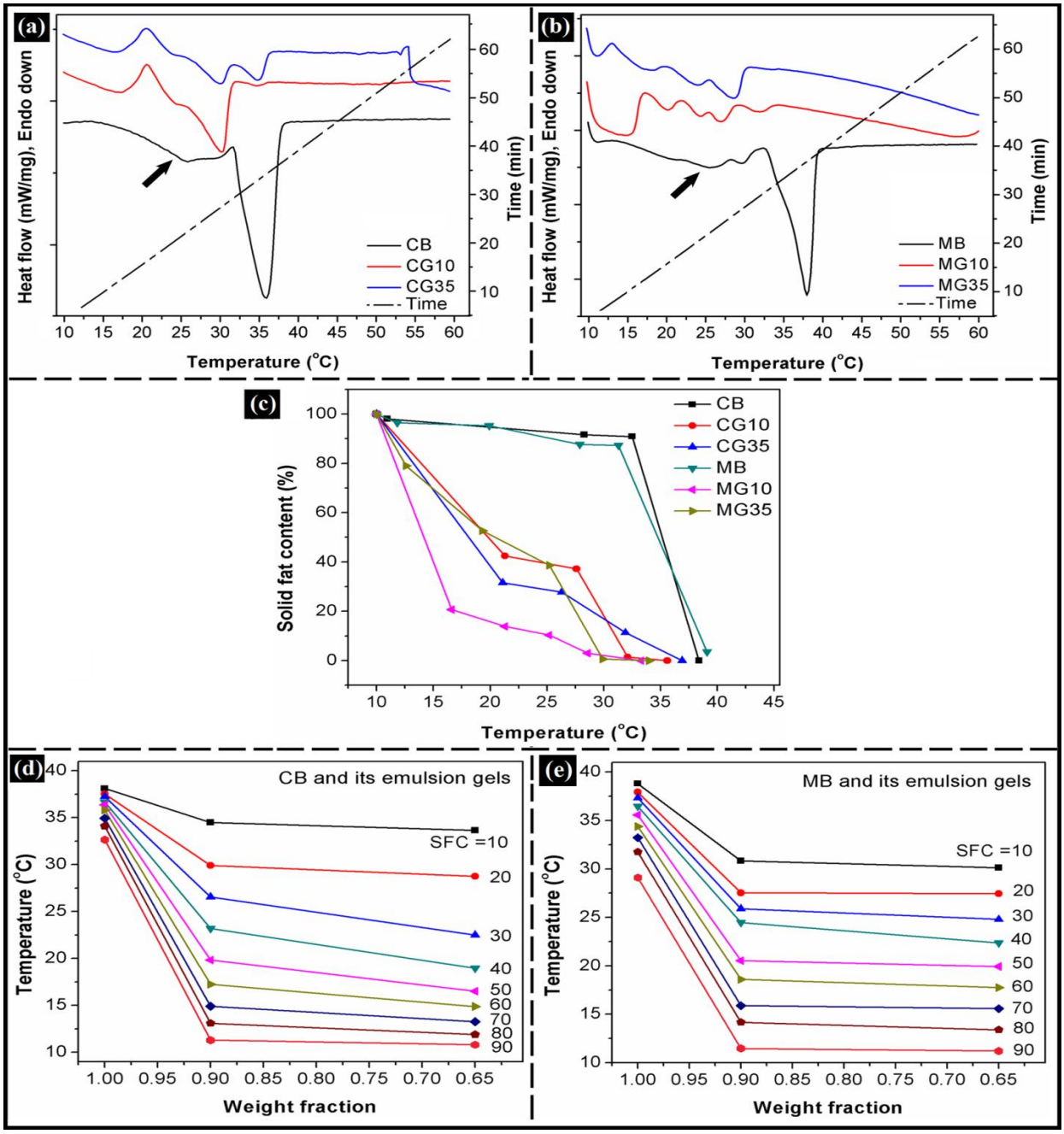

Figure 4.8: Melting endotherms of: (a) cocoa butter organogels, and (b) mango butter organogels; Isosolid diagrams of (c) cocoa butter gels, and (b) mango butter gels; and (e) SFC of the gels.

Table 4.3: Melting analysis of the cocoa butter (CB), mango butter (MB) and their gels.

Sample	**Polymorphic state**														
	A			**β`$_2$**			**β`$_1$**			**β**					
	T(ºC)	**ΔH(J/g)**	**SFC**	**T(ºC)**	**ΔH(J/g)**	**SFC**	**T(ºC)**	**ΔH(J/g)**	**SFC**	**T(ºC)**	**ΔH(J/g)**	**SFC**			
CB	10.9	1.5	2.0	26.8	4.7	6.4	30.9	0.53	0.71	36.7	66.7	90.8			
CG10	18.2	36.3	45.2	25.1	3.3	5.2	31.1	12.6	25.8	35.3	9.1	11.4			
CG35	17.3	31.8	68.4	25.2	1.8	3.8	30.8	7.6	16.4	35.6	5.3	11.3			
Sample	**Polymorphic state**														
	1 ~ sub α or γ			**2~ α**			**3 ~ β`$_2$**			**4 ~ β`$_1$**			**5 ~ β**		
	T(ºC)	**ΔH (J/g)**	**SFC**	**T (ºC)**	**ΔH (J/g)**	**SFC**	**T (ºC)**	**ΔH (J/g)**	**SFC**	**T (ºC)**	**ΔH (J/g)**	**SFC**	**T (ºC)**	**ΔH (J/g)**	**SFC**
MB	11.1	5.4	3.5	19.9	0.6	1.2	25.5	3.8	7.6	29.6	1.4	0.4	38.0	41.4	83.7
MG10	15	37.1	79.3	20.1	3.2	6.9	24.4	1.6	3.5	27.0	3.5	7.4	31.9	1.4	2.9
MG35	11.1	5.3	20.9	18.3	6.7	26.4	24.0	3.6	13.9	28.6	9.7	38.1	33.4	0.2	0.6

The change in the enthalpy during the endothermic events was calculated by integrating the area under the peak [142-143]. The peak temperatures (T) of the endotherms, change in enthalpies (ΔH) and SFC associated with the corresponding endotherms (polymorphic states) have been tabulated in Table 4.3. SFC of the β polymorphic state was higher in pure cocoa butter and mango butter, whereas, SFC of the α and β` polymorphic states was increased in the organogels. Figure 4.8c shows the SFC profiles of the organogels at different temperatures. Melting points of α and β` polymorphic states of mango butter were found to be lower than cocoa butter whereas, melting point of the β polymorphic state was found to be higher than cocoa butter. This suggested that the pure mango butter was softer than cocoa butter at low temperatures but retained more number of solids at higher temperatures. This was due to the presence of the higher oleic acid content which might have a "dilution effect" on the saturated fatty acids thereby increasing the softness of mango butter [1]. On the other hand, mango butter contains longer chain fatty acids such as behenic and lignoceric acids. These fatty acids contributed to the induction of the stable β polymorphic state, which resulted in the higher melting point of mango butter.

SFC content of cocoa butter and mango butter was drastically decreased when water was added. There was no significant difference in the rate of decrease in SFC of CG10 and CG35, but it was significant in MG10 and MG35. MG35 lost almost ~80 % of the SFC below 15 °C. This may be the reason that mango butter could not form stable organogels beyond 35 % (w/w) aqueous phase. This indicated that the organogels became softer than the pure fats and their thermal stability was greatly influenced. To measure the compatibility of the emulsion gel components and their effects on the gel softening, isosolid diagrams were drawn (Figure 4.8d and 4.8e).

In general, isosolid diagrams links the points of different samples with equal solid content in weight fraction-temperature graphs. As a matter of fact, if the isosolid lines are parallel and approximately horizontal to each other, then the components are said to be compatible to each other [1]. Isosolid diagrams suggested that the mango butter organogels were softer than the cocoa butter organogels. This may be explained by the lower melting points of the mango butter organogels than the cocoa butter organogels at the equal SFC. Sudden decrease in the melting points of the isosolid lines was observed when 10 % (w/w) of gelatin solution was added to either cocoa butter or mango butter. The decrease in the melting temperature indicated softening of the organogels. The results suggested that the softening effect was more pronounced when 10 % (w/w) aqueous phase was added to cocoa butter and mango butter.

Upon further addition of aqueous phase (35 % w/w), no significant softening effect was observed which resulted in almost parallel lines. The isosolid lines of the mango butter organogels were more parallel to each other than the cocoa butter organogels. This indicated that the softening was continuing in cocoa butter organogels but a plateau phase was reached in mango butter organogels. Since the isosolid lines were not horizontal and parallel to each other up to the 90 % solid fraction, the gel components (butter and gelatin solution) seemed to be not compatible with each other. But the compatibility was improved when the aqueous portion was raised to 35 % (w/w). 100 % compatibility amongst the fat (cocoa butter and mango butter) and aqueous phase cannot be expected due to the thermodynamic instability amongst them. But the compatibility of the fat and the aqueous phase was improved when higher amount of gelatin (20 % w/w) solution was added. Comparatively, the components of the mango butter organogels were more compatible than the cocoa butter organogels. This can be explained by the fact that the isosolid lines were more parallel and horizontal to each other in mango butter organogels. This may be due to the presence of the higher amount of unsaturated fatty acids in mango butter. Disordered packing of unsaturated fatty acids might have allowed the incorporation of the aqueous phase in the organogels and subsequent improvement of the compatibility of the fat and the aqueous phases.

Crystallization studies

Isothermal crystallization studies of the organogels were performed by holding them at 60 ºC for 10 min (to eliminate the crystal memory of the fats) and subsequently cooled to 10 ºC at 1 ºC/min, followed by holding at 10 ºC for 1 h. The crystallization exotherms of cocoa butter and mango butter organogels can be divided into three exothermal events (Figure 4.9a and 4.9b). The first exotherm (~19 ºC) was not distinctly separated but exist as a shoulder peak of the second exotherm at ~22.5 ºC. The intensity of the shoulder peak was reduced when water was added to the fats. The third exotherm was recorded during the isothermal stage that spans over a wide time range. These kind of exothermic events were similar to the fat mixtures of cocoa butter [141, 143]. Crystallization of the fats started at 22.5 ºC and continued up to 10 ºC leading to a broad exotherm. Evolution of this kind of exotherm is a characteristic feature of hexagonal packing of triacylglycerol chains in α form [141]. Literature suggests that the progressive crystallization of triacylglycerides arrange themselves from liquid crystalline to double-chain length (2L) organization in α form [141]. The first exothermic peak (shoulder peak) corresponded to the crystallization of the high-melting saturated fatty acids [141]. The second (major) exothermic event was due to the transformation of monounsaturated fatty

acids [141]. During crystallization, a steep increase of the second exotherm at 15.4 ºC and 15.1 ºC was noticed in cocoa butter and mango butter organogels, respectively. Based on these events, it can be inferred that the saturated fatty acids acted like seed crystals for the transformation of the liquid crystalline fat. Since the crystal growth of the saturated fatty acids was coinciding with the transformation of the unsaturataed fatty acids, the first exotherm in DSC thermogram existed as the shoulder peak. The transformation of the fatty acids continued even during the isothermal stage. Crystallization at 10 ºC suggested the transformation of the liquid crystalline fatty acids into α polymorphic state [129]. Since the crystallization at 10 ºC resulted in a broad exotherm, it was expected that some of the α polymorphic fatty acids might have converted to β` polymorphic state (found in DSC melting and XRD profiles as well) [129, 141]. Overall, the peak positions did not change, but the enthalpies associated with the exotherms of organogels were changed due to the difference in the peak intensities. The overall crystallization enthalpies of the pure fats and the organogels have been provided in Table 4.4. Based on the difference in crystallization enthalpies, Avrami equation (equation 4) was used to predict the nucleation and crystal growth in organogels [142].

$$\ln\left[\ln\left(1/1-X_t\right)\right] = \ln k + n\ln t \qquad (4.4)$$

where, X is the fraction of the crystals formed at time t during crystallization, k is the crystallization rate constant (measure of crystallization) which depends on the crystallization temperature and n is the Avrami exponent. Avrami exponent determines the dimensionality of crystallization. Crystal fraction (X) at a given time was calculated by the ratio of partial enthalpy (ΔH_x) to the total crystallization enthalpy (ΔH_c).

Figures 9c and 9d indicate that the crystal formation was very rapid during the early stages of the crystallization. Subsequently, the rate of formation was slowed and ultimately reached a stationary phase. The shape of the curves (X vs. *time*) illustrates the crystallization mechanism of the substance [144]. The shape of the curves did not change, indicating that the crystallization mechanism was not affected by the incorporation of the aqueous phase [144]. To better understand the crystallization mechanism, the crystal fraction (X) was used to calculate the Avrami parameters (n and k). Crystallization data of the organogels showed good fitting ($R^2 > 0.95$) to the Avrami equation (Figure 4.9e and 4.9f). The Avrami parameters calculated from the fit curves have been given in Table 4.4. n values were found to be in the range of 0.9 to 1.5. This suggested the occurrence of instantaneous nucleation during the crystallization process [129]. n values below 2 suggest that the nucleation rate was very rapid at the beginning, but decreased as the time progressed (as predicted by X vs. *time* curves) [142]. n values indicated needle-like growth of the crystals along one or two dimensions.

Formation of the spherulitic crystals were reported by the growth of the small needle like crystals during suspension crystallization with agitation [145]. Since static crystallization (no agitation) was studied in DSC, needle-like crystals might have not aggregated to spherulites.

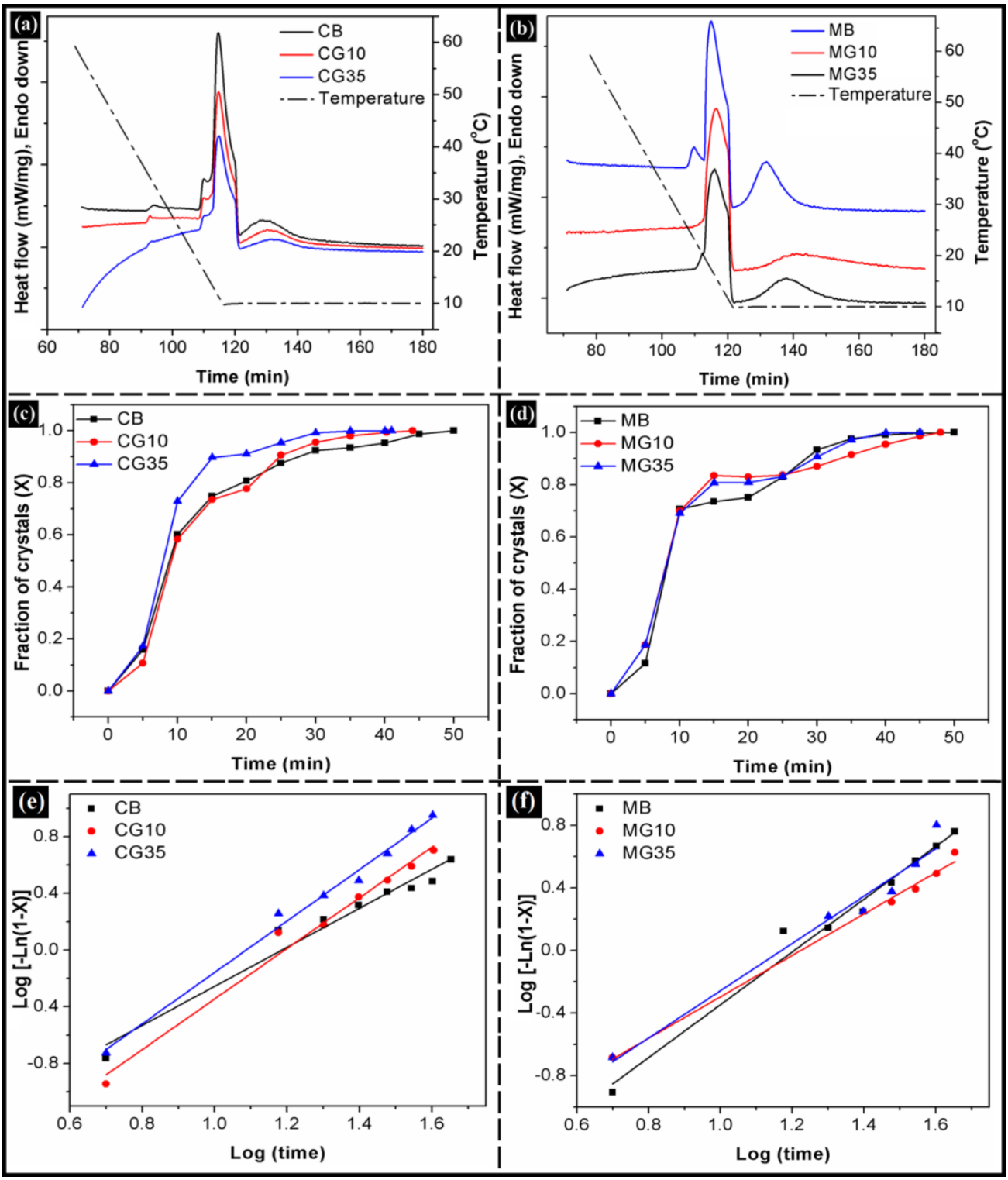

Figure 4.9: Crystallization exotherms of: (a) cocoa butter gels, and (b) mango butter gels; Crystal fraction of (c) cocoa butter gels, and (d) mango butter gels; and Avrami analysis of (e) cocoa butter gels, and (f) mango butter gels.

Table 4.4: Avrami analysis of the DSC exotherms.

Sample	ΔH_c(J/g)	n	k X 10^{-3} (min)	$t_{1/2}$ (min)
Cocoa butter	2.28	0.94	103.0	7.56
CG10	1.55	1.26	42.7	9.10
CG35	0.96	1.63	19.5	8.88
Mango butter	1.94	1.05	82.0	7.65
MG10	1.41	1.32	24.1	12.68
MG35	0.94	1.45	17.1	12.85

On the other hand, high *k* values (Table 4.4) suggested rapid crystallization in cocoa butter, followed by mango butter and the organogels, respectively. Rate of crystallization was influenced by the presence of water. CG10 and MG10 were having higher rate of crystallization as compared to CG35 and MG35, respectively. Presence of aqueous phase might have prevented the growth of the crystals in quick time. Increase in the crystallization time might also have lead to the change in dimensionality of the growing crystals [142]. Hence, *n* values suggested the possibility of two dimensional growth of the crystals. Change in the crystallization times was determined by calculating the half-time of the crystallization ($t_{1/2}$). Since *k* is dependent on nucleation, crystal growth and temperature, it can be directly related to the half-time of crystallization ($t_{1/2}$).

$$\left(t_{1/2}\right)^n = 0.693/k \qquad (4.5)$$

$t_{1/2}$ is a function of both *n* and *k*. It provides information about the time taken to form 50 % of the crystals. The $t_{1/2}$ values were lower in pure fats as compared to the organogels (Table 4.4). This indicated that the rate of crystallization was highest in cocoa butter and mango butter followed by CG10, CG35, MG10 and MG35 under the experimental conditions. As the rate of fat crystallization was slower in organogels with higher water proportions, water droplets coalescence has lead to the formation of unstable organogels. Higher crystallization rates in cocoa butter organogels facilitated the cocoa butter to tolerate high amounts of water. Since rate of crystallization was slower in mango butter organogels, the water droplets might have coalesced prior to the fat crystallization. Hence, stable cocoa butter organogels were formed even at high proportion of water (70 % (w/w)) as compared to the mango butter organogels (35 % (w/w)).

4.3.5. Mechanical analysis

During the cyclic uni-axial compression test, fracturing of pure cocoa butter and mango butter (shown by an arrow in Figure 4.10a and 4.10b) indicated the brittle nature of the pure fats. Fracture points were also seen during the second cycle of compression in the pure fats. Organogels, except CG10, did not show fracture points. This indicated a decrease in the brittleness with the addition of the aqueous phase. Higher brittleness can be attributed to the higher cohesive strength of the pure fats (Table 4.5). The triacylglycerols in pure fats are tightly packed either in double or triple chain length structures [146]. This kind of orientation favors ordered arrangement of the triacylglycerols and imparts higher cohesive strength [146]. Presence of aqueous phase might have disturbed the orientation of the triacylglycerols which resulted in the decrease in the cohesiveness, hardness and gumminess of the organogels (Table 4.5). This indicated that the organogels became softer with the incorporation of the aqueous phase (as predicted during melting studies). Increase in the softness might have enhanced the adhesive nature and spreadability of the organogels. Interestingly, adhesiveness of the cocoa butter and mango butter organogels was enhanced when lower amount of aqueous phase was added but a reverse trend was observed when higher amount of aqueous phase was added. Presence of gelatin in the aqueous phase might be responsible for the enhancement in the adhesive nature of the organogels but at higher amounts of gelatin, the intermolecular attraction (cohesive interactions) between the gelatin molecules might have dominated the adhesive forces [147]. Increase in the spreadable nature of the organogels was confirmed by spreadability studies (Figure 4.10c and 4.10d). Application of force during spreadability test did not result in the syneresis of water. Since the water droplets were physically locked within the fat continuous phase (evident from the microscopic studies), syneresis did not occur, which in turn, imparted physical stability to the organogels. CG35 and MG35 showed higher spreadability than CG10, MG10 followed by cocoa butter and mango butter. Increase in the softness may be associated with the spreadability of the organogels. During cyclic compression studies, springiness of the organogels did not vary significantly. This indicated that the elastic nature of the pure fats was not altered in the organogels. To confirm this and to critically evaluate the viscoelastic properties of the organogels, stress relaxation studies were conducted.

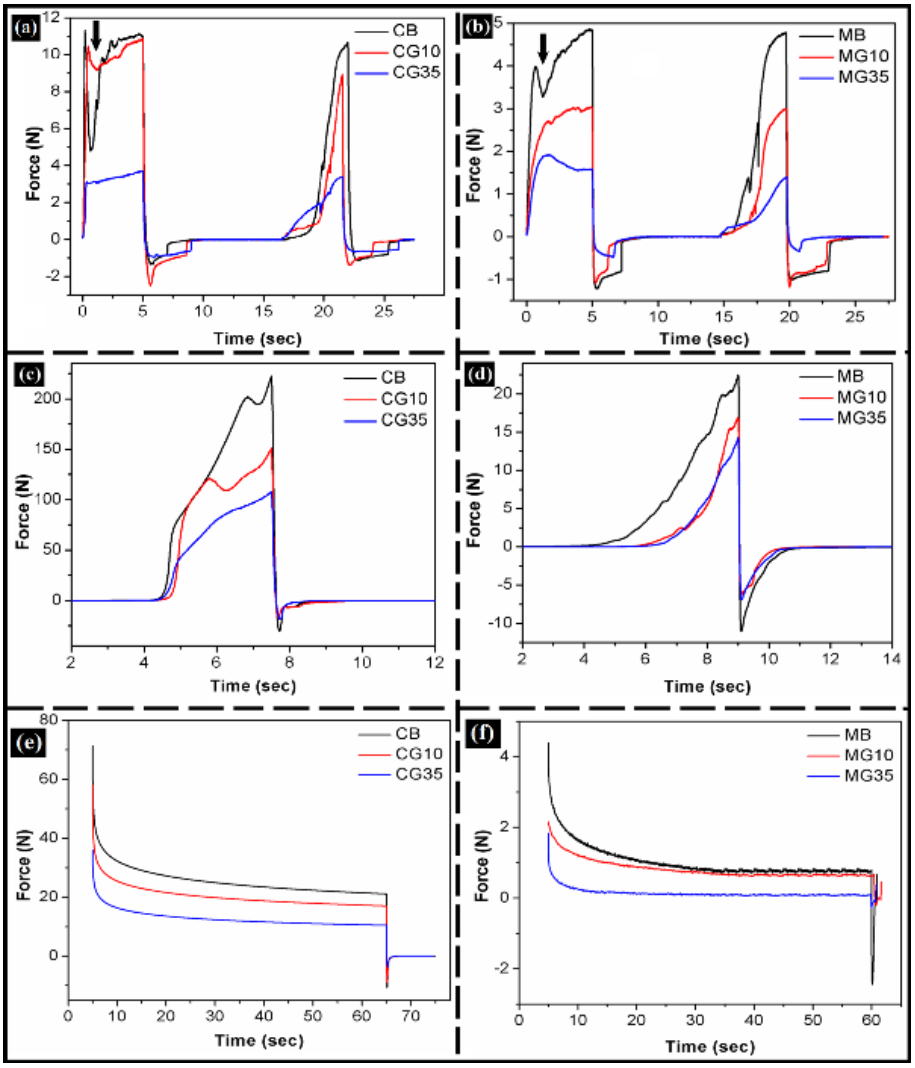

Figure 4.10: Compression cycle of: (a) CB and (b) MB-based gels; Spreadability of: (c) CB and (d) MB-based gels; and Stress relaxation of: (e) CB and (f) MB-based gels.

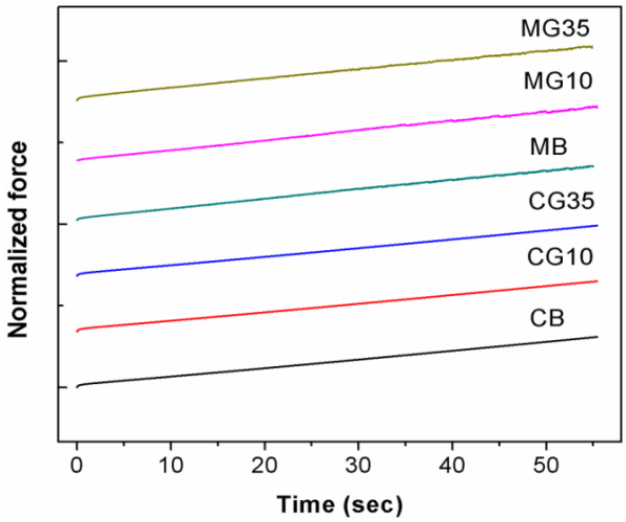

Figure 4.11: Normalized force vs. time (modified Peleg's analysis).

Table 4.5: Mechanical properties of CB, MB and organogels.

Sample	Hardness (N)	Cohesiveness	Adhesiveness (N.sec)	Springiness	Gumminess (N)	Spreadability $(N.sec)^{-1}$
CB	11.33	0.42	1.99	1.00	4.79	0.23
CG10	10.87	0.23	4.44	1.00	2.56	0.31
CG35	3.72	0.13	2.99	1.01	2.0	0.44
MB	4.87	0.57	2.17	1.00	2.76	2.51
MG10	3.04	0.47	2.21	1.00	1.43	5.78
MG35	1.92	0.37	0.74	1.00	0.71	6.44

The stress relaxation profiles of the organogels have been shown in Figure 4.10e and 4.10f. The firmness (F_0) and the residual force (F_r) were higher in cocoa butter and mango butter as compared to the organogels. F_0 and F_r decreased with the increase in the aqueous phase. This was due to the decrease in the SFC of the organogels. The stress relaxation profiles of the organogels followed an exponential decay function. The force decay with respect to time (F(t)) during the relaxation of the organogels was analyzed by fitting the data in modified Peleg's equation [148].

$$\frac{(F_0 - F(t))t}{F_0} = k_1 + k_2 t \qquad (4.6)$$

where, F_0 is the maximum force attained after loading; k_1 and k_2 represent the initial rate and extent of the relaxation, respectively.

Normalized stress relaxation data from modified Peleg's equation yielded a straight line with good fitting ($R^2 > 0.995$) (Figure 4.11). Curve analysis indicated that the initial rate of relaxation (k_1) was decreased with the increase in the proportion of the aqueous phase but the extent of relaxation (k_2) did not vary significantly in both kind of organogels (Table 4.6). Though k_2 (slope) represents the total relaxation behavior of the formulations, almost similar values were obtained. To find the viscoelastic nature and to know the stress relaxation behavior, asymptotic residual force was calculated from the stress relaxation curve (F^*) [149].

$$F^* = \frac{F_r}{F_0} \qquad (4.7)$$

Where, F_r is the residual force after relaxation and F_0 is the maximum force attained prior to the relaxation.

For viscoelastic materials, F^* lies in the range of 0.0 to 1.0. 'F^*' value close to 1.0 indicates that the material is an elastic material. There was a reduction in the F^* values with the decrease in the SFC of the organogels. This indicated that the elastic nature of the cocoa butter and mango butter decreased with the increase in the aqueous phase. Cocoa butter and mango butter organogels have shown F^* values in the range of 0 to 1, suggesting that the developed organogels were viscoelastic in nature. % relaxation was calculated using equation 8.

$$\%\ relaxation = \left(\frac{F_0 - F_r}{F_0} \right) * 100 \qquad (4.8)$$

Mango butter organogels showed more relaxation more than cocoa butter organogels (Table 4.6). Since mango butter organogels were amorphous than the cocoa butter organogels (as per XRD studies), relaxation of the mango butter organogels was more than the cocoa butter organogels.

Table 4.6: Textural parameters of the gels from stress relaxation studies after modified Peleg's analysis.

Samples	**F_0 (N)**	**F_r (N)**	**k_1**	**k_2**	**F^***	**% relaxation**
CB	71.37	21.09	0.036	0.001	0.29	78.45
CG10	58.17	15.03	0.031	0.016	0.26	74.16
CG35	35.98	8.42	0.015	0.001	0.24	76.60
MB	4.39	0.74	0.041	0.017	0.17	95.17
MG10	2.15	0.26	0.013	0.017	0.12	87.74
MG35	1.85	0.08	0.005	0.017	0.04	93.60

4.3.6. *In vitro* drug delivery studies

In vitro drug delivery studies were carried out in phosphate buffer (pH 7.2) (Figure 4.12a). The release of the drug was higher from MGM35 (52.78 %) followed by CGM35 (23.24 %), CGM10 (18.34 %) and MGM10 (10.83 %), respectively. Organogels with higher aqueous phase showed higher drug release than the others. The results suggested that the mango butter organogels released more drug than the cocoa butter organogels of similar composition. This may be due to the amorphous nature of the mango butter organogels compared to the cocoa butter organogels (predicted by XRD studies). Presence of higher amount of liquid triacylglycerols in mango butter organogels might have contributed to the higher release of

the drug. To understand the drug release kinetcis, the drug release data was fit in different drug release kinetics models (Figure 4.13). The best fit model was found to be Weibull model (Table 4.7). This indicated that the developed formulations were homogeneous planar matrix type delivery vehicles [150]. The ‘n’ value (Fickian value) was calculated from the Korsemeyer-Peppas (KP) model. The ‘n’ values indicated that the release of the drugs was diffusion mediated. The diffusion of the drug from the cocoa butter organogels followed non-Fickian diffusion while it was Fickian diffusion from the mango butter organogels (Table 4.7).

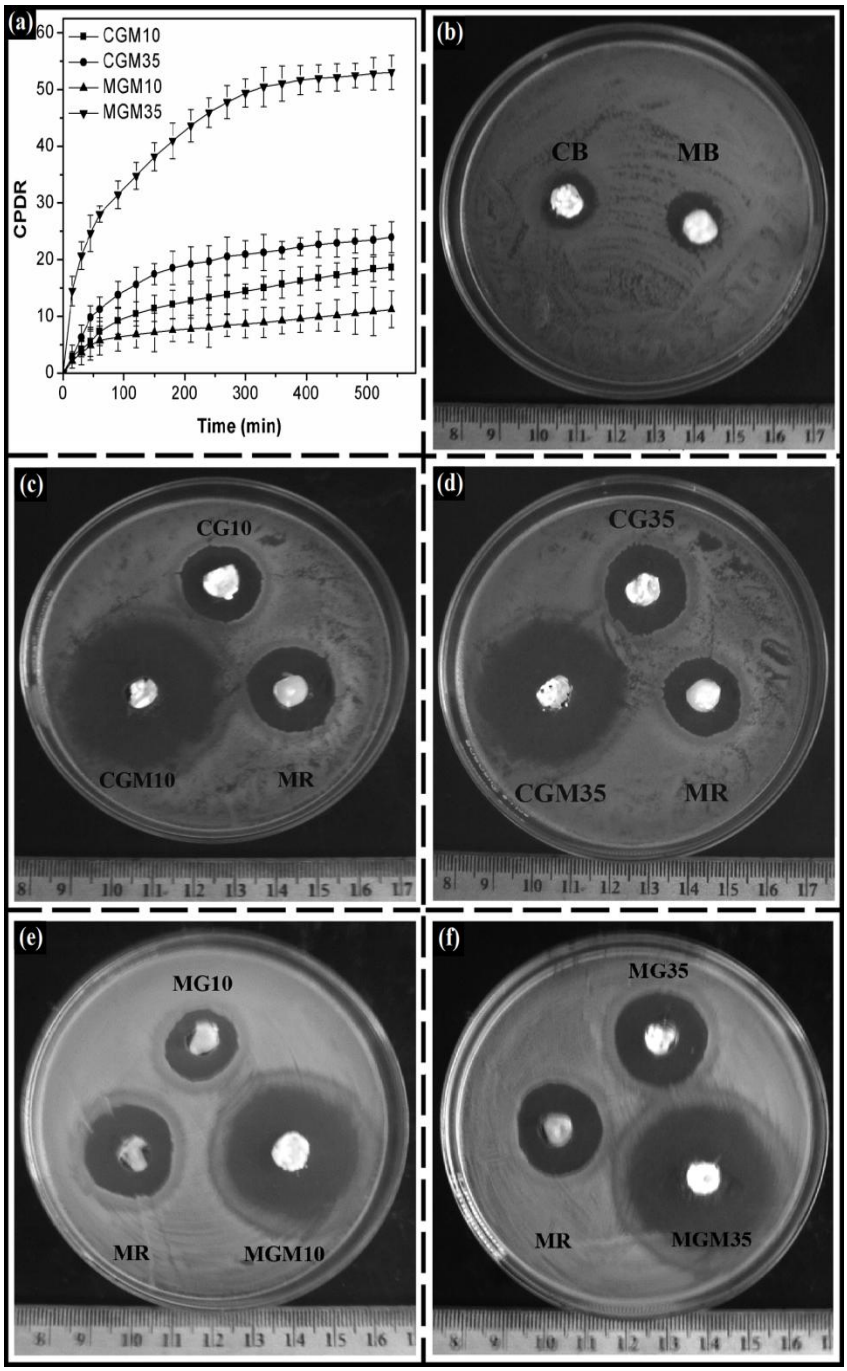

Figure 4.12: Drug release from the gels: (a) CPDR vs. time; (b-f) antimicrobial activity of the gels against *E. coli*.

Table 4.7: The drug release kinetics of the gels

Samples	Zero order (R^2)	Higuchi (R^2)	Weibull (R^2)	Best fit	KP model	
					n	Type of flow
CGM10	0.617	0.985	0.983	Weibull	0.50	Non-Fickian
CGM35	0.363	0.922	0.950	Weibull	0.51	Non-Fickian
MGM10	0.262	0.913	0.951	Weibull	0.39	Fickian
MGM35	0.405	0.89	0.988	Weibull	0.36	Fickian

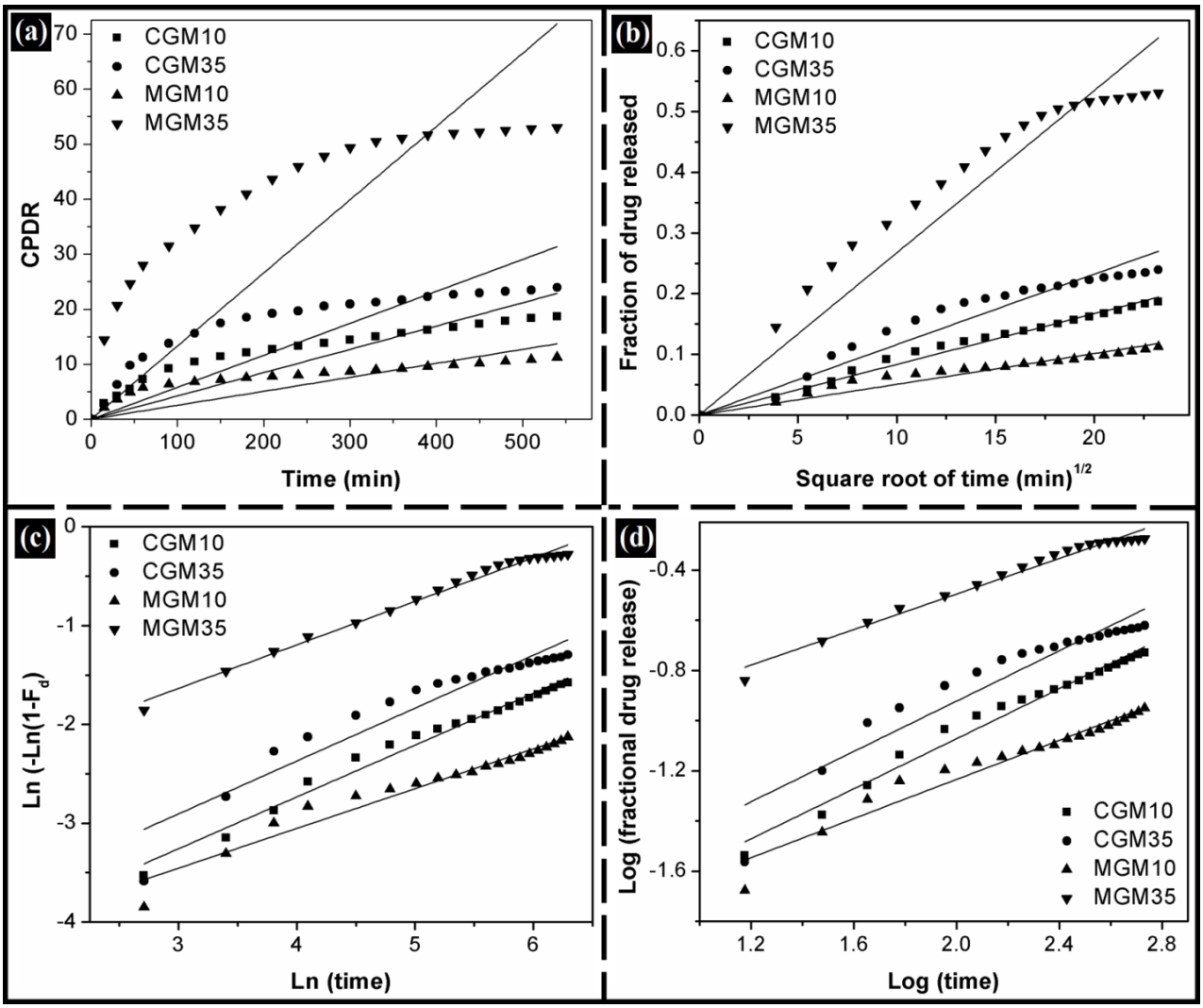

Figure 4.13: Drug release kinetics from the organogels: (a) Zero order, (b) Higuchi model, (c) Weibull model, and (d) KP model.

Pure cocoa butter and mango butter have shown antimicrobial activity against *E. coli* (Figure 4.12b). Polyphenols present in cocoa butter and mango butter were responsible for the antimicrobial action [118]. Metronidazole loaded formulations showed very good antimicrobial activity. This might be associated with the synergistic activity of the polyphenols and the drug. The antimicrobial activity of the cocoa butter and mango butter organogels were much higher than Metrogyl® (Figure 4.12d and 4.12e). Difference in the antimicrobial activity of the cocoa butter and mango butter organogels against Metrogyl® was found to be statistically significant ($p < 0.05$). The differences in the antimicrobial action of the cocoa butter and mango butter organogels were statistically insignificant ($p > 0.05$).

4.4. Conclusion

In conclusion, stable gelatin-based cocoa butter and mango butter organogels were formed by a simple hot emulsification method. Cocoa butter incorporated high amounts of aqueous fraction (70 % (w/w)) as compared to mango butter (35 % (w/w)). The water droplets were dispersed within the fat continuous matrix. Presence of fat around the water droplets imparted physical stability to the organogels (evident from the spreadability studies). Since water droplets were locked within the crystallized fats, microbial contamination can be arrested. Avrami analysis indicated that the rate of fat crystallization was higher in cocoa butter and it was decreasing with the increase in water proportion. High fat crystallization rate in cocoa butter might be responsible for the high tolerance capacity of the water as compared to mango butter. X-ray diffractograms indicated the fats present in the organogels were having stable β polymorphic state even after tempering. Effect of tempering was lowered as the organogels were prepared by melting the fats at lower temperature (45 ºC). DSC results suggested that the organogels showed high percentage of SFC as β polymorphic form and intermediary polymorphic forms ($\beta`_1$ and $\beta`_2$). As the intermediary polymorphic forms possess the melting point at ~ 30 ºC, the organogels may have high chances of consumer acceptance if employed in the preparation of chocolates and/or other confectionaries. Increase in softness and spreading nature of the organogels with respect to the pure fats also will favor the consumer acceptance. Mango butter organogels are found to be softer than the cocoa butter organogels, which may be due to the presence of high amounts of liquid-like unsaturated fatty acids. Based on the observations, it can be suggested that the mango butter organogels can be used as cocoa butter equivalents in food and pharmaceutical industries.

Part B: Encapsulation of cocoa butter and mango butter organogels in alginate microparticles

Overview:

Cocoa butter and mango butter based gels with 35 % (w/w) aqueous portion were chosen for the encapsulation studies. The organogels were encapsulated within the alginate microparticles by ionotropic gelation method. Palm oil containing alginate microparticles were synthesized for the comparative studies, because, palm oil has been regarded as one of the cocoa butter equivalents. Microscopy, XRD and DSC studies confirmed that both kinds of the organogels (CG35 and MG35) were successfully encapsulated within the microparticles. Confocal micrographs showed the presence of alginate layer around the liquid palm oil droplets and semi-solid organogels. Leaching of palm oil was noticed when the microparticles were incubated at room-temperature for 2 h. Leaching of palm oil resulted in the lower DEE (model drug: metronidazole). In case of fat containing microparticles, presence of organogels improved the DEE by preventing the leaching of the drug. Biocompatibility studies suggested that the developed microparticles were cytocompatible in nature when tested against mammalian L929 fibroblast cells. The organogel containing microparticles showed better mucoadhesivity against goat small intestine as compared to palm oil containing microparticles. *In vitro* drug release studies showed super case-II mode of drug delivery from the formulations and showed good antimicrobial activity when tested against *E. coli*.

4.5. Introduction

In general, biopolymeric microparticles are porous in nature which lead to the leaching of the encapsulated bioactive agents [151-152]. Over the years, this problem was tried to overcome using blended polymers [152]. Additionally, the problem of leaching was negotiated by loading higher amount of drugs within the microparticles [153]. Unfortunately, in many cases higher drug loading results in severe complications *viz.*, drug toxicity and drug resistance [154]. In the recent times, another approach, i.e. core-shell type of microparticles, has been employed to overcome the problems. This allowed an improvement in the drug carrying capacity of the microparticles [155]. This approach seems to have solved the problem associated with the enhancement of the drug encapsulation efficiency. But, difficulty in the diffusion of the drugs from the solid shell is another concern associated with the core-shell microparticles. In general, core-shell microparticles are being synthesized using synthetic polymers or composite polymers [155]. The synthetic polymers remain in the body even after the completion of the task [156]. The use of biopolymers for the synthesis of the core-shell microparticles may solve the problem. Unfortunately, the leaching of the internal phase from the biopolymeric microparticles had prevented the use of the biopolymers for the synthesis of core-shell microparticles. In this study, we are proposing an alternative approach to solve the problem by encapsulating vegetable fat based organogels.

Alginate was chosen as the biopolymeric shell material. Alginate has been reported to form porous microparticles [105]. Often, the problem of leaching of the internal phase is overcome by coating the microparticles with polymers (eg. chitosan and gelatin) [100, 152]. Over the years, cocoa butter has been used as topical and transdermal bases in gels, ointments and suppositories. The use of cocoa butter in oral delivery of bioactive agents is very limited. Keeping this in mind, we intended to explore the use of cocoa butter organogels in oral delivery applications. Mango butter formulations were also prepared to use as the cocoa butter equivalent. Amongst the stable cocoa butter and mango butter organogels, organogels with 35 % (w/w) gelatin solution (CG35 and MG35) were chosen for the encapsulation studies. As per the literature, palm oil has been used as cocoa butter equivalent because of its high saturated fatty acid content. Palm oil based microparticles were used as the control [117].

4.6. Materials and methods

4.6.1. Preparation of the organogels

Composition of the cocoa butter and the mango butter based organogels has been given in Table 4.8. Organogels were prepared as per the protocol mentioned in chapter 3.2.1.

Table 4.8: Composition of the organogels.

Sample	Cocoa butter (% w/w)	Mango butter (% w/w)	Gelatin solution (% w/w)	Tween 80 (% w/w)	Metronidazole (% w/w)
CG	64.0	--	35.0	1.0	--
MG	--	64.0	35.0	1.0	--
CGD	63.0	--	35.0	1.0	1.0
MGD	--	63.0	35.0	1.0	1.0

4.6.2. Preparation and characterization of the microparticles.

Accurately weighed 5 g of the gels or palm oil were used to prepare the primary emulsions and they were subsequently processed to synthesize the microparticles by ionotropic elation method as explained in chapter 3.2.5. Experimental details for the characterization of the microparticles have been explained in chapter 3.3. Bright field microscopy, confocal microscopy, XRD, FTIR, DSC, leaching, biocompatiblitbility, mucoadhesivity, *in vitro* drug delivery and antimicrobial studies were conducted during the study.

4.7. Results and discussion.

4.7.1. Preparation of the organogels.

Stable organogels were formed and are shown in Figure 4.14. Mechanism of the formation of organogels was explained in part A of this chapter.

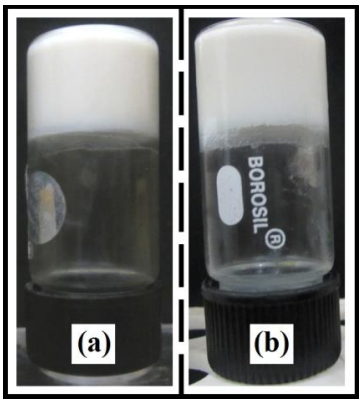

Figure 4.14: Pictographs of the organogels: (a) CG and (b) MG.

4.7.2. Preparation of the microparticles

Addition of the primary emulsion to the bulk sunflower oil (external oil phase) (300 rpm and 4 ^{o}C) resulted in the formation of internal phase-in-water-in-oil type multiple emulsion. Addition of the acidified oil resulted in the gelation of the alginate layer to form microparticles. Under acidic conditions, the calcium ions replaced the monovalent sodium ions and ionically cross-linked the carboxyl groups of the guluronic monomers (of sodium alginate). Cross-linking of the alginate layer resulted in the encapsulation of the internal phase. The stability of the microparticles was improved by treating the microparticles with 0.5 M calcium chloride solution. Sunflower oil was washed from the surface of the microparticles with excess water containing 1 % (w/w) Tween 80. Thereafter, the microparticles were collected by filtration and subsequently stored at 4 ºC. Stable microparticles were also formed when the drug containing organogels and palm oil were used. The compositions of the microparticles have been tabulated in Table 4.9.

Table 4.9: Composition of the microparticles.

Sample	Internal phase
MPO	Palm oil
MCG	CG
MMG	MG
MPOD	Palm oil with drug*
MCGD	CGD
MMGD	MGD

*1% (w/w) metronidazole

4.7.2. Microscopy

The bright field micrographs of MCG and MMG were found to be spherical in shape, whereas, MPO showed the presence of both spherical and oval shaped microparticles (Figure 4.15a-c). Formation of oval shaped microparticles may be explained by the presence of liquid palm oil (internal phase) in MPO. Since MCG and MMG encapsulated the semi-solid organogels, sphericity was retained and resulted in the formation of large sized microparticles. Size distribution analysis of the microparticles (Figure 4.16a) indicated that the average diameter of the microparticles was in the order of MCG (295.95 ± 8.2 µm) > MMG (292.70 ± 6.6 µm) > MPO (266.82 ± 10.6 µm). The differences in the sizes of the microparticles can be attributed to their internal compositions. The diameter of the 50 % population of the microparticles was determined from the cumulative percentage frequency

plot (Figure 4.16b). Results suggested that the diameter of the 50 % of the microparticles was nearly equal to the average diameter of the microparticles. Formation of core and shell type of microparticles was evaluated by confocal laser scanning microscopy. The confocal images showed the presence of black alginate layer around the internal phase of the microparticles (Figure 4.15d-f) (indicated by arrow) Confocal images confirmed the formation of core and shell type of hybrid microparticles. The confocal images also showed the presence of the oil droplets within MPO and uniformly dispersed internal phase within MCG and MMG. This confirmed the presence of semi-solid organogels within the microparticles.

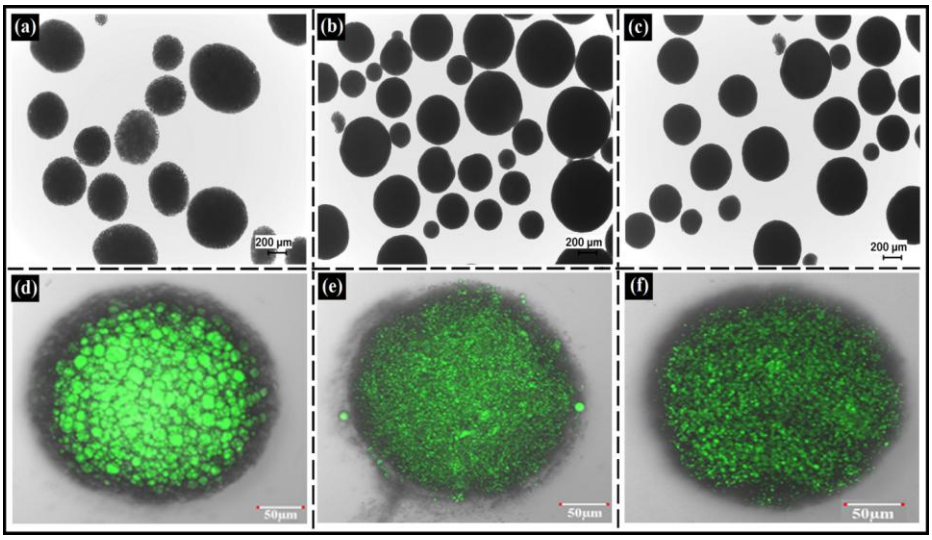

Figure 4.15: BFM images of: (a) MPO, (b) MCG, and (c) MMG; CLSM images of (d) MPO, (e) MCG, and (f) MMG.

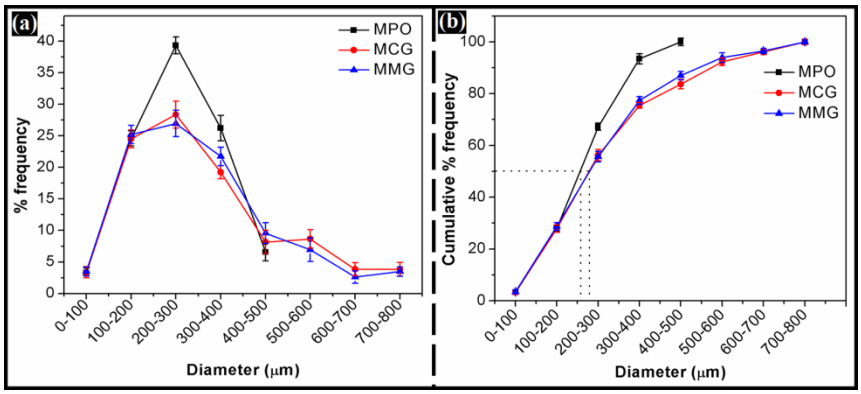

Figure 4.16: Size distribution analysis of the microparticles: (a) % frequency, and (b) cumulative % frequency.

4.7.3. XRD studies

The X-ray diffraction profiles of the organogels and the prepared microparticles have been shown in Figure 4.17a. MCG and MMG showed the peaks corresponding to cocoa butter and

mango butter (shown as dotted lines in Figure 4.17a), suggesting the existence of organogels within the microparticles. The *d*-spacings of the peaks of the fats did not vary even after encapsulation within the microparticles. This suggested that the polymorphic structure of the fats did not change during the preparation of the microparticles. The microparticles retained the stable β polymorphic state and the intermediary polymorphic state (β_2) of the fats. Results indicated that the presence of the stable β polymorphic fats in MCG and MMG. The crystal size of the fats within the microparticles was checked by Debey-Sherrer equation (equation 2 in part A of chapter 3).

The peak corresponding to the β polymorphic state was chosen for the determination of the crystal size. The crystallite sizes of the cocoa butter and the mango butter were found to be higher in MCG and MMG as compared to CG and MG, respectively (Table 4.10). This suggested that the microparticle processing conditions have altered the crystallite sizes of the fats.

Table 4.10: XRD parameters of microparticles and organogels.

Sample	**FWHM* of peak at ~19.3º 2θ**	**Crystallite size (nm)**
CG	0.25	33.68
MG	0.26	32.72
MCG	0.23	35.65
MMG	0.23	35.60

The peaks of the fats were superposed over a broad peak (~ 20º 2θ) in MCG and MMG. On the other hand, MPO showed only one broad peak with a peak maximum at ~ 20º 2θ. Presence of triacylglyerols within the microparticles resulted in the formation of broad peaks [157]. This is an indication of the predominant amorphous nature of the microparticles. MPO seemed to be more amorphous as compared to MCG and MMG (showed crystalline peaks of the vegetable fats).

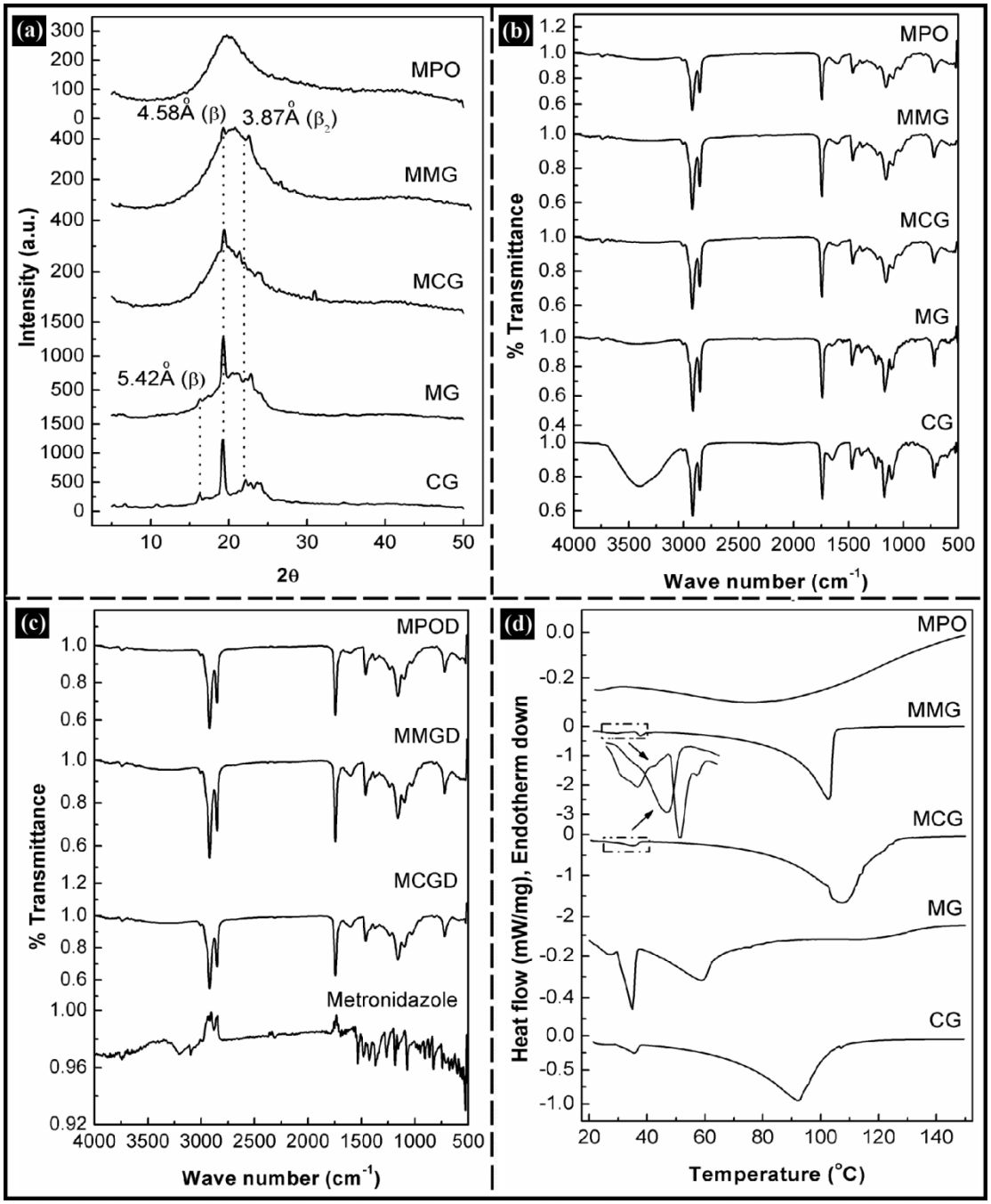

Figure 4.17: a) X-ray diffractograms of organogels and microparticles; FTIR spectra of: (b) the organogels and microparticles; (c) drug and drug containing microparticles; and (d) DSC thermograms of the organogels and the microparticles.

4.7.4. FTIR studies

Figure 4.17b and 4.17c shows the FTIR spectra of the microparticles and metronidazole loaded microparticles. All the microparticles showed the characteristic peaks associated with the alginate molecules as per the reported literature [158]. The characteristic peaks of alginate were observed due to the $–COO^-$ and C-O-H stretching vibrations. The peaks at 1620 $cm^{-1}$and

1410 cm^{-1} correspond to the $–COO^-$ stretching vibrations. Peak at 3450 cm^{-1} was due to the O-H stretching vibrations of secondary and tertiary alcohols. Presence of secondary and tertiary alcohols was confirmed by the presence of C-OH stretching vibrations at 1110 cm^{-1} and 1150 cm^{-1}, respectively [158]. Since palm oil, cocoa butter and mango butter possess similar kind of saturated and unsaturated fatty acids in their composition, microparticles and organogels showed the characteristic peaks of triacylglycerols/fatty acyl molecules. Microparticles showed strong stretching peaks of C-H or C=H bonds at ~2800 cm^{-1} and 1450 cm^{-1} [137]. These peaks correspond to the fatty acyl chains (tails) of the triglycerides. Pure metronidazole showed the characteristic peaks at 3219 cm^{-1} (OH stretching vibrations), 3101 cm^{-1} (C=CH stretching vibrations), 1535 cm^{-1} (NO_2 and NO stretching vibrations) and 1074 cm^{-1} (C-OH and C-O stretching vibrations) [140]. Since metronidazole was present at very low concentration, the peaks associated with the drug molecules were not observed. Though the peaks corresponding to the drug were not detected, absence of new peaks and shift in the peaks indicated that the drug did not chemically interacted with the components of the microparticles [12].

4.7.5. Thermal studies

Figure 4.17d shows the thermograms of the organogels and the microparticles. CG and MG showed an endothermic peak at ~37 ºC, indicating the melting of the cocoa butter and the mango butter, respectively. In addition to the endothermic peak of the fats, CG and MG also showed peaks at ~91 ºC and ~62 ºC, respectively. These peaks correspond to the evaporation of the water molecules associated with the organogels. The melting peaks of fat in MCG and MMG are associated with shoulder peaks at lower temperatures (showed as an insert in Figure 4.17d). Presence of these endothermic peaks indicated the presence of unstable α and/or β` polymorphic state(s) of cocoa butter and mango butter in MCG and MMG [129]. Presence of unstable polymorphic states of cocoa butter and mango butter was also observed in XRD studies. Apart from the peaks at ~37 ºC, MCG and MMG showed another peak at ~110 ºC. This may be due to the evaporation of water associated with the organogels or alginate layer of the microparticles. Since 100 % evaporation of the water is not possible from the alginate microparticles, endothermic peak was seen [159]. This confirmed that the organogels were present within the microparticles. MPO showed only one broad endothermic band. The peak was due to the evaporation of the water molecules associated with the alginate layer.

4.7.6. Leaching studies

MPO showed leaching of palm oil but MCG and MMG did not show leaching of the internal phase (Figure 4.18a-c). Leaching of the palm oil was identified by the formation of a dark oily zone around MPO after the incubation (Figure 4.18a). Presence of semi-solid organogels within MCG and MMG might have prevented the leaching of the internal phase. Absence of leaching can also be correlated to the increase in the viscosity of the internal phase of MCG and MMG. The increased viscosity might have prevented the leaching of the internal phase from MCG and MMG. The leaching of the internal phase was quantified (Figure 4.18d). % leaching was found to be very high in MPO as compared to MCG and MMG ($p < 0.05$). Swelling power of the microparticles was higher in MCG and MMG as compared to MPO but the difference was not significant ($p > 0.05$) (Figure 4.18d).

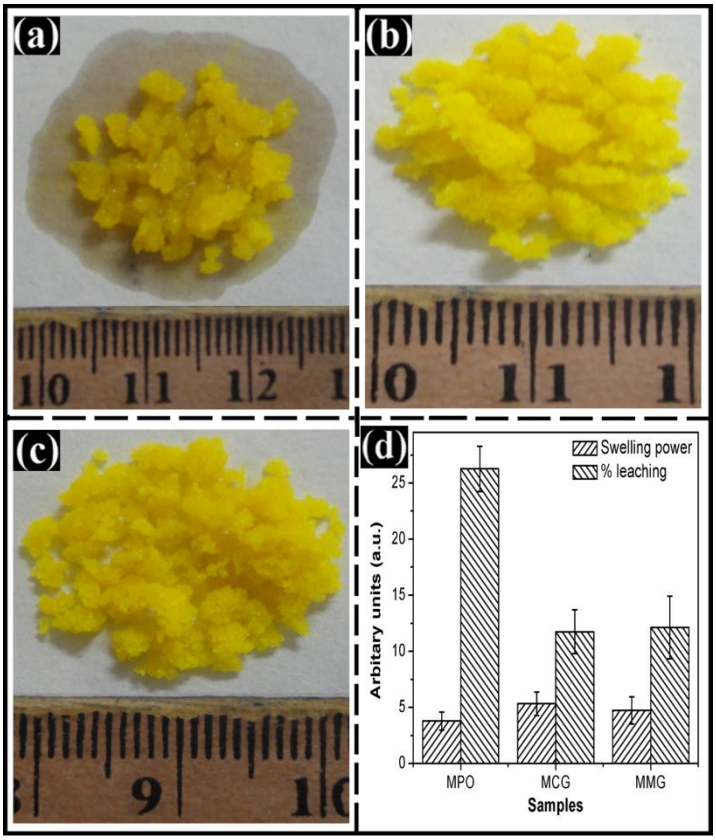

Figure: 4.18: Leaching studies: (a) MPO, (b) MCG, and (c) MMG, and (d) Bar graphs showing the swelling power and % leaching of the microparticles.

4.7.7. Drug encapsulation efficiency

MCGD (71.3 ± 2.1) and MMGD (70.2 ± 1.6) showed higher % DEE as compared to MPOD (44.3 ± 3.4). The results indicated that the % DEE of MCGD and MMGD was nearly twice that of MPOD. The difference in % DEE was due to the leaching of the internal phase from

MPOD. As a result, lower % DEE was observed in MPOD. The results indicated that the gelling of the internal phase enhanced the drug carrying capacity of the microparticles.

4.7.8. Biocompatibility studies

Fibroblast cells (L929 cell line) showed good growth in the presence of the microparticles leachate (Figure 4.19a). The difference in cell viability index of the microparticles against the control (cell growth in the absence of leachate) was insignificant ($p > 0.05$). The results suggested that the microparticles are cytocompatible in nature.

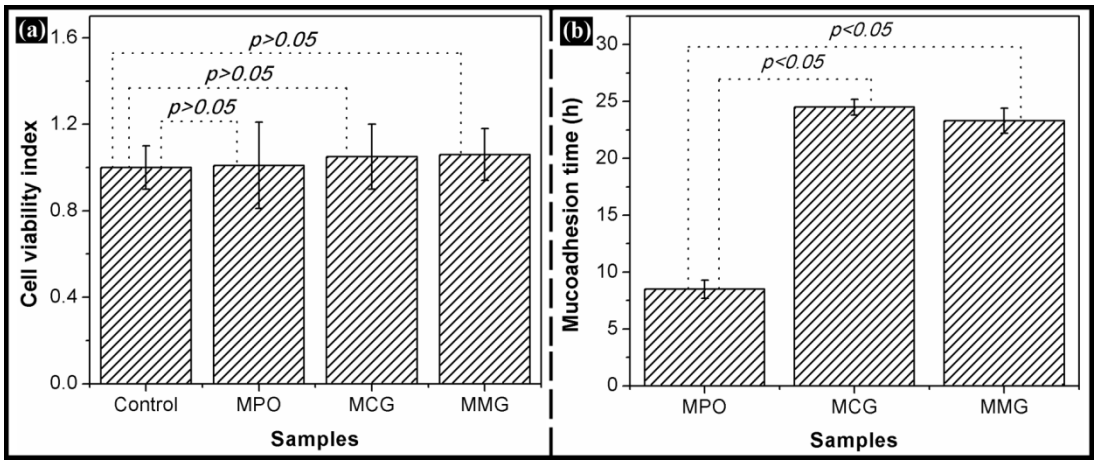

Figure 4.19: (a) Biocompatibility studies, and (b) Mucoadhesion times of the microparticles.

4.7.9. Mucoadhesivity studies

The mucoadhesive properties of the microparticles were evaluated using small intestine of goat by wash-off method. The mucoadhesion times were in the order of MCG > MMG >> MPO (Figure 4.19b). The difference in the mucoadhesion times of the microparticles was significant amongst MPO, MCG and MMG. In general, alginate shows good mucoadhesion via non-specific and non-covalent interactions *viz.,* electrostatic interactions, hydrogen and hydrophobic bonding [160]. The leaching of the palm oil might have hindered the mucoadhesive property of MPO. Absence of leaching in MCG and MMG improved mucoadhesion. Observation of higher mucoadhesion times may facilitate the use of MCG and MMG for sustained drug release applications.

4.7.10. *In vitro* drug delivery studies

The cumulative percentage drug release (CPDR) profiles of the drug containing microparticles have been shown in Figure 4.20a. MPOD showed higher CPDR as compared to MCGD and MMGD. Higher CPDR in MPO was due to the leaching of the palm oil. On the other hand, presence of semi-solid organogels prevented the free movement of the drug

molecules from the microparticles into the dissolution medium. To better understand the drug release phenomenon, the drug release profiles of the microparticles were fitted in different drug release kinetic models.

Microparticles showed good fit against zero order and Baker's Lonsdale (BL) models (Table 4.11) (Figure 4.21). Zero order release kinetics suggested that the drug release was independent of the drug concentration [161]. BL model suggested that the drug release was from non-disintegrating spherical formulations [150, 161]. The mechanism of drug diffusion was predicted using Korsmeyer-Peppas (KP) model. The Fickian constant (n-value) was found to be > 0.89. This indicated that the diffusion of the drug was via anomalous or super case-II diffusion [150].

The drug release from the microparticles was further evaluated by performing antimicrobial studies against *E. coli*. The drug containing microparticles showed a clear zone of inhibition. The blank microparticles did not show any zone of inhibition (Figure 4.20b-d). This indicated that metronidazole inhibited the growth of the *E. coli*. The difference in zone of inhibition was insignificant amongst the microparticles ($p < 0.05$). The antimicrobial studies suggested that the drug was released in its active state from the microparticles.

Table 4.11: The drug release kinetics from the microparticles.

Samples	**Zero order (R^2)**	**Higuchi (R^2)**	**BL model**	**Best fit**	**KP model**	
			(R^2)		**n**	**Type of flow**
MPOD	0.96	0.83	0.98	Zero order	0.90	Super case-II
MCGD	0.97	0.93	0.95	Zero order	1.26	Super case-II
MMGD	0.98	0.86	0.95	Zero order	1.02	Super case-II

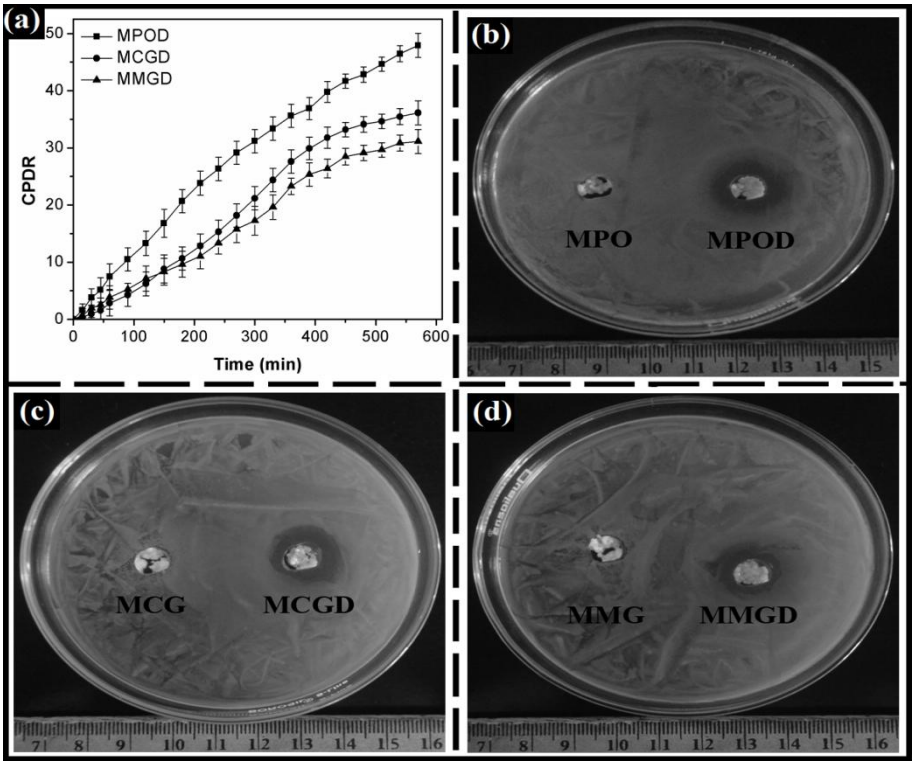

Figure 4.20: (a) CPDR vs. time, and (b-d) Antimicrobial studies of the microparticles.

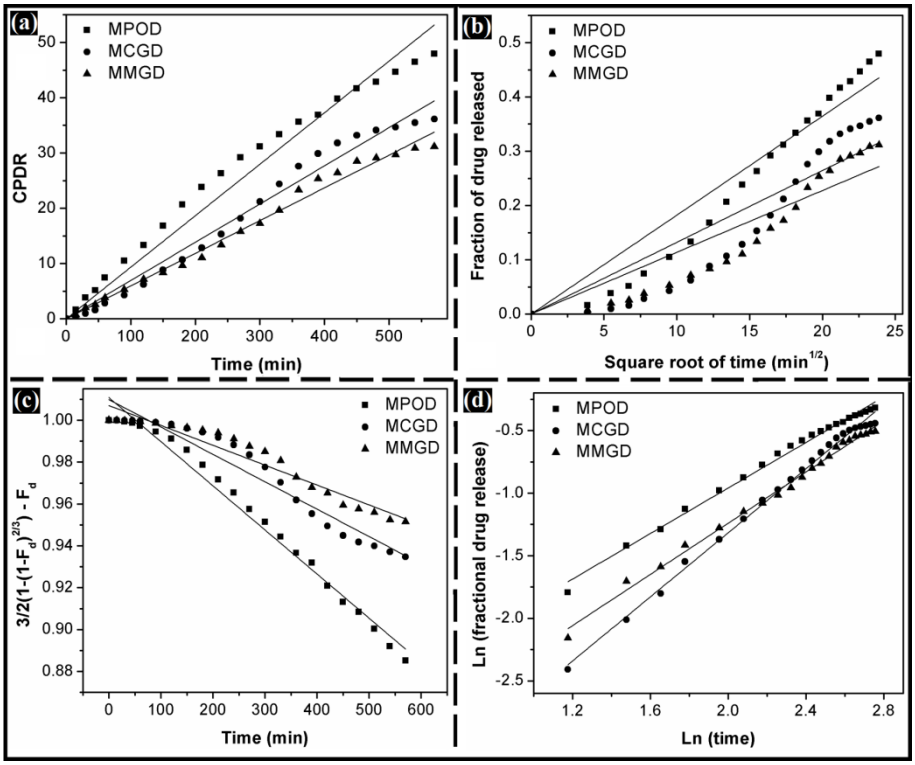

Figure 4.21: Drug release kinetics: (a) Zero order; (b) Higuchi model; (c) BL model and (d) KP model.

4.8. Conclusion

In this study, core (cocoa butter organogels and its equivalents) and shell (alginate) microparticles were successfully synthesized using internal gelation method. Presence of organogels and palm oil as the core materials of the microparticles were critically evaluated by microscopic techniques, X-ray diffraction and differential scanning calorimetric methods. Palm oil containing microparticles showed leaching of the internal phase making them unsuitable for the controlled delivery applications. Mango butter formulations proved that they can be used as alternatives for the cocoa butter formulations. The cocoa butter and mango butter containing microparticles showed similar drug encapsulation, CPDR and antimicrobial properties. Based on the results, it can be concluded that the microparticles with mango butter organogels can be used as equivalents or alternatives to the microparticles with cocoa butter organogels. The developed vegetable fat based formulations may be used as carriers for the oral delivery of nutraceutical and pharmaceutical bioactive agents.

Chapter 5

Encapsulation of lanolin based organogels in alginate microparticles

Abstract

Stable semi-solid lanolin-based organogels were prepared using hot-emulsification method. The gels were formed when the lanolin: water proportions were maintained at 2:1, 1:1 and 1:2 (w/w). The gels were characterized by microscopy, XRD, FTIR, DSC and viscosity studies. Non-Fickian mode of drug release was identified from the planar gel matrices. Stable microparticles were formed when organogel with lanolin:water proportion was-2:1. Blank microparticles and microparticles with lanolin were served as the controls. Microparticles with lanolin and lanolin based organogel did not leach out any internal components. XRD, DSC studies confirmed the encapsulation of organogels within microparticles. Encapsulation of organogels improved the DEE of (metronidazole was used as the model drug). Formulations showed good biocompatibility and antimicrobial action against L929 fibroblast cells and *E. coli*, respectively.

Graphical abstract

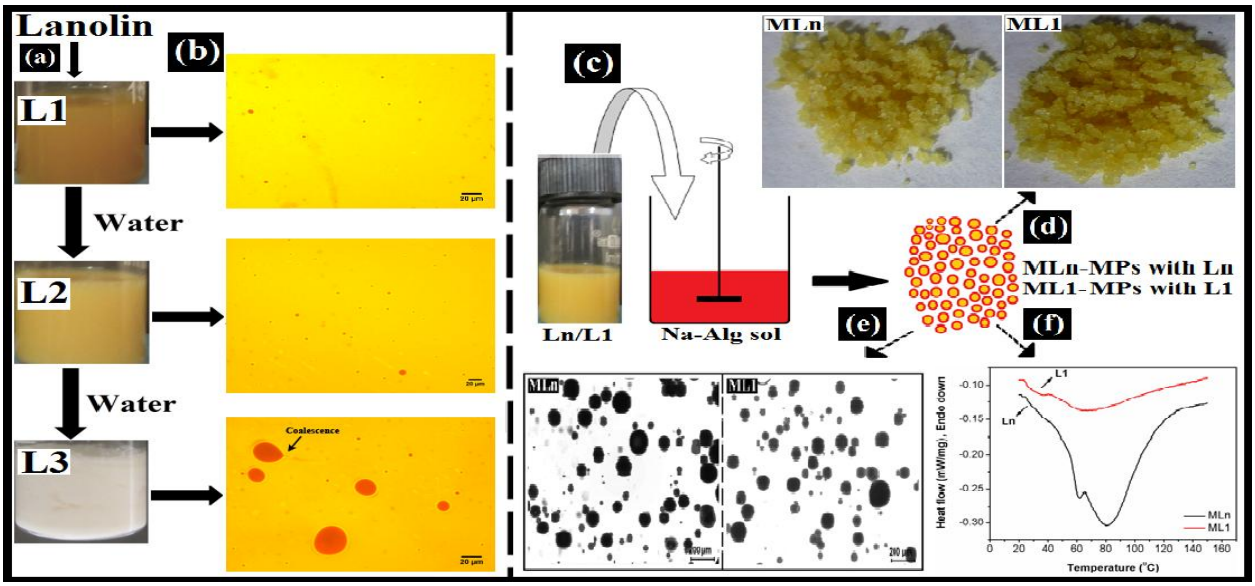

Part A: Preparation and characterization of lanolin-based organogels

Overview

Lanolin-based organogels were prepared by hot emulsification method. Stable semi-solid organogels were formed when the lanolin:water proportions were maintained at 2:1, 1:1 and 1:2 (w/w). Bright-field, phase contrast and fluorescent micrographs showed the circular water droplets (red color) in the formulations. Coalescence of water droplets was observed in gels containing higher proportion of water. XRD studies suggested an increase in amorphousness of the gels with the incorporation of water into the gel structure. The gels showed non-Newtonian and thixotropic flow behavior. The melting temperatures of the gels were identified by DSC thermal analysis. DSC thermograms indicated an increase in thermal stability with the increase of water content in the gels. Metronidazole (model drug) was released from matrix kind of formulations by non-Fickian mode of diffusion with good antimicrobial efficacy against *E. coli*.

5.1. Introduction

Lanolin (Ln) is an animal wax, devoid of glycerides, which is secreted from the sebaceous glands of sheep and other animals [162]. Lanolin coats the hair present on the body of the animals. anolin mainly consists of mono-, di- and poly- hydroxyesters of sterols (e.g. cholesterol, dihydrocholesteol), trimethyl sterols (lanosterol and dihydrolanosterol), triterpene alcohols, aliphatic alcohols (C_{14}-C_{37}) and free hydrocarbons [163]. The biocompatibility of lanolin has been attributed to its similar chemical nature as that of human sebum [164]. The significant difference between the refined anolin and human sebum is that the former is completely devoid of triglycerides and free fatty acids [164]. The increase in permeability of the bioactive agents through skin in the presence of lanolin has also been related to the similar chemical properties of lanolin as that of human sebum. It has found extensive applications in the formulation of moisturizers [165], cosmetics [166], sunscreen lotions [166], shaving creams [166-167] and emollient products due to its ability to incorporate large amount of water into its structure. Various pharmaceutical products meant for the topical, transdermal, subcutaneous and ophthalmic deliveries of drugs have employed anolin due to its inherent biocompatibility and water-holding capacity. The water-holding capacity of lanolin helps formulating emulsion-based formulations having improved stability [168]. Chemical composition of lanolin shows 33 different hydroxy and polyhydroxy esters of alcohols (sterols) and 36 free fattyacids which can act as organogelators to form organogels when polar phase was added [169-170]. In recent past, it was shown that nanoemulsions derived from the lanolin carries potential drug delivery properties [171]. Taking inspiration from the above, it seems quite feasible to develop lanolin-based semi-solid topical and transdermal formulations. Within this framework, the objective of the current study deals with the development of lanolin-based emulsion gels and characterizing them to check their suitability to be used as matrices for drug delivery.

5.2. Experimental section

5.2.1. Preparation of organogels

Organogels were prepared as per the protocol given in 3.2.2. The composition of the formulations has been shown in Table 5.1. Characterization of the gels (bright field microscopy, fluorescent microscopy, XRD, FTIR, DSC, viscosity studies, mechanical studies and *in vitro* drug release studies) was carried out as per the methods described in chapter 3.3.

Table 5.1: Composition of the formulations.

Formulation	Weight (% w/w)			
	Lanolin	**Water**	**Span 80**	**Metronidazole**
L1	65.66	33.33	1.0	--
LD1	65.66	33.33	1.0	1.0
L2	50.0	49.0	1.0	--
LD2	50.0	49.0	1.0	1.0
L3	33.33	65.66	1.0	--
LD3	33.33	65.66	1.0	1.0

5.3. Results and discussion

5.3.1. Preparation of the organogels

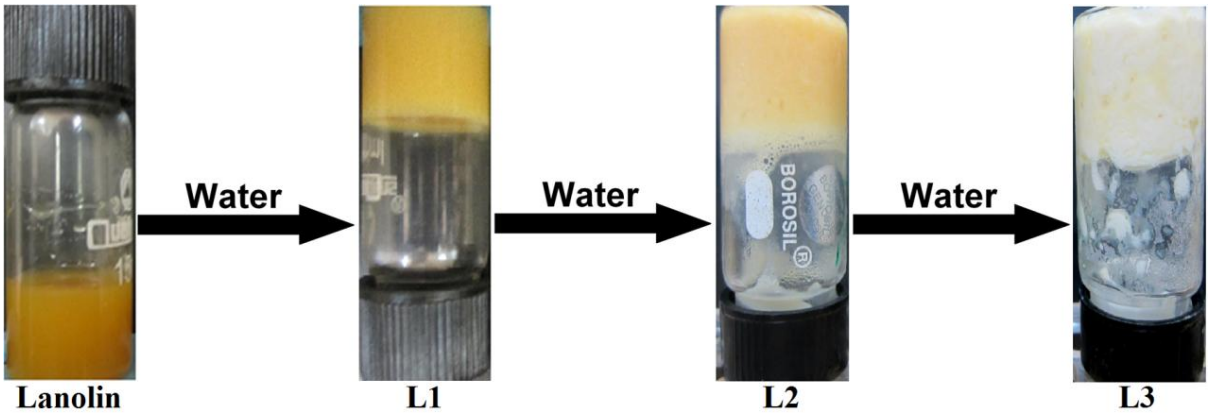

Figure 5.1: Conversion of Lanolin to emulsified gel.

Homogenization of lanolin and water resulted in the formation of white colored emulsion. The emulsion, so obtained, turned into pale yellow colored gels upon cooling to room-temperature (RT). Stable semi-solid emulsion gels were formed when the Lanolin:water proportions were 1:0.5, 1:1 and 1:2 (w/w) (Figure 5.1). As the proportion of water was increased further, the formulations were found to leach water. This may be attributed to the water holding capacity of the lanolin, which can absorb water only twice its original weight [168]. The metronidazole loaded samples were regarded as LD1, LD2 and LD3 respectively. Since the aqueous layer formed the internal phase and lanolin formed a continuous phase, the developed gels may be regarded as organogels. The prepared formulations were stable for 12+ months and stored at room-temperature.

5.3.2. Microscopic studies

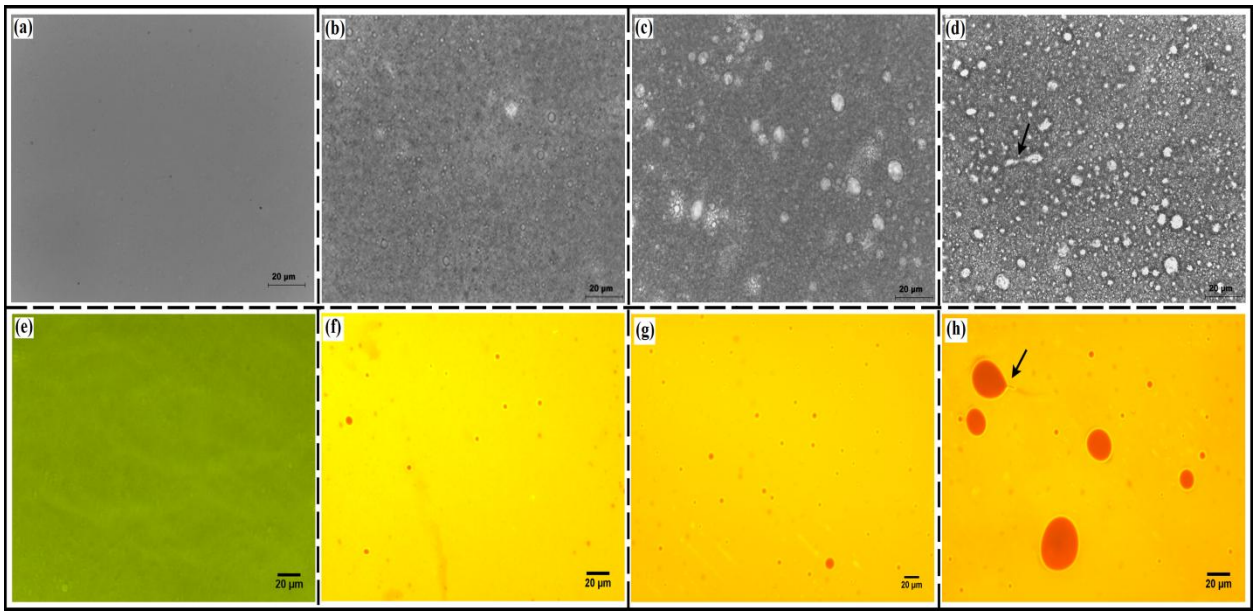

Figure 5.2: Bright field micrographs of: (a) Lanolin, (b) L1, (c) L2, and (d) L3 (Size bar: 20 µm); and fluorescent micrographs of: (e) Lanolin, (f) L1, (g) L2, and (h) L3.

Figure 5.2a-d shows the bright-field light microscopic images of the lanolin and the formulations. The micrographs of the lanolin did not show any visible microstructure indicating that the composition of lanolin was homogenous. As water was incorporated, the micrographs showed a uniform distribution of circular water droplets within the continuous phase of lanolin. The size of water droplets increased with the increase in the proportion of water in the gels. Similar variation in sizes and distribution of water droplets was observed by fluorescent microscope (Figure 5.2d-g). The aqueous phase (containing rhodamine) appeared as red colored droplets in the lanolin continuum phase. The L3 micrographs showed the tendency of the water droplets to undergo coalescence as the proportion of the water was increased in the gels. The coalesced water droplets try to separate out from the continuum phase, if the water proportion increases further [172]. This phenomenon may be attributed to the phase separation as the Lanolin:water ratio was increased above 1:2 (w/w).

5.3.3. XRD studies

Figure 5.3a shows the XRD diffractograms of Lanolin and the organogels. Broad humps in the diffractograms may be attributed to the presence of isotropic liquids present within the physical structure of the formulations [173]. XRD pattern did not show any sharp diffraction peaks suggesting that the gels are amorphous or ultrafine crystalline materials where the diffraction peaks cannot be resolved. The diffractogram analysis indicated that there was a

decrease in % crystallinity of the organogels as the water content in the emulsion gels increased (Table 5.2). The diffractograms of the gels showed a sharp peak at ~21.3^{o} 2θ as compared to 21.67^{o} 2θ in lanolin. This slight shift of the peak position may be due to the change in the physical properties of the gels at the molecular level. In addition to this, the *d*-spacing of Lanolin (4.09 Å) was found to be lower as compared to the emulsion gels (~4.15 Å). The peak shift and increase in d-spacing in the diffractograms of the gels as against Lanolin were due to the incorporation of water [174].

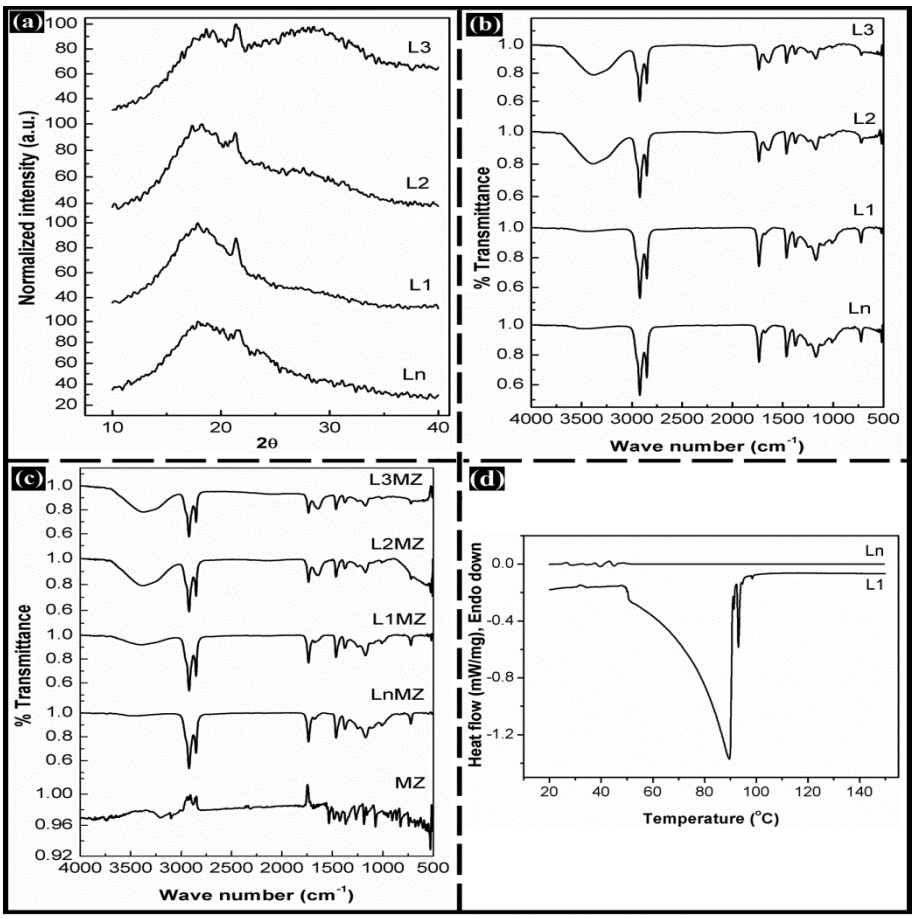

Figure 5.3: X-ray diffractograms of: (a) lanolin and organogels; FTIR spectra of (b-c) lanolin, organogels and metronidazole; and DSC thermograms of (d) lanolin, and L1.

Table 5.2: Change of % crystallinity of the gels, deduced from the XRD pattern data.

Formulation	Peak position	% crystallinity	d-spacing (Å)
Lanolin	21.67	27.0	4.097
L1	21.38	19.65	4.15
L2	21.29	18.5	4.168
L3	21.30	14.23	4.158

5.3.4. FTIR studies

The chemical interactions amongst the organogels were studied using ATR-FTIR spectrophotometer (Figure 5.3b). The peaks obtained for the lanolin were in exact match with the lanolin FTIR literature data [175]. All the characteristic peaks of lanolin were conserved in the formulations. This suggested that there were no significant chemical alterations in the lanolin molecular structure, although the other gel components were added. The shallow peak at 3361 cm^{-1} may be associated with the –OH stretching of the alcohol hydroxyl groups present in lanolin. With the incorporation of water into the gels, the peak at ~ 3361 cm^{-1} became more prominent in the formulations which may be attributed to the intermolecular hydrogen bonding amongst the alcohol group of lanolin and the water molecules [176]. Peaks corresponding to the drug were not identified, indicating that the drug was completely dispersed within the gel matrix. Absence of additional peaks suggested that the drug was present in its native state.

5.3.5. Thermal analysis

The differential scanning calorimetric thermogram of lanolin showed a combination of exotherm and endotherm peaks [175]. The thermal profiles of the formulations were different from that of the lanolin indicating that there has been a complete change in the physical properties of the lanolin as water was incorporated into its structure (Figure 5.3d, Table 5.3). The melting point (T_m) of formulations was higher than lanolin indicating that the formulations were having higher thermal stability than the raw material [170]. The ΔH_m (change in enthalpy) and ΔS_m (change in entropy) values during the melting endotherm followed the same trend as that of T_m values. The ΔH_m and ΔS_m values indicate the cohesive energy for packing of the gel structure [170]. The higher ΔH_m of L3 and LD3 samples suggested the presence of higher gelator (lanolin)- water interactions which may be associated to the intermolecular hydrogen bonding. The DSC results may also be correlated with the spreadability of the gels. As per the reported literatures, higher T_m values are often associated with higher firmness or lower spreadability indices [177].

Table 5.3: Thermal properties of the formulations.

Sample	**T_m (°C)**	**ΔH_m (J/g)**	**ΔS_m (mJ/g.K)**
Lanolin	41.1	-6.882	-896.7
L3	48.7	0.233	5.31
LD3	47.4	-2.562	-136.3

5.3.6.Viscosity studies

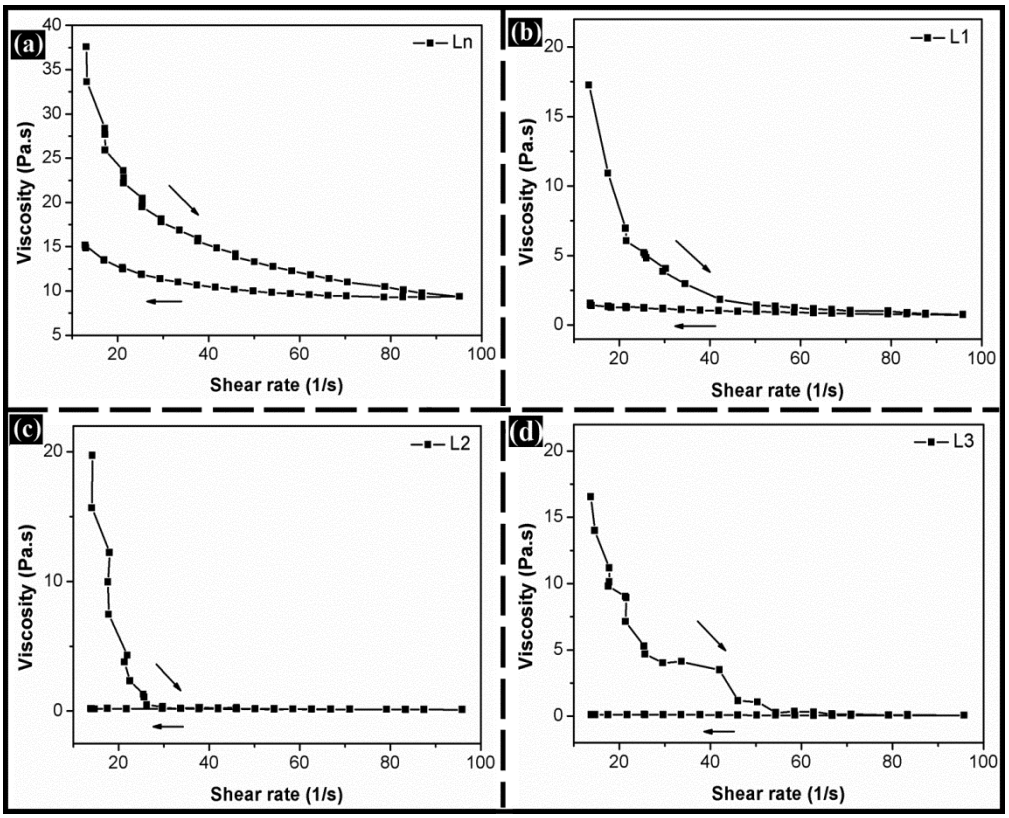

Figure 5.4: Shear rate vs. viscosity of lanolin, and the organogels.

The rheological behaviour of the formulations has been shown in Figure 5.4. Lanolin showed an increase in the shear stress as the shear rate was increased. Lanolin showed a gradual decrease in the viscosity whereas the gels showed an exponential decrease in the viscosity as the shear rate was increased. Lanolin and the formulations showed higher apparent viscosities when the shear rate was increased as compared to when the shear rate was lowered. This resulted in the formation of hysteresis loop. Decrease in the viscosity as the shear rate was increased and formation of hysteresis loop due to closed shear cycle indicate viscoelastic properties of the gels (shear thinning and thixotropy, respectively) [106]. Though 100 % structural recovery was not there, many of the junction points were recovered. The observed hysteresis loop suggested that the total structure recovery did not take place under the experimental conditions. Such profiles are very common in pharmaceutical formulations such as ointments, creams and gels [178-179]. The non-Newtonian flow behavior of the gels were confirmed by analyzing the rheological data using power law or Ostwald-de Waelae relationship [110].

$$\tau = K \cdot \gamma^{n} \qquad (5.1)$$

where, τ is the shear stress (Pa) at γ shear rate (s^{-1}), K is the flow consistency index (Pa.s), and n is the flow behaviour index.

The value of n governs the type of rheological behavior. If the value of n is < 1, =1 and > 1, then the formulations may be regarded as pseudoplastic, Newtonian and dilatant, respectively [110]. In the current study, the n value was determined by plotting the graph between log (shear stress) and log (shear rate). All the n values were found to be less than 1, indicating the pseudoplastic nature of the gels. The thixotropic behavior of the emulsion gels were evaluated by measuring the area enclosed within the hysteresis loop [109]. In general, the thixotropy of the gels decreased non-linearly with the addition of water (Figure 5.4). The decrease in thixotropy with the increase in the water proportions in the formulations indicated that the gels would take more time to regain their initial viscosity once their internal structure was disturbed by applying external shear stress.

5.3.7. Mechanical studies

Figure 5.5a shows the mechanical profile of lanolin and the organogels after performing the cyclic uni-axial compression test. Lanolin showed the maximum hardness and the hardness was found to be decreasing with the increase in water proportion of the gels (Table 5.4). Decrease in hardness influenced the gumminess of the formulations. As the water proportion was enhanced, adhesiveness of the organogels was also decreased, whereas, cohesiveness of the formulations seem to be unaffected. The difference between the cohesiveness of the organogels was insignificant ($p > 0.05$). Decrease in hardness of the samples helped in increasing the spreadable nature of the organogels (Figure 5.5b and Table 5.4). This property may facilitate the use of lanolin in the development of topical formulations. Mechanical properties of the formulations were further tested by stress relaxation studies. When force was applied, the formulations developed approximately uniform stress (F_0). When the stress was maintained for 60 seconds, the formulations showed different relaxation behavior (Figure 5.5c). % relaxation was calculated using the equation 4.8 in chapter 4. Lanolin was found to have relaxed more as compared to organogels (Table 5.5). In general, the difference in relaxation behavior is associated with the viscoelastic nature of the formulations. The viscoelastic nature of the organogels was predicted by fitting the stress relaxation data in modified Peleg's equation (equation 5.2) ($R^2 > 0.95$) (Figure 5.5f). The Stress relaxation parameters of the Peleg's analysis *viz.*, initial rate of relaxation (k_1) and extent of relaxation (k_2) remain unchanged in all the formulations (Table 5.5). In this regard, area (S^*) and asymptotic residual force (F^*) of the normalized stress relaxation curve were calculated. The

obtained S^* and F^* values were less than 1 (Table 5.5). Since these values are in between 0.0 and 1.0, the developed organogels are viscoelastic in nature.

$$\frac{(F_0 - F(t))t}{F_0} = k_1 + k_2 t \qquad (5.2)$$

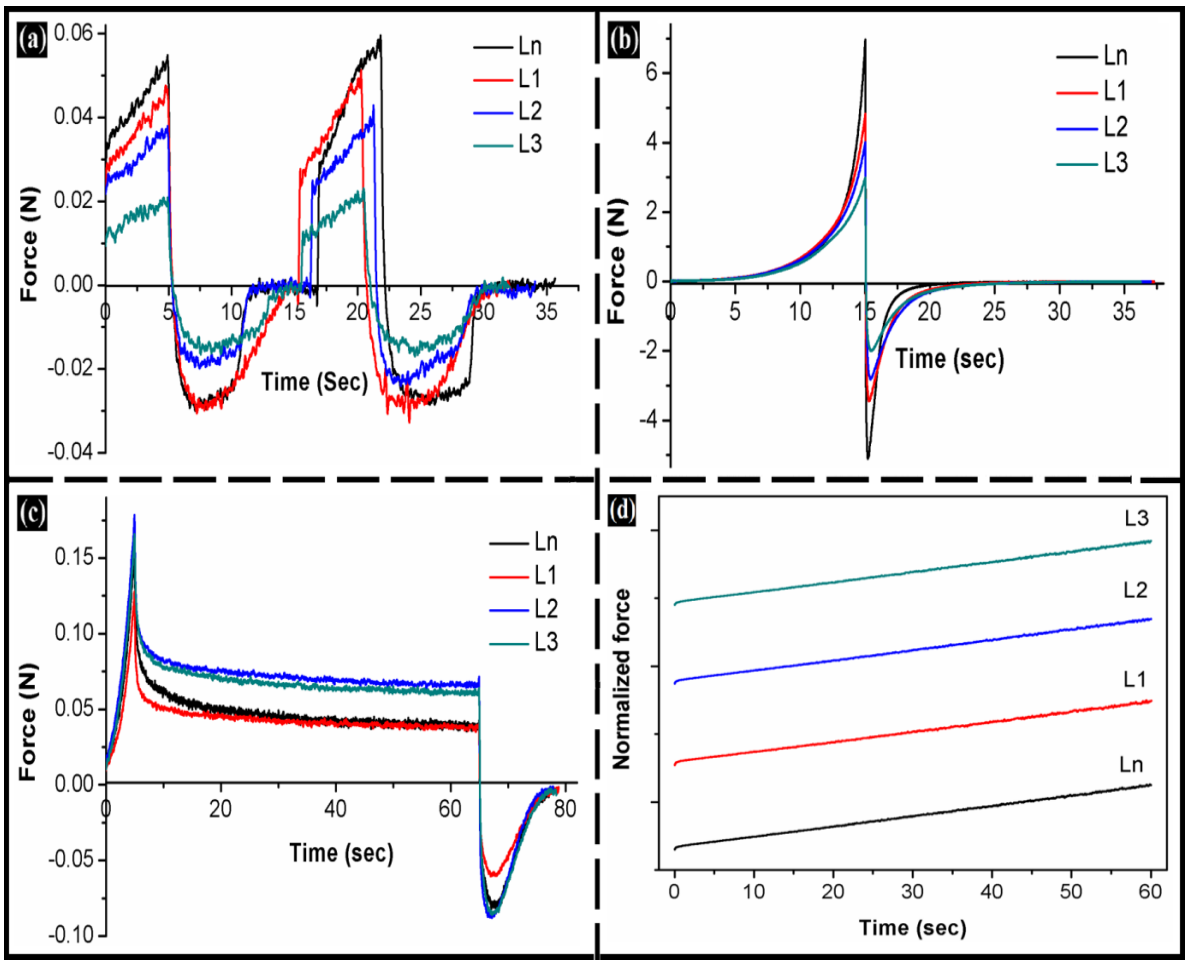

Figure 5.5: Mechanical studies of lanolin and the organogels: (a) Cyclic uni-axial compression studies; (b) Spreadability studies; (c) Stress relaxation studies; and (d) Stress relaxation profiles (modified Peleg's analysis).

Table 5.4: Mechanical properties of lanolin and organogels.

Sample	Hardness (N)	Cohesiveness	Adhesiveness (N.sec)	Gumminess (N)	Spreadability ($N.sec^{-1}$)
Lanolin	5.60	1.04	14.14	5.82	0.082
L1	4.86	1.03	13.69	5.01	0.088
L2	3.86	1.02	9.51	3.94	0.098
L3	2.13	1.02	9.64	2.17	0.118

Table 5.5: Mechanical parameters of lanolin and the organogels.

Samples	F_0 (N)	F_r (N)	k_1	k_2	S^*	F^*	% relaxation
Lanolin	0.16	0.04	0.042	0.015	0.92	0.23	76.56
L1	0.13	0.04	0.045	0.015	0.92	0.30	69.30
L2	0.18	0.06	0.045	0.015	0.92	0.36	63.83
L3	0.17	0.06	0.042	0.015	0.92	0.33	66.92

5.3.8. *In vitro* drug delivery studies

The release profiles of the drug from the formulations have been shown in figure 8. The results indicated that there was 25 %, 36 %, 38 % and 41 % drug release from LD, LD1, LD2 and LD3 formulations, respectively, suggesting that as the water proportion was increased in formulations the rate of release of the drug was higher. This may be due to the increased partition of the drug into aqueous phase of the formulations and subsequent quicker diffusion into the dissolution media. The results can be correlated with the results obtained from the XRD and antimicrobial studies, where it was predicted that with the increase in the water content in the formulations will result in the increase in the amorphous nature of the gels and increased drug release rate [180]. This indicated that the release rate may be tailored by altering the composition of the gels.

Table 5.6: Drug release kinetics of the formulations.

Sample	Zero-order	Higuchi model	KP model		Type of release
	R^2 value	R^2 value	R^2 value	n value	Non-Fickian
LnD	0.761	0.995	0.993	0.557	Non-Fickian
LD1	0.717	0.998	0.992	0.53	Non-Fickian
LD2	0.63	0.992	0.991	0.504	Non-Fickian
LD3	0.85	0.991	0.998	0.576	Non-Fickian

To get an insight into the drug release mechanism, drug release kinetics from the gels was evaluated using different drug release kinetics models (Figure 5.6c-d, Table 5.6). The formulations followed Higuchi kinetics indicating that the formulations were homogeneous-planar matrix type and did not lose their structural integrity during the course of the study [181]. The Fickian value (n) was calculated from the KP model and was found to be ~ 0.5 for all the formulations. This suggested that the release of SA from the gels showed non-Fickian release.

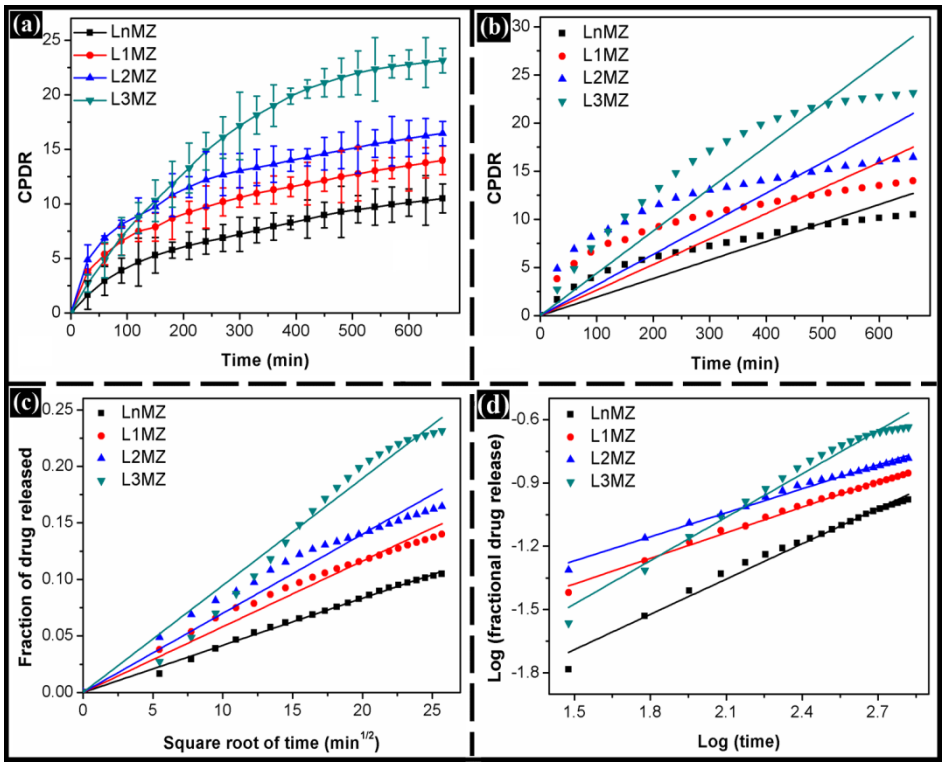

Figure 5.6: Drug release kinetics: (a) CPDR vs. time; (b) Zero order; (c) Higuchi kinetics; and (d) KP kinetics.

5.3.9 Antimicrobial studies

The results of the antimicrobial study are shown in Figure 5.7. The results indicated that the blank gels did not inhibit the growth of the bacteria. Metronidazole loaded formulations showed the antimicrobial activity as the water content in the formulations was increased. The results suggested that the antimicrobial activity of the drug loaded gels were due to the presence of metronidazole as the blank gels did not show any antimicrobial activity. Also, an increase in drug diffusion from the gels containing higher water content may be related to the increase in the amorphous nature of the gels, as evident from the XRD studies.

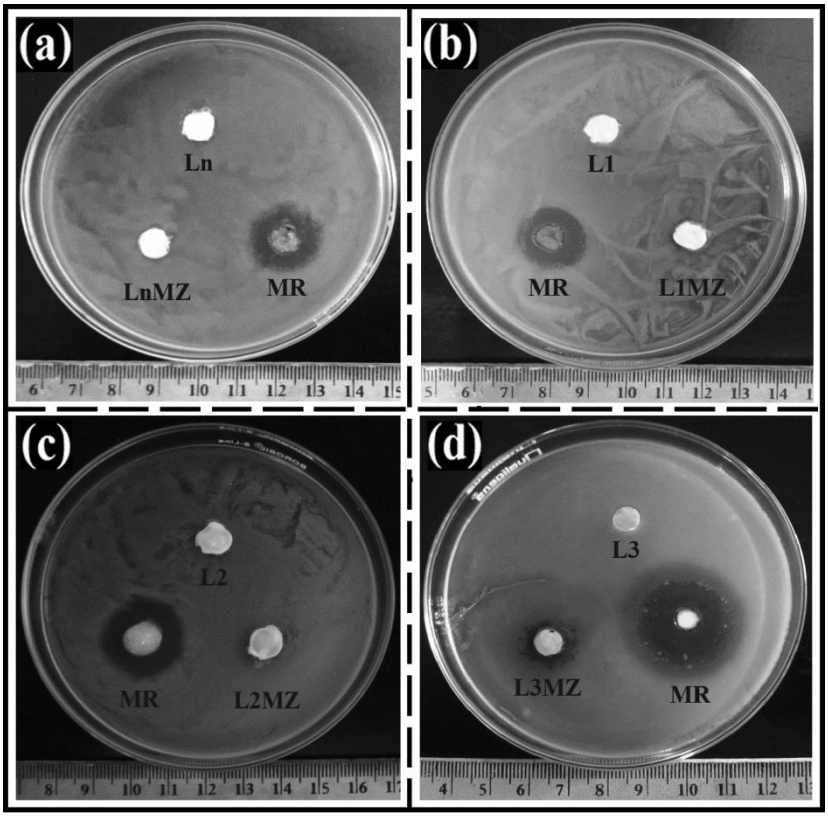

Figure 5.7: Antimicrobial studies of lanolin and the organogels against *E. coli*.

5.4. Conclusion

The present study dealt with the successful development of the Lanolin based emulsion gels. There were no chemical interactions amongst drug and lanolin molecules, indicating that the gel matrices were inert and may be used as carrier for various bioactive agents. The increase in amorphousness due to the addition of water has influenced the drug release pattern. The developed formulations have shown increased thermal stability compared to the raw material, which suggested that the formulations may be stored for a long time. Apart from the flow behavior (thixotropic and shear thinning properties), the developed gels showed sufficient spreadability and biocompatibility for pharmaceutical applications. This ensures a uniform application of the dosage form without any irritation to the skin during topical drug delivery. In addition, drug loaded gels showed good antimicrobial activity against *E. coli*. In short, the developed Lanolin based gels may be tried as carrier matrices for topical drug delivery.

Part B: Encapsulation of lanolin organogels within alginate microparticles

Overview

The developed lanolin-based organogels were tried to encapsulate within the alginate microparticles by internal gelation method. Synthesis of the alginate microparticles was possible only when L1 (Ln:water-2:1) was used but not with L2 (Ln:water-1:1) and L3 (Ln:water-1:2). This was due to the unstability of L2 and L3 during thermal processing, associated with the preparation of microparticles. Blank microparticles and microparticles with lanolin were served as the controls. Ln and L1 components did not leach out of the microparticles when incubated at RT for 2h. Microscopy, FTIR, XRD and DSC studies confirmed the presence of organogels within the microparticles. Encapsulation of organogels improved the DEE (metronidazole was used as the model drug). Non-Fickian mode of drug release was seen from the matrix kind of microparticles and showed antimicrobial activity against *E. coli*. The developed microparticles possess good biocompatibility and mucoadhesivity against mammalian L929 fibroblast cells and goat small intestine, respectively.

5.5 Introduction

The stable lanolin-based organogels (L1, L2 and L3) were tried to encapsulate within the alginate microparticles. Lanolin based formulations have been studied in topical and oral drug delivery [182-183]. If the organogels gets encapsulated, it is expected that there will be reduction in the loss of bioactive agents (associated with leaching) and lanolin organogels may be tried for the oral delivery applications. Metronidazole was used as the model drug.

5.6. Materials and methods

5.6.1 Preparation of the lanolin-based organogels and microparticles

Lanolin based organogels were prepared as per the protocol described in chapter 3.2.2. Microparticles were prepared as per the protocol given in chapter 3.2.5. Experimental procedures for the characterization of microparticles (bright field microscopy, SEM, XRD, FTIR, DSC, leaching studies, *in vitro* biocompatibility, mucoadhesivity and drug delivery studies) are given in chapter 3.3.

5.7. Results and discussion

5.7.1. Preparation of lanolin based organogels

The compositions of the organogels used in this study have been tabulated in Table 5.7. Mechanism of organogel formation of organogels was explained in part A of this chapter.

Table 5.7: Composition of the organogels.

Sample	Lanolin:Water (% W)	Span 80 (% W)	Metronidazole (% W)
L1	2:1	1.0	--
L2	1:1	1.0	--
L3	1:2	1.0	--
L1MZ	2:1	1.0	1.0

5.7.2. Preparation of microparticles

The microparticles were prepared by double emulsification/internal gelation method. Stable microparticles were formed when lanolin and L1 organogels were used as the internal phase. The use of L2 and L3 organogels did not result in the formation of microparticles. This may be associated with the lower stability of L2 and L3 organogels [12]. Due to this reason, L2 and L3 containing microparticles were not investigated further. The compositions of the prepared microparticles have been tabulated in Table 5.8.

Table 5.8: Internal phase composition of the microparticles.

Samples	Internal phase	Observation
BM	Nil	Stable microparticles were formed
MLn	Lanolin	Stable microparticles were formed
ML1	L1	Stable microparticles were formed
ML2	L2	Microparticles were not formed
ML3	L3	Microparticles were not formed
BMMZ	MZ	Stable microparticles were formed
MLnMZ	LnMZ	Stable microparticles were formed
ML1MZ	L1MZ	Stable microparticles were formed

5.7.3. Microscopy

BM microparticles were semi-transparent, which may be associated with the absence of any internal phase. On the other hand, MLn and ML1 were opaque, which may be accounted to the presence of lanolin and L1 within the microparticles (Figure 5.8). As lanolin and L1 are semi-solid and opaque at RT, encapsulation resulted in the formation of opaque microparticles [162].

The size distribution of the microparticles revealed that lanolin and L1 containing microparticles showed a broad size distribution compared to BM microparticles (Figure 5.9). The average diameter (D_{avg}) of the microparticles was found out by estimating the size of the 50 % population of the microparticles. The size of the microparticles was in the order of ML1 (130.14 ± 21.2) > MLn (111.28 ± 17.6) > BM (94.7 ± 10.2). The size distribution analysis of the microparticles has been provided in Table 5.9. Since lanolin and L1 are viscous in nature, this might have resulted in the formation of non-homogeneous alginate mixture which, in turn, resulted in the formation of microparticles of wide size distribution [12]. Apart from the physical nature of the internal phase, the homogenization speed also plays an important role in governing the size distribution of the microparticles.

In general, homogenization at lower speeds exerts lower dispersive forces thereby resulting in the formation of larger sized microparticles. Increase in viscosity of the emulsion also results in the lower dispersive force. Hence it may be expected that the effective dispersive force during the preparation of BM microparticles might have resulted in the formation of uniform and small vesicles as compared to lanolin and L1 containing microparticles where larger sized particles were formed [92]. The micrographs of the dried microparticles, as

observed under SEM, have been shown in Figure 5.8. All types of the microparticles were found to be spherical and smooth in nature.

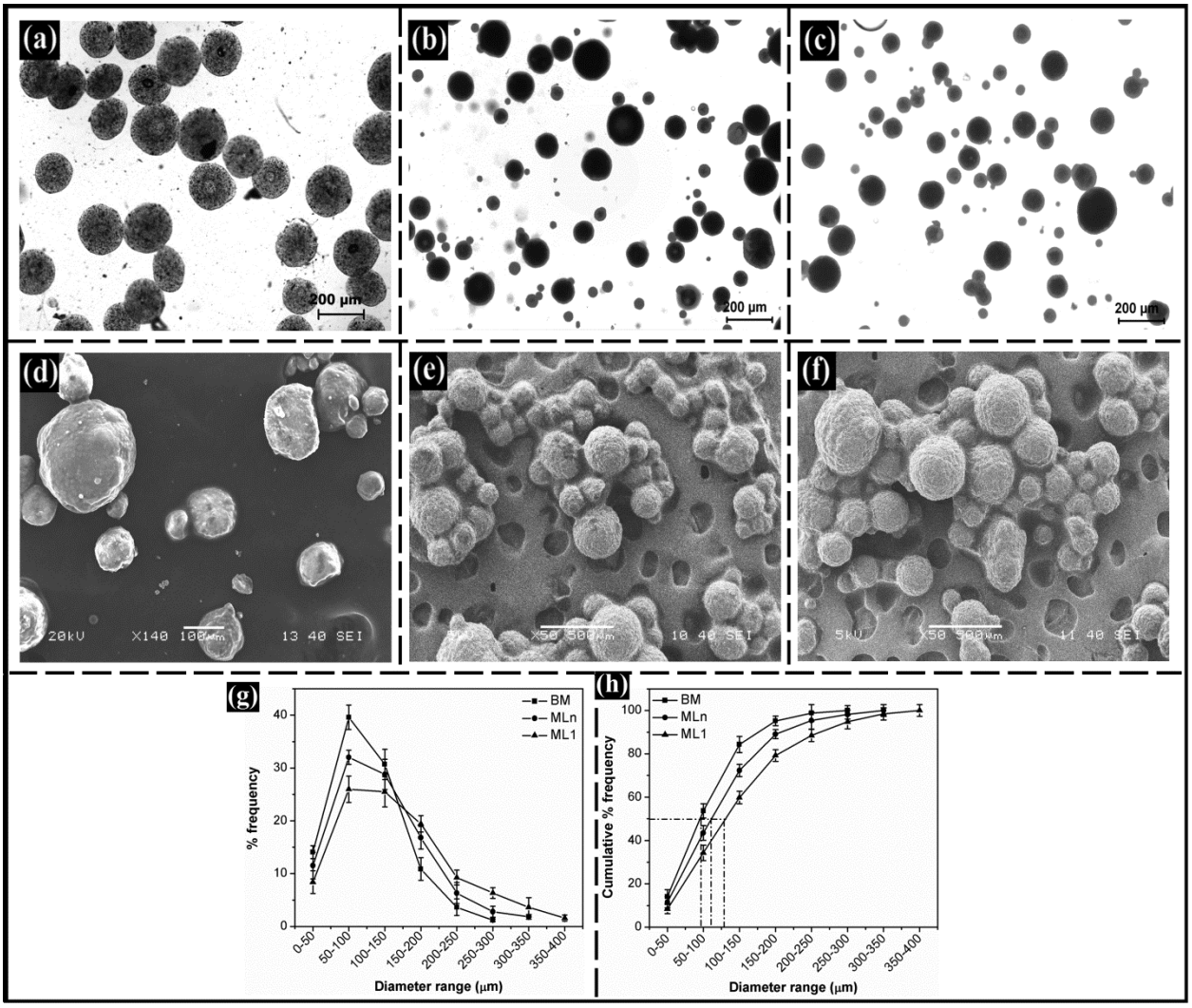

Figure 5.8: The bright field microscopic images of: (a) BM, (b) MLn, and (c) ML1; SEM images of: (d) BM, (e) MLn, and (f) ML1; and Size distribution analysis of the microparticles: (g) % frequency, and (h) cumulative % frequency.

5.7.4. Leaching studies

The leaching of the internal phase from the microparticles was monitored (Figure 5.10). Lanolin and L1 containing microparticles did not show any signs of leakage at the end of the study (2h). Leakage was checked by monitoring the wetting of the filter paper with the internal phase. The absence of leakage of the internal phase may be associated with the gelation of the internal phase at RT. This prevented the migration of the internal phase out of the polymeric layer. This ensures that the encapsulation of organogels within the

microparticles prevents the leakage of bioactive agents which, in turn, can improve the drug entrapment efficiency of the microparticles.

5.7.5 Drug entrapment efficiency

The dried microparticles were used to calculate the drug entrapment efficiency. The encapsulation efficiencies of the microparticles have been tabulated in Table 5.10. The drug entrapment efficiency of MLnMZ (82.0 ± 2.5) and ML1MZ (85.0 ± 3.4) were higher than BMMZ (46.0 ± 2.7). MLnMZ and ML1MZ have shown %DEE > 85 %, which is nearly the 1.8 times the drug entrapment efficiency of BM. The restricted movement of the drug within the organogels might have yielded higher encapsulation efficiency in MLn and ML1 than in BM. In other words, the semisolid nature of the organogels behaved as a barrier for the movement of the drugs. MLnMZ and ML1MZ did not show any leaching (Figure 5.9). This might have also contributed in the increase drug entrapment efficiency.

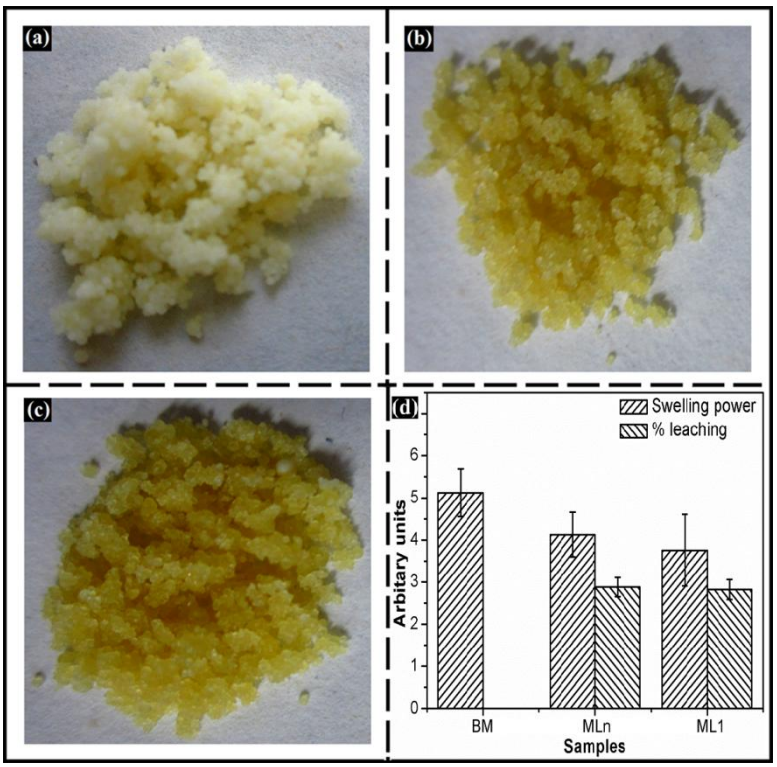

Figure 5.9: Leaching studies: (a) BM, (b) MLn, and (c) ML1; and bar graphs of: (d) Swelling power and % leaching.

5.7.6. Molecular interaction studies

XRD profiles of the microparticles have been shown in Figure 5.10a. BM showed a broad hump at ~12^{o} 2θ [129]. MLn and ML1 have shown additional peaks corresponding to their internal phase apart from the broad peak of the alginate [12]. Microparticles have shown

distinct x-ray diffraction profiles, which varied on the composition of the internal phase. The characteristic peaks of lanolin and L1 (21.67° and 21.3° 2θ, respectively, given in part A of this chapter) were conserved in their respective microparticles, indicating their presence without any change in the physical properties.

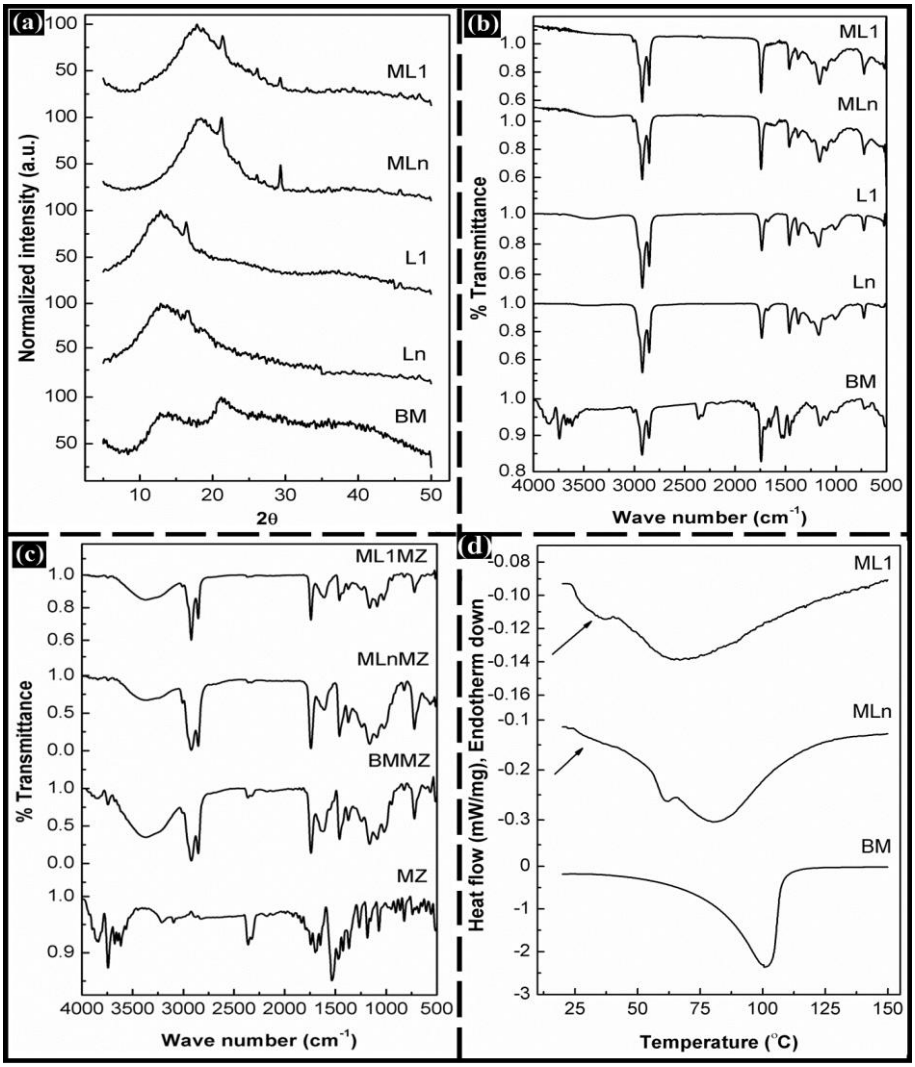

Figure 5.10: (a) XRD profiles, (b-c) FTIR spectra, and (d) DSC thermograms of the microparticles.

All the microparticles were found to be amorphous in nature as suggested by the presence of a broad peak at ~20° 2θ. The change in the amorphousity was compared by calculating full width half maximum (FWHM) of the broad peak at ~20º [184]. In general, higher degree of amorphousity is associated with higher FWHM [12]. The FWHM of lanolin and L1 was found to be 10.76 and 10.00, respectively. BM have shown highest FWHM and may be attributed to the presence of water within the microparticles [173]. Results suggested that MLn and ML1 have lower amorphousity than BM.

The FTIR spectra of the microparticles showed the characteristic peaks of alginate, indicating that the addition of lanolin and L1 did not change the chemical nature of the alginate polymer (Figure 5.10b-c). L1 showed a narrow peak at 3400 cm^{-1} which was not present in lanolin. This may be associated with the intermolecular hydrogen bonding due to the presence of water in L1. MLn and ML1 have shown peaks corresponding to lanolin and L1, respectively, suggesting their presence within the microparticles. The intensity of the peak at 3400 cm^{-1} for L1, as L1 contained water which might have promoted intermolecular hydrogen bonding [12]. Absence of additional peaks in the microparticles suggested that there was no chemical interaction amongst the drug molecules and the components of the microparticles.

5.7.7. Thermal studies

The thermograms of lanolin and L1 have been reported in part A of this chapter. MLn and ML1 have shown endothermic peaks at ~38 °C (as shoulder peaks, pointed with arrows in the Figure 5.10d), corresponding to the melting endotherms of lanolin and L1. This confirmed the encapsulation of lanolin and L1 within the alginate microparticles. As per the literature, polysaccharides show high affinity towards water molecules and lose/release water at different temperatures depending on the interactions with the water. Water is reported to form hydrogen bonds with the –OH groups of the alginate polymers [185]. MLn and ML1 have shown peaks at ~67 °C. These endothermic peaks have been reported due to the evaporation of the loosely bound water [159]. MLn has shown additional endothermic peak at ~80 ^{o}C. This is due to the evaporation of tightly bound water molecules. ML1 showed a single broad endothermic peak for the evaporation of the water molecules. This might have resulted due to the evaporation of the water molecules (both loosely bound and tightly bound water) in tandem. BM did not contain any internal phase which resulted in the stronger association of the water molecules with the –OH groups of alginate. This explains the occurrence of the endotherm peak at 100 ºC. No shoulder peak was obtained as there was no gel entrapped within the core of the microparticles.

5.7.8. *In vitro* Biocompatibility and mucoadhesivity studies

Biocompatibility of the microparticles was determined by studying the relative proliferation of fibroblast cells in the presence of the microparticles extracts. The cell proliferation was measured using MTT assay. The results indicated that the cell viability index in presence of the leachates of the microparticles were either ~1 or better than 1 indicating the biocompatible nature of the microparticles (Figure 5.11a). The change in cell viability index was found to be insignificant ($p > 0.05$) with respect to control.

The detachment times of BM, MLn and ML1 from the mucous membranes was found to be 28.25 ± 2.2 h, 24.5 ± 1.5 h and 25.5 ± 3.25 h, respectively (Figure 5.11b). All the microparticles showed high affinity towards the mucousal membrane. This may be associated with the anionic nature of the alginate molecules [186]. The statistical analysis suggested that the difference in mucoadhesion times was insignificant ($p > 0.05$). Since there was negligible leaching of the internal phase from MLn and ML1, this accounted for their similar mucoadhesive behavior as that of BM microparticles.

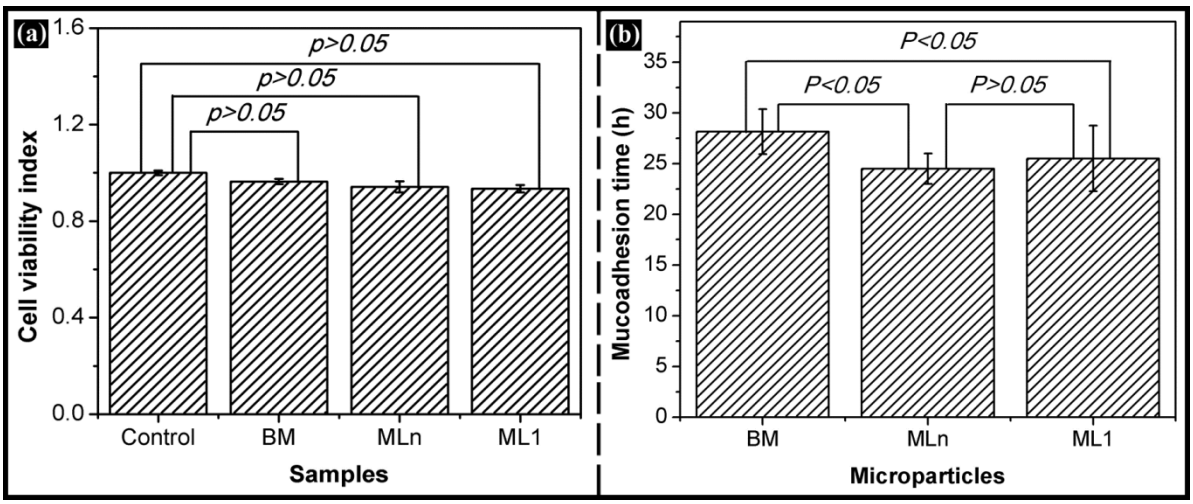

Figure 5.11: (a) *In vitro* biocompatibility, and (b) Mucoadhesivity studies of the microparticles.

5.7.9. *In vitro* drug delivery studies

The release of the drugs was affected by the physical nature of the microparticles. Under the given conditions, BMMZ have shown highest *in vitro* CPDR value (Figure 5.12a), followed by ML1MZ and MLnMZ. The difference in the drug release behavior may be attributed to the internal composition of the organogels. Difference in CPDR values was also noticed during antimicrobial studies. Higher zone of inhibition was noticed against BMMZ, followed by ML1MZ and MLnMZ (Figure 5.12b-d). Presence of water might have facilitated the transportation of the drug from the microparticles.

The speculation of the mechanism of release of the drugs was carried out by fitting the drug release profile information in the zero-order, first order, Higuchi, Baker-Lonsdale model and Korssmeyer-Peppas models (Figure 5.13). The parameters of the best fit models have been tabulated in Table 5.9. All the release patterns followed Higuchi and Baker-Lonsdale models ($R^2 > 0.95$). The results suggested that the developed microparticles may be considered as swollen matrix type as the release profile can be easily described by the Baker-Lonsdale

model [187-188]. The Fickian value (n) was calculated from Korssmeyer-Peppas model (R^2 > 0.95). As per the n value, MLnMZ and ML1MZ followed non-Fickian kinetics. The non-Fickian/anomalous behavior of drug release may be due to polymer relaxation, erosion and degradation. The non-Fickain and anomalous release behavior of the drugs from the alginate microparticles have also been reported [189-190].

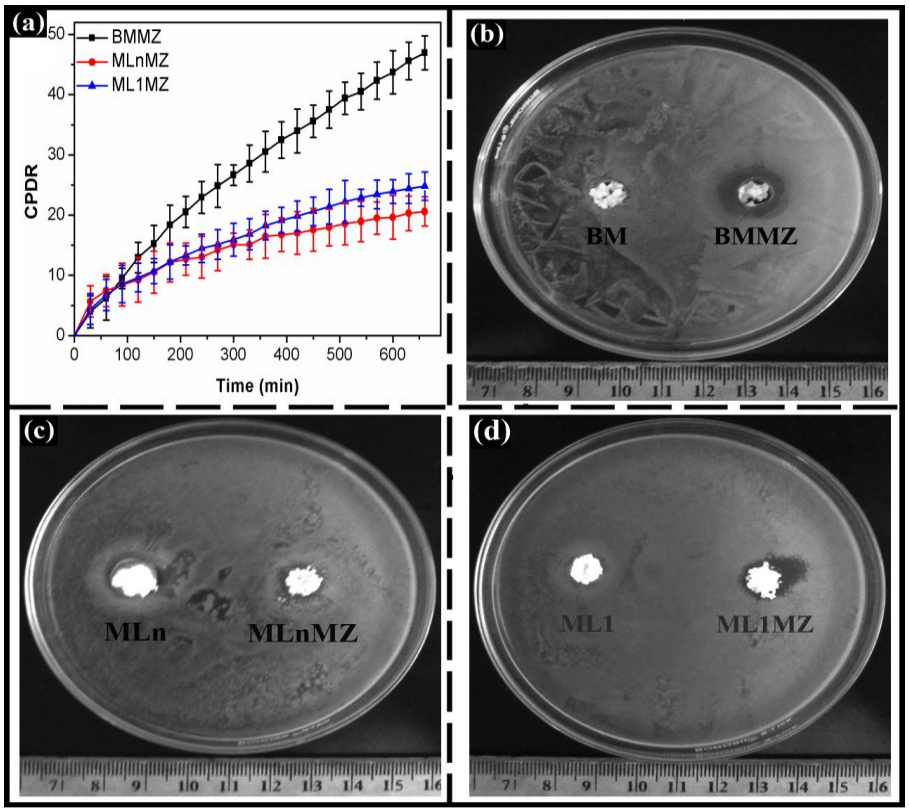

Figure 5.12: (a) CPDR profiles of the microparticles, and (b-d) antimicrobial studies of the microparticles against *E. coli*.

Table 5.9: Drug release kinetics from the microparticles

Sample	Zero order R^2	Higuchi R^2	BL model R^2	Best fit	KP model		
					R^2	'n'	Diffusion
BMMZ	0.957	0.937	0.983	BL	0.995	0.80	Non-Fickian
MLnMZ	0.55	0.988	0.996	BL	0.995	0.53	Non-Fickian
ML1MZ	0.80	0.993	0.993	BL	0.998	0.56	Non-Fickian

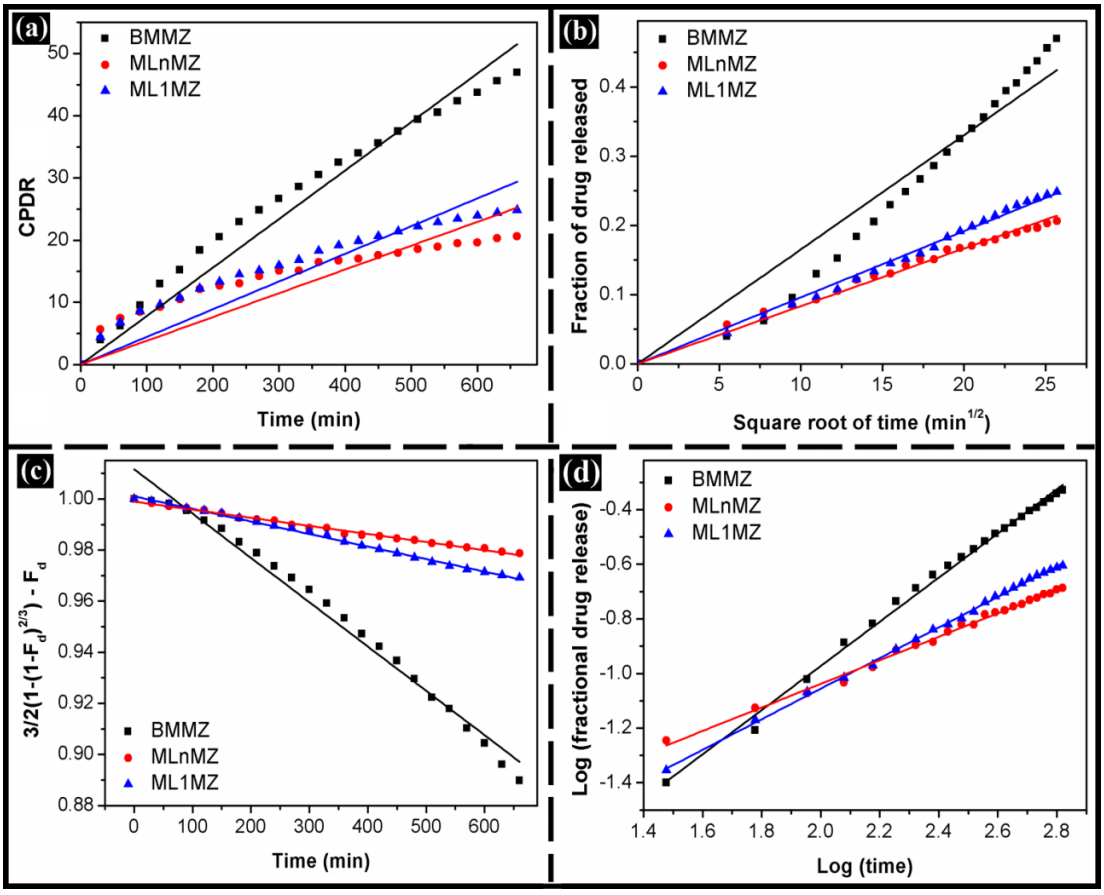

Figure 5.13: Drug release kinetics: (a) Zero order; (b) Higuchi kinetics; (c) BL model; and (f) KP model.

5.8. Conclusion

Lanolin-based organogels have been successfully encapsulated within the alginate microparticles prepared by ionotropic gelation method. DSC and XRD studies confirmed the encapsulation of organogels within the microparticles. Drug entrapment efficiency of the organogel containing microparticles was found to be higher than the blank microparticles. Encapsulation of the organogels has enhanced the drug carrying capacity of the microparticles. The cytocompatibility and mucoadhesivity studies suggested the biocompatible and mucoadhesive nature of the microparticles. *In vitro* drug release studies suggested that lanolin and L1 containing microparticles may be tried for controlled delivery applications.

Chapter 6

Encapsulation of stearate based organogels in alginate microparticles

Abstract

Edible oil (sesame oil and soy bean oil) based organogels were synthesized using stearic acid as the organogelator. In depth analysis of gel kinetics, gel microstructure, molecular interactions, thermal and mechanical behaviors of the organogels was performed. The properties of the organogels were dependent on the type of the vegetable oil used and the concentration of the stearic acid. Avrami analysis indicated heterogeneous nucleation coupled with one-dimensional growth of gelator fibers was the key phenomenon in the formation of organogels. Alginate (shell) microparticles were prepared by encapsulating semi-solid organogel (core) by ionotropic gelation method. Confocal microscopic studies have shown the existence of organogel as the core of the microparticles. The presence of organogel as the core material of the microparticle was confirmed by X-ray diffraction and differential scanning calorimetric analyses. Entrapment of the organogel within the microparticles has improved the drug encapsulation efficiency by preventing the leaching of the internal phase. *In vitro* drug release studies showed sustained release of ciprofloxacin from the organogel containing microparticles. The drug loaded microparticles was found to have good antimicrobial activity when tested against *E. coli*. The microparticles were found to be mucoadhesive and biocompatible in nature. The preliminary results suggested that the developed microparticles hold promise as carriers for controlled delivery applications.

Graphical abstract

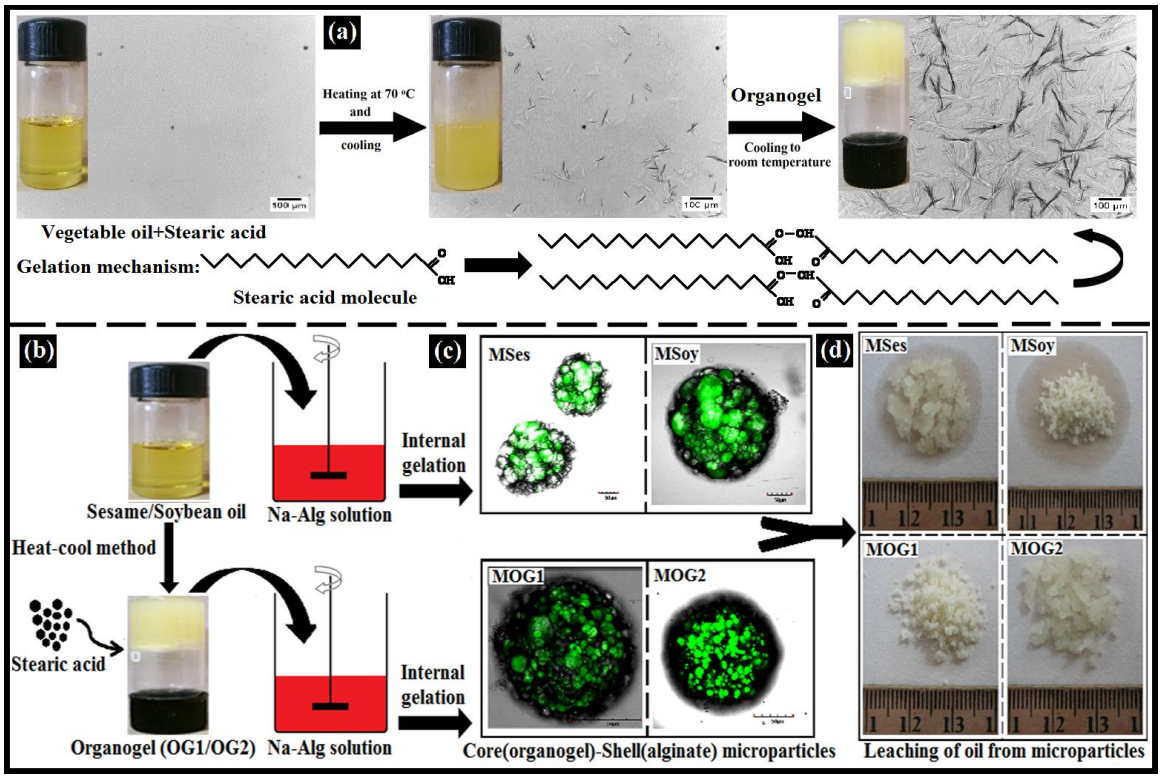

Part A: Preparation and characterization of stearate organogels

Overview:

Stearic acid based organogels were prepared by hot emulsification method using sesame oil and soy bean oil as the organic solvents. Critical gelator concentration (CGC) of stearic acid was found to be 16 % (w/w) and 19 % (w/w) for the synthesis of sesame oil and soy bean oil organogels, respectively. For further characterization and comparison, sesame oil and soy bean organogels with CGC, 22 % (w/w) and 25 % (w/w) gelator concentrations were chosen. Organogel microstructure and gelation kinetics indicated that the gels were formed by heterogeneous nucleation and one-dimensional growth of gelator fibers. The gelation mechanism was confirmed by performing Avrami analysis on DSC thermograms. Based on the XRD, FTIR and DSC analyses it was identified that the stearic acid molecules were arranged themselves in layered fashion by forming hydrogen bonds amongst their carboxyl head groups. The change in the crystallite size of stearic acid in organogels was evaluated by XRD studies. Viscoelastic and pseudoplastic nature of the organogels was analyzed in-depth by fitting the stress relaxation data in modified Peleg's model and rheological studies, respectively. Textural studies revealed the coexistence of hydrogen bond dissipation and formation of new bonds when stress applied on the organogels. Ciprofloxacin (model drug) was released from the organogels via diffusion with good antimicrobial activity against *E. coli*.

6.1. Introduction

In general, organogels are grouped as physical gels and chemical gels. Since the chemical organogels have wide range of applications beyond biomedical, food and cosmetic applications, their mechanism of formation and physical properties have been well documented [191]. But limited research has been carried out on the physical organogels, especially edible oil organogels (organogels). The gelation mechanism and in-depth analysis of physical properties of organogels have not been well explored.

Stearic acid has several health benefits when consumed orally or applied locally over the skin. It is octadecanoic acid, an 18 carbon chain fatty acid. It is the second most naturally abundant saturated fatty acid after palmitic acid. Sesame and soy bean oils are edible oils obtained from the seeds of *Sesamum indicum* and *Glycine max*, respectively. These oils are rich in natural antioxidants. Sesame oil contains vitamin E and sesamol whereas phytic acid is present in soy bean oil [192-194]. These oils also possess excellent anti-inflammatory properties. Although these oils possess intriguing features, limited research has been done on these oils for food, cosmetic and pharmaceutical applications. In this study, we report for the in-depth analysis of the gelation kinetics, molecular interactions, thermal and mechanical properties of the stearic acid based organogels. Sesame oil and soy bean oil were used as the representative vegetable oils. *In vitro* drug release and antimicrobial studies were carried out using ciprofloxacin loaded organogels to determine the capability of the organogels as carriers for controlled drug delivery.

6.2. Materials and methods

Stearate based organogels were prepared as per the protocol given in section 3.2.3 of chapter 3. Characterization of the organogels, *in vitro* drug delivery studies and antimicrobial studies were performed as per the protocols given in section 3.3 of chapter 3. Characterization studies include, bright field microscopy, gelation kinetics, XRD, FTIR, DSC and mechanical studies.

6.3. Results and discussion

6.3.1. Preparation of the organogels

Organogels were prepared by dissolving stearic acid in the vegetable oil (sesame oil and soy bean oil). At higher temperatures, the stearic acid solution was transparent. As the solution was cooled down to room-temperature, the solution became opaque. Formation of organogels was confirmed by inverted tube method (Figure 6.1) [107]. Above the critical gelator

concentration (CGC), stearic acid induced gelation. The CGCs for sesame oil and soy bean oil were different. 16 % (w/w) and 19 % (w/w) of stearic acid was needed to induce the gelation of sesame oil and soy bean oil, respectively. CGC of > 15 % is quite common for fatty acyl non-ionic organogelators in vegetable oils and organic solvents [106]. At CGC, each stearic acid molecule immobilized ~1.7 molecules of sesame oil and ~1.4 molecules of soy bean oil. The CGC of the gels did not change even after the addition of 0.5 % (w/w) ciprofloxacin. The developed gels were opaque, smooth and semi-solid and their composition has been tabulated in Table 6.1. Color of the gels was dependent on the vegetable oil used. The organogels are thermoreversible in nature and stable at RT for more than 12 months. During this period, syneresis of the oil was not observed. No fungal contamination of the samples was found during this period. Sesame oil formed yellow colored gels while white colored gels were formed when soy bean oil was used.

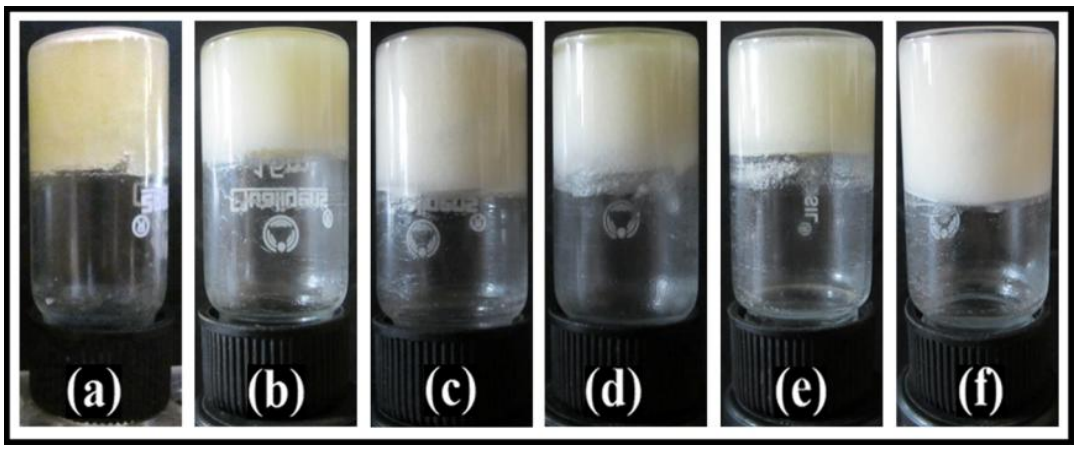

Figure 6.1: Pictographs of: (a) Ses1, (b) Ses2, (c) Ses3 (d) Soy1, (e) Soy2, and (f) Soy3.

The minimum concentration of stearic acid (CGC) to induce gelation was different for the oils. This is due to the solvent induced nucleation of the gelator molecules and may be attributed to the difference in the polarity of the oils used. The difference in the polarity of the oils may be described by the degree of unsaturation of the oils. Sesame oil contains high oleic acid fraction whereas soy bean oil contains high linolenic and linoleic acid fraction [195-196]. These differences lead to the change in polarity of the oils, which in turn, affected the gelling ability of stearic acid. This kind of phenomenon was observed in 12-hydroxy stearic acid/canola oil organogels [197].

Table 6.1: Composition of the organogels under investigation.

Sample	Stearic acid (% w/w)	Sesame oil (% w/w)	Soy bean oil (% w/w)	Ciprofloxacin (% w/w)
Ses1	16.0	84.0	--	--
Ses2	22.0	78.0	--	--
Ses3	25.0	75.0	--	--
Soy1	19.0	--	81.0	--
Soy2	22.0	--	78.0	--
Soy3	25.0	--	75.0	--
Ses1C	16.0	83.5	--	0.5
Ses2C	22.0	77.5	--	0.5
Ses3C	25.0	76.5	--	0.5
Soy1C	19.0	--	81.5	0.5
Soy2C	22.0	--	78.5	0.5
Soy3C	25.0	--	75.5	0.5

6.3.2. Gelation kinetics

Since the developed formulations were transparent liquids at 70 ^{o}C, the kinetics of the organogelation was studied by measuring the absorbance of the gels when the molten gels were cooled to room-temperature. The gel setting time was considered as the time required in reaching the equilibrium phase. Equilibrium phase was first achieved by Ses3 and Soy3, where the concentration of stearic acid was highest (Figure 6.2). As the stearic acid concentration was reduced there was a decrease in the gel setting time.

The gel setting time was calculated from the measurement of the absorbance of the molten gels during cooling. The shape of the absorption profile was sigmoidal. The gelation time per gram of the gel was calculated (Figure 6.2c). The initial slow transformation rate can be attributed to the time required for forming the significant number of nuclei. Alteration in the gelator concentration resulted in the changes of induction time (T_i), fibrillar growth time (T_f) and equilibration time (T_e). In comparison to the induction time, fibrillar growth time was very fast and was about ~1 min for all the gels. The change in gelator concentration has mainly affected the induction time and the equilibration time of the gels. The equilibration time (gel setting time) decreased with the increase in the concentration of the stearic acid. Sigmoid profile along with long-term equilibrium state signifies that growth of the fiber aggregates was may be one-dimensional and followed first-order kinetics [198]. One-

dimensional growth of the aggregates results in the formation of long fibers having high length: width ratio. Formation of fibers with high length: width ratio was confirmed from the microscopic studies (Figure 6.3).

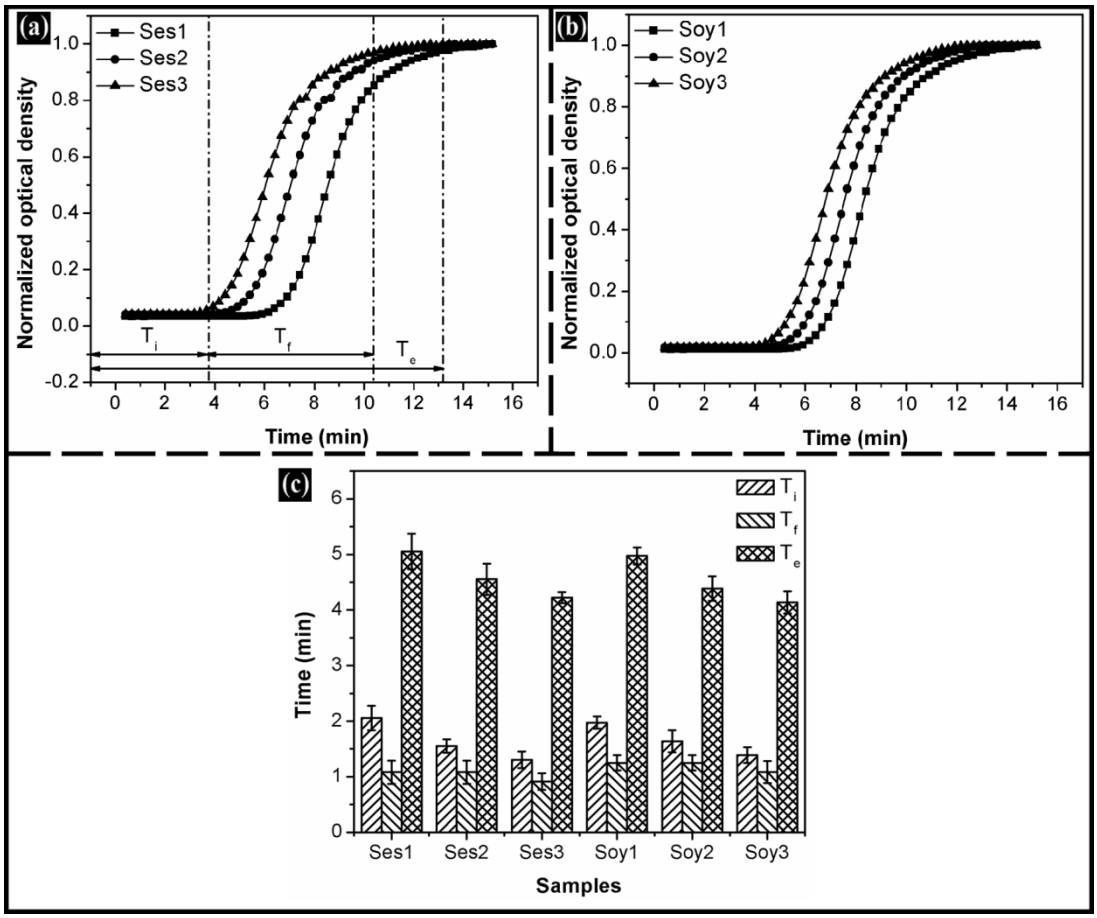

Figure 6.2: Gelation kinetics of: (a) sesame oil based organogels, and (b) soy bean oil organogels; and (c) Gelation parameters of the organogels.

The micrographs (bright field microscopy) showed the presence of fibrous network of stearic acid in vegetable oils (Figure 6.3). The gelator fibers were dispersed throughout the continuous phase and were entangled to form a coherent network. The orientation of the thin fibers into discrete fibrillar bundles/aggregates was noticed in all the organogels. This kind of phenomenon is commonly associated with physical organogels [199]. The network density was higher in gels with higher gelator concentration. Figure 6.3 (g-i) shows the formation of gelator network of Ses3 oleogel at different time intervals during cooling. Network formation was initiated by random nucleation of stearic acid, followed by fiber growth and subsequent branching. Branching and entanglement of fibers has been shown by an arrow in Figure 6.3i. Formation of nucleation points were observed during the fiber growth. This suggested that the nucleation in the gels was a random and continuous process and not a spontaneous

process. The fibers started growing away from the nucleation point. The fibers showed a continuous branching at the tips and/or side faces.

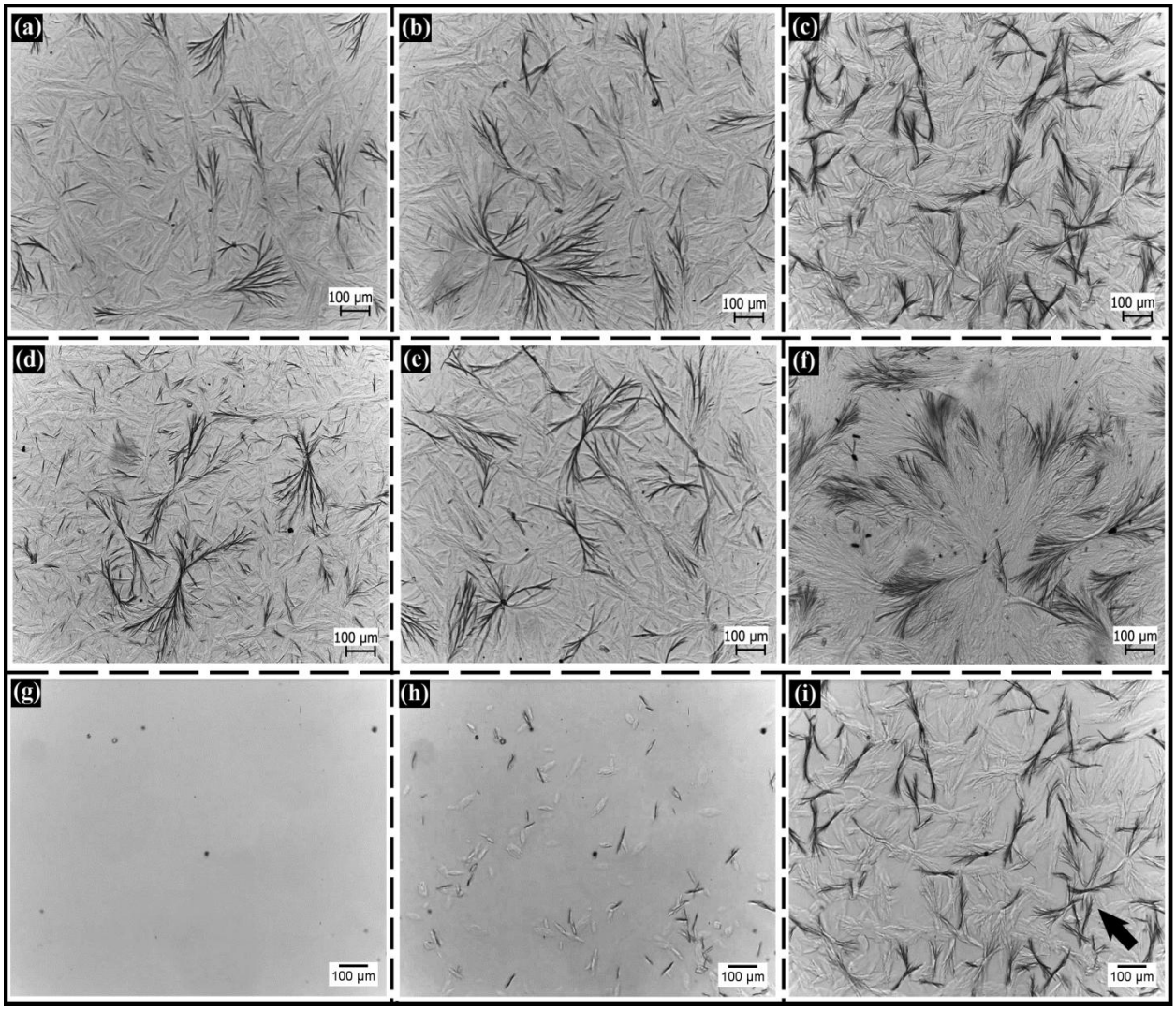

Figure 6.3: Microscopic images of: (a) Ses1, (b) Ses2, (c) Ses3, (d) Soy1, (e) Soy2, and (f) Soy3 organogels; Formation of Ses3 organogel at: (g) zero sec, (h) 30 sec, and (i) 1 min of gelation (Ses3 was shown as the representative).

The gelator molecules self-assembled as the temperature of the molten organogels was reduced (Figure 6.3). Nucleation was governed by the diffusion of stearic acid molecules from the molten phase to the solid phase. Phase conversion lead to the formation of fibers with low-dimensional or liquid crystalline ordering of stearic acid molecules. This suggested heterogeneous nucleation was prevalent in the formation of the stearic acid fibers [200]. There was an increase in the fiber growth and branching as the concentration of the gelator was increased. The increase in the proportion of stearic acid has resulted in the increase in the branching.

6.3.3. Molecular interaction studies

Table 6.2: Peak analysis of stearic acid's X-ray diffractogram.

Type of peaks	Peak position (°2θ)	d-spacing (Å)	Interplanar spacing
Long spacing peaks	6.89	12.82	[003]
	11.5	7.69	[005]
Short spacing peaks	20.29	4.37	[007]
	21.37	4.15	[110]
	23.7	3.75	

Molecular interactions amongst the gel components were studied by XRD and FTIR studies. Stearic acid exists in different polymorphic forms. Based on the peak analysis, the polymorphic form of stearic acid was estimated (Figure 6.4, Table 6.2). The peak positions and *d*-spacings of stearic acid diffractograms are closely matching with the C-form of stearic acid [157]. The position of the major peaks and the *d*-spacings of stearic acid were conserved in the organogels (Figure 6.4). This suggests that the polymorphic form of stearic acid was not altered during the formation of organogels. The diffractograms of both stearic acid and the organogels showed the presence of both long-spacing peaks [00l] and short-spacing peaks [hk0]. The long spacing and short spacing peaks provide information about the order and the lateral packing of the molecular layers, respectively [157]. Although the peak positions of long and short spacing peaks were not altered, their intensities were different. The intensity of the long spacing peaks was more intense than the short spacing peaks in the stearic acid diffractogram. On the other hand, a reverse trend was observed in the prepared organogels, i.e. the intensity of the short spacing peaks were higher than the long spacing peaks. This suggested that the addition of the vegetable oils in the stearic acid resulted in the rearrangement of the molecular packing of stearic acid.

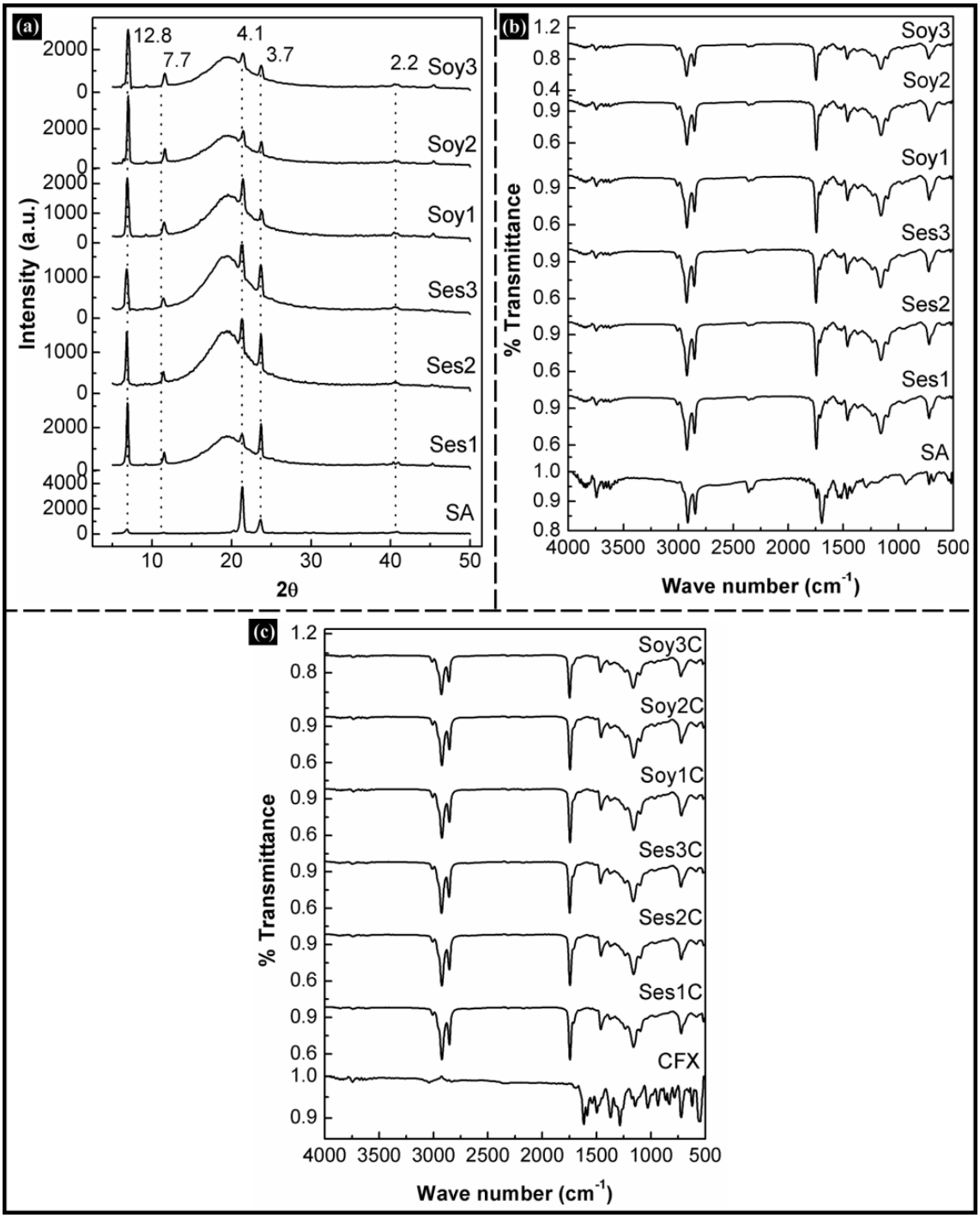

Figure 6.4: (a) XRD of organogels; FTIR spectra of: (b) organogels, and (c) CFX and CFX containing organogels.

Previous study using oleanolic acid (a pentacyclic triterpenoid acid) reported that the long spacing peaks of stearic acid are not manifested in the X-ray diffractograms. This is due to the destruction of the order of molecular layers of stearic acid in the organogels [157]. In the present study, inclusion of oils has exposed the crystal planes of long spacing region. This resulted in the increase in the peak intensity of the long spacing peaks. Retention of peaks in

the long spacing region revealed that the order of stearic acid molecular layers was not disturbed even in the organogels. As peak positions in the organogels were in match with the pure stearic acid, the gelator molecules exist in the same molecular packing arrangement [201].

Table 6.3: The XRD parameters of SA and organogels.

Samples	*d*-spacing of [110] plane (Å)	FWHM of [110] peak (º2θ)	D (nm)
SA	4.15	0.157	51.4
Ses1	4.15	0.324	24.9
Ses2	4.15	0.195	41.5
Ses3	4.15	0.192	
Soy1	4.14	0.292	27.7
Soy2	4.14	0.227	35.6
Soy3	4.14		

The molecular packing of stearic acid in gelator fibers was determined by the angle ratios or Bragg distance ratios. The ratios of position of the 1st (6.89º 2θ), 2nd (11.5º 2θ) and 3rd (21.37º 2θ) low angle peaks of the gels with respect to lowest angle peak position (6.89º 2θ) was studied to identify the packing of the gelator molecules [201]. The XRD profiles of the developed gels showed that the ratios were nearly 1:1, 2:1 and 3:1, respectively. This type of arrangement supports the layered packing of the stearic acid molecules in the organogels [201]. During the preparation of the gels, there is a possibility of the incorporation of the vegetable oils within the layers of stearic acid molecules. Association of the vegetable oils within the layers of stearic acid has been reported to affect the crystallite size of stearic acid. Based on the peak width, average crystallite size (D) was calculated using Debey-Scherrer equation (equation 4.2 in chapter 4).

The estimation and comparison of the average crystallite size was done using the peak at 21.37º 2θ. Addition of oil resulted in the distinct variation of the crystallite sizes of stearic acid (Table 6.3). Decrease in the crystallite size of the gelator molecules leads to the increase in the amorphousity (or decrease in the crystallinity) of the organogels and vice versa [136]. The amorphous peak (19.5º 2θ) associated with the XRD profiles of the organogels was due to the presence of liquid triacylglycerols in sesame oil and soy bean oil [202]. The crystallite size values suggested that the organogels with lower proportions of stearic acid were having lowest crystallinity. This was attributed to the interactions amongst the stearic acid and the

solvents. Presence of oil prevents the crystal growth of stearic acid [203]. This resulted in the formation of short stearic acid fibers in the organogels with higher proportions of oils and vice versa. During the formation of the organogels, the branching of the gelator fibers occurred at the tip and/or the side faces of the gelator fibers (Figure 6.3f). Addition of new crystal layers (layered/lamellar arrangement) during crystal growth lead to the structural mismatch with the crystallographic orientation of the parent fiber. This crystallographic mismatch branching (CMB) was responsible for the splitting of growing fibers. In the nucleation-growth mechanism (as predicted earlier), growth was favored by CMB. One-dimensional growth of fibers is favored when the CMB is very high, which in turn, is associated with the high degree of supersaturation of the gelator [197].

The possible chemical interactions for the lamellar arrangement of the stearic acid molecules were explained by the FTIR studies. FTIR spectrum of stearic acid showed its characteristic bands at about 1,710 and 940 cm^{-1} (Figure 6.4). The bands at 1,710 cm^{-1} and 940 cm^{-1} were due to the stretching vibration of carbonyl group and bending vibrations of hydrogen bond (OH-H) involving carboxylic acid, respectively [204]. The characteristic peaks of stearic acid were retained in the FTIR spectra of the organogels. These peaks were shifted towards lower wave number in the organogels. This may be due to the involvement of the carboxylic group of stearic acid in the non-covalent interactions (hydrogen bonding) during gelation [205]. Fatty acids present in sesame oil and soy bean oil have been involved in the formation of hydrogen bonds with the stearic acid molecules. This resulted in the incorporation of the vegetable oils within the lamellar structure of the stearic acid. Coexistence of stearic acid molecules and vegetable oils resulted in the change in the molecular packing of the stearic acid in the organogels. Ciprofloxacin showed characteristic bands at 1,610 and 1,260 cm^{-1} due to the stretching vibration of the phenyl network conjugated to –COOH and of C-F bond, respectively [206]. The bands of ciprofloxacin were subsided by the bands of the gel components.

6.3.4. Thermal studies

Melting and crystallization behavior of stearic acid and organogels was tested below 100 ºC. This was done to avoid sublimation of stearic acid. The melting and crystallization events in organogels were observed in broad temperature ranges as compared to pure stearic acid (Figure 6.5). The occurrence of phase change in the broad temperature range suggested that the sol-to-gel and gel-to-sol transitions were not an instantaneous process but a continuous process. The $T_{onset,m}$ (melting onset temperature), T_m (melting temperature), $T_{onset,c}$

(crystallization onset temperature), T_c (crystallization temperature), ΔH_m (melting enthalpy) and ΔH_c (crystallization enthalpy) of the organogels and stearic acid were tabulated in Table 6.4. Enthalpy changes involved during the thermal events was measured by integrating the area under the curve. The onset temperatures and change in the enthalpies associated with the organogels were found to be less than the pure stearic acid (Table 6.4).

In general, the melting endotherm is a combination of two events, i.e. fiber melting and dissolution of the fibers. The effect of the gelator concentration during phase change was studied using Schroder-Van Laar equation [207].

$$\ln\left[X_g\right] = \Delta H_g / RT \qquad (6.1)$$

where, X_g is the mole fraction of gelator in organogels; ΔH_g is the enthalpy involved due to phase change of stearic acid during melting; R is the universal gas constant and T is the melting temperature.

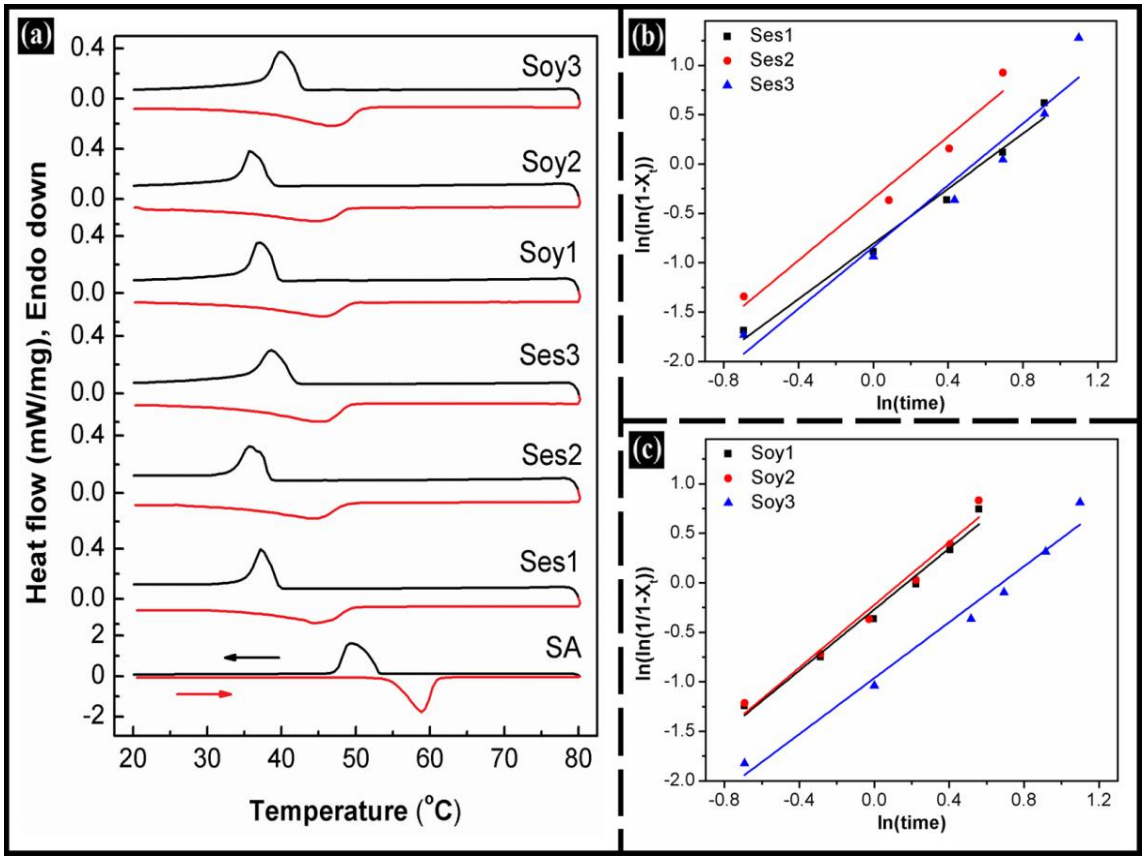

Figure 6.5: (a) DSC thermogrms of SA and organogels (arrow in red indicates heating and arrow in black indicates cooling); (b) and (c) are the Fitting curves of the Avrami equation.

The change in the enthalpies (ΔH_g) was found to be higher in organogels with the increase in the concentration of the stearic acid (Table 6.4). The change in the enthalpies due to the gelator melting was found to be less than the total enthalpy of the melting process. The excess heat involved during the phase change might have contributed to the dissolution of the fibers. This suggested that the fiber melting and the dissolution of the fibers into the solvent occurred in tandem, which in turn, resulted in the formation of broad endothermic peaks.

Microscopic studies suggested that the fiber formation/crystallization in organogels was a 2-step process, i.e. nucleation and crystal growth. Crystallization at the nucleation site was driven by the non-covalent interactions amongst the stearic acid molecules and the stearic acid–vegetable oil molecules. This allowed the system to attain a low energy-state by releasing heat (exothermic reaction). The released heat was calculated as the crystallization enthalpy of the reaction (Table 6.4). This driving force was countered by the entropic forces associated with the phase separation/demixing of the gelator fibers from the homogeneous solution. The change in the entropies during the crystallization events was calculated by using the following equation:

$$\Delta G = \Delta H_c - T_c \Delta S \qquad (6.2)$$

where, ΔG and ΔS are the Gibb's free energy and change in entropy involved during crystallization.

Table 6.4: Thermal properties obtained by DSC studies.

Sample	Melting, Endotherm				Crystallization, Exotherm			
	$T_{onset,m}$ (°C)	T_m (°C)	ΔH_m (J/g)	ΔH_g (J/g)	$T_{onset,c}$ (°C)	T_c (°C)	ΔH_c (J/g)	ΔS (J/g/K)
SA	55.0	58.8	863.55	--	53.2	49.4	863.55	17.48
Ses1	35.0	44.5	65.24	33.77	39.6	35.9	236.92	1.82
Ses2	35.1	44.6	71.55	29.31	38.4	37.3	245.29	1.92
Ses3	36.7	45.2	106.32	34.16	41.9	38.6	253.08	2.75
Soy1	34.9	44.5	55.0	28.85	38.5	35.6	226.45	1.54
Soy2	35.5	44.4	62.58	26.71	38.5	35.7	251.92	1.75
Soy3	37.0	46.7	107.35	28.23	42.8	39.9	374.32	2.69

ΔG tends to be zero at the crystallization temperature. The change in the entropies was calculated at the crystallization temperature (Table 6.4) [208]. The change in entropy is due to the crystal-solvent interfacial tension and forms a key parameter for the nucleus formation

during crystallization [209]. The loss of entropy was found to be higher in the organogels having higher proportions of stearic acid. Hence, the organogels with higher proportions of stearic acid lead to the formation of organogels with higher thermodynamic stability. Increase in the loss of entropy indicated a reduction in the crystal-solvent interfacial tension. In other words, the crystal-solvent interfacial tension was decreased with the increase in the concentration of the stearic acid.

The results suggested that the rearrangement of the stearic acid molecules happened to minimize the interactions amongst the polar head groups of the stearic acid and the apolar groups of the vegetable oil. The minimal interfacial interactions lead to the decrease in the interfacial tension and hence resulted in the formation of a stable nucleus. This explained the thermodynamic stability of the organogels with higher proportions of stearic acid. The possible orientation of stearic acid molecules within the organogels has been shown in Figure 6.6. The polar head groups of stearic acid molecules interact via intermolecular hydrogen bonding (as predicted in FTIR studies). This minimizes the interfacial tension by hiding the polar groups and exposing the hydrophobic tails to the vegetable oils. This orientation resulted in bilayered arrangement of stearic acid molecules during the formation of gelator fibers. Layered arrangement of stearic acid molecules was confirmed by the XRD studies.

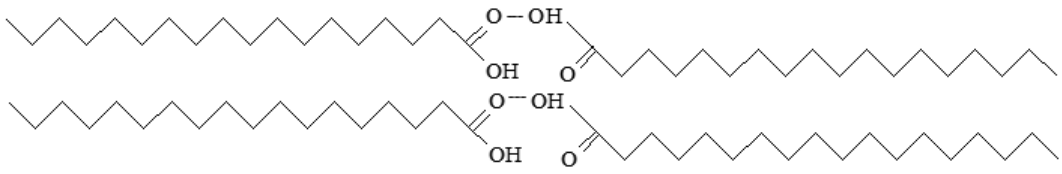

Figure 6.6: Schematic sketch of the possible orientation of stearic acid molecules in the organogels.

Crystallization studies

Table 6.5: Crystallization kinetics of organogels.

Sample	**Avrami analysis**			**% crystallinity**
	n	**K, (s^{-1})**	**R^2**	
Ses1	1.396	0.984	0.981	7.55
Ses2	1.568	0.969	0.969	8.28
Ses3	1.563	0.948	0.95	12.31
Soy1	1.541	0.981	0.981	6.37
Soy2	1.583	0.977	0.975	7.25
Soy3	1.611	0.975	0.97	12.43

Gelation/crystallization kinetics of the organogels was evaluated by Avrami equation (equation 4.4 in chapter 4). Avrami exponents were obtained from the slopes of the Avrami plots (Figure 6.5, Table 6.5). The exponent values were non-integer values and were in between 1 and 2. This indicated that the nucleation followed first-order kinetics and the fiber formation happened in a linear fashion [210]. In this kind of nucleation mechanism, nucleation of the fibers does not occur instantaneously but occurs throughout the gelation process. This kind of nucleation is called heterogeneous or simultaneous nucleation [200]. Heterogeneous nucleation in the prepared organogels can be visualized in the Figure 6.3h. The n value was higher in the organogels with higher concentration of stearic acid (Table 6.5). The change in the n value suggested a change in the order of the crystal growth. A n value nearer to 2.0, suggest that the crystallization process might be approaching towards two-dimensional growth of the stearic acid fibers. Change in the order of the crystal growth may be associated with the secondary crystallization process occurring during the crystal growth. The fractional n values indicate that the secondary crystallization must have occurred by heterogeneous nucleation process during gelation. Existence of secondary crystallization during gelation can also be proved by observing the regression coefficient (R^2) values of Avrami plots (Table 6.5) [200]. The R^2 values were found to be decreasing with the increase in the concentration of stearic acid. In general, Avrami equation is limited to low degrees of crystallinity. At high concentration of stearic acid, impringement of crystals with one another and/or secondary crystallization will affect the crystallization kinetics (Avrami equation). Secondary crystallization of the gelators must have occurred during the gelation, as was evident from the fractional n values. The decrease in the R^2 values with the increase in the concentration of the stearic acid indicated that the secondary crystallization was regulated by the change in the concentration of the gelator. Avrami analysis indicated a change in the order of crystallization during crystal growth. Hence, it can be inferred that there are high chances of secondary crystallization during gelation. Since the crystal growth took place at different crystal layers, the occurrence in the structural mismatch lead to the crystallographic mismatch and subsequent branching. This kind of branching leads to splitting of fibers and results in irregular shaped fibers. The non-integer Avrami exponent values also indicated the existence of irregular shaped crystals.

Based on the organogelation kinetics, XRD, DSC and FTIR studies, the mechanism of gelation of stearic acid in vegetable oil organogels was predicted. During gelation, heterogeneous nucleation was associated with one dimensional crystal growth and followed

by splitting of fibers due to CMB. The stearic acid molecules arrange themselves as bilayers to reduce the interfacial tension during fiber growth. Finally, the entanglement of the irregularly shaped fibers leads to the formation of the gelator network.

6.3.5. Mechanical analysis

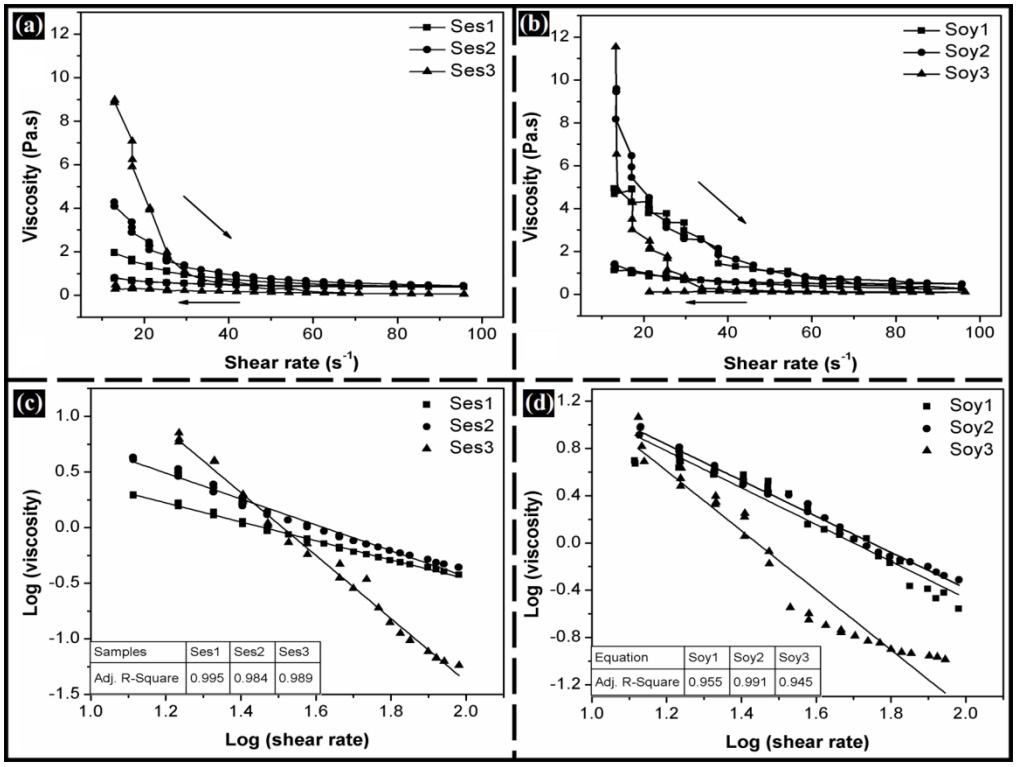

Figure 6.7: Viscosity studies of organogels: (a, b) Viscosity curves and (c,d) modified power law fitting curves.

The mechanical analyses of the gels were done by small scale deformation (viscosity measurement) and large scale deformation (stress relaxation and spreadability using dynamic mechanical tester) studies. During small scale deformation studies, the flow behavior of the organogels was predicted by applying a cyclic shear rate in the range of 10 s^{-1} to 95 s^{-1}. The initial apparent viscosity of Ses3 and Soy3 were found to be higher than the other gels (Figure 6.7a and 6.7b). With the increase in the gelator concentration, there was an increase in viscosity of the organogels thereby indicating the formation of stronger organogels. There was an exponential decrease in the viscosity of the organogels when the shear rate was increased. When the shear rate was reduced, there was an incomplete structural reversal resulting in the formation of an open hysteresis loop. Presence of hysteresis is a common feature in gels [179]. 100 % recovery of the initial apparent viscosity was not achieved in any of the organogels and may be associated to the complete disruption of the gel architecture.

The results have suggested that the apparent viscosities of the organogels were reduced with the increase in the shear rate and vice versa. This indicated shear thinning behavior of the organogels. The non-Newtonian behavior of the organogels was confirmed by fitting obtained data in the modified power law equation [211].

$$\tau = K.\gamma^{m-1} \qquad (6.3)$$

where, τ is the shear stress (Pa) at γ shear rate (s^{-1}); K is the flow consistency index (Pa.s), and m is the flow behavior index.

The flow behaviour indices (Table 6.5) of the organogels were found to be < 1, suggesting the pseudoplastic nature of the organogels [211]. The K value (Table 6.5) suggested that the organogels with higher proportions of stearic acid have higher consistency. Amongst the sesame oil and soy bean oil organogels, apparent viscosity and consistency of the soy bean oil organogels was higher.

Cyclic uni-axial compression test showed that hardness, adhesiveness and gumminess of the organogels increased with the increase in stearic acid concentration (Table 6.6). On the other hand, cohesiveness was decreased. The same trend was followed in both the kind of organogels. Increase in hardness may also be regarded as firmness (F_0) and higher firmness was observed for Ses3 and Soy3 organogels during stress relaxation studies. In general, organogels have been described as viscoelastic semisolids. The viscoelastic nature of the organogels was confirmed by stress relaxation studies (Figure 6.8). The stress relaxation profiles of the organogels were closely related to the stress relaxation profiles of viscoelastic solids [149]. During relaxation, when the strain was kept constant, the recorded force decreased quickly and reached a near constant asymptotic value. This value is called residual force or resistance encountered by the elastic part of the material [212]. Ses3 and Soy3 have shown higher gel strength as initial force and residual force were found to be higher than the others.

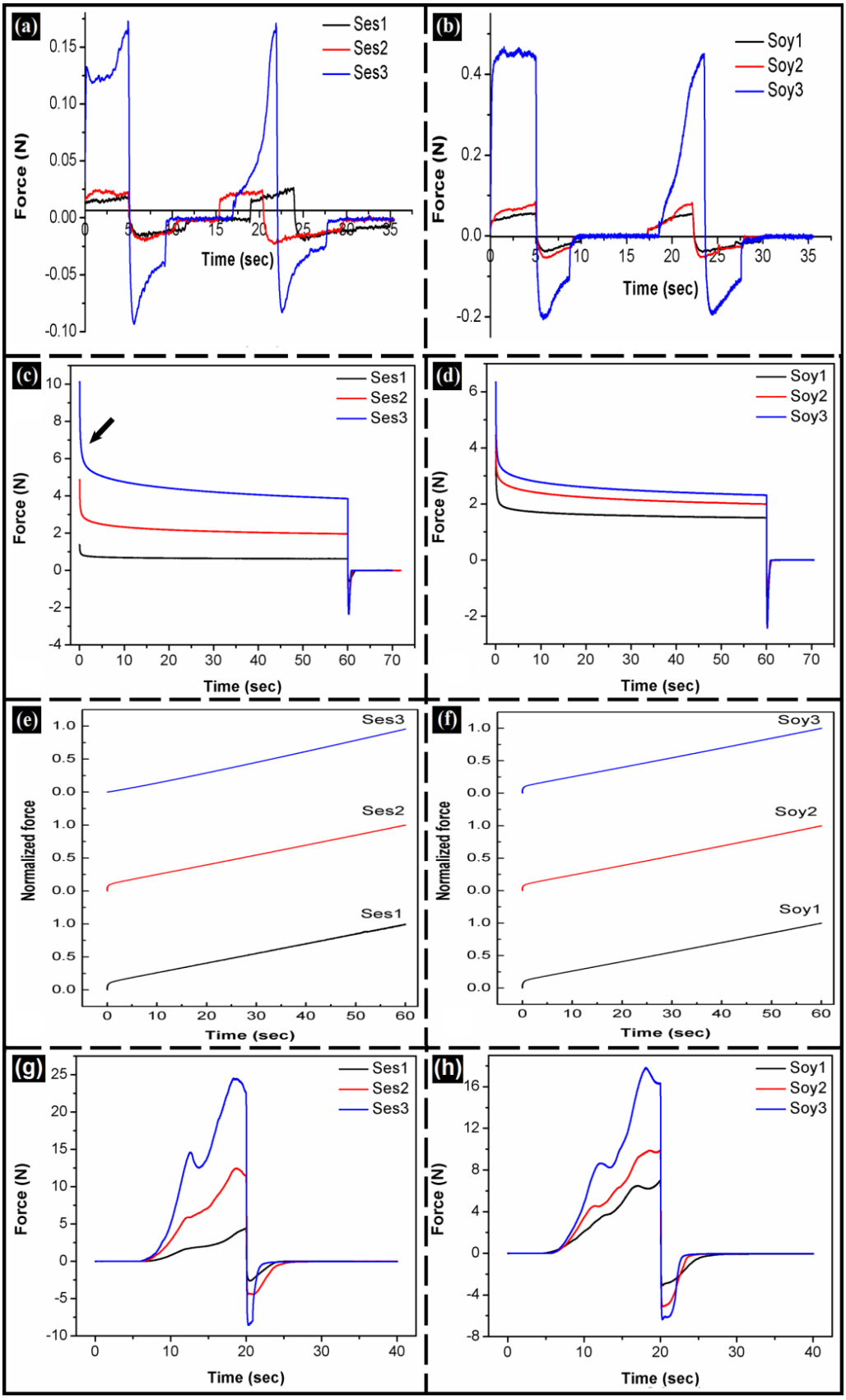

Figure 6.8: Mechanical studies of organogels: (a, b) Stress relaxation studies, (c, d) Fitting curves (Modified Peleg's equation), and (e, f) Spreadability studies.

Table 6.6: Mechanical properties of organogels.

Sample	Hardness (N)	Cohesiveness	Adhesiveness (N.sec)	Gumminess (N)
Ses1	0.019	1.251	0.083	0.022
Ses2	0.024	0.955	0.089	0.022
Ses3	0.167	0.489	0.241	0.082
Soy1	0.061	0.815	0.123	0.049
Soy2	0.084	0.727	0.157	0.061
Soy3	0.468	0.550	0.560	0.257

The stress relaxation profiles followed an exponential decaying function. The force decay of the curve with respect to time (F(t)) of the organogels was analyzed by fitting the data in modified Peleg's equation (Equation 4.6 of chapter 4). Curve fitting ($R^2 > 0.995$) of the normalized stress relaxation data using modified Peleg's equation was shown in Figure 6.8 and the fitting parameters have been tabulated in Table 6.7. The initial rate of the relaxation (k_1) was lower in the organogels with higher proportions of stearic acid. The extent of the relaxation (k_2) of the organogels was almost equal. k_1 mainly illustrates the distribution of force decay rates and does not represent the whole stress relaxation curve. k_2 is the overall slope of the normalized stress relaxation data during modified Peleg's analysis. The slope of the modified Peleg's fitting curve was strongly influenced by the asymptotic residual force (F_r). Due to the above reasons, k_2 is a good parameter to estimate the complete relaxation behavior of the organogels. But the fitting analysis indicated that k_2 values were ambiguous and very near to each other. Analysis using modified Peleg's equation is efficient in identifying the relaxation behavior but it is unable to quantify the viscoelastic properties of the organogels. To quantify the viscoelastic properties, asymptotic residual value in the normalized stress relaxation curve (F^*) and the area under the normalized stress relaxation curve (S^*) are calculated [149].

$$F^* = \frac{F_r}{F_0} \qquad (6.4)$$

$$S = \int_a^b F(t).dt \qquad (6.5)$$

$$S_0 = \left(\frac{S}{b-a} \right) a \qquad (6.6)$$

$$S^* = \frac{S}{S_0} \qquad (6.7)$$

where, 'a' and 'b' are the lower and upper limits of the time, respectively.

Area under the curve (S) is a simple and sensitive estimator of the changes in the relaxation behavior of materials. For viscoelastic materials S^* varies in the range of 0-1. Materials with greater elastic-like behavior possesses S^* close to 1.0. In the present study, the area under the curves was found to be > 0.5. This indicated that the organogels were viscoelastic semi-solid in nature. The organogels with higher stearic acid concentration showed higher S^* values, which indicated higher elastic strength of the organogels as compared to the organogels with lower concentration of stearic acid. The crosslinking density of the organogels might have contributed to the differences in the viscoelastic properties of the organogels.

Table 6.7: Mechanical parameters of organogels.

Samples	**F_0 (N)**	**F_r (N)**	**k_1**	**k_2**	**S^***	**F^***	**% relaxation**	**Spreadability $(N.sec)^{-1}$**
Ses1	1.373	0.628	0.111	0.014	0.857	0.457	4.017	4E-2
Ses2	4.866	1.959	0.097	0.015	0.859	0.403	13.16	1.1E-2
Ses3	10.12	3.564	0.025	0.016	0.864	0.352	26.49	0.5E-2
Soy1	3.849	1.504	0.112	0.014	0.858	0.390	9.828	1.9E-2
Soy2	4.455	1.993	0.086	0.015	0.859	0.387	13.44	1.3E-2
Soy3	6.351	2.313	0.101	0.014	0.861	0.364	15.63	0.8E-2

The modified Peleg's analysis and the calculated parameters (F^* and S^*) suggested that the relaxation behavior of the organogels was dependent on the gelator concentration. The difference in the relaxation behavior of the organogels can be attributed to the crosslinking density of the stearic acid in the organogels. Higher crosslinking density in the Ses3 and Soy3 organogels may be associated with the higher intermolecular hydrogen bonding (predicted in FTIR studies) amongst the stearic acid and the vegetable oil molecules. Application of the force resulted in the breakage of the hydrogen bonds amongst the gelator molecules. Disruption of the hydrogen bonds lead to the sudden decrease in the stress applied upon the gels (denoted by arrow in Figure 6.8a). The rate of decay was higher in Ses3/Soy3, followed

by Ses2/Soy2 and Ses1/Soy1. The rate of decay was also dependent on the gelator concentration. Since the hydrogen bonding was more pronounced in Ses3 and Soy3 than the other gels, disruption of bonds resulted in the greater decay of the applied stress. Force induced unbinding lead to the local gelator network rearrangement in the organogels. Interestingly though the hydrogen bonds were disrupted, the gelator network retained its elasticity even under plastic flow conditions. This has lead to the availability of residual stress at the end of relaxation. More amount of residual stress was retained in the organogels with higher gelator concentration. Retaining of residual stress was due to the formation of new hydrogen bonds amongst the gelator molecules during relaxation [213]. This suggests that the hydrogen bond disruption due to the application of stress is subsequently associated with the formation of new bonds. The coexistence of bond dissipation and the elastic recovery due to the formation of new bonds is possible if the gelator molecule can readily undergo crosslinking [213]. Based on the stress relaxation studies, the relaxation behavior of the organogels can be ranked as Ses3 > Ses2 > Ses1 and Soy3 > Soy2 > Soy1.

The ranking of the relaxation behavior was also predicted by calculating the % relaxation. % relaxation was calculated using equation 6.8 [214].

$$\%\ relaxation = \left(\frac{F_0 - F_r}{F_0} \right) * 100 \qquad (6.8)$$

% relaxation indicated that the relaxation was higher in oleogels with higher proportions of stearic acid. % relaxation information further confirmed the viscoelastic nature of the oleogels.

The spreadable nature of the organogels was checked and shown in Figure 6.8e and 6.8f. Spreadability of Ses3 and Soy3 was very low, i.e. a very high force was needed to spread the gels. Gels with lower concentration of stearic acid showed better spreadability. The spreadability of the organogels was predicted by calculating the inverse of the area under the positive curve (Table 6.7). Lower spreadability of Ses3 and Soy3 may be associated with the higher elastic nature of the organogels (confirmed by stress relaxation studies) as compared to the others. The mechanical parameters followed a similar trend for both sesame oil and soy bean oil organogels. The results only varied quantitatively. This was due to the gelator-solvent interactions.

6.3.6. *In vitro* drug delivery studies

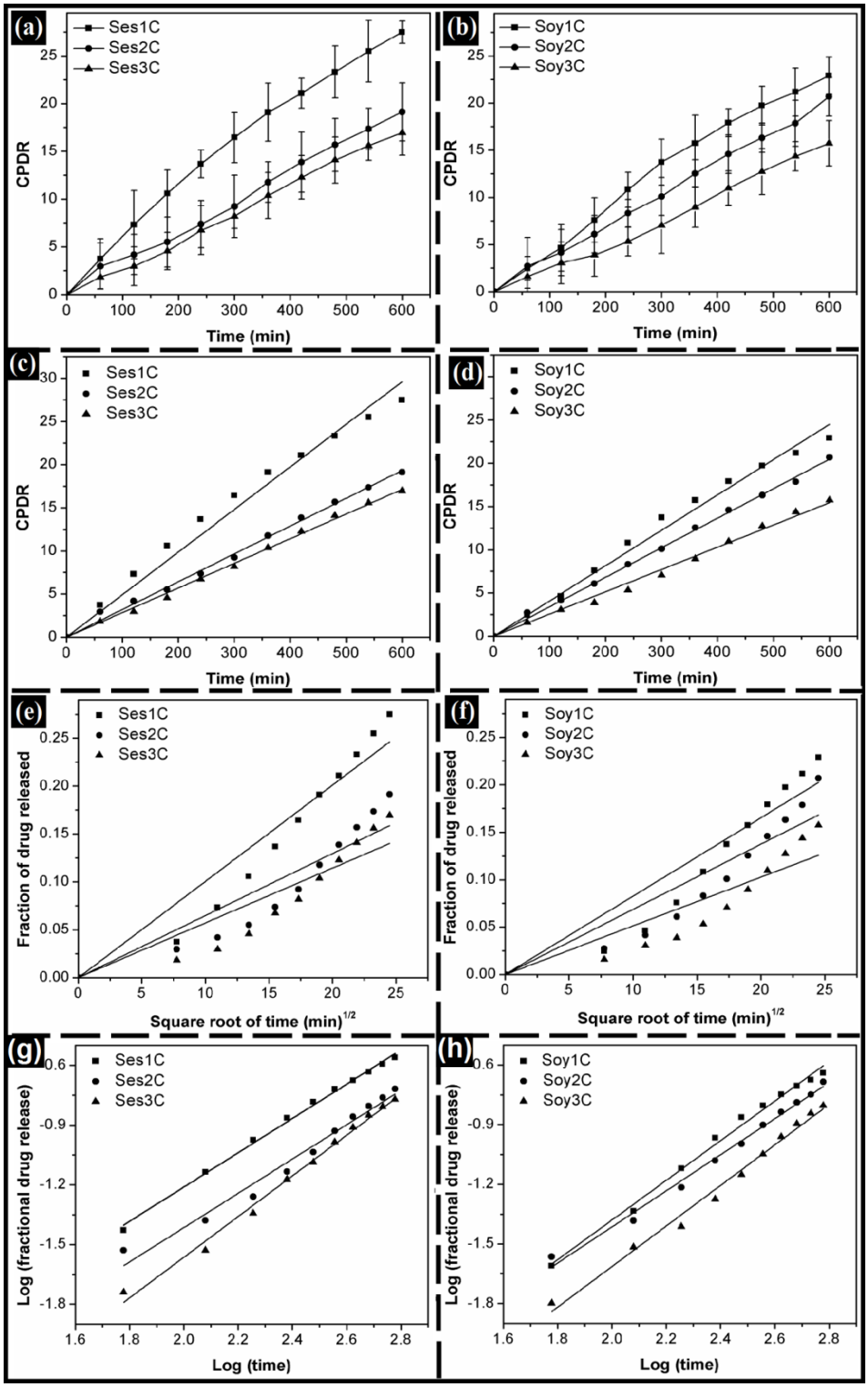

Figure 6.9: Drug release kinetics from the organogels: (a, b) CPDR vs. time; (c, d) Zero order, (e, f) Higuchi model, and (g, h) KP model.

The CPDR was higher in the gels with lower proportions of stearic acid (Figure 6.9). Presence of dense network of gelator fibers in organogels with higher stearic acid

concentration might have prevented the movement of the drug molecules. The drug release from the organogels followed zero-order kinetics ($R^2 > 0.95$) (Table 6.8). Traditionally, zero-order kinetics is followed by poorly water-soluble drugs [150]. The slope (n) or Fickian value (KP kinetics) was found to be in between 0.45 and 0.89 for Ses1C, suggesting non-Fickian diffusion [150]. In general, non-Fickian diffusion is followed when the release mechanism is not well known or when more than one mechanism is involved. The 'n' value was found to be 0.89 for Ses2C and Soy1C, suggesting case-II diffusion transport mechanism [150]. The n value for Soy2C is near 0.89, which can be considered as case-II transportation of drugs. Case-II transport mechanism has been associated with the zero order release, i.e. time independent release of the drugs [150]. Fickian value exceeded 1.0 in Ses3C and Soy3C, indicating super case-II transport of drugs.

Table 6.8: Drug release kinetics from the organogels.

Samples	**Zero order (R^2)**	**Higuchi (R^2)**	**Best fit**	**KP model**	
				n	**Type of flow**
Ses1C	0.97	0.93	Zero order	0.86	Non-Fickian
Ses2C	0.99	0.87	Zero order	0.89	Case-II transport
Ses3C	0.99	0.90	Zero order	1.02	Super case-II transport
Soy1C	0.97	0.93	Zero order	0.89	Case-II transport
Soy2C	0.99	0.87	Zero order	0.91	Case-II transport
Soy3C	0.99	0.82	Zero order	1.02	Super case-II transport

The release of the drug in its active form was checked by performing antimicrobial studies. Presence of clear zones around the wells of the drug loaded organogels indicated that ciprofloxacin was released in its active form (Figure 6.10). Higher drug release from Ses1C and Soy1C resulted in larger zone of inhibition. The antimicrobial efficiency of the drug loaded organogels was much better than the Ciplox® formulation. This may be due to the sustained release of the drug from the organogels over a prolonged period of time. The *in vitro* release studies suggested that the release of the drugs can be controlled by tailoring the concentration of stearic acid in the organogels.

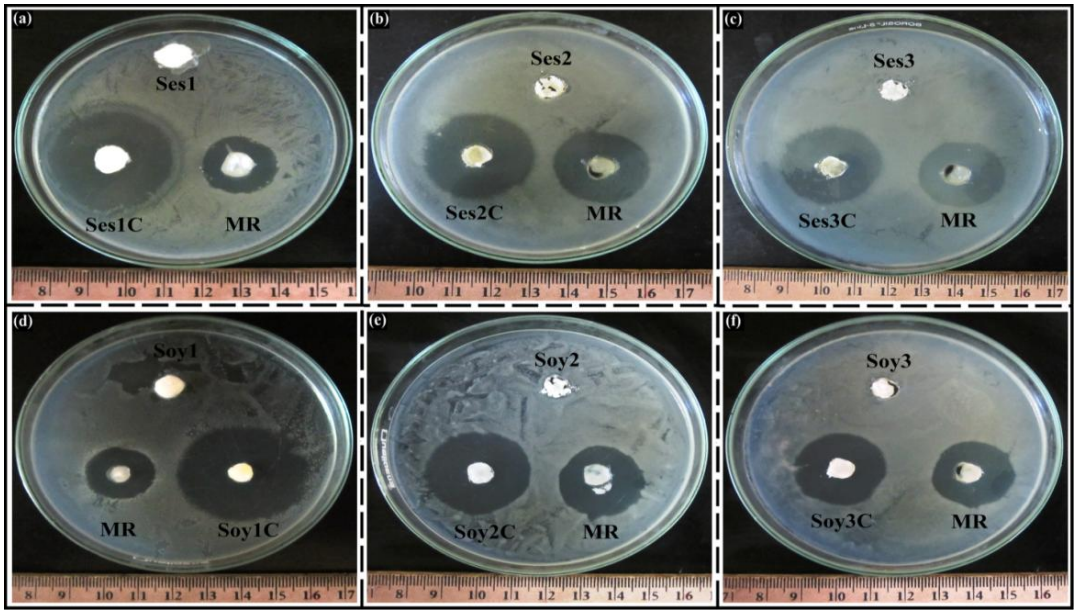

Figure 6.10: Antimicrobial studies of organogels against *E. coli*.

6.4. Conclusion

Stearic acid was able to induce gelation of sesame oil and soy bean oil. The CGC for both the oils was different and was attributed to the differences in the chemical composition of the oils. The gelator-solvent interactions have significantly influenced the gelation and viscoelastic properties of the organogels. The physicochemical properties of the organogels were altered as the compositions of the organogels were changed. Gel kinetics, XRD and thermal analyses indicated that the formation of organogels was accompanied with the heterogeneous nucleation coupled with one-dimensional growth of the gelator fibers. The predicted gelation mechanism in stearic acid-edible oil organogels was via nucleation-CMB-crystal growth-nucleation-. The *in vitro* drug release studies have suggested that the developed organogels may be tried as topical controlled drug delivery vehicles.

Part B: Encapsulation of stearate organogels in alginate microparticles

Overview:

Alginate microparticles were synthesized by encapsulating sesame oil and soy bean oil organogels with 22 % (w/w) stearic acid concentration (core) by ionotropic gelation method. Vegetable oil (sesame oil and soy bean oil) containing microparticles were used as the controls. Confocal microscopic studies showed the existence of distinct shell material around the organogel core. This was confirmed by XRD and DSC analyses. Control microparticles showed leaching, whereas, organogel containing microparticles did not show any leaching. Semi-solid nature of organogels prevented the leaching internal phase which in turn improved the drug encapsulation efficiency of microparticles (ciprofloxacin was used as the model drug). *In vitro* drug release studies showed the controlled release of ciprofloxacin from the organogel containing microparticles with significant antimicrobial activity against *E. coli*. Further, microparticles showed good mucoadhesivity and cytocompatibility against goat small intestine and mammalian L929 fibroblast cells, respectively.

6.5. Introduction

Stearic acid-based sesame oil and soy bean oil organogels are tried to encapsulate within the alginate microparticles. These oils have antioxidant properties which may improve the shelf-life of the formulations. Oral consumption of stearic acid has been reported to lower the LDL cholesterol [215]. These health benefits of microparticulate components will help improving the efficiency of the formulations. Ciprofloxacin (CFX) was chosen as the model drug to study the drug release kinetics from the developed microparticles. It is a 2^{nd} generation fluoroquinolone antibiotic with broad spectrum of activity against bacterial infections *viz.*, urinary tract, gastrointestinal, abdomen and respiratory infections [216]. The drug has been recommended to treat the infections especially caused by Gram negative bacteria. In this regard, antimicrobial efficiency of the developed formulations was tested against *E. coli*. In general, systemic administration of ciprofloxacin is being done via oral (tablets or suspension) or intravenous (solution) routes. In oral drug delivery, for the immediate release, ciprofloxacin hydrochloride salt and for the extended release, ciprofloxacin base have been employed. Since attempts were made to design controlled release dosage forms, ciprofloxacin base was chosen. Ciprofloxacin therapy often includes nausea (2.5% of patients) and vomiting (1% of patients) [217]. These problems can be overcome by taste masking the antibiotic via the developed microparticles.

In nut shell, this chapter describes the synthesis and characterization of alginate-based microparticles containing organogels as the internal phase (core). Sesame oil and soy bean oil containing microparticles were used as controls.

6.6. Materials and methods

Stearate organogels were prepared as per the protocol described in section 3.2.3 of chapter 3. Ses2 and Soy2 were chosen for the encapsulation studies and they were labeled as OG1 and OG2, respectively. 2.5 g of OG1/OG2 or sesame oil/soy bean oil were encapsulated within the microparticles as mentioned in section 3.2.5 of chapter 3. Sesame oil and soy bean oil containing microparticles served as the controls for OG1 and OG2 containing microparticles, respectively. Bright field microscopy, SEM, confocal microscopy, XRD, FTIR, DSC, biocompatibility studies, mucoadhesivity studies, *in vitro* drug delivery studies and antimicrobial studies were conducted as per the methods described in section 3.3 of chapter 3.

6.7. Results and discussion

6.7.1. Preparation of organogels

Stable organogels were prepared and the composition was given in Table 6.9. The mechanism of organogel formation has been explained in part A of this chapter.

Table 6.9: Composition of the organogels.

Sample	Stearic acid (% w/w)	Sesame oil (% w/w)	Soy bean oil (% w/w)	Ciprofloxacin (% w/w)
OG1	22.0	88.0	--	--
OG2	22.0	--	88.0	--
OG1C	22.0	87.5	--	0.5
OG2C	22.0	--	87.5	0.5

6.7.2. Preparation of the microparticles

Stable microparticles were formed when organogels and vegetable oils were used as the internal phases. Table 6.10 illustrates the composition of the microparticles.

Table 6.10: Composition of the microparticles.

Sample	Internal phase	Ciprofloxacin (% w/w)
MSes	Sesame oil	--
MSoy	Soybean oil	--
MOG1	OG1	--
MOG2	OG2	--
MSesC	Sesame oil + CFX	0.5
MSoyC	Soybean oil + CFX	0.5
MOG1C	OG1 + CFX	0.5
MOG2C	OG2 + CFX	0.5

6.7.3. Microscopy

The structural analysis of the microparticles was investigated in detailed by different microscopic techniques. BFM images of MSes, MSoy showed droplets as the internal phase, whereas, MOG1 and MOG2 are opaque in nature (Figure 6.11a-d). Micrographs suggested the formation of spherical microparticles. The size distribution analysis of the microparticles suggested a broad size distribution profile for the vegetable oil containing microparticles, whereas, organogel containing microparticles showed a narrow size distribution profile

(Figure 6.12a). The average diameter (D_{avg}) of the microparticles was calculated as the size of the 50% of the total microparticles population (shown as dotted lines in Figure 6.12b). The average diameter of the organogel containing microparticles was higher (MOG1: 210.24 ± 5.8 µm; MOG2: 226.10 ± 4.7 µm) than the vegetable oil (MSes: 130.52 ± 3.5 µm; MSoy: 178 ± 3.8 µm) containing microparticles. Increase in the sizes of the organogel containing microparticles was due to the higher viscosity of the organogels. Due to this reason, large droplets of primary emulsion were formed during the formation of the multiple emulsions when organogels were used as the internal phase.

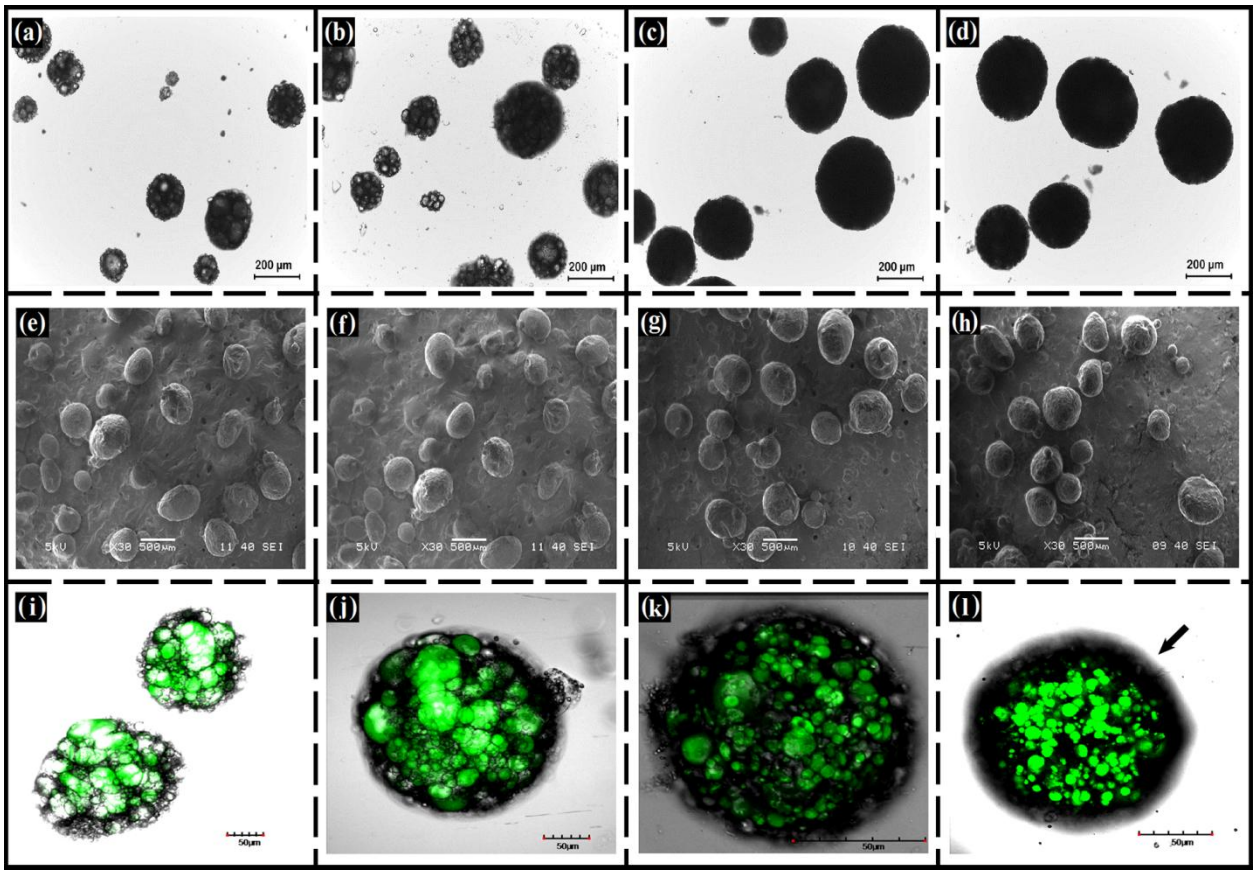

Figure 6.11: BFM images (size bar: 200 µm) of: (a) MSes, (b) MSoy, (c) MOG1, and (d) MOG2; SEM images (size bar: 500 µm) of: (e) MSes, (f) MSoy, (g) MOG1, and (h) MOG2; and confocal images (size bar: 50 µm) of: (i) MSes, (j) MSoy, (k) MOG1, and (l) MOG2.

The scanning electron micrographs showed that the microparticles were spherical in nature and had a smooth surface after drying (Figure 6.11e-h). The organogel entrapped microparticles were nearly spherical, whereas, the spherical nature of the oil containing microparticles was lost to a great extent. This can be explained by the physical nature of the internal phase of the microparticles. The presence of semi-solid organogels within the core

prevented deformation of the microparticle architecture during drying. On the other hand, the vegetable oils were not able to resist the inward force of the alginate layer when the microparticles were dried. This resulted in the formation of the deformed structures.

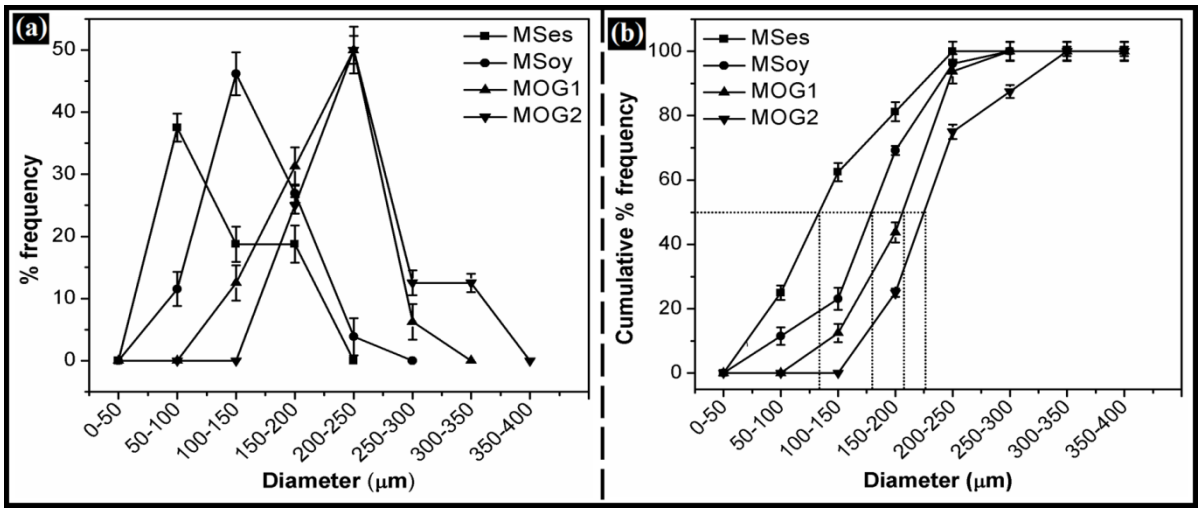

Figure 6.12: Size distribution analysis of the microparticles: (a) % frequency and (b) Cumulative % frequency.

The internal structure of the microparticles was investigated using confocal micrographs. Confocal images of MSes and MSoy showed the presence of oil globules (green in color) in different sizes (Figure 6.11i and 6.11j). On the other hand, MOG1 and MOG2 have shown homogeneous globular structures of uniform sizes of the internal phase (Figure 6.11k and 6.11l). The difference can be attributed to the structuring of oils by the gelator (stearic acid) molecules in MOG1 and MOG2 [218]. Some of the oil globules in MSes and MSoy seemed to be closer to the alginate boundary layer. This kind of microstructure may promote leaching of the internal phase oil. On the other hand, MOG1 and MOG2 showed globular structures uniformly surrounded by an alginate layer. This kind of encapsulated structure is preferred to prevent the leaching so as to enhance the encapsulation efficiency. Confocal images of MOG1 and MOG2 showed the presence of the black alginate layer surrounding the internal phase (indicated by an arrow). Encapsulation of the organogels within the alginate microparticles was further confirmed by thermal (DSC) studies.

6.7.4. Leaching studies

The results of the leaching studies (filter paper method) indicated that the vegetable oil containing microparticles showed extensive leaching of the internal phase (marked by the formation of a dark zone) from the dried microparticles as against the organogel containing microparticles (Figure 6.13a and 6.13b). This may be accounted to the porous nature of the

alginate microparticles [151]. The dark zone was not observed for the organogel containing microparticles (Figure 6.13c and 6.13d). Absence of leaching from the organogel containing microparticles can be attributed to the gelation of the vegetable oils using stearic acid; due to which apparent viscosity of the oils was increased. This in turn, prevented the leaching of the internal phase due to the immobilization of the oil within the fibrous matrix of stearic acid.

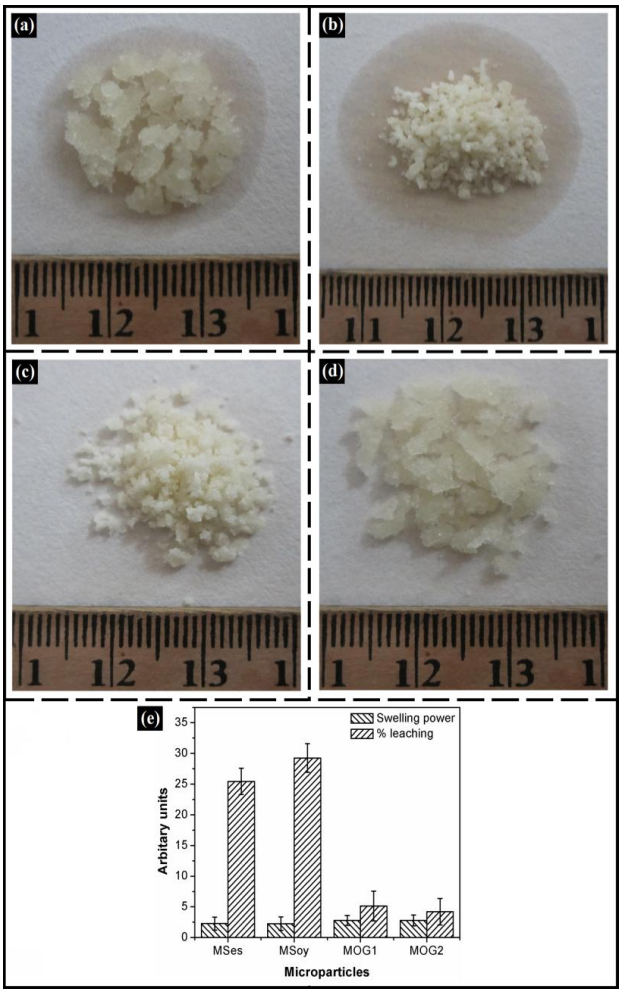

Figure 6.13: Leaching studies: (a) MSes, (b) MSoy, (c) MOG1, and (d) MOG2; and bar graphs showing the (e) Swelling power, and % leaching of the microparticles.

The leaching of the internal phase was quantified by incubating the microparticles in phosphate buffer (pH 7.4) (Figure 6.13e). The studies indicated higher leaching of the internal phase from the vegetable oil containing microparticles (> 25 %) as compared to the organogel containing microparticles which showed much lower leaching (~5 %). The results were significantly different ($p < 0.05$) and supported the observation of the qualitative leaching studies. The swelling power of the microparticles was in the range 2.0 -2.7. Though not much difference was observed in the swelling power of the microparticles, organogel

containing microparticles have shown slightly higher swelling power (Figure 6.13e). This may be accounted to the ability of the fatty acid organogels to accommodate water within their architecture [219]. But the back pressure created by the alginate layer on to the internal phase might have been a limiting factor for the organogels to accommodate higher proportions of water molecules within them.

6.7.5. Drug encapsulation efficiency

Drug encapsulation efficiency of the organogel containing microparticles (MOG1C: 77.0 ± 2.9, MOG2C: 82.0 ± 2.5) was much higher as compared to the vegetable oil containing microparticles (MSesC: 48.0 ± 2.8, MSoyC: 45.0 ± 3.2). This may be explained by the increased viscosity of the organogels which decreased the diffusion of the drug molecules (evident from the *in vitro* drug release studies). This reduced the loss of the drug from the microparticles during the preparation and washing stages. Also, leaching of the internal phase from the microparticles played an important role.

6.7.6. Molecular characterization studies

X-ray diffraction analysis of sodium alginate, stearic acid, organogels (OG1, OG2) and the developed microparticles was performed (Figure 6.14a and 6.14b). Presence of vegetable oil in MSes and MSoy changed the diffraction pattern of sodium alginate (Na-Alg) to show a single broad peak. The fatty acyl molecules in the vegetable oils were responsible for the appearance of the hump at ~20º 2θ [157]. Even though, the organogels were amorphous in nature the crystalline peaks of stearic acid were observed. These peaks were also found in the diffractograms of MOG1 and MOG2. This indicated that MSes and MSoy were comparatively more amorphous than MOG1 and MOG2. The crystalline peaks in MOG1 and MOG2 indicated the existence of stearic acid molecules within the microparticles. The crystalline peaks of stearic acid were conserved and retained at almost the same 2θ (Bragg's angle) in MOG1 and MOG2. This suggested the presence of the stearic acid without any changes in the physical nature of the organogels [157]. MOG1 and MOG2 showed "Long spacing" (6.8º and 11.4º 2θ) and "short spacing" (21.37º and 23.7º 2θ) peaks of stearic acid. Although the peaks of stearic acid were conserved in MOG1 and MOG2, their intensities were poor when compared with stearic acid and OG1 and OG2, respectively. Presence of alginate layer around the organogels might have reduced the peak intensity in MOG1 and MOG2. This suggested that stearate organogels were encapsulated within the alginate microparticles without any major alterations in the organogel structure.

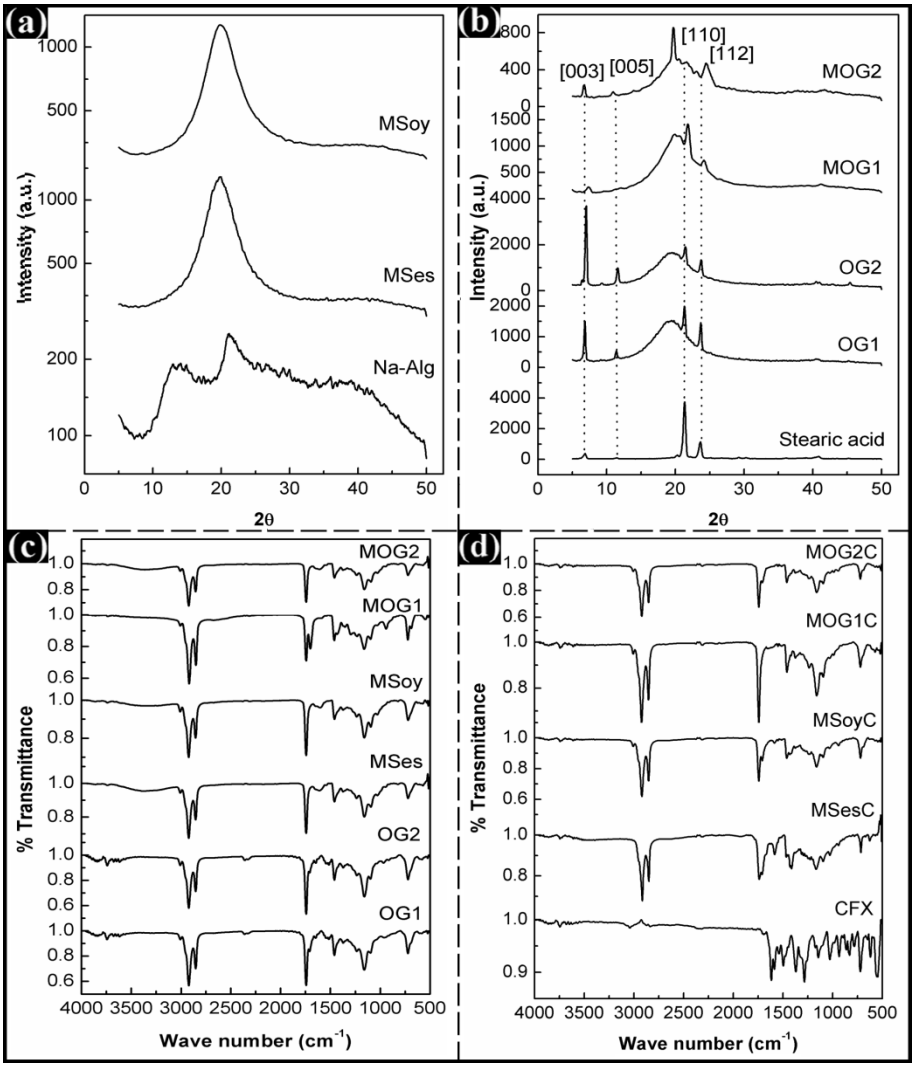

Figure 6.14: (a-b) X-ray diffractograms, and (c-d) FTIR spectra of the microparticles.

Figure 6.14b shows the interplanar spacings [hkl] of the peaks and their corresponding *d*-values have been listed in the Table 6.11. In general, intensities of all the peaks of the organogels were decreased after encapsulation, but the effect was more pronounced in long spacing peaks. The major changes in the pattern of the peaks revealed that the order of the molecular layers was significantly altered due to the presence of the other components of the microparticles [157]. There were negligible changes in the *d*-values of the short spacing peaks in microparticles as compared to the organogels. Along with the decrease in the peak intensity and changes in *d*-value; crystallite size (D) of the stearic acid was also changed when the organogels were incorporated within the microparticles. *d*-value of the crystalline peaks in microparticles was not in actual match with that of the pure stearic acid and organogels (Table 6.11). The crystallite size was calculated based on the [110] crystal plane (at 2θ 21.37º) of stearic acid. The crystal size was calculated using Debey-Scherrer equation (equation 4.2 in chapter 4).

Crystallite size (D) of stearic acid was found to be higher when it was in pure form, followed by encapsulated organogels and organogels, respectively. This suggested that the stearic acid in microparticles was structurally closer to its native form than in the organogels. Increase in the crystallite size also suggested an increase in the crystallinity of the stearic acid in microparticles than in the organogels. This was supported by the FWHM values which showed that the FWHM values were lower in the organogel encapsulated microparticles as compared to organogels.

Table 6.11: XRD analysis of the organogels and the microparticles.

Sample	*d*-value of peaks (Å)				FWHM of 21.3° 2θ	*D* (nm)
	[003] or 6.8° 2θ	[005] or 11.4° 2θ	[110] or 21.3° 2θ	[112] or 23.7° 2θ		
SA	12.82	7.69	4.15	3.75	0.157	51.4
OG1	12.89	7.74	4.15	3.74	0.195	41.5
OG2	12.53	7.60	4.13	3.73	0.227	35.6
MOG1	11.83	--	4.05	3.66	0.162	49.8
MOG2	13.01	8.09	4.49	3.63	0.194	41.4

The FTIR spectra of the prepared microparticles have been shown in Figure 6.14c and 6.14d. The microparticles have shown the characteristic peaks associated with the alginate. The characteristic peaks of stearic acid were observed at ~1,710 and ~940 cm^{-1}. The peak at 1,710 cm^{-1} overlapped with the $–COO^-$ vibrations of the alginate. Co-existence of the stearic acid and alginate peaks suggested that the stearic acid based organogels might have been encapsulated within the alginate microparticles. In drug containing microparticles, peaks corresponding to ciprofloxacin (1,610 and 1,260 cm^{-1}, due to phenolic groups conjugated to $–COO^-$ and CF bond, respectively) were observed apart from the peaks associated with the alginate and stearic acid molecules. There was no shift in the absorption bands of ciprofloxacin indicating that the drug molecules were present in its native state.

6.7.7. Thermal studies

Vegetable oil containing microparticles showed a broad endothermic peak at ~70 °C (Figure 6.15a). This may be due to the evaporation of the bound water from the alginate layer. Though dried microparticles were used for the thermal analysis, 100 % removal of water from the alginate microparticles was not possible [159]. The organogels showed endothermic peaks, associated with the melting of the organogels, at ~44 °C. The melting endotherms of

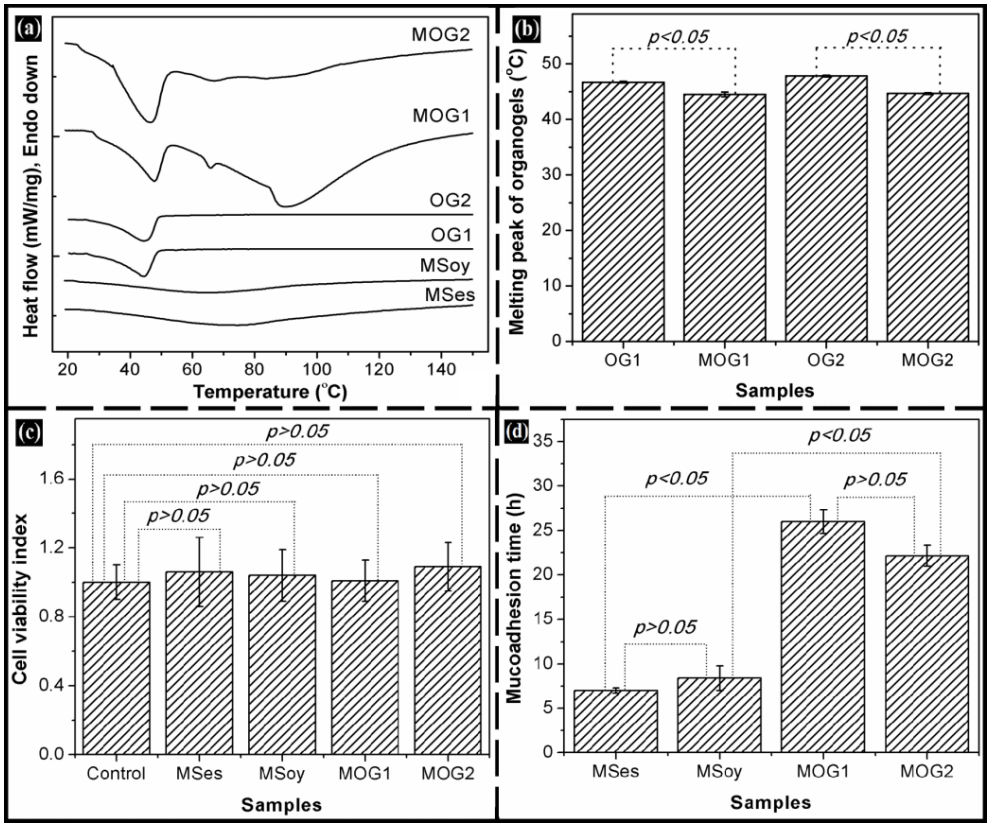

Figure 6.15: (a) DSC curves of the microparticles and organogels, (b) Melting point of organogels, (c) Cell viability index, and (d) Mucoadhesion times of the microparticles.

the organogels were also observed in the thermograms of the organogel containing microparticles, suggesting the presence of organogels within the microparticles. The differences in the melting temperatures between OG1, OG2 and MOG1, MOG2, respectively were found to be significant ($p < 0.05$) (Figure 6.15b). This indicates that encapsulation has improved the stability of the organogels. In addition to the melting peaks of the organogels, microparticles showed additional peaks at ~70 ºC and ~100 ºC. The peak at ~70 ºC was due to the evaporation of the bound water in the alginate layer, whereas, the peak at ~100 ºC was due to the evaporation of the water molecules absorbed by the organogels (within the microparticles) during microparticle preparation [220]. Literature suggests that it is quite possible that the water molecules can exist within the dynamic and transient microstructures of the fatty acyl organogels [219]. Evaporation of water over a range of 60-120 ºC, suggested the involvement of dipole-dipole interactions amongst the –OH groups of the water molecules and the fatty acid molecules. There is a high probability of dipole-dipole interactions amongst the water molecules and the alginate molecules [185]. Thermal analysis revealed that the organogels have been successfully entrapped within the alginate microparticles.

6.7.8. Biocompatibility and mucoadhesivity studies

Cytocompatibility of the microparticles was checked using L929 fibroblast cells. The leachants of the microparticles were used in the study. MTT assay indicated that the relative proliferation of the cells in the presence of the leachants and the control was statistically insignificant *(p* > 0.05) thereby suggesting the cytocompatibility of the prepared microparticles (Figure 6.15c). *In vitro* cell cytocompatibility studies have confirmed that the developed formulations were biocompatible in nature and may be employed for the *in vivo* applications.

In addition to the biocompatibility studies, mucoadhesivity of the microparticles was checked using goat small intestine. Microparticles showed different adhesion times (depending on the composition) from the mucosal surface of the small intestine. Detaching times/mucoadhesion times were found to be more in organogel containing microparticles (Figure 6.15d). Leaching of oil from the MSes and MSoy might have reduced these interactions between the alginate layer and the mucosal surface. This has lead to the quick detachment of MSes and MSoy as compared to MOG1 and MOG2. Higher mucoadhesive nature is expected to promote the residence time of MOG1 and MOG2 in the gastrointestinal tract and lead to the lower dosage administration frequency. Statistical analysis suggested that the mucoadhesion times varied significantly when the internal phase was changed from oil to organogel ($p < 0.05$). This suggested an improved mucoadhesive efficiency of the microparticles when organogels were encapsulated.

6.7.9. *In vitro* drug delivery studies

In vitro drug release was higher from MSesC and MSoyC as compared to MOG1C and MOG2C (Figure 6.16a). This might be associated with the leaching of oils from MSesC and MSoyC. The drug release kinetics from the microparticles was estimated (Figure 6.16b-e). MSesC and MSoyC followed zero order kinetics, whereas MOG1C and MOG2C followed Higuchian kinetics (Table 6.12). It indicated that drug release from MSes and MSoy was concentration dependent. But in case of MOG1C and MOG2C, drug release was affected/controlled by the presence of organogel as the core of the microparticles. The drug release from the microparticles followed the Baker's Lonsdale (BL) model. The results suggested that the developed formulations may be regarded as spherical matrices [150]. From the Korsmeyer-Peppas (KP) model, it was found that the release of the drug was diffusion mediated and followed non-Fickian (0.4 > n > 0.89) diffusion mechanism. The 'n' value of MSesC and MSoyC is near 0.89, which in general associates with the case-II diffusion or

zero order kinetics [150]. *In vitro* drug release studies suggested that the drug release behavior was altered due to the incorporation of organogels within the microparticles.

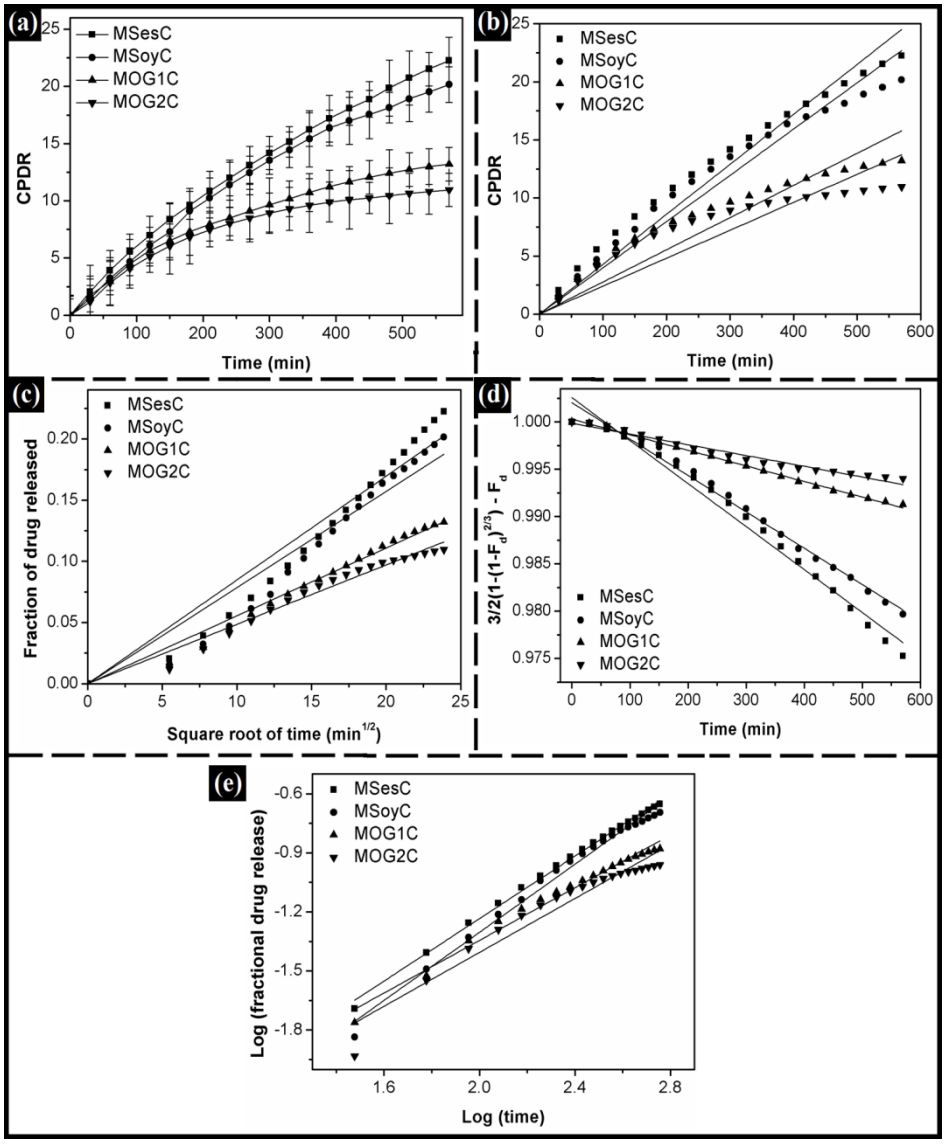

Figure 6.16: Drug release kinetics from the microparticles: (a) CPDR vs. time, (b) Zero order, (c) Higuchi model, (d) BL model, and (e) KP model.

Table 6.12: The drug release kinetics from the microparticles

Samples	Zero order (R^2)	Higuchi (R^2)	BL model (R^2)	Best fit	KP model	
					n	Type of flow
MSesC	0.96	0.90	0.98	BL	0.80	Non-Fickian
MSoyC	0.95	0.91	0.99	BL	0.85	Non-Fickian
MOG1C	0.83	0.98	0.99	BL	0.67	Non-Fickian
MOG2C	0.71	0.95	0.97	BL	0.68	Non-Fickian

6.7.10. Antimicrobial studies

Ciprofloxacin is a quinolene antibiotic, found to be active against *E. coli*. After an overnight incubation of nutrient agar plates, zone of inhibition was found around the drug loaded microparticles but not around the microparticles without drugs (Figure 6.17). This suggested that the zone of inhibition was due to the release of ciprofloxacin from the microparticles. Zone of inhibition was found to be more against MSesC and MSoyC than MOG1C and MOG2C, respectively. This may be due to the leaching of the oils from the microparticles at 37 ºC which in turn increased the availability of drug and hence larger zone of inhibition. This was also evident from the *in vitro* drug release studies. Antimicrobial studies indicate that the drug was releasing in its active state from the microparticles.

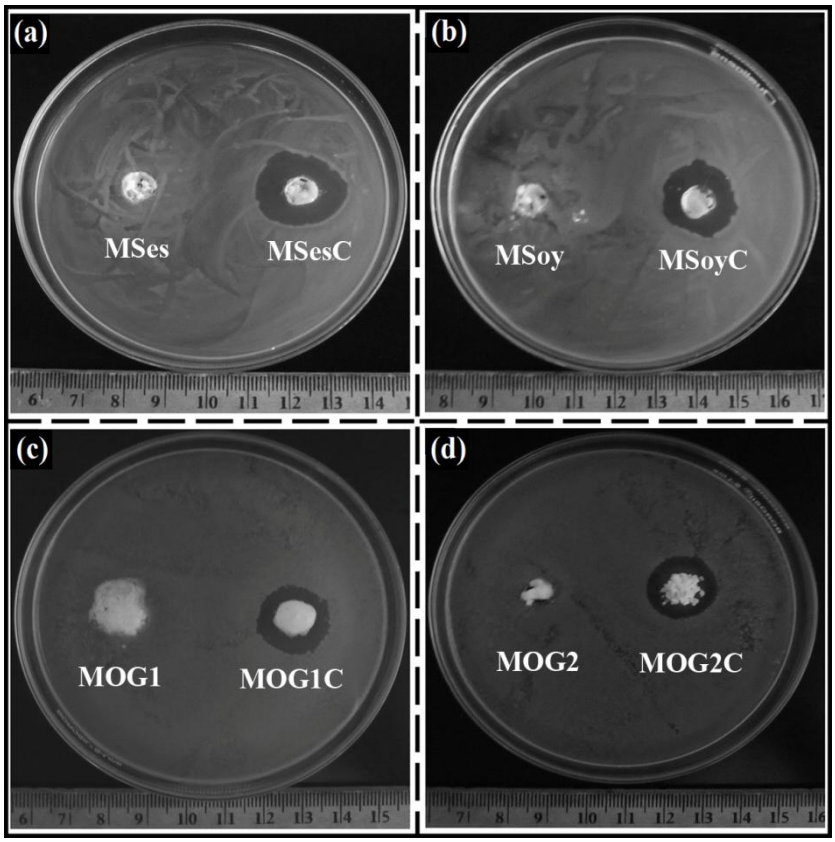

Figure 6.17: Antimicrobial studies of the microparticles against *E. coli*.

6.8. Conclusion

Ionotropic gelation method was successfully employed to synthesize organogel entrapped microparticles using alginate as the polymer matrix. The organogel entrapped microparticles showed improved drug entrapment efficiency by preventing the leaching of the internal phase. Controlled release of ciprofloxacin from the microparticles was noticed and the release

was super case-II diffusion transport mediated. The developed microparticles seem to have huge potential in controlled delivery applications.

Chapter 7

Encapsulation of Span 80-Tween 80 based organogels in alginate microparticles

Abstract

Sunflower oil based organogels were prepared using a gelator mixture containing Span 80 and Tween 80 (1:2 (w/w)). The organogel composition involves 52.5 % (w/w) of gelator mixture, 35.0 % (w/w) of water and 12.5 % (w/w) of sunflower oil. The organogel was characterized by microscopic, FTIR, thermal and mechanical studies. Drug release kinetics suggested that metronidazole (model drug) was released from organogel matrices in non-Fickian fashion and the drug was found to be active against *E. coli*. The synthesized organogel was encapsulated within the alginate microparticles by ionotropic gelation method. Blank microparticles and sunflower oil containing microparticles were synthesized as the controls. The microparticles were characterized by microscopy, XRD, FTIR and DSC studies. Microscopic studies revealed that oil droplets were present within sunflower oil containing microparticles whereas, organogel containing microparticles were opaque in nature. The difference in microstructure can be attributed to the gelation of sunflower oil by organogelators which in turn, prevented the oil leaching. Prevention of oil has improved the DEE, biocompatibility (against mammalian L929 fibroblasts) and mucoadhesivity (against goat small intestine) of the microparticles. The release of drugs from the microparticles followed non-Fickian diffusion and showed good antimicrobial activity against *E. coli*.

Graphical abstract

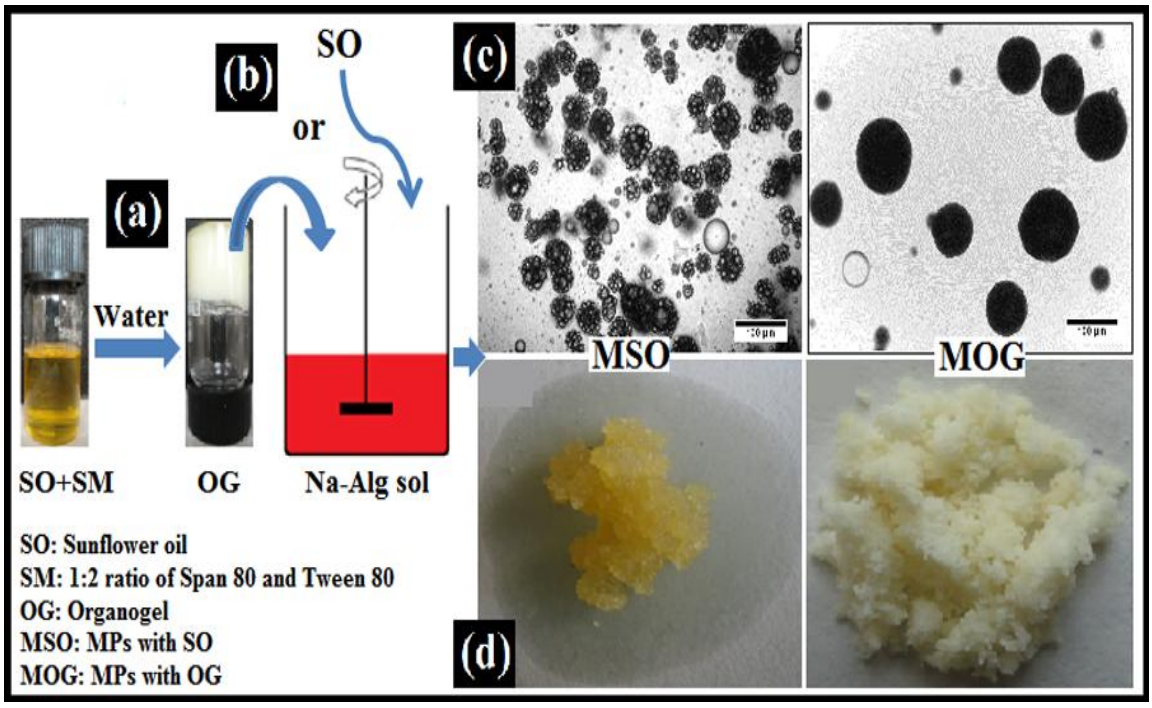

Part A: Preparation and characterization of Span 80-Tween 80 based organogels

Overview

Span 80-Tween 80 based organogels were prepared by mixing the surfactants in the ratio of 1:2 (w/w), sunflower oil and water. Microscopic studies revealed the presence of circular emulsion droplets within the organogel matrix. FTIR studies indicated that intermolecular hydrogen bonding between the organogelators (surfactants) and water molecules might be responsible for the formation of organogels. Since the water molecules are associated with the organogel components, thermal studies yielded a single large endotherm. This was resulted due to the gel-to-sol transition at lower temperature and evaporation of water at higher temperature. Mechanical properties of the organogel were identified by performing mechanical studies. Stress relaxation studies indicated that the developed organogel is a viscoelastic semi-solid. Drug release kinetics showed that metronidazole was released in non-Fickian mode from organogel matrices. The released drug was found to be effective against *E. coli*.

7.1. Introduction

In general, the mechanism of organogelation may be achieved by forming 3D networked structures either by solid fibre or by fluid filled fibre structures. The organogelation has been achieved by using ionic surfactants (e.g. sodium lauryl sulphate, sodium stearate etc) and non-ionic surfactants (e.g. polysorbates, sorbitan esters, poloxamer etc) [221]. Unlike ionic surfactants, non-ionic surfactants are non-irritant in nature. This property of the non-ionic surfactants has facilitated the exploitation of non-ionic surfactants for the development of organogels. A broad category of sorbitan esters based non-ionic surfactants have gained wide applications in pharmaceutical and food industries [222-224]. This may be associated with the versatility and biocompatibility of these organogels [32].

7.2. Materials and methods

Span 80 and Tween 80 based organogels were prepared as per the protocol given in section 3.2.4 of chapter 3, characterization of the organogels (microscopy, FTIR studies, thermal studies and mechanical studies), *in vitro* drug release studies and antimicrobial studies were explained in detail in section 3.3 of chapter 3.

7.3. Results and discussion

7.3.1. Preparation of organogels

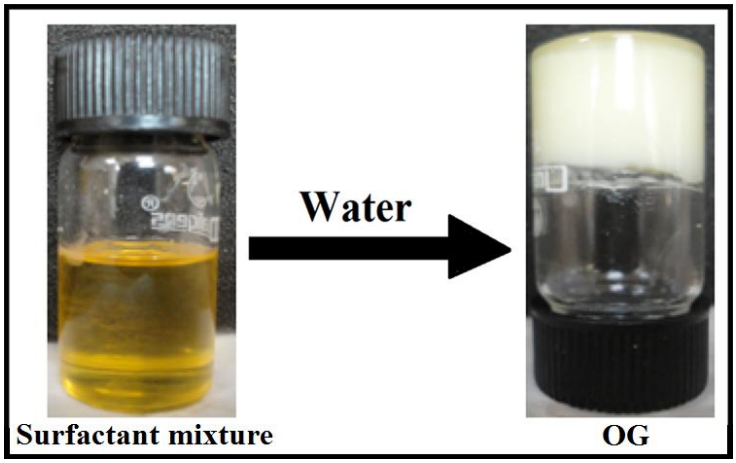

Figure 7.1: Schematic representation of the preparation of organogels.

A clear and homogeneous solution was formed after mixing Span 80: Tween 80 in the ratio of 1:2 (w/w) (surfactant mixture) and sunflower oil. Drop-wise addition of water (under constant stirring) has lead to the transformation of the clear solution to turbid. Formation of organogel was confirmed by inverted test-tube method (Figure 7.1) [221]. The organogel was labelled as “OG”. Metronidazole (1 % w/w) containing organogels were found to be stable at

room-temperature and labelled as "OGMZ". The organogels were stable for more than 12 months at room-temperature. Dilution test revealed that the formed organogels are oil-in-water (O/W) type of organogels. This indicated that the oil was dispersed in the organogels. Microstructure of the organogel was analyzed in bright field microscope. The microscopic analysis revealed the presence of uniformly dispersed emulsion droplets within the continuous matrix of organogel (Figure 7.2).

7.3.2. Microscopic studies

Microstructure of the organogel was analyzed in bright field microscope. The microscopic analysis revealed the presence of uniformly dispersed emulsion droplets within the continuous matrix of organogel (Figure 7.2).

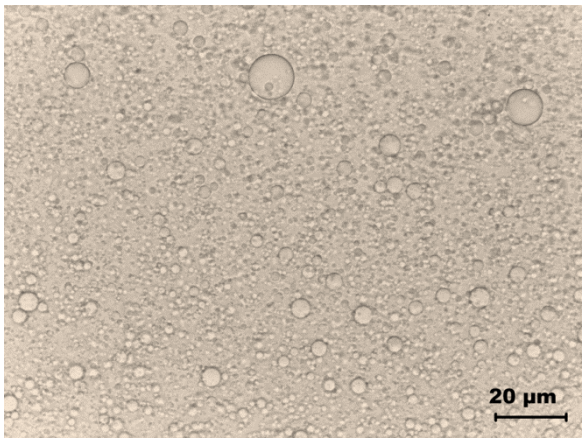

Figure 7.2: Microstructure of the organogel.

7.3.3. FTIR studies

FTIR spectra of organogels and organogel components have been shown in Figure 7.3a. FTIR spectra of organogels and the surfactant mixture are similar to each other with some variations. Difference in peak intensity was found for the FTIR band at ~3,300 cm^{-1}. In general, peak at ~3,300 cm^{-1} corresponds to the –OH stretching vibrations. Increase in peak intensity was due to the presence of water within the organogels. Incorporation of water might have lead to the intermolecular hydrogen bonding between the water molecules and surfactant molecules [176]. It has been established that gelation mechanism in fluid-type organogels involves hydrogen bonds and hydrophobic interactions amongst the gel components [176]. Addition of drug to the organogel did not alter the position of the peaks in the FTIR spectrum of organogel. Absence of new peaks indicated that the drug was completely dispersed in the organogel. This also indicated that no chemical interactions exist between the organogel components and drug molecules.

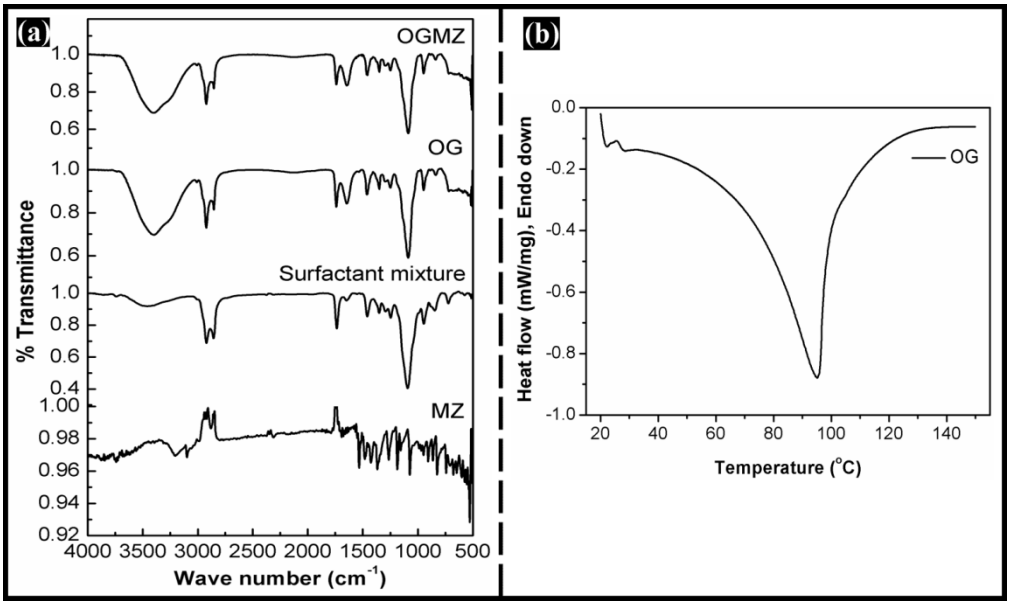

Figure 7.3: (a) FTIR spectra of the organogels, surfactant mixture and drug (metronidazole); and (b) DSC thermogram of the organogel.

7.3.4. Thermal studies

Organogel was heated from 20 ^{o}C to 150 ^{o}C at a scan rate of 1 ^{o}C/min. When heated, organogel yielded a single large endotherm with a peak maximum at ~95 ^{o}C. Endotherm was resulted due to the combination of two evens namely, gel-to-sol transition of the organogel and evaporation of water associated with the organogel. FTIR studies also indicated that the water molecules are associated with the organogel components. In general, gel-to-sol transition temperature of the Span 80-Tween 80-type of organogel is present at ~ 55 ^{o}C. Since gel-to-sol transition of the organogel was associated with the evaporation of water, no separate peak was identified.

7.3.5. Mechanical studies

Figure 7.4a shows the two cycled uni-axial compression test of the organogel. The mechanical parameters calculated from the compression test have been tabulated in Table 7.1. Spreadability studies indicated that OG possesses good spreadability. The viscoelastic nature of the organogel was investigated by stress relaxation studies. When the applied stress was released, a sudden decrease in force was noticed and reached a constant force during the relaxation time. This indicated that when stress was applied, OG released the stress in quick time. % relaxation of the organogel was calculated using equation 1. It was found to be 86.52 %. Higher % relaxation indicated the liquid-like nature of the organogel. This was confirmed by calculating the viscoelastic properties (F^{*} and S^{*}) of the organogel.

$$\%\ relaxation = \left(\frac{F_0 - F_r}{F_0} \right) * 100 \qquad (7.1)$$

where, F_0 and F_r are the maximum load after the application of stress and the residual force after the relaxation, respectively.

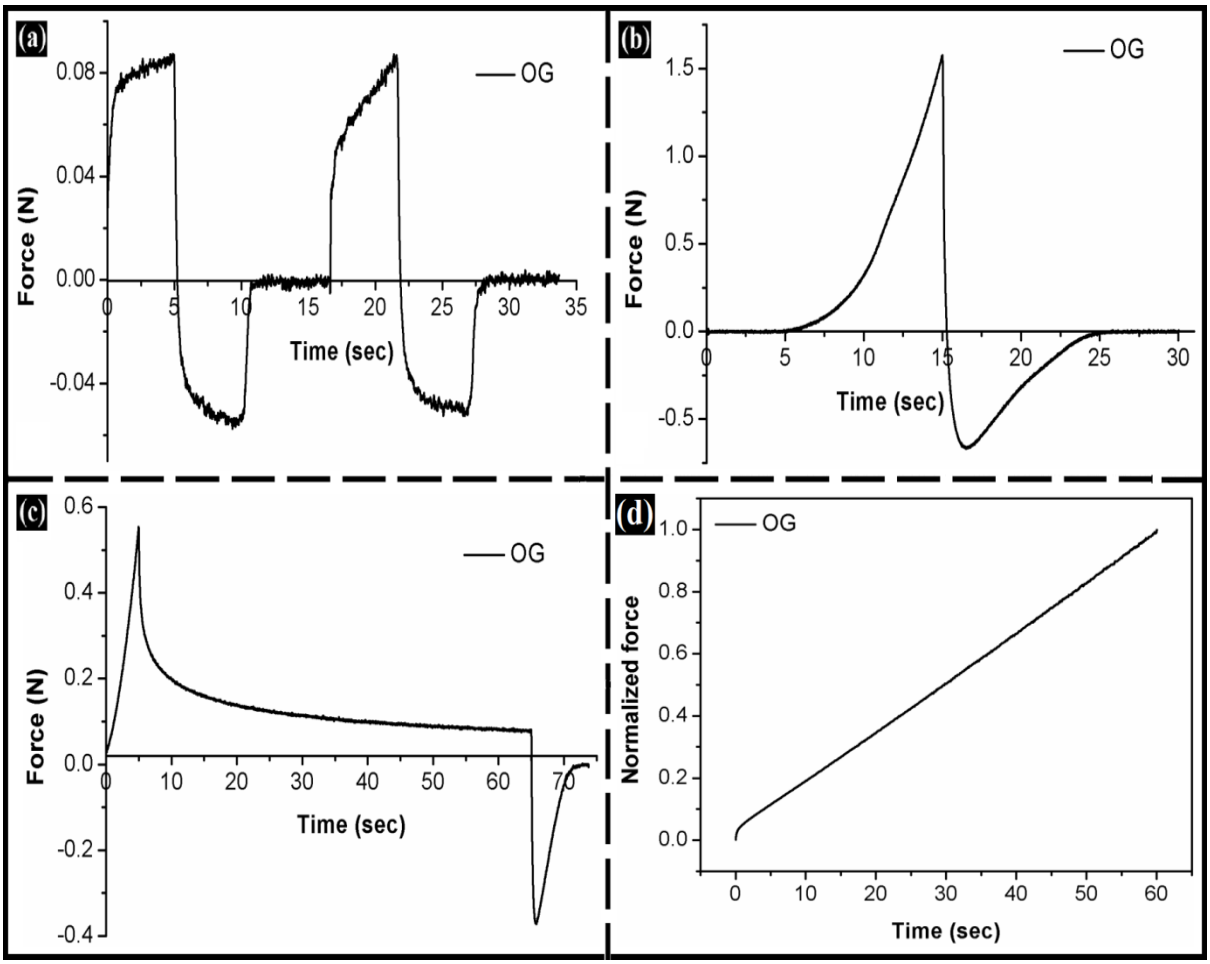

Figure 7.4: Mechanical studies: (a) Cyclic compression; (b) Spreadability; (c) Stress relaxation curves and (d) Normalized stress relaxation curve (modified Peleg's analysis).

The viscoelastic properties, asymptotic residual value in the normalized stress relaxation curve (F^*) and the area under the normalized stress relaxation curve (S^*) are calculated using the following equations [149].

$$S = \int_a^b F(t).dt \qquad (7.2)$$

$$S_0 = \left(\frac{S}{b-a} \right) a \qquad (7.3)$$

$$S^* = \frac{S}{S_0} \qquad (7.4)$$

where, 's' is the area under the stress relaxation curve; 'a' and 'b' are the lower and upper limits of the time, respectively.

Area under the curve (S) is a simple and sensitive estimator of the changes in the relaxation behavior of materials. For viscoelastic materials S^* varies in the range of 0 to1. Elastic-like materials possesses S^* close to 1.0. On the other hand, if S^* is near to zero, then the materials can be regarded as viscous materials. Since S^* was found to be in between 0 to 1 (Table 7.1), OG can be regarded as viscoelastic semi-solid.

Table 7.1: Mechanical properties of the organogel.

Sample	**Hardness (N)**	**Cohesiveness**	**Adhesiveness (N.sec)**	**Gumminess (N)**	**Spreadability ($N.sec^{-1}$)**	**S^***
OG	0.087	0.855	0.25	0.074	0.002	0.347

7.3.6. *In vitro* drug delivery studies

In vitro drug release studies showed that ~ 54 % of metronidazole was released from OGMZ (Figure 7.5a). To predict the drug release behaviour, the drug release data was fitted in different drug kinetic models (Figure 7.5b-d). After fitting, it was found that the drug release pattern was not following zero order kinetics ($R^2 > 0.95$), but following Higuchi kinetics ($R^2 > 0.95$) (Table 7.2). Following Higuchi kinetics suggested that the drug was released from planar matrices. The drug release behaviour was further investigated by fitting the data in KP kinetics ($R^2 > 0.95$). The Fickian value (n) was found to be in between 0.4 and 0.85 which suggested that non-Fickian mode of drug release was observed (Table 7.2). Based on the drug release kinetic models, it was inferred that metronidazole was released in non-Fickian mode from matrix-kind of organogel.

Table 7.2: Drug release kinetics.

Sample	**Zero-order**	**Higuchi model**	**Best fit**	**KP model**		
	R^2	**R^2**		**R^2**	**n value**	**Type of release**
OGMZ	0.915	0.973	Higuchi	0.99	0.667	Non-Fickian

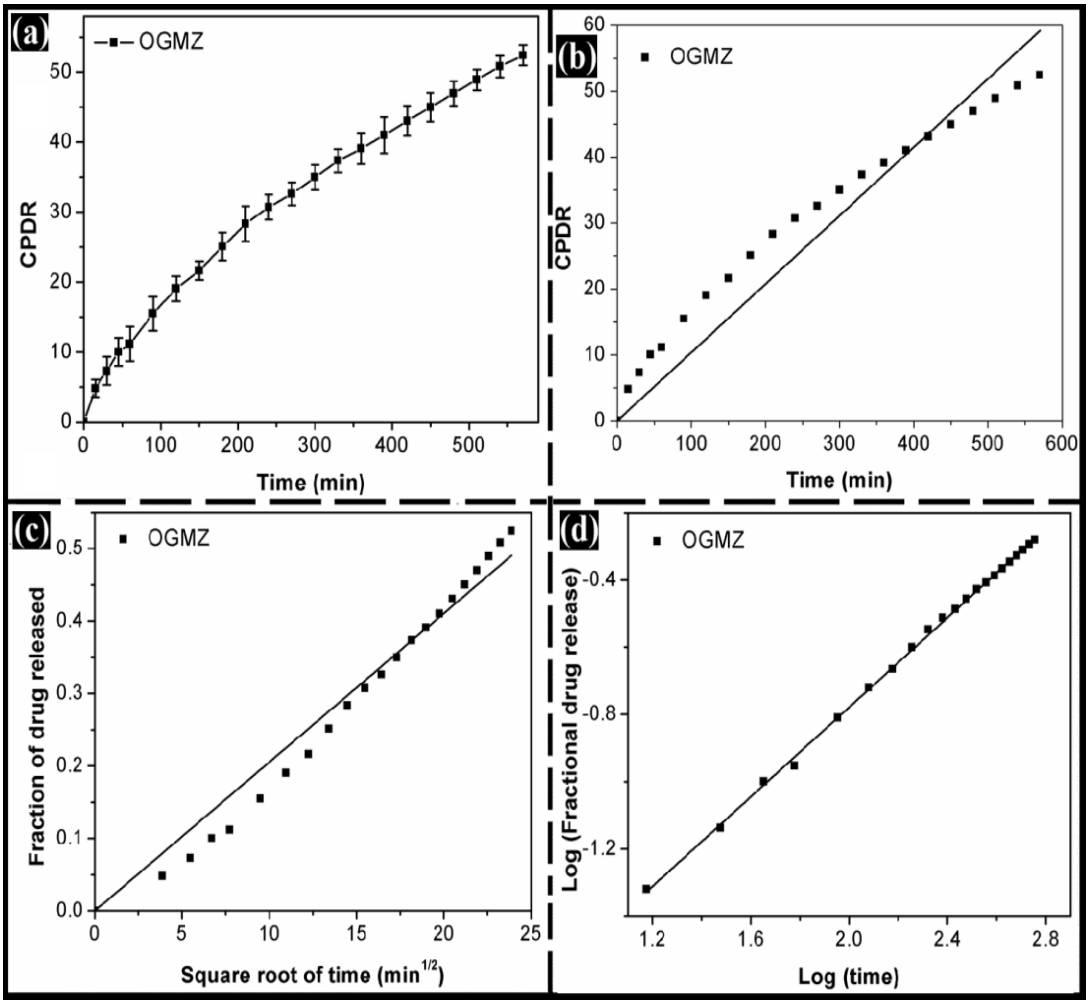

Figure 7.5: Drug release kinetics: (a) CPDR vs. time, (b) Zero order, (c) Higuchi model, and (d) KP model.

7.3.7. Antimicrobial studies

Antimicrobial nature of the organogel and release of the drug from OGMZ was confirmed by testing the gels against *E. coli*. A clear zone of inhibition was noticed around OGMZ, but the zone of inhibition was not found for OG. This indicated that metronidazole has been released in its active form and antimicrobial activity was only due to the action of the drug. Zone of inhibition (diameter: ~1.7 cm) due to OGMZ was found to be almost same as that of metrogyl® (diameter: ~1.6 cm). Difference in zone of inhibition was found to insignificant ($p > 0.05$).

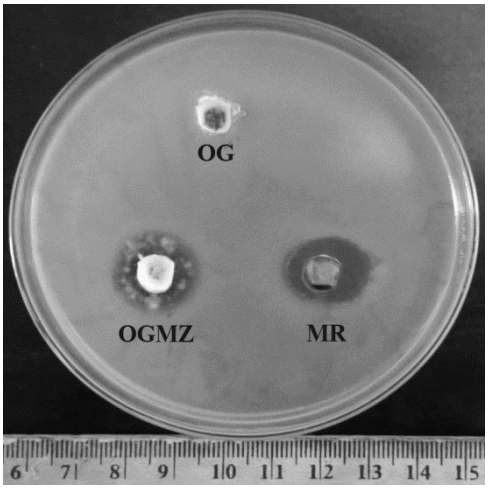

Figure 7.6: Antimicrobial studies of the organogels against *E. coli.*

7.4. Conclusion

Stable organogel was prepared using Span 80-Tween 80 in the ratio of 1:2 (w/w), sunflower oil and water. Microscopic, FTIR and thermal studies were conducted to characterize the organogel. Mechanical properties of the organogel were elucidated by conducting uni-axial compression studies, spreadability studies and stress relaxation studies. Stress relaxation studies revealed that the organogel is viscoelastic semisolid in nature. Drug release kinetics suggested that metronidazole was released in non-Fickian mode from organogel matrices. The organogel showed good antimicrobial activity against *E. coli* as that of metrogyl®.

Part B: Encapsulation of Span 80-Tween 80 based organogels in alginate microparticles

Abstract

Sunflower oil based organogels were prepared using a gelator mixture containing Span 80 and Tween 80 (1:2 (w/w)). The organogel composition involves 52.5 % (w/w) of gelator mixture, 35.0 % (w/w) of water and 12.5 % (w/w) of sunflower oil. The synthesized organogel (core) was encapsulated within the alginate microparticles by internal gelation method. Blank microparticles and sunflower oil containing microparticles were also synthesized as the controls. The microparticles were characterized by microscopy, XRD, FTIR and DSC studies. Microscopic studies revealed that oil droplets were present within sunflower oil containing microparticles whereas, organogel containing microparticles were opaque in nature. The difference in microstructure can be attributed to the gelation of sunflower oil by organogelators which in turn, prevented the oil leaching. Prevention of oil has improved the DEE (metronidazole), biocompatibility (against mammalian L929 fibroblasts) and mucoadhesivity (against goat small intestine) of the microparticles. The release of drugs from the microparticles followed non-Fickian diffusion and showed good antimicrobial activity against *E. coli*.

7.5. Introduction

In this chapter, we tried to encapsulate sunflower oil via polysorbates-based organogels. All the components used in this study are GRAS (Generally Regarded As Safe) materials and FDA approved for oral administration [225-226]. Blank microparticles (microparticles without any internal phase) and microparticles with sunflower oil served as controls.

7.6. Materials and methods

7.6.1. Preparation and characterization of the microparticles

Microparticles were prepared as per the protocol given in section 3.2.5 of chapter 3. 5 g of Span 80-Tween 80-based organogel and sunflower oil were used during the preparation of organogel and sunflower oil containing microparticles, respectively. Blank microparticles and sunflower oil containing microparticles were used as the controls of the study.

Experimental details for the characterization of the microparticles are given in section 3.3 of chapter 3.

7.7. Results and discussion

7.7.1. Preparation of the microparticles

The composition of the internal phase of the microparticles has been listed in Table 7.3. Primary emulsions were prepared by dispersing either sunflower oil or organogel in alginate solution. Addition of the primary emulsion to the external phase sunflower oil resulted in the formation of oil-in-water-in-oil multiple emulsion. Crosslinking of the alginate molecules under acidic conditions resulted in the formation of stable microparticles.

Table 7.3: The internal phase composition of the microparticles.

Samples	**Internal phase**
BM	No internal phase
MSO	Sunflower oil
MOG	Organogel
BMMZ	Blank microparticles with 1 % (w/w) metronidazole
MSOMZ	Sunflower oil containing 1 % (w/w) metronidazole
MOGMZ	Organogel containing 1 % (w/w) metronidazole

7.7.2. Microscopy

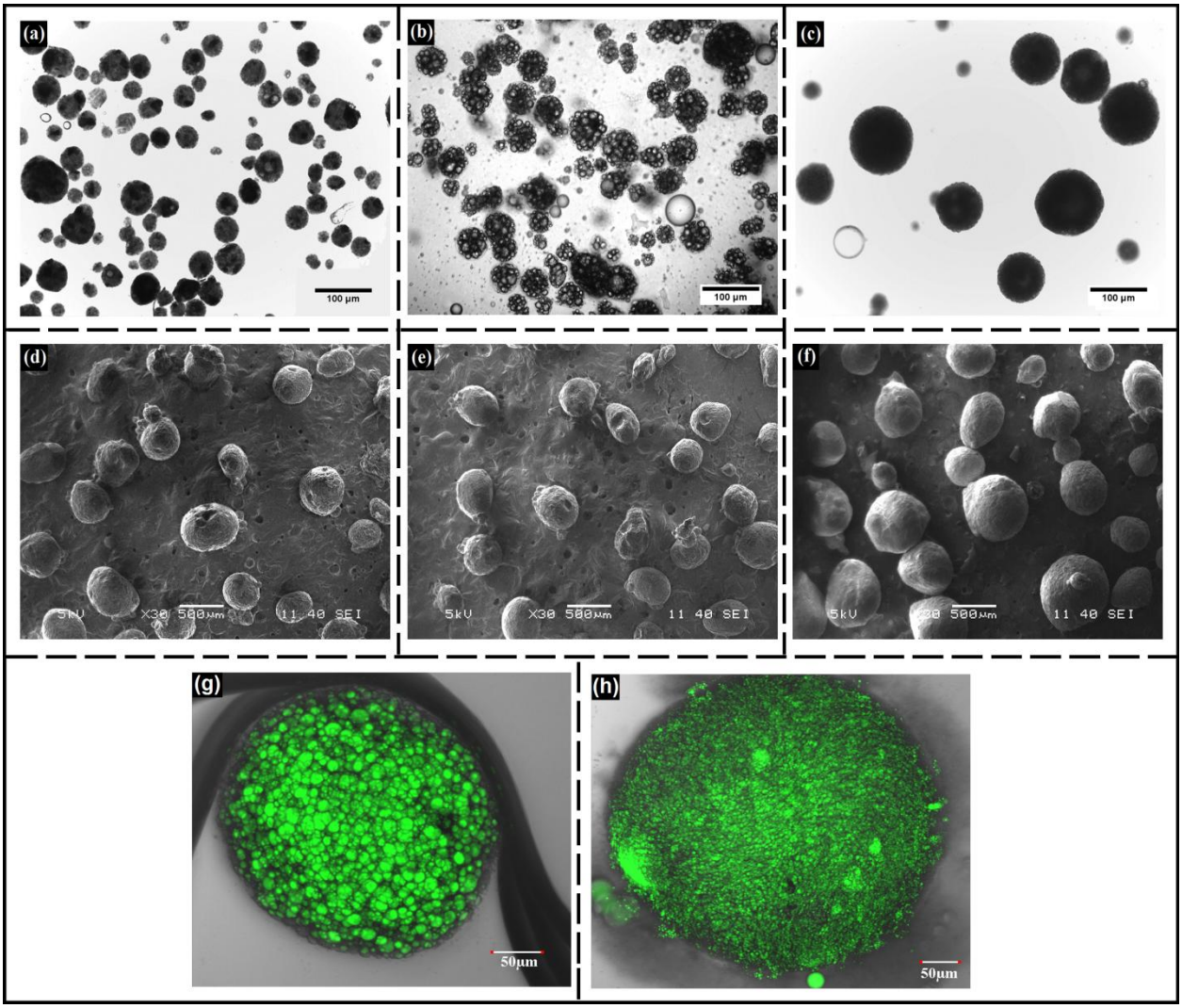

Figure 7.7: Bright field microscopic images (scale bar: 100 µm) of: (a) BM, (b) MSO, and (c) MOG; SEM images (scale bar: 500 µm) of: (d) BM, (e) MSO, and (f) MOG; and Confocal images of: (g) MSO, and (h) MOG.

The microparticles have shown distinct variation in their internal structure (Figure 7.7). BM was semi-transparent due to the absence of any internal phase within the microparticles. MSO showed globular droplets suggesting the entrapment of sunflower oil within the alginate particles. Oil droplets were clearly seen in confocal image of MSO (Figure 7.7g). MOG were more opaque than BM and MSO as was evident from the darker nature of the microparticles (Figure 7.7c). This may be associated with the presence of the semi-solid organogel, which prevented the transmission of the light through the microparticles [227]. Confocal image of MOG showed uniformly dispersed organogel matrix (Figure 7.7h). Sunflower oil was

dispersed within the organogel matrix. Absence of large oil droplets helps in preventing the oil leaching.

The average diameter of the microparticles was found to be highest for MOG followed by MSO and BM (Figure 7.8a). MOG had broad size distribution over MSO and BM (Figure 7.8a and 7.8b). Presence of viscous organogels in the primary emulsions might have lead to the larger and wide size distribution of MOG microparticles. SEM studies suggested that the microparticles are circular but are having polydispersity (Figure 7.7d-f). The sizes of the microparticles were smaller as compared to the particle size obtained from light microscopy. This is due to the fact that the microparticles for SEM analysis were completely dried. The evaporation of water has lead to the shrinkage of the microparticles which resulted in loss of spherical nature to a certain extent. The extent of loss of sphericity was more in BM and MSO as compared to MOG. The microscopic studies indicated that the physical nature of the internal phase was affecting the appearance of the microparticles.

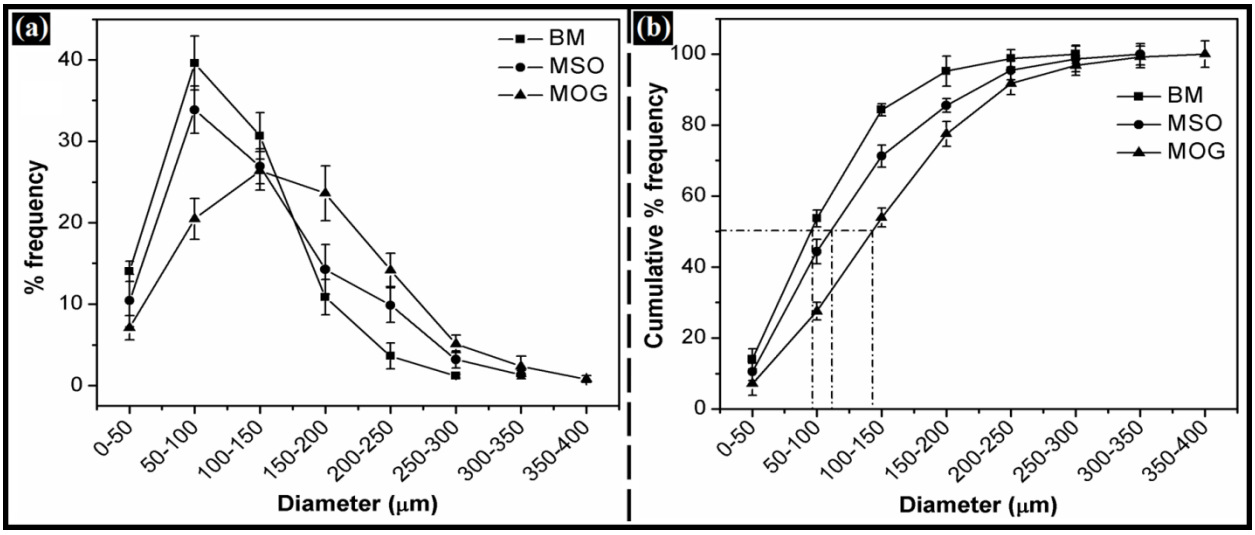

Figure 7.8: Size distribution analysis: (a) % frequency and (b) Cumulative % frequency of the microparticles.

7.7.3. Leaching studies

Leaching of internal phase from the MSO showed a darker region surrounding the microparticles (Figure 7.9). This indicated that sunflower oil was leaking out of the microparticles. On the other hand, MOG did not show any signs of leakage until the end of the experiment (2 h). This may be attributed to the gelation of the sunflower oil due to which apparent viscosity was increased. The increase in viscosity might have prevented the leaching of the internal phase. Quantification of oil leaching by another study also demonstrated the similar kind of results. % leaching was very high in MSO (~ 45 %) as compared to MOG

(~10 %). This study shows that the leakage of oil from microparticles may be overcome by inducing gelation of the internal phase.

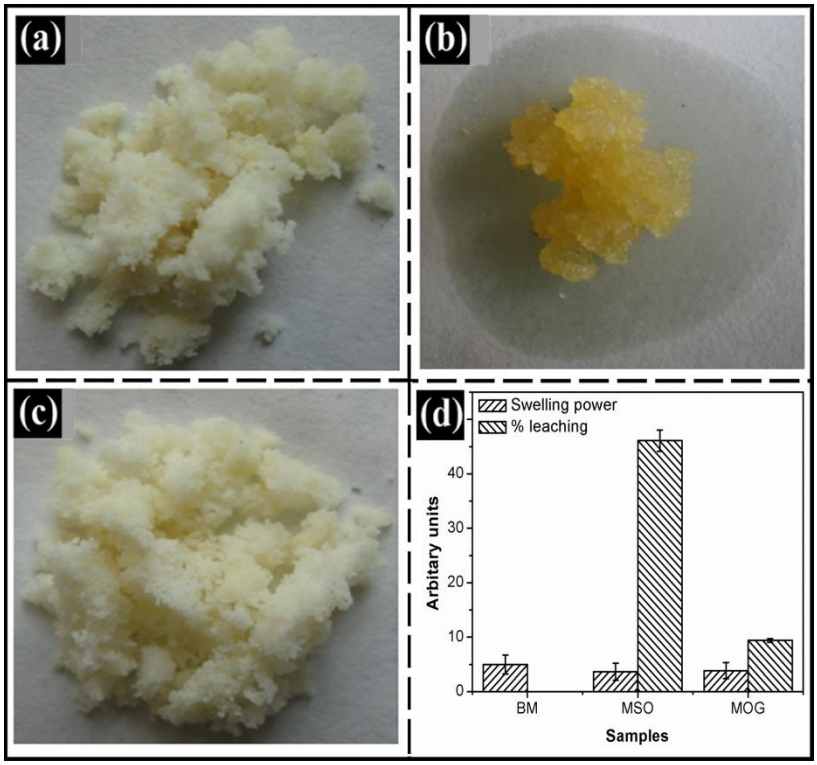

Figure 7.9: Leaching studies: (a) BM, (b) MSO, and (c) MOG; and bar graphs showing the: (d) Swelling power and % leaching of the microparticles.

7.7.4. Drug entrapment efficiency

The percentage of drug encapsulation efficiency (% DEE) of microparticles was varying with nature of the internal phase. The lowest % DEE of BMMZ (44.0 ± 2.7) may be associated with the absence of the internal phase. Drug might have diffused out of the porous alginate microparticles by diffusion during the preparation of the microparticles [92]. The % DEE of MSOMZ (49.0 ± 2.5) was slightly better than BMMZ and may be associated with the partitioning effect. The %DEE was highest in MOGMZ (74.0 ± 3.4) which may be due to the combined effect of partitioning and increased viscosity of the internal phase. The semi-solid organogels might have restricted the diffusion of drugs and resulted in higher % DEE.

7.7.5. Molecular interaction studies

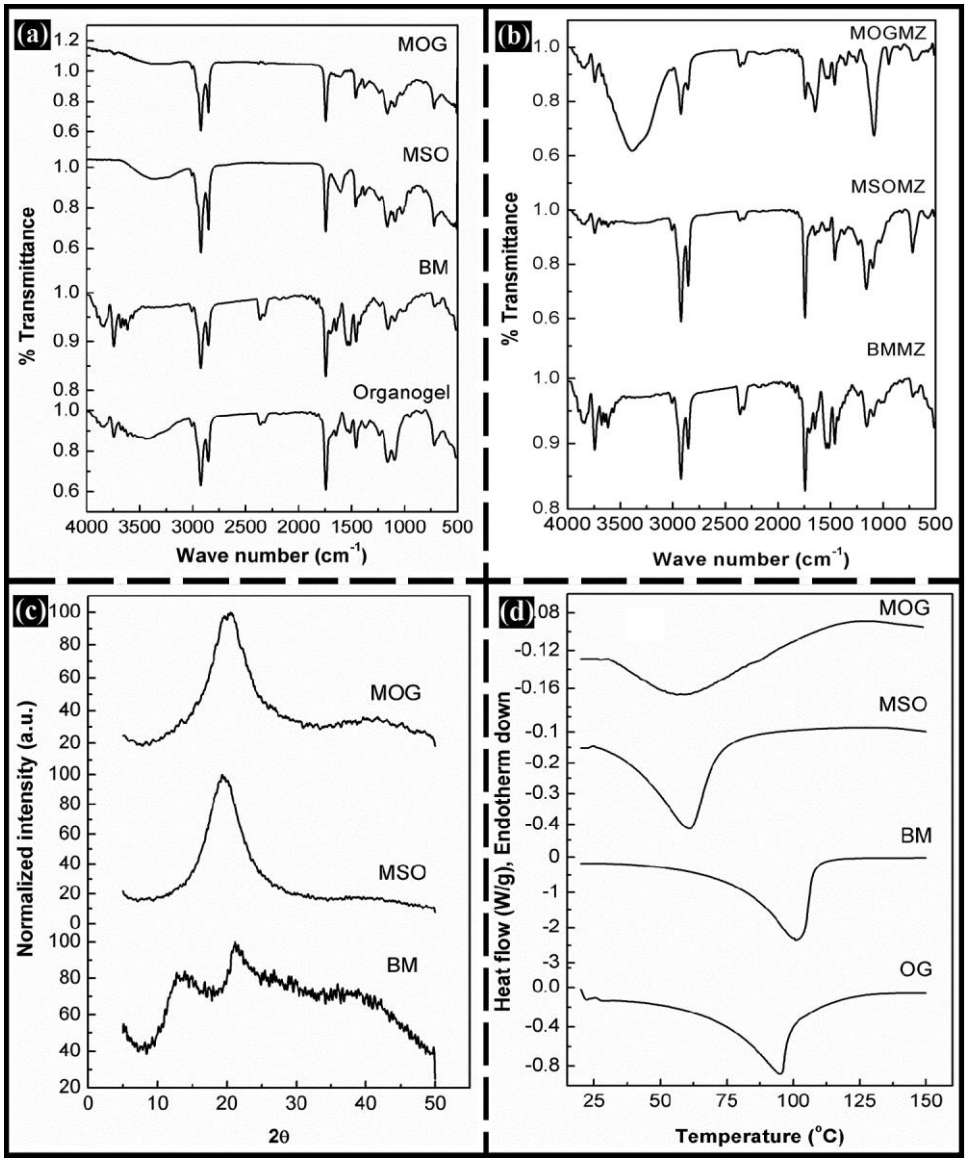

Figure 7.10: (a-b) FTIR spectra, (c) XRD profiles, and (d) DSC thermograms of the microparticles.

The FTIR spectra of the microparticles showed peaks corresponding to calcium alginate (Figure 7.10a-b). The peak at ~3370 cm^{-1} was broadened and shifted towards lower wave numbers in MSO and MOG, suggesting an increase in hydrogen bonding [228]. The drug containing microparticles showed characteristic peaks of metronidazole, in addition to the peaks associated with calcium alginate. The peaks at 1238 cm^{-1} (ester carbonyl peak), 1747 cm^{-1} (carbonyl stretching) and 1593 cm^{-1} (asymmetric nitro stretch), associated with metronidazole, were observed in drug containing microparticles [229]. Though the peaks of the drugs were conserved in the microparticles, the characteristic peaks of the alginate

backbone (1200–950 cm^{-1}) were shifted slightly towards lower wave number. This suggested a strong association of the drugs with the components of the microparticles [230]. At the same time, absence of any new characteristic peak in the spectra suggested that the drugs are in their native state and there were no chemical interactions between the drugs and the microparticles.

The X-ray diffractogram of BM showed two peaks at 13.7º 2θ and 23º 2θ, whereas the diffractograms of MSO and MOG showed only one peak at 23º 2θ (Figure 7.10c). The peak at 13.7º 2θ of BM was not visible in MSO and MOG. On the other hand, the peak at 23º 2θ was intensified. This may be due to the interactions amongst the alginate and the internal phase molecules, which resulted in the alteration in the molecular packing of the alginate molecules.

7.7.6. Thermal studies

Figure 7.10d shows the thermograms of the organogel and developed microparticles. The thermogram of sunflower oil showed an endothermic peak at ~34ºC. The organogel showed a broad endothermic peak at ~95 ºC. This is due to the combined effect of melting of the organogel and evaporation of water present in the organogel [231]. BM showed an endothermic peak at ~100ºC which may be attributed to the evaporation of the bound water associated with the alginate. Although dried microparticles were used, the thermal profile suggested that it was not possible to remove the bound water completely. MSO and MOG have shown endothermic peaks at ~60ºC. This endothermic peak may be associated with the heating of sunflower oil. Gel to sol transition temperature of the span 80 and tween 80 organogels was found to be 55 to 70 ºC [107]. The endothermic peak of MOG was broader than MSO. This can be explained by the simultaneous evaporation of the water present in the organogel. Thermal analysis suggests that the organogels were successfully encapsulated within the microparticles.

7.7.7. Biocompatibility and physical interaction studies

Biocompatibility of the microparticles was determined by studying the relative proliferation of MG63 cells in the presence of the microparticles extracts. The cell proliferation was measured using MTT assay. The results indicated that the cell viability index in presence of the leachates of the microparticles were either ~1 or better than 1 indicating the biocompatible nature of the microparticles (Figure 7.11a). The change in cell viability index was found to be insignificant ($p > 0.05$) with respect to control.

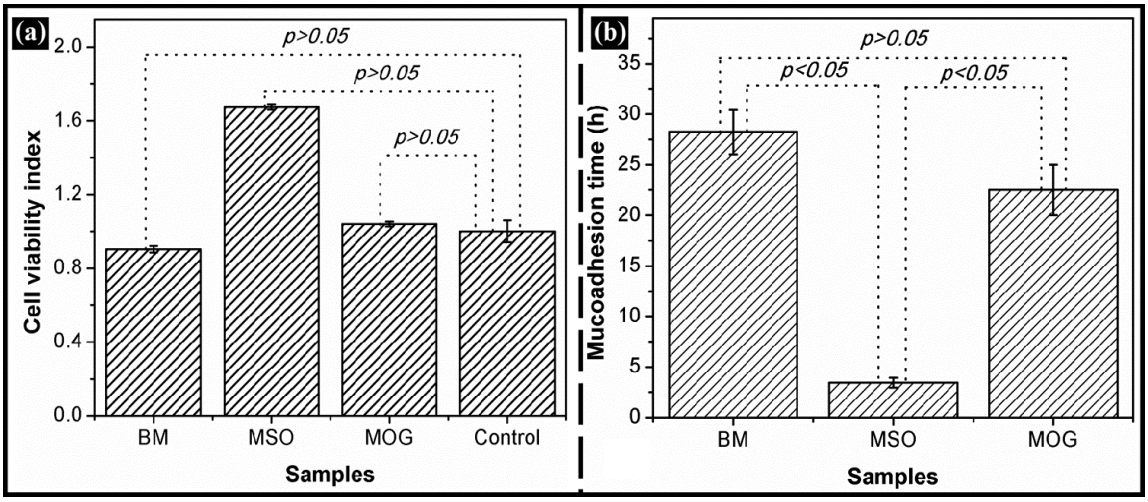

Figure 7.11: (a) Biocompatibility and (b) Mucoadhesion times of the microparticles.

Physical interaction of microparticles with mucous membrane was studied by *in vitro* wash-off method (Figure 7.11b). In general, alginate constructs possess high affinity towards intestinal mucousal layer. Under the experimental conditions, MSO (3.45 ± 0.5) detached quicker than MOG (22.5 ± 2.5) and BM (28.25 ± 2.2). This may be accounted to the leaching of sunflower oil from MSO which was evident from the leaching studies. The mucoadhesive time of MOG was increased almost by 7 fold as compared to MSO. This is due to the prevention of oil leaching from MOG, due to the gelation of the internal phase. The differences in mucoadhesivity of microparticles were found to be significant ($p < 0.05$) as per paired t-test analysis. The significant rise in the mucoadhesive nature of MOG is self-explanatory about the importance of the structuring of the edible oil within the microparticles. The results suggested that the MOG may be tried as mucoadhesive microparticulate delivery vehicle.

7.7.8. *In vitro* drug release studies

Figure 7.12 shows the *in vitro* cumulative percentage drug release (CPDR) profiles of the microparticles. The drug release from BMMZ and MSOMZ was higher than MOGMZ. This may be associated with the leaching of the drugs from BMMZ and MSOMZ.

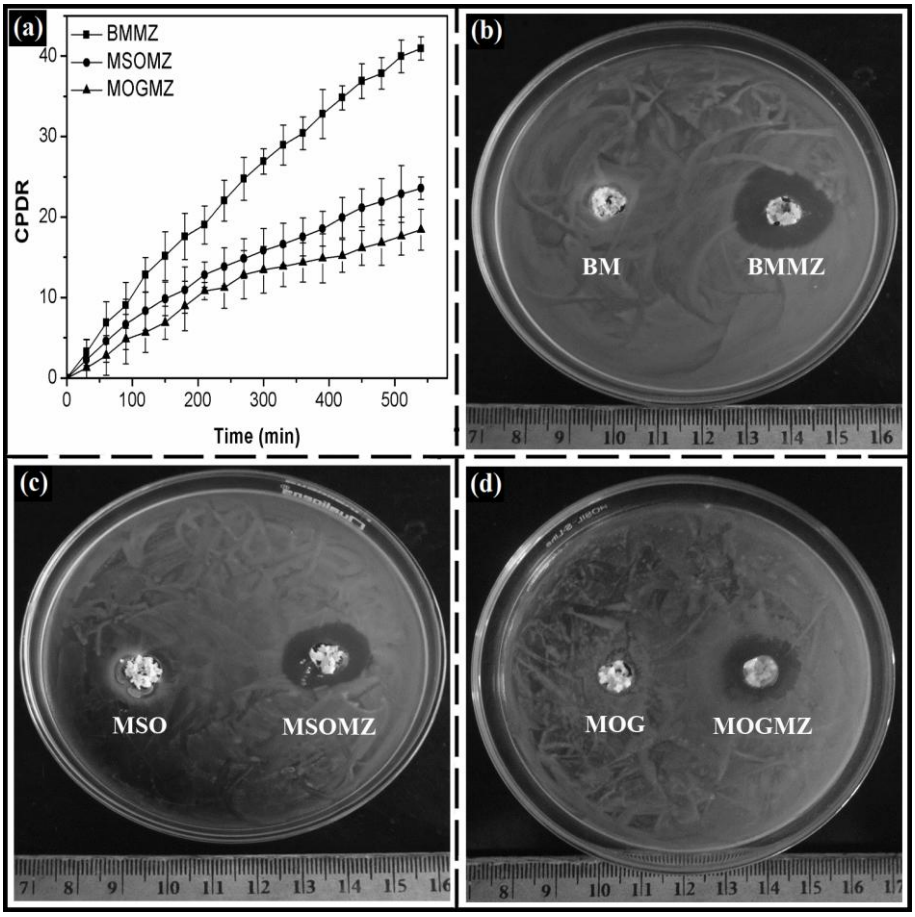

Figure 7.12: (a) CPDR profiles of the microparticles, and (b-d) antimicrobial studies of the microparticles against *E. coli*.

The drug release kinetics was studied by finding the best-fit release model after fitting in zero-order, First-order, Higuchi and Baker-Lonsdale models. The diffusion of the drugs was figured out by calculating 'n' value using KP model. The acceptable regression coefficient for fitting of the models was > 0.95 and the best fit models have been tabulated in Table 7.4 and shown in Figure 7.13. The results suggested that the drug release from the microparticles followed Higuchian and BL kinetic models, indicating that the developed microparticles were spherical matrix type. The release behavior of the drugs from the microparticles followed non-Fickian diffusion. The non-Fickian diffusion of the drugs may be attributed to the polymer relaxation, erosion and degradation [232].

The drug containing microparticles have shown considerable antimicrobial activity thereby suggesting that that the incorporated drugs were bioactive even after encapsulation (Figure 7.12b-d). Comparatively, BMMZ (diameter of the zone of inhibition: 2.2 cm) and MSOMZ (diameter of the zone of inhibition: 1.9 cm) microparticles showed higher zone of inhibition over MOGMZ (diameter of the zone of inhibition: 1.6 cm). This may be attributed to the

quick release of the drugs from BMMZ and MSOMZ microparticles. Similar results were also evident from the *in vitro* drug release studies. The results suggested that the organogels containing microparticles may be tried for the controlled delivery applications.

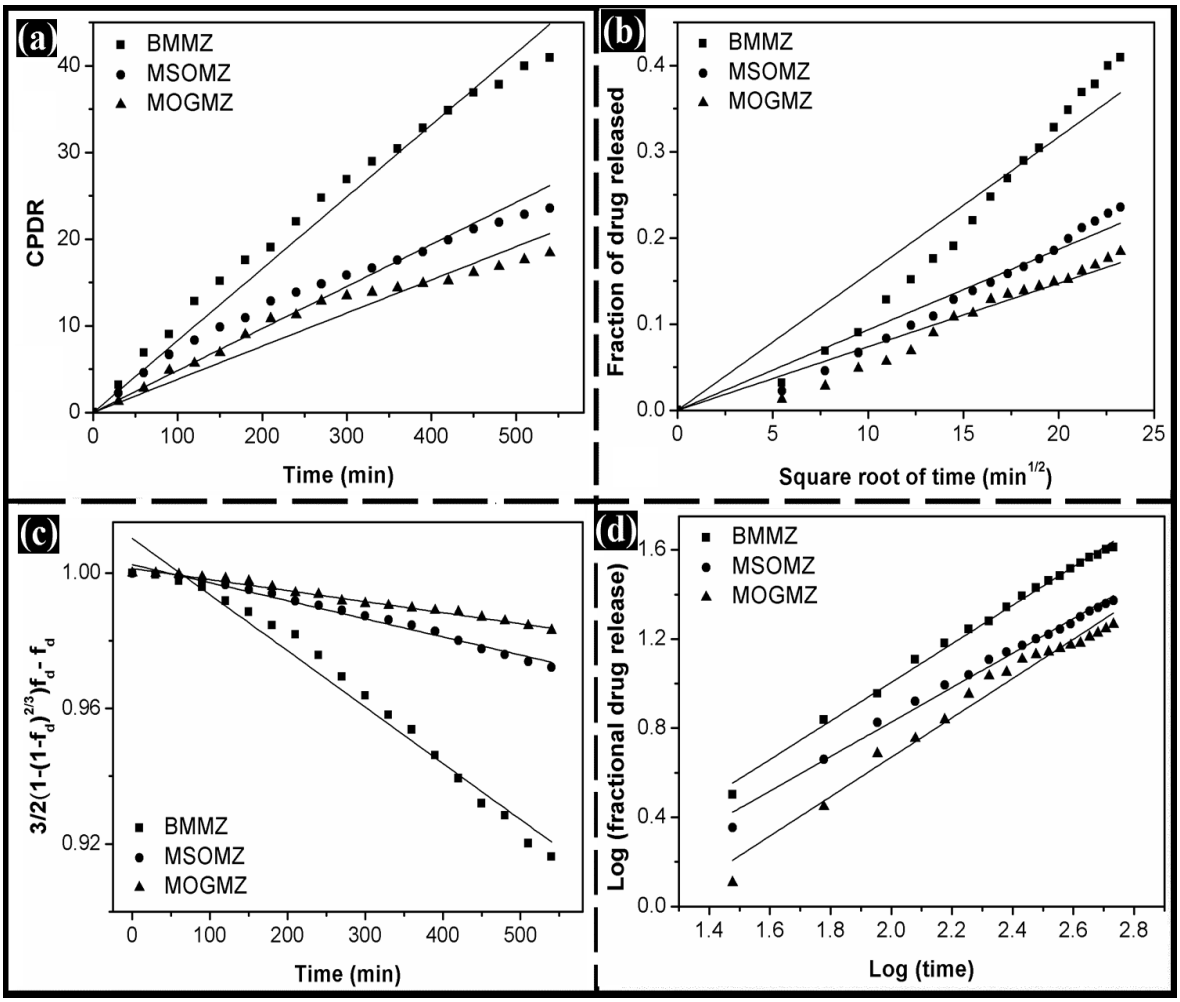

Figure 7.13: The drug release kinetics from the microparticles: (a) Zero order; (b) Higuchi model; (c) BL model and (d) KP model.

Table 7.4: Drug release kinetics from the microparticles.

Sample	Zero order R^2	Higuchi model R^2	BL model R^2	Best fit model	KP model	
					n	Type of diffusion
BMMZ	0.95	0.92	0.96	BL	0.84	Non-Fickian
MSOMZ	0.92	0.95	0.99	BL	0.75	Non-Fickian
MOGMZ	0.89	0.95	0.99	BL	0.84	Non-Fickian

7.8. Conclusion

Encapsulation of the organogels prevented leaching of the internal phase of the microparticles, a common phenomenon when oil is encapsulated. The encapsulation efficiency of the drugs was improved after the encapsulation of organogels. The mucoadhesivity of the microparticles was improved by many-fold when the oil was encapsulated via organogel. Based on the preliminary results, the developed organogel containing microparticles are best suited to prevent the leakage of the internal phase and controlled delivery applications.

Chapter 8

Comparison of the organogel loaded microparticles

8.1. Preparation and characterization of the microparticles

Organogels of different nature (plant-based, animal-based, plant and animal-based and synthetic polysorbates-based) were successfully encapsulated within the alginate microparticles by ionotropic gelation method (Table 8.1). The comparative account of the microparticles is provided in Table 8.2. All the microparticles were found to be stable at room-temperature. Microscopic studies revealed that the microparticles are spherical in nature with broad size distribution. Broad size distribution of the microparticles can be attributed to the increased viscosity of the primary emulsion (due to the addition of organogels) and the method used for the preparation of microparticles. The average size (D_{avg}) of the microparticles differed from each other. The difference in sizes can be attributed to the internal composition of the microparticles. Average size was highest for MCG (cocoa butter organogel containing microparticles) and lowest for ML1 (lanolin organogel containing microparticles. The order of average sizes is MCG > MMG > MOG2 > MOG1 > MOG and ML1. Encapsulation of organogels within the microparticles was confirmed by DSC, FTIR and XRD studies. DSC thermograms of the microparticles showed endothermic peaks corresponding to the melting point of the encapsulated organogels. This indicated that the organogels were encapsulated within the microparticles. XRD studies also showed the peaks corresponding to the gelators of the organogels. It was found that the stable polymorphic state of vegetable fats (cocoa butter and mango butter) and stearic acid was retained in the microparticles. The characterization studies confirmed that the encapsulated organogels are present in their native state within the microparticles.

Table 8.1: Description of the microparticles

Sample	Description
MCG	Cocoa butter organogel (CG35) containing microparticles
MMG	Mango butter organogel (MG35) containing microparticles
ML1	Lanolin organogel (L1) containing microparticles
MOG1	Sesame oil/stearate-based organogel (Ses2) containing microparticles
MOG2	Soy bean oil/stearate-based organogel (Soy2) containing microparticles
MOG	Span 80-Tween 80-based organogel (OG) containing microparticles

Table 8.2: Comparison of the organogel loaded microparticles*.

Sample	D_{avg} (µm)	% leaching	% DEE	Cell viability index	Mucoadhesive time (h)	*In vitro* drug delivery	Zone of inhibition (cm)
MCG	295.95	11.74	71.3	1.05	18.2	Super case-II	1.9
MMG	292.70	12.12	70.2	1.06	17.4	Super case-II	2.0
ML1	130.14	2.82	85.0	0.93	25.5	Non-Fickian	1.0
MOG1	210.24	5.20	77.0	1.01	26.0	Super case-II	1.7
MOG2	226.10	4.20	82.0	1.03	22.15	Super case-II	1.7
MOG	142.0	9.40	74.0	1.01	22.5	Non-Fickian	1.2

*average values are provided

8.2. Leaching studies

The microparticles showed significant variation in leaching of the internal phase (Table 8.2). Higher % leaching was found in vegetable fat containing organogels (MCG and MMG). This was may be due to the melting of cocoa butter and mango butter. DSC studies of the CG35 and MG35 showed that these organogels can melt (partially) at room-temperature. Molten solid fat content of the organogels might have leached out of MCG and MMG and resulted in higher % leaching. Next to MCG and MMG, % leaching was higher from MOG. This can be explained with respect to the strength of the gels. Mechanical studies revealed that OG (Span 80-Tween 80 based organogel) was having lowest gel strength and higher spreadability than the others. In general, lower gel strength and higher spreadable nature reduces the immobilization capacity of the microparticles. Since MOG possesses lower immobilization capacity, there is a high chance for the leaching. MOG1 and MOG2 showed lower % leaching as compared to MOG. Since stearate organogels are having higher gel strength and lower spreadability, MOG1 and MOG2 showed less amount of leaching. % leaching was found to be lowest in ML1 which can be attributed to the higher viscosity and stickiness of the lanolin-based organogels than the other organogels. The difference in % leaching has directly influenced the drug encapsulation efficiency of the microparticles. % drug encapsulation efficiency was in the order of ML1 > MOG2 > MOG1 > MOG > MCG > MMG.

8.3. *In vitro* biocompatibility studies

The cell viability index of all microparticles was found to be near one (the cell viability index of the control) (Table 8.2). This suggests that the microparticles are supporting the growth of the L929 fibroblast cells. The organogel containing microparticles showed higher mucoadhesivity. Leaching of the internal phase affected the mucoadhesivity of the microparticles. Lowest mucoadhesive time was observed for vegetable fat containing organogels and highest for the lanolin containing organogels (Table 8.2). Since these microparticles showed longer mucoadhesion times, these microparticles may be used as the controlled drug delivery vehicles.

8.4. *In vitro* drug delivery studies

The microparticles showed two kinds of drug diffusion. KP kinetics was used to predict the type of diffusion from the microparticles. Non-Fickian mode of drug diffusion was present in ML1 and MOG, whereas, super case-II type of diffusion was associated with MCG, MMG and MOG1

and MOG2. Super case-II mode of diffusion resulted in higher CPDR from the microparticles than the others.

Chapter 9
Conclusion

The present work was aimed at developing a new strategy in negotiating the problem of leaching from the microparticles. To achieve this, hydrophobicity of the microparticles was improved by encapsulating semi-solid organogels within the alginate microparticles. Semi-solid organogels were prepared using plant-derived cocoa butter, mango butter, animal-derived lanolin, stearic acid having both plant and animal origin and synthetic polysorbates (Mixture of Span 80 and Tween 80 in the ratio of 1:2 w/w). The microscopic, physicochemical, thermal and mechanical properties of the organogels were studied. Gelation mechanism in vegetable fat and stearate-based organogels was predicted. Instantaneous nucleation coupled with one or two dimensional growth of the fat crystals was followed by cocoa butter and mango butter organogels. On the other hand, stearate organogels followed heterogeneous nucleation coupled with one-dimensional growth of organogelators. *In vitro* drug release studies were carried out from the organogels using metronidazole and cirprofloxacin (in stearate organogels) as the model drugs. Antimicrobial properties of the organogels were evaluated by checking against *E. coli*.

The developed organogels were successfully encapsulated within the alginate microparticles by ionnotropic/internal gelation method. The presence of organogels as the core material of the microparticles was confirmed by microscopic, XRD and DSC studies. To check the efficiency of the microparticles in preventing the leaching of internal phase, leaching studies were carried out qualitatively and quantitatively. Both the studies showed that the leaching of internal phase from the developed microparticles was found to be negligible when compared with controls. Presence of semi-solid organogels prevented the leaching of the internal phase at room-temperature, which in turn improved the drug encapsulation efficiency of the microparticles. Increase in drug encapsulation efficiency was found to be almost 2-fold as compared to the controls. Prevention of leaching has enhanced the mucoadhesivity of the organogel containing microparticles by almost 2 to 3-fold with respect to the controls. The microparticles showed controlled release of the drugs under *in vitro* conditions and they showed antimicrobial property when tested against *E. coli*. The biocompatibility of the microparticles was checked by incubating their leachates with mammalian fibroblast cells. Based on the results, it was concluded that the developed formulations (organogels and microparticles) may be tried as the controlled delivery vehicles for *in vivo* applications.

References

1. Solís-Fuentes, J.A. and M.C. Durán-de-Bazúa, *Mango seed uses: thermal behaviour of mango seed almond fat and its mixtures with cocoa butter.* Bioresource Technology, 2004. **92**(1): p. 71-78.
2. Gershanik, T. and S. Benita, *Self-dispersing lipid formulations for improving oral absorption of lipophilic drugs.* European Journal of Pharmaceutics and Biopharmaceutics, 2000. **50**(1): p. 179-188.
3. Yeo, Y., N. Baek, and K. Park, *Microencapsulation methods for delivery of protein drugs.* Biotechnology and Bioprocess Engineering, 2001. **6**(4): p. 213-230.
4. Egilmez, N.K., et al., *In situ tumor vaccination with interleukin-12-encapsulated biodegradable microspheres: induction of tumor regression and potent antitumor immunity.* Cancer research, 2000. **60**(14): p. 3832-3837.
5. Sinha, V. and A. Trehan, *Biodegradable microspheres for protein delivery.* Journal of Controlled Release, 2003. **90**(3): p. 261-280.
6. Tamber, H., et al., *Formulation aspects of biodegradable polymeric microspheres for antigen delivery.* Advanced drug delivery reviews, 2005. **57**(3): p. 357-376.
7. Eun, Y.-J., et al., *Encapsulating bacteria in agarose microparticles using microfluidics for high-throughput cell analysis and isolation.* ACS chemical biology, 2010. **6**(3): p. 260-266.
8. He, P., et al., *Preparation of novel organometallic derivatives of cholesterol and their gel-formation properties.* Colloids and Surfaces A: Physicochemical and Engineering Aspects, 2010. **362**(1–3): p. 127-134.
9. Gharsallaoui, A., et al., *Applications of spray-drying in microencapsulation of food ingredients: An overview.* Food Research International, 2007. **40**(9): p. 1107-1121.
10. George, M. and R.G. Weiss, *Molecular organogels. Soft matter comprised of low-molecular-mass organic gelators and organic liquids.* Accounts of chemical research, 2006. **39**(8): p. 489-497.
11. Sarkar, S., et al., *Hydrophobic derivatives of guar gum hydrolyzate and gum arabic as matrices for microencapsulation of mint oil.* Carbohydrate Polymers, 2013. **95**(1): p. 177-182.

12. Sagiri, S., et al., *Organogels as Matrices for Controlled Drug Delivery: A Review on the Current State.* Soft Materials, 2013(just-accepted).
13. Vintiloiu, A. and J.-C. Leroux, *Organogels and their use in drug delivery—a review.* Journal of Controlled Release, 2008. **125**(3): p. 179-192.
14. Hashizaki, K., H. Taguchi, and Y. Saito, *A novel reverse worm-like micelle from a lecithin/sucrose fatty acid ester/oil system.* Colloid & Polymer Science, 2009. **287**(9): p. 1099-1105.
15. Kumar, R. and O.P. Katare, *Lecithin organogels as a potential phospholipid-structured system for topical drug delivery: a review,* . AAPS Pharm. Sci. Tech, 2005. **6**(298).
16. Pernetti, M., et al., *Structuring edible oil with lecithin and sorbitan tri-stearate.* Food Hydrocolloids, 2006. **21**(5-6): p. 855-861.
17. Trickett, K., et al., *Microemulsion-based organogels containing inorganic nanoparticles.* Soft Matter, 2010. **6**(6): p. 1291-1296.
18. Vemula, P.K. and G. John, *Crops: A Green Approach toward Self-Assembled Soft Materials.* Accounts of Chemical Research, 2008. **41**(6): p. 769-782.
19. Trivedi, D.R., et al., *Structure–Property Correlation of a New Family of Organogelators Based on Organic Salts and Their Selective Gelation of Oil from Oil/Water Mixtures.* Chemistry – A European Journal, 2004. **10**(21): p. 5311-5322.
20. Abdallah, D.J. and R.G. Weiss, *n-Alkanes Gel n-Alkanes (and Many Other Organic Liquids).* Langmuir, 1999. **16**(2): p. 352-355.
21. Schaink, H.M., et al., *Crystal network for edible oil organogels: Possibilities and limitations of the fatty acid and fatty alcohol systems.* Food Research International, 2007. **40**(9): p. 1185-1193.
22. Terech, P. and R.G. Weiss, *Low molecular mass gelators of organic liquids and the properties of their gels.* Chemical Reviews, 1997. **97**(8): p. 3133-3160.
23. Liu, K., et al., *Supramolecular gels based on organic diacid monoamides of cholesteryl glycinate.* Journal of Colloid and Interface Science, 2008. **327**(1): p. 233-242.
24. Tu, T., et al., *An Air-Stable Organometallic Low-Molecular-Mass Gelator: Synthesis, Aggregation, and Catalytic Application of a Palladium Pincer Complex.* Angewandte Chemie International Edition, 2007. **46**(33): p. 6368-6371.

25. Li, Y., et al., *Amino Acid Derivatives of Cholesterol as "Latent" Organogelators with Hydrogen Chloride as a Protonation Reagent.* Langmuir, 2006. **22**(16): p. 7016-7020.
26. Löfman, M., et al., *Bile acid alkylamide derivatives as low molecular weight organogelators: Systematic gelation studies and qualitative structural analysis of the systems.* Journal of Colloid and Interface Science, 2011. **360**(2): p. 633-644.
27. Suzuki, M., et al., *New gemini organogelators linked by oxalyl amide: organogel formation and their thermal stabilities.* Tetrahedron letters, 2003. **44**(36): p. 6841-6843.
28. Brosse, N., D. Barth, and B. Jamart-Grégoire, *A family of strong low-molecular-weight organogelators based on aminoacid derivatives.* Tetrahedron letters, 2004. **45**(52): p. 9521-9524.
29. Willimann, H.-L. and P.L. Luisi, *Lecithin organogels as matrix for the transdermal transport of drugs.* Biochemical and Biophysical Research Communications, 1991. **177**(3): p. 897-900.
30. Bot, A., A.R. den, and E. Roijers, *Fibrils of γ-Oryzanol + β-Sitosterol in edible oil organogels.* Journal of the American Oil Chemists' Society, 2008. **85**(12): p. 1127-1134.
31. Yoza, K., et al., *Sugar-integrated gelators of organic fluids on their versatility as building-blocks and diversity in superstructures.* Chem. Commun.,, 1998: p. 907-908.
32. Murdan, S., *Organogels in drug delivery.* Expert Opinion on Drug Delivery, 2005. **2**(3): p. 489-505.
33. Engel, R.H., S.J. Riggi, and M.J. Fahrenbach, *Insulin: Intestinal absorption as water-in-oil-in-water emulsions.* Nature, 1968. **219**(5156): p. 856-857.
34. Lee, G.-S., D.-H. Lee, and H.-B. Pyo, *Preparation and characterization of encapsulation of multiple lipid carrier (MLC) using vegetable fat.* Journal of Industrial and Engineering Chemistry, 2011. **17**(3): p. 421-426.
35. Kita, Y., S. Matsumoto, and D. Yonezawa, *Viscometric method for estimating the stability of W/O/W-type multiple-phase emulsions.* Journal of Colloid And Interface Science, 1977. **62**(1): p. 87-94.
36. Cournarie, F., et al., *Insulin-loaded W/O/W multiple emulsions: comparison of the performances of systems prepared with medium-chain-triglycerides and fish oil.* European Journal of Pharmaceutics and Biopharmaceutics, 2004. **58**(3): p. 477-482.

37. Cunha, A.S., et al., *Insulin in w/o/w multiple emulsions: preparation, characterization and determination of stability towards proteases in vitro.* Journal of microencapsulation, 1997. **14**(3): p. 311-319.
38. Schuster, D., *Encyclopedia of Emulsion Technology: Basic theory, measurement, applications*. Vol. 3. 1987: CRC Press.
39. Kumar, R., M.S. Kumar, and N. Mahdevan, *Multiple emulsions: a review.* International Journal of Recent Advances in Pharmaceutical Research, 2012. **2**(1): p. 9-19.
40. Morais, J.M., P.A. Rocha-Filho, and D.J. Burgess, *Relationship between rheological properties and one-step W/O/W multiple emulsion formation.* Langmuir, 2010. **26**(23): p. 17874-17881.
41. Khan, A.Y., et al., *Multiple emulsions: an overview.* Current Drug Delivery, 2006. **3**(4): p. 429-443.
42. Yoshida, K., et al., *Stability of vitamin A in oil-in-water-in-oil-type multiple emulsions.* Journal of the American Oil Chemists' Society, 1999. **76**(2): p. 1-6.
43. Souto, E.B., W. Mehnert, and R.H. Müller, *Polymorphic behaviour of Compritol®888 ATO as bulk lipid and as SLN and NLC.* Journal of microencapsulation, 2006. **23**(4): p. 417-433.
44. Dams, S.S. and I.M. Walker, *[5] Multiple emulsions as targetable delivery systems.* Methods in enzymology, 1987. **149**: p. 51-64.
45. Sohi, H., Y. Sultana, and R.K. Khar, *Taste masking technologies in oral pharmaceuticals: recent developments and approaches.* Drug development and industrial pharmacy, 2004. **30**(5): p. 429-448.
46. Garti, N., et al., *Double emulsions of water-in-oil-in-water stabilized by α-form fat microcrystals. Part 1: Selection of emulsifiers and fat microcrystalline particles.* Journal of the American Oil Chemists' Society, 1999. **76**(3): p. 383-389.
47. Hom, F., S. Veresh, and W. Ebert, *Soft gelatin capsules II: Oxygen permeability study of capsule shells.* Journal of pharmaceutical sciences, 1975. **64**(5): p. 851-857.
48. Cole, E.T., D. Cadé, and H. Benameur, *Challenges and opportunities in the encapsulation of liquid and semi-solid formulations into capsules for oral administration.* Advanced drug delivery reviews, 2008. **60**(6): p. 747-756.

49. Liu, S., N. Low, and M.T. Nickerson, *Entrapment of flaxseed oil within gelatin-gum arabic capsules.* Journal of the American Oil Chemists' Society, 2010. **87**(7): p. 809-815.
50. Chang, C.P. and T. Dobashi, *Preparation of alginate complex capsules containing eucalyptus essential oil and its controlled release.* Colloids and Surfaces B: Biointerfaces, 2003. **32**(3): p. 257-262.
51. Lertsutthiwong, P., et al., *Preparation of alginate nanocapsules containing turmeric oil.* Carbohydrate Polymers, 2008. **74**(2): p. 209-214.
52. Bilia, A.R., et al., *Essential Oils Loaded in Nanosystems: A Developing Strategy for a Successful Therapeutic Approach.* Evidence-Based Complementary and Alternative Medicine, 2014. **2014**.
53. Hosseini, S.F., et al., *Two-step method for encapsulation of oregano essential oil in chitosan nanoparticles: Preparation, characterization and in vitro release study.* Carbohydrate Polymers, 2013. **95**(1): p. 50-56.
54. Paula, H.C.B., et al., *Lippia sidoides essential oil encapsulation by angico gum/chitosan nanoparticles.* Journal of the Brazilian Chemical Society, 2010. **21**: p. 2359-2366.
55. de Oliveira, E.F., H.C.B. Paula, and R.C.M.d. Paula, *Alginate/cashew gum nanoparticles for essential oil encapsulation.* Colloids and Surfaces B: Biointerfaces, 2014. **113**(0): p. 146-151.
56. ALHaj, N.A., et al., *Characterization of Nigella sativa L. essential oil-loaded solid lipid nanoparticles.* American Journal of Pharmacology and Toxicology, 2010. **5**(1): p. 52.
57. Lai, F., et al., *SLN as a topical delivery system for Artemisia arborescens essential oil: In vitro antiviral activity and skin permeation study.* International journal of nanomedicine, 2007. **2**(3): p. 419.
58. Shi, F., et al., *Preparation and characterization of solid lipid nanoparticles loaded with frankincense and myrrh oil.* International journal of nanomedicine, 2012. **7**: p. 2033.
59. Moghimipour, E., Z. Ramezani, and S. Handali, *Solid Lipid Nanoparticles as a Delivery System for Zataria multiflora Essential Oil: Formulation and Characterization.* Current Drug Delivery, 2013. **10**(2): p. 151-157.
60. Chan, E.-S., *Preparation of Ca-alginate beads containing high oil content: Influence of process variables on encapsulation efficiency and bead properties.* Carbohydrate Polymers, 2011. **84**(4): p. 1267-1275.

61. Durante, M., et al., *Effects of Sodium Alginate Bead Encapsulation on the Storage Stability of Durum Wheat (Triticum durum Desf.) Bran Oil Extracted by Supercritical CO2.* Journal of agricultural and food chemistry, 2012. **60**(42): p. 10689-10695.
62. Rubilar, M., et al., *Development of a soup powder enriched with microencapsulated linseed oil as a source of omega-3 fatty acids.* European Journal of Lipid Science and Technology, 2012. **114**(4): p. 423-433.
63. Can Karaca, A., N. Low, and M. Nickerson, *Encapsulation of Flaxseed Oil Using a Benchtop Spray Dryer for Legume Protein–Maltodextrin Microcapsule Preparation.* Journal of agricultural and food chemistry, 2013. **61**(21): p. 5148-5155.
64. Paula, H.C.B., et al., *Preparation and characterization of chitosan/cashew gum beads loaded with Lippia sidoides essential oil.* Materials Science and Engineering: C, 2011. **31**(2): p. 173-178.
65. Lopez, M., et al., *Development of formulations to improve the controlled-release of linalool to be applied as an insecticide.* Journal of agricultural and food chemistry, 2012. **60**(5): p. 1187-1192.
66. Fernandes, R.V.d.B., S.V. Borges, and D.A. Botrel, *Gum arabic/starch/maltodextrin/inulin as wall materials on the microencapsulation of rosemary essential oil.* Carbohydrate Polymers, 2014. **101**: p. 524-532.
67. Soottitantawat, A., et al., *Microencapsulation of l-menthol by spray drying and its release characteristics.* Innovative Food Science & Emerging Technologies, 2005. **6**(2): p. 163-170.
68. Sagiri, S.S., et al., *Encapsulation of vegetable organogels for controlled delivery applications.* Designed Monomers and Polymers, 2012. **16**(4): p. 366-376.
69. Sagiri, S.S., et al., *Encapsulation of Sorbitan Ester-Based Organogels in Alginate Microparticles.* AAPS PharmSciTech, 2014: p. 1-12.
70. Sagiri, S.S., K. Pal, and P. Basak, *Encapsulation of animal wax-based organogels in alginate microparticles.* Journal of Applied Polymer Science, 2014.
71. Siqueira-Moura, M.P., et al., *Gelled oil particles: A new approach to encapsulate a hydrophobic metallophthalocyanine.* Journal of colloid and interface science, 2013. **401**: p. 155-160.

72. Park, J., M. Ye, and K. Park, *Biodegradable polymers for microencapsulation of drugs.* Molecules, 2005. **10**(1): p. 146-161.
73. Venkatesan, P., R. Manavalan, and K. Valliappan, *Microencapsulation: a vital technique in novel drug delivery system.* Journal of Pharmaceutical Sciences and Research, 2009. **1**(4): p. 26-35.
74. Lv, Y., et al., *Formation of heat-resistant nanocapsules of jasmine essential oil via gelatin/gum arabic based complex coacervation.* Food Hydrocolloids, 2014. **35**(0): p. 305-314.
75. Soliman, E.A., et al., *Microencapsulation of Essential Oils within Alginate: Formulation and in Vitro Evaluation of Antifungal Activity.* Journal of Encapsulation and Adsorption Sciences, 2013. **3**: p. 48.
76. Yang, Y.-Y., T.-S. Chung, and N. Ping Ng, *Morphology, drug distribution, and in vitro release profiles of biodegradable polymeric microspheres containing protein fabricated by double-emulsion solvent extraction/evaporation method.* Biomaterials, 2001. **22**(3): p. 231-241.
77. Silva, C.M., et al., *Alginate microspheres prepared by internal gelation: Development and effect on insulin stability.* International Journal of Pharmaceutics, 2006. **311**(1–2): p. 1-10.
78. Koo, S.Y., et al., *Microencapsulation of peppermint oil in an alginate–pectin matrix using a coaxial electrospray system.* International Journal of Food Science & Technology, 2014. **49**(3): p. 733-739.
79. Almeida, A.P., et al., *Microencapsulation of oregano essential oil in starch-based materials using supercritical fluid technology.* Innovative Food Science & Emerging Technologies, 2013. **20**(0): p. 140-145.
80. Roccia, P., et al., *Influence of spray-drying operating conditions on sunflower oil powder qualities.* Powder Technology, 2014. **254**(0): p. 307-313.
81. Gallo, L., et al., *Influence of spray-drying operating conditions on Rhamnus purshiana (Cáscara sagrada) extract powder physical properties.* Powder Technology, 2011. **208**(1): p. 205-214.
82. Turchiuli, C., et al., *Use of different supports for oil encapsulation in powder by spray drying.* Powder Technology, 2014. **255**(0): p. 103-108.

83. Carneiro, H.C.F., et al., *Encapsulation efficiency and oxidative stability of flaxseed oil microencapsulated by spray drying using different combinations of wall materials.* Journal of Food Engineering, 2013. **115**(4): p. 443-451.
84. Mohanty, B. and H. Bohidar, *Systematic of alcohol-induced simple coacervation in aqueous gelatin solutions.* Biomacromolecules, 2003. **4**(4): p. 1080-1086.
85. Lazko, J., Y. Popineau, and J. Legrand, *Soy glycinin microcapsules by simple coacervation method.* Colloids and Surfaces B: Biointerfaces, 2004. **37**(1): p. 1-8.
86. Mauguet, M., et al., *Gliadin matrices for microencapsulation processes by simple coacervation method.* Journal of microencapsulation, 2002. **19**(3): p. 377-384.
87. Wu, K.G. and Q. Xiao, *Microencapsulation of fish oil by simple coacervation of hydroxypropyl methylcellulose.* Chinese Journal of Chemistry, 2005. **23**(11): p. 1569-1572.
88. Weiβ, G., et al., *Simple coacervation of hydroxypropyl methylcellulose phthalate (HPMCP) II. Microencapsulation of ibuprofen.* International journal of pharmaceutics, 1995. **124**(1): p. 97-105.
89. Prabaharan, M. and J. Mano, *Chitosan-based particles as controlled drug delivery systems.* Drug delivery, 2004. **12**(1): p. 41-57.
90. Latha, M., et al., *Bioavailability of theophylline from glutaraldehyde cross-linked casein microspheres in rabbits following oral administration.* Journal of controlled release, 1995. **34**(1): p. 1-7.
91. Lin, S.Y. and J.C. Yang, *Bioavailability studies of theophylline ethylcellulose microcapsules prepared by using ethylene-vinyl acetate copolymer as a coacervation-inducing agent.* Journal of pharmaceutical sciences, 1987. **76**(3): p. 219-223.
92. Maji, T.K., et al., *Microencapsulation of Zanthoxylum limonella oil (ZLO) in glutaraldehyde crosslinked gelatin for mosquito repellent application.* Bioresource Technology, 2007. **98**(4): p. 840-844.
93. Weinbreck, F., et al., *Complex coacervation of whey proteins and gum arabic.* Biomacromolecules, 2003. **4**(2): p. 293-303.

94. Burgess, D. and J. Carless, *Microelectrophoretic studies of gelatin and acacia for the prediction of complex coacervation.* Journal of Colloid and interface Science, 1984. **98**(1): p. 1-8.
95. Schmitt, C., et al., *Complex coacervation between [beta]-lactoglobulin and acacia gum in aqueous medium.* Food Hydrocolloids, 1999. **13**(6): p. 483-496.
96. Tsung, M. and D.J. Burgess, *Preparation and stabilization of heparin/gelatin complex coacervate microcapsules.* Journal of pharmaceutical sciences, 1997. **86**(5): p. 603-607.
97. Thimma, R. and S. Tammishetti, *Study of complex coacervation of gelatin with sodium carboxymethyl guar gum: microencapsulation of clove oil and sulphamethoxazole.* Journal of microencapsulation, 2003. **20**(2): p. 203-210.
98. Singh, O. and D. Burgess, *Characterization of Albumin-Alginic Acid Complex Coacervation.* Journal of pharmacy and pharmacology, 1989. **41**(10): p. 670-673.
99. Hwang, D.S., J.H. Waite, and M. Tirrell, *Promotion of osteoblast proliferation on complex coacervation-based hyaluronic acid-recombinant mussel adhesive protein coatings on titanium.* Biomaterials, 2010. **31**(6): p. 1080-1084.
100. Saravanan, M. and K.P. Rao, *Pectin-gelatin and alginate-gelatin complex coacervation for controlled drug delivery: Influence of anionic polysaccharides and drugs being encapsulated on physicochemical properties of microcapsules.* Carbohydrate Polymers, 2010. **80**(3): p. 808-816.
101. Zhang, L., et al., *Coaxial electrospray of microparticles and nanoparticles for biomedical applications.* Expert Review of Medical Devices, 2012. **9**(6): p. 595-612.
102. Loscertales, I.G., et al., *Micro/Nano Encapsulation via Electrified Coaxial Liquid Jets.* Science, 2002. **295**(5560): p. 1695-1698.
103. Xie, J., et al., *Encapsulation of protein drugs in biodegradable microparticles by co-axial electrospray.* Journal of colloid and interface science, 2008. **317**(2): p. 469-476.
104. Varona, S., et al., *Supercritical impregnation of lavandin (Lavandula hybrida) essential oil in modified starch.* The Journal of Supercritical Fluids, 2011. **58**(2): p. 313-319.
105. Peniche, C., et al., *Formation and stability of shark liver oil loaded chitosan/calcium alginate capsules.* Food Hydrocolloids, 2004. **18**(5): p. 865-871.
106. Jibry, N., R. Heenan, and S. Murdan, *Amphiphilogels for Drug Delivery: Formulation and Characterization.* Pharmaceutical Research, 2004. **21**(10): p. 1852-1861.

107. Sagiri, S.S., et al., *Effect of composition on the properties of tween-80–span-80-based organogels.* Designed Monomers and Polymers, 2012. **15**(3): p. 253-273.
108. Ranathunge, K. and L. Schreiber, *Water and solute permeabilities of Arabidopsis roots in relation to the amount and composition of aliphatic suberin.* Journal of Experimental Botany, 2011. **62**(6): p. 1961-1974.
109. Desai, H., N.R. Biswal, and S. Paria, *Rheological Behavior of Pyrophyllite− Water Slurry in the Presence of Anionic, Cationic, and Nonionic Surfactants.* Industrial & Engineering Chemistry Research, 2010. **49**(11): p. 5400-5406.
110. Jones, D.S., et al., *Physicochemical Characterization of Bioactive Polyacrylic Acid Organogels as Potential Antimicrobial Implants for the Buccal Cavity.* Biomacromolecules, 2008. **9**(2): p. 624-633.
111. L. W. Chan, L.T.L., P. W. S. Heng, *Microencapsulation of oils using sodium alginate.* Journal of Microencapsulation, 2000. **17**(6): p. 757-766.
112. Bordenave, N., S. Janaswamy, and Y. Yao, *Influence of glucan structure on the swelling and leaching properties of starch microparticles.* Carbohydrate Polymers, 2014. **103**(0): p. 234-243.
113. Fischer, D., et al., *In vitro cytotoxicity testing of polycations: influence of polymer structure on cell viability and hemolysis.* Biomaterials, 2003. **24**(7): p. 1121-1131.
114. Miller, K.B., et al., *Antioxidant Activity and Polyphenol and Procyanidin Contents of Selected Commercially Available Cocoa-Containing and Chocolate Products in the United States.* Journal of Agricultural and Food Chemistry, 2006. **54**(11): p. 4062-4068.
115. Jahurul, M.H.A., et al., *Cocoa butter fats and possibilities of substitution in food products concerning cocoa varieties, alternative sources, extraction methods, composition, and characteristics.* Journal of Food Engineering, 2013. **117**(4): p. 467-476.
116. Yanus, R.L., et al., *Trace elements in cocoa solids and chocolate: An ICPMS study.* Talanta, 2014. **119**(0): p. 1-4.
117. Lipp, M. and E. Anklam, *Review of cocoa butter and alternative fats for use in chocolate—Part A. Compositional data.* Food Chemistry, 1998. **62**(1): p. 73-97.
118. Kabuki, T., et al., *Characterization of novel antimicrobial compounds from mango (Mangifera indica L.) kernel seeds.* Food Chemistry, 2000. **71**(1): p. 61-66.

119. Norton, J.E. and P.J. Fryer, *Investigation of changes in formulation and processing parameters on the physical properties of cocoa butter emulsions.* Journal of Food Engineering, 2012. **113**(2): p. 329-336.
120. Boutin, C., et al., *Characterization and acid-induced gelation of butter oil emulsions produced from heated whey protein dispersions.* International Dairy Journal, 2007. **17**(6): p. 696-703.
121. Ibrahim, M.M., S.A. Hafez, and M.M. Mahdy, *Organogels, hydrogels and bigels as transdermal delivery systems for diltiazem hydrochloride.* Asian Journal of Pharmaceutical Sciences, 2013. **8**(1): p. 48-57.
122. Satapathy, D., et al., *Sunflower-oil-based lecithin organogels as matrices for controlled drug delivery.* Journal of Applied Polymer Science, 2013. **129**(2): p. 585-594.
123. Ghotra, B.S., S.D. Dyal, and S.S. Narine, *Lipid shortenings: a review.* Food Research International, 2002. **35**(10): p. 1015-1048.
124. di Bari, V., J.E. Norton, and I.T. Norton, *Effect of processing on the microstructural properties of water-in-cocoa butter emulsions.* Journal of Food Engineering, 2014. **122**(0): p. 8-14.
125. Norton, J.E., et al., *Development and characterisation of tempered cocoa butter emulsions containing up to 60% water.* Journal of Food Engineering, 2009. **95**(1): p. 172-178.
126. Ghosh, S. and D. Rousseau, *Fat crystals and water-in-oil emulsion stability.* Current Opinion in Colloid & Interface Science, 2011. **16**(5): p. 421-431.
127. Himawan, C., V. Starov, and A. Stapley, *Thermodynamic and kinetic aspects of fat crystallization.* Advances in colloid and interface science, 2006. **122**(1): p. 3-33.
128. MacMillan, S.D., et al., *In Situ Small Angle X-ray Scattering (SAXS) Studies of Polymorphism with the Associated Crystallization of Cocoa Butter Fat Using Shearing Conditions.* Crystal Growth & Design, 2002. **2**(3): p. 221-226.
129. Marangoni, A.G. and S.E. McGauley, *Relationship between Crystallization Behavior and Structure in Cocoa Butter.* Crystal Growth & Design, 2002. **3**(1): p. 95-108.
130. Campos, R., M. Ollivon, and A.G. Marangoni, *Molecular Composition Dynamics and Structure of Cocoa Butter.* Crystal Growth & Design, 2009. **10**(1): p. 205-217.

131. Hindle, S., M.W. Povey, and K. Smith, *Characterizing cocoa butter seed crystals by the oil-in-water emulsion crystallization method.* Journal of the American Oil Chemists' Society, 2002. **79**(10): p. 993-1002.
132. Fredrick, E., et al., *Isothermal crystallization behaviour of milk fat in bulk and emulsified state.* International Dairy Journal, 2011. **21**(9): p. 685-695.
133. Bricknell, J. and R. Hartel, *Relation of fat bloom in chocolate to polymorphic transition of cocoa butter.* Journal of the American Oil Chemists' Society, 1998. **75**(11): p. 1609-1615.
134. Ramananarivo, H.R., et al., *Tunable Structure of Zirconia Nanoparticles by Biopolymer Gelation: Design, Synthesis and Characterization.* European Journal of Inorganic Chemistry, 2012. **2012**(33): p. 5465-5469.
135. Hodate, Y., et al., *Ultrasonic velocity measurement of crystallization rates of palm oil in oil-water emulsions.* Colloids and Surfaces A: Physicochemical and Engineering Aspects, 1997. **128**(1): p. 217-224.
136. Niu, H.J. and D.P. Hampshire, *Fabrication of nanocrystalline and amorphous Chevrel phase PbMo6S8 powder by ball milling.* Physica C: Superconductivity, 2002. **372–376, Part 2**(0): p. 1145-1147.
137. Goodacre, R. and E. Anklam, *Fourier transform infrared spectroscopy and chemometrics as a tool for the rapid detection of other vegetable fats mixed in cocoa butter.* Journal of the American Oil Chemists' Society, 2001. **78**(10): p. 993-1000.
138. Lam, P.-L., et al., *Development of formaldehyde-free agar/gelatin microcapsules containing berberine HCl and gallic acid and their topical and oral applications.* Soft Matter, 2012. **8**(18): p. 5027-5037.
139. Wang, M., et al., *Investigation of Water Diffusion in Low-Density Polyethylene by Attenuated Total Reflectance Fourier Transform Infrared Spectroscopy and Two-Dimensional Correlation Analysis.* Industrial & Engineering Chemistry Research, 2011. **50**(10): p. 6447-6454.
140. Herculano, R.D., et al., *On the release of metronidazole from natural rubber latex membranes.* Materials Science and Engineering: C, 2011. **31**(2): p. 272-275.
141. Lopez, C., et al., *Definition of a model fat for crystallization-in-emulsion studies.* Journal of the American Oil Chemists' Society, 2001. **78**(12): p. 1233-1244.

142. Metin, S. and R. Hartel, *Thermal analysis of isothermal crystallization kinetics in blends of cocoa butter with milk fat or milk fat fractions.* Journal of the American Oil Chemists' Society, 1998. **75**(11): p. 1617-1624.
143. Foubert, I., et al., *Influence of Chemical Composition on the Isothermal Cocoa Butter Crystallization.* Journal of Food Science, 2004. **69**(9): p. E478-E487.
144. Sharples, A., *Introduction to polymer crystallization.* 1966.
145. Ahza, A.B., *Kinetics of milk fat crystallization in a continuous crystallizer*. 1995: University of Wisconsin--Madison.
146. Smith, K.W., *Cocoa butter and cocoa butter equivalents.* Structured and modified lipids. New York: Marcel Dekker, 2001: p. 401-22.
147. Abruzzo, A., et al., *Mucoadhesive chitosan/gelatin films for buccal delivery of propranolol hydrochloride.* Carbohydrate Polymers, 2012. **87**(1): p. 581-588.
148. Peleg, M., *CHARACTERIZATION OF THE STRESS RELAXATION CURVES OF SOLID FOODS.* Journal of Food Science, 1979. **44**(1): p. 277-281.
149. Bellido, G.G. and D.W. Hatcher, *Asian noodles: Revisiting Peleg's analysis for presenting stress relaxation data in soft solid foods.* Journal of Food Engineering, 2009. **92**(1): p. 29-36.
150. Dash, S., et al., *Kinetic modeling on drug release from controlled drug delivery systems.* Acta Pol Pharm, 2010. **67**(3): p. 217-223.
151. Lee, K.Y. and D.J. Mooney, *Alginate: Properties and biomedical applications.* Progress in Polymer Science, 2012. **37**(1): p. 106-126.
152. Liu, L.-S., et al., *Controlled release of interleukin-2 for tumour immunotherapy using alginate/chitosan porous microspheres.* Journal of Controlled Release, 1997. **43**(1): p. 65-74.
153. Rahmani, S., et al., *Multimodal delivery of irinotecan from microparticles with two distinct compartments.* Journal of Controlled Release, 2013. **172**(1): p. 239-245.
154. Florea, A.-M. and D. Büsselberg, *Cisplatin as an anti-tumor drug: cellular mechanisms of activity, drug resistance and induced side effects.* Cancers, 2011. **3**(1): p. 1351-1371.
155. Shenoy, D.B., et al., *Layer-by-Layer Engineering of Biocompatible, Decomposable Core−Shell Structures.* Biomacromolecules, 2003. **4**(2): p. 265-272.

156. Rincon, A., et al., *Biocompatibility of elastin-like polymer poly (VPAVG) microparticles: in vitro and in vivo studies.* Journal of Biomedical Materials Research Part A, 2006. **78**(2): p. 343-351.
157. Teixeira, A.C.T., et al., *Phase behaviour of oleanolic acid, pure and mixed with stearic acid: Interactions and crystallinity.* Chemistry and Physics of Lipids, 2010. **163**(7): p. 655-666.
158. Tan, R., et al., *Preparation and characterization of an injectable composite.* Journal of Materials Science: Materials in Medicine, 2009. **20**(6): p. 1245-1253.
159. Ostrowska-Czubenko, J. and M. Gierszewska-Drużyńska, *Effect of ionic crosslinking on the water state in hydrogel chitosan membranes.* Carbohydrate Polymers, 2009. **77**(3): p. 590-598.
160. Ponchel, G. and J.-M. Irache, *Specific and non-specific bioadhesive particulate systems for oral delivery to the gastrointestinal tract.* Advanced drug delivery reviews, 1998. **34**(2): p. 191-219.
161. Costa, P. and J.M. Sousa Lobo, *Modeling and comparison of dissolution profiles.* European Journal of Pharmaceutical Sciences, 2001. **13**(2): p. 123-133.
162. Kilonzo, C., et al., *Prevalence and Molecular Characterization of Escherichia coli O157: H7 by Multiple-Locus Variable-Number Tandem Repeat Analysis and Pulsed-Field Gel Electrophoresis in Three Sheep Farming Operations in California.* Journal of Food Protection&# 174;, 2011. **74**(9): p. 1413-1421.
163. Dee, G.J., et al., *Vegetable substitutes for lanolin*. 2009, EP Patent 1,673,055.
164. Morganti, P., *Beauty and Wellness at 360°.* Journal of applied cosmetology, 2010. **28**(1): p. 13-24.
165. Jacob, S.E., C. Matiz, and E.M. Herro, *Compositae-Associated Allergic Contact Dermatitis from Bisabolol.* Dermatitis, 2011. **22**(2): p. 102.
166. Malcolm, D.R.B. and L. Ulceres, *Core tutorials in dermatology for promary care.* Psoriasis. p7. Available from Dermal Laboratories contact, 2011. **1462**: p. 458866.
167. Kalejman, H., *Cosmetic composition comprising camel milk or components thereof*. 2011, Google Patents.
168. Lee, B. and E. Warshaw, *Lanolin allergy: history, epidemiology, responsible allergens, and management.* Dermatitis, 2008. **19**(2): p. 63.

169. Maity, G.C., *Low Molecular Mass Gelators of Organic Liquids.* Journal of Physical Sciences, 2007. **11**: p. 156-171.

170. Dassanayake, L., et al., *Physical Properties of Rice Bran Wax in Bulk and Organogels.* Journal of the American Oil Chemists' Society, 2009. **86**(12): p. 1163-1173.

171. Flockhart, I.R., I. Steel, and G. Kitchen, *Nanoemulsions derived from lanolin show promising drug delivery properties.* Journal of Pharmacy and Pharmacology, 1998. **50**(S9): p. 141-141.

172. Dunstan, T.S. and P.D.I. Fletcher, *Compartmentalization and Separation of Aqueous Reagents in the Water Droplets of Water-in-Oil High Internal Phase Emulsions.* Langmuir, 2011.

173. Abdallah, D.J., S.A. Sirchio, and R.G. Weiss, *Hexatriacontane organogels. The first determination of the conformation and molecular packing of a low-molecular-mass organogelator in its gelled state.* Langmuir, 2000. **16**(20): p. 7558-7561.

174. Wright, A. and A. Marangoni, *Formation, structure, and rheological properties of ricinelaidic acid-vegetable oil organogels.* Journal of the American Oil Chemists' Society, 2006. **83**(6): p. 497-503.

175. Rissmann, R., et al., *Lanolin-derived lipid mixtures mimic closely the lipid composition and organization of vernix caseosa lipids.* Biochimica et Biophysica Acta (BBA) - Biomembranes, 2008. **1778**(10): p. 2350-2360.

176. Gupta, S., et al., *Composition dependent structural modulations in transparent poly(vinyl alcohol) hydrogels.* Colloids and Surfaces B: Biointerfaces, 2009. **74**(1): p. 186-190.

177. Bot, A., et al., *Effect of Sterol Type on Structure of Tubules in Sterol + γ-Oryzanol-Based Organogels.* Food Biophysics, 2009. **4**(4): p. 266-272.

178. Korhonen, M., et al., *Rheological properties of creams with four different surfactant combinations - effect of storage time and conditions.* International Journal of Pharmaceutics, 2001. **221**(1–2): p. 187-196.

179. Jones, D.S., A.F. Brown, and A.D. Woolfson, *Rheological characterization of bioadhesive, antimicrobial, semisolids designed for the treatment of periodontal diseases: Transient and dynamic viscoelastic and continuous shear analysis.* Journal of Pharmaceutical Sciences, 2001. **90**(12): p. 1978-1990.

180. Frank, A., S.K. Rath, and S.S. Venkatraman, *Controlled release from bioerodible polymers: effect of drug type and polymer composition.* Journal of Controlled Release, 2005. **102**(2): p. 333-344.
181. Varshosaz, J., M. Tabbakhian, and Z. Salmani, *Designing of a thermosensitive chitosan/poloxamer in situ gel for ocular delivery of ciprofloxacin.* The Open Drug Delivery Journal, 2008. **2**: p. 61-70.
182. Lauer, A., et al., *Transfollicular Drug Delivery.* Pharmaceutical Research, 1995. **12**(2): p. 179-186.
183. Newsham, E., J.W. Forrester, and D.J. Rowley, *Moistureless oral drug delivery formulation and method for preparing same*. 1989, Google Patents.
184. Cai, W., et al., *Synthesis of Boehmite Hollow Core/Shell and Hollow Microspheres via Sodium Tartrate-Mediated Phase Transformation and Their Enhanced Adsorption Performance in Water Treatment.* The Journal of Physical Chemistry C, 2009. **113**(33): p. 14739-14746.
185. Avella, M., et al., *Addition of glycerol plasticizer to seaweeds derived alginates: Influence of microstructure on chemical-physical properties.* Carbohydrate Polymers, 2007. **69**(3): p. 503-511.
186. Patel, F.M., A. Patel, and K. Rathore, *Release of metformin hydrochloride from ispaghula–sodium alginate beads adhered cock intestinal mucosa.* International Journal of Current Pharmaceutical Research, 2011. **3**(3): p. 52-55.
187. Glavas Dodov, M., et al., *Wheat germ agglutinin-conjugated chitosan–Ca–alginate microparticles for local colon delivery of 5-FU: Development and in vitro characterization.* International Journal of Pharmaceutics, 2009. **381**(2): p. 166-175.
188. Md, S., et al., *Gastroretentive drug delivery system of acyclovir-loaded alginate mucoadhesive microspheres: Formulation and evaluation.* Drug Delivery, 2011. **18**(4): p. 255-264.
189. Sultana, Y., et al., *Preparation and in vitro characterization of diltiazem hydrochloride loaded alginate microspheres.* Pharmaceutical Development and Technology, 2009. **14**(3): p. 321-331.

190. Patil, S.B. and K.K. Sawant, *Development, optimization and in vitro evaluation of alginate mucoadhesive microspheres of carvedilol for nasal delivery.* Journal of Microencapsulation, 2009. **26**(5): p. 432-443.
191. Zhang, T. and Q. Guo, *High internal phase emulsion (HIPE) organogels prepared from charge-driven assembled polymer organogels.* Chemical Communications, 2013. **49**(100): p. 11803-11805.
192. Ramachandran, S., N.R. Prasad, and S. Karthikeyan, *Sesamol inhibits UVB-induced ROS generation and subsequent oxidative damage in cultured human skin dermal fibroblasts.* Archives of dermatological research, 2010. **302**(10): p. 733-744.
193. Dimitrios, B., *Sources of natural phenolic antioxidants.* Trends in Food Science & Technology, 2006. **17**(9): p. 505-512.
194. Graf, E. and J.W. Eaton, *Antioxidant functions of phytic acid.* Free Radical Biology and Medicine, 1990. **8**(1): p. 61-69.
195. Bahkali, A., M. Hussain, and A. Basahy, *Protein and oil composition of sesame seeds (Sesamum indicum, L.) grown in the Gizan area of Saudi Arabia.* International Journal of Food Sciences and Nutrition, 1998. **49**(6): p. 409-414.
196. Liu, X., et al., *Transesterification of soybean oil to biodiesel using SrO as a solid base catalyst.* Catalysis Communications, 2007. **8**(7): p. 1107-1111.
197. Rogers, M.A., A.J. Wright, and A.G. Marangoni, *Nanostructuring fiber morphology and solvent inclusions in 12-hydroxystearic acid / canola oil organogels.* Current Opinion in Colloid & Interface Science, 2009. **14**(1): p. 33-42.
198. Nielsen, L., et al., *Effect of environmental factors on the kinetics of insulin fibril formation: elucidation of the molecular mechanism.* Biochemistry, 2001. **40**(20): p. 6036-6046.
199. Terech, P., *Networks of surfactant-made physical organogels*, in *Gels*, M. Zrínyi, Editor. 1996, Steinkopff. p. 64-70.
200. Lopes-da-Silva, J.A. and J.A.P. Coutinho, *Analysis of the Isothermal Structure Development in Waxy Crude Oils under Quiescent Conditions.* Energy & Fuels, 2007. **21**(6): p. 3612-3617.
201. Mallia, V.A., P. Terech, and R.G. Weiss, *Correlations of Properties and Structures at Different Length Scales of Hydro- and Organo-gels Based on N-Alkyl-(R)-12-*

Hydroxyoctadecylammonium Chlorides. The Journal of Physical Chemistry B, 2011. **115**(43): p. 12401-12414.

202. Gao, J., et al., *Nanoscale and microscale structural changes alter the critical gelator concentration of self-assembled fibrillar networks.* CrystEngComm, 2013. **15**(22): p. 4507-4515.
203. Moniruzzaman, M. and P. Sundararajan, *Morphology of blends of self-assembling long-chain carbamate and stearic acid.* Pure and applied chemistry, 2004. **76**(7): p. 1353-1363.
204. Xiong, G., et al., *Characterization of perovskite-type LaCoO3 nanocrystals prepared by a stearic acid sol--gel process.* Journal of Materials Science Letters, 1997. **16**(13): p. 1064-1068.
205. Fringeli, U.P. and H.H. Günthard, *Infrared membrane spectroscopy*. 1981: Springer.
206. Wang, Q., et al., *Controlled release of ciprofloxacin hydrochloride from chitosan/polyethylene glycol blend films.* Carbohydrate Polymers, 2007. **69**(2): p. 336-343.
207. Bag, B.G., et al., *Self-Assembly of Esters of Arjunolic Acid into Fibrous Networks and the Properties of their Organogels†.* Langmuir, 2009. **25**(15): p. 8663-8671.
208. Lam, R.S.H. and M.A. Rogers, *Activation Energy of Crystallization for Trihydroxystearin, Stearic Acid, and 12-Hydroxystearic Acid under Nonisothermal Cooling Conditions.* Crystal Growth & Design, 2011. **11**(8): p. 3593-3599.
209. Cao, S., Y. Zhang, and Y. Zhang, *Nucleation and Morphology of Monosodium Aluminate Hydrate from Concentrated Sodium Aluminate Solutions.* Crystal Growth & Design, 2010. **10**(4): p. 1605-1610.
210. Huang, X., et al., *Kinetics of 5α-Cholestan-3β-yl N-(2-Naphthyl)carbamate/n-Alkane Organogel Formation and Its Influence on the Fibrillar Networks.* Journal of the American Chemical Society, 2005. **127**(12): p. 4336-4344.
211. Halley, P.J. and M.E. Mackay, *Chemorheology of thermosets—an overview.* Polymer Engineering & Science, 1996. **36**(5): p. 593-609.
212. Drissi-Alami, H., et al., *The effects of the tabletting machine speed on physical characteristics of pharmaceutical powders.* Journal de pharmacie de Belgique, 1993. **48**(1): p. 43.

213. Yang, Y., et al., *Microrheology of highly crosslinked microtubule networks is dominated by force-induced crosslinker unbinding.* Soft Matter, 2013. **9**(2): p. 383-393.
214. Ebba, F., et al., *Stress relaxation studies of granules as a function of different lubricants.* European Journal of Pharmaceutics and Biopharmaceutics, 2001. **52**(2): p. 211-220.
215. Hunter, J.E., J. Zhang, and P.M. Kris-Etherton, *Cardiovascular disease risk of dietary stearic acid compared with trans, other saturated, and unsaturated fatty acids: a systematic review.* The American Journal of Clinical Nutrition, 2010. **91**(1): p. 46-63.
216. Karageorgopoulos, D., et al., *Antimicrobial activity of prulifloxacin in comparison with other fluoroquinolones against community-acquired urinary and respiratory pathogens isolated in Greece.* European journal of clinical microbiology & infectious diseases, 2013. **32**(11): p. 1417-1422.
217. Fass, R., *Efficacy and safety of oral ciprofloxacin in the treatment of serious respiratory infections.* The American journal of medicine, 1987. **82**(4A): p. 202.
218. Pernetti, M., et al., *Structuring of edible oils by alternatives to crystalline fat.* Current Opinion in Colloid & Interface Science, 2007. **12**(4): p. 221-231.
219. Willimann, H., et al., *Lecithin organogel as matrix for transdermal transport of drugs.* Journal of pharmaceutical sciences, 1992. **81**(9): p. 871-874.
220. Behera, B., et al., *Modulating the physical properties of sunflower oil and sorbitan monopalmitate-based organogels.* Journal of Applied Polymer Science, 2013. **127**(6): p. 4910-4917.
221. Behera, B., et al., *Span-60-based organogels as probable matrices for transdermal/topical delivery systems.* Journal of Applied Polymer Science.
222. Xuan, X.Y., Y.L. Cheng, and E. Acosta, *Lecithin-Linker Microemulsion Gelatin Gels for Extended Drug Delivery.* Pharmaceutics, 2012. **4**(1): p. 104-129.
223. Peltola, S., et al., *Microemulsions for topical delivery of estradiol.* International journal of pharmaceutics, 2003. **254**(2): p. 99-107.
224. Lee, P.J., R. Langer, and V.P. Shastri, *Novel microemulsion enhancer formulation for simultaneous transdermal delivery of hydrophilic and hydrophobic drugs.* Pharmaceutical research, 2003. **20**(2): p. 264-269.

225. Pouton, C.W. and C.J. Porter, *Formulation of lipid-based delivery systems for oral administration: materials, methods and strategies.* Advanced drug delivery reviews, 2008. **60**(6): p. 625-637.
226. Peshkovsky, A.S., S.L. Peshkovsky, and S. Bystryak, *Scalable high-power ultrasonic technology for the production of translucent nanoemulsions.* Chemical Engineering and Processing: Process Intensification, 2013. **69**(0): p. 77-82.
227. Martins, S., et al., *Insulin-loaded alginate microspheres for oral delivery – Effect of polysaccharide reinforcement on physicochemical properties and release profile.* Carbohydrate Polymers, 2007. **69**(4): p. 725-731.
228. Jia-hui, Y., D. Yu-min, and Z. Hua, *Blend films of chitosan-gelatin.* Wuhan University Journal of Natural Sciences, 1999. **4**(4): p. 476-476.
229. Vaidya, A., et al., *Pectin–metronidazole prodrug bearing microspheres for colon targeting.* Journal of Saudi Chemical Society, (0).
230. Coates, J., *Interpretation of Infrared Spectra, A Practical Approach*, in *Encyclopedia of analytical chemistry*. 2006, John Wiley & Sons, Ltd.
231. Dong, Z., Q. Wang, and Y. Du, *Alginate/gelatin blend films and their properties for drug controlled release.* Journal of Membrane Science, 2006. **280**(1–2): p. 37-44.
232. Pasparakis, G. and N. Bouropoulos, *Swelling studies and in vitro release of verapamil from calcium alginate and calcium alginate–chitosan beads.* International Journal of Pharmaceutics, 2006. **323**(1–2): p. 34-42.

CURRICULUM VITAE

Sai Sateesh Sagiri
R.No: 121, Dhuirubhai Ambani Hall of Residence,
NIT, Rourkela,
Orissa, India-769008
Email:biotech.satishsai@gmail.com
Phone:+ 91-9439783308

Objective: To pursue a career in the scientific world that provides an innovative, research and competitive environment and offers an opportunity for widening and continuum of my knowledge in science.

Education:

Pursuing **Ph.D** in the Department of Biotechnology and Medical Engineering at NIT, Rourkela, Odisha, India.

M. Tech. in Biotechnology (2007-09) CGPA: 8.3 out of 10
Vellore Institute of Technology University
Vellore, T.N, India.

B. Tech in Biotechnology (2003-07) Percentage: 72.3%
Bapatla Engineering College, ANU,
Guntur, A.P, India.

Academic Achievements:

To my credit I got an All India Rank of 346 (96.88 percentile) in GATE-2007.

Academic Projects:

I am doing my Ph.D project, entitled **"Studies on the synthesis and characterization of encapsulated organogels for controlled delivery applications"** at National Institute of Technology, Rourkela, India.

I have done my M.Tech project, entitled "**Studies to identify the redox partners of WhiB1/Rv3219 of *Mycobacterium tuberculosis* H37Rv**" at Institute of Microbial Technology (IMTECH) (CSIR), Chandigarh, India.

My B.Tech project was "**Studies on the production of Streptokinase with reduced antigenicity**" In my project I have written a computer program in C language for "Identification of the antigenic sites in a given protein's amino acid sequence".

Publications and presentations: Annexure I

Research Experience:

Total research experience is 5 years

Work Experience:

Worked as a lecturer in the Department of Biotechnology at RVR&JC College of Engineering, Guntur, A.P for six months (a semester). In this period I taught Cancer biology, Gene delivery & Environmental Studies to final year, third year & second year B.Tech students, respectively.

Laboratory Skills and Technical Expertise:

Biomaterials characterization: Differential scanning calorimetry, Mechanical analysis using texture analyzer, FTIR and UV-Visible spectrophotometry.

Molecular Biology: Nucleic acid isolation from bacteria, Bacterial transformation, gene cloning, Sequence analysis, Restriction digestion, Agarose gel Electrophoresis, PCR.

Protein engineering: Immobilized metal affinity chromatography, Thioredoxin affinity chromatography, 2-D gel electrophoresis, Mass spectroscopy by MALDI-TOF, HPLC, Column chromatography, thin layer chromatography, Paper chromatography, Dialysis, SDS-PAGE.

Immunology: Blood grouping**,** Immunoelectrophoresis**,** ELISA, Western blot, Widal test, Differential count of WBC, Immunocytochemistry.

References:

Dr. Kunal Pal

Assistant professor,

NIT, Rourkela, Odisha.

Email: pal.kunal@yahoo.com

Phone: +91-8763366085

Dr. P. Krishnakanth

Assistant professor,

CBST, VITU, Vellore, T.N.

Email:pkkanth2006@gmail.com

Phone: +91-9441790250

Declaration:

I here by declare that all the above information is correct to the best of my knowledge.

(Sai Sateesh Sagiri)

ANNEXURE-I

JOURNAL PUBLICATIONS

1. **Sagiri, S. S**., V. K. Singh**,** K. Pal*, I. Banerjee and Piyali Basak, *Stearic acid based oleogels: A study on the molecular, thermal and mechanical properties*, submitted to Materials Science and Engineering C. ***Accepted, in press, Available online*** (SCI, Impact factor: 2.596)

2. **Sagiri, S. S**., V. K. Singh**,** S. Kulanthaivel**,** K. Pal*, I. Banerjee, Krishna Pramanik and Piyali Basak, *Gelatin hydrogel and stearate organogel based bigels: Physico-chemical characterization and application as drug delivery vehicle* submitted to Journal of Mechanical behavior of Biomedical materials. ***Accepted, in press, Available online*** (SCI, Impact factor: 3.487)

3. **Sagiri, S. S**., V.K. Singh, K. Pal*, I. Banerjee, Krishna Pramanik and Piyali Basak, *Core-shell-type organogel-alginate hybrid microparticles: A controlled delivery vehicle*, submitted to Chemical Engineering Journal. **2015**, 264, pp. 134-145. (SCI, Impact factor: 3.691)

4. **Sagiri, S. S**., V. Sharma, K. Pal*, and Piyali Basak, *Mango butter emulsion gels as cocoa butter equivalents: Physical, thermal and mechanical analyses* submitted to Journal of Agricultural and Food Chemistry**. 2014** 62(47), pp. 11357-11368. (SCI, Impact factor: 2.906)

5. **Sagiri S. S.**, Kunal Pal*, Piyali Basak, Usman Ali Rana, Imran Shakir, and Arfat Anis, Encapsulation of Sorbitan Ester-Based Organogels in Alginate Microparticles. AAPS pharmaSciTec, **2014**, 15(5), pp. 1197-1208. (SCI, Impact factor: 1.906)

6. **Sagiri S. S.**, Kunal Pal*, Piyali Basak, Encapsulation of animal wax-based organogels in alginate microparticles. Journal of Applied Polymer Science, **2014**, 131(20), pp. 49010. (SCI, Impact factor: 1.4)

7. V. K. Singh, **Sagiri S. S,** M. K Bhattacharya, S. M. Khade*, Kunal Pal Development and characterization of gelatin–polysaccharide based phase-separated hydrogels for prevention of sexually transmitted diseases Journal of Applied Polymer Science, ***Accepted, in press***. (SCI, Impact factor: 1.4)

8. V. K. Singh, **Sagiri S. S.**, K. Pal*, S. M. Khade, D. K. Pradhan and M. K. Bhattacharya, Gelatin-carbohydrate phase-separated hydrogels as bioactive carriers in vaginal delivery:

Preparation and Physical characterizations, Journal of Applied Polymer Science, **2014**, 131(13), pp. 40445. (SCI, Impact factor: 1.4)

9. S. P. Mallick, **Sagiri S. S.**, V. K. Singh, K. Pal*, D. K. Pradhan and M. K. Bhattacharya, Effect of processed starches on the properties of gelatin based physical hydrogels: Characterization, *in vitro* drug release and antimicrobial studies, Polymer-Plastics Technology and Engineering, **2014**, 53(7), pp. 700-715. (SCI, Impact factor: 1.481)
10. **Sagiri S. S.**, D. Satapathy, K. Pal* and K. Pramanik, Development of mustard oil and groundnut oil based Span 40 organogels as matrices for controlled drug delivery, Designed Monomers and Polymers, **2014**, 17(6), pp. 545-556. (SCI, Impact factor: 1.34)
11. S. M. Khade, B. Behera, **Sagiri S. S.**, V. K. Singh, A. Thirugnanam, K. Pal*, S. S. Ray, D. K. Pradhan and M. K. Bhattacharya, Gelatin-PEG based metronidazole-loaded vaginal delivery systems: preparation, characterization and in vitro antimicrobial efficiency, Iranian Polymer Journal, **2014,** 23(3), pp. 171-184. (Impact factor: 1.053)
12. S. Pradhan, **Sagiri S. S.**, V. K. Singh, K. Pal*, S. S. Ray and D. K. Pradhan, Palm oil based organogels and microemulsions for delivery of antimicrobial drugs, Journal of Applied Polymer Science, **2014,** 131(6), pp. 39979. (SCI, Impact factor: 1.4)
13. **Sagiri S. S.**, B. Behera, C. Bhattacharya, K. Pal*, I. Banerjee, R. Rafanan and D. Rousseau, Organogels as matrices for controlled drug delivery: A review on the current state, Soft Materials, **2014**, 12(1), pp. 47-72. (SCI, Impact factor: 1.6)
14. **Sagiri S. S.**, J. Sethy, K. Pal*, I. Banerjee, K. Pramanik and T. K. Maiti, Encapsulation of vegetable organogels: A prospective new generation drug delivery vehicle, Designed Monomers & Polymers, **2013**, 16(4), pp. 366-376. (SCI, Impact factor: 1.34)
15. D. K. Shah, **Sagiri S. S.**, B. Behera, K. Pal* and K. Pramanik, Development of olive oil based organogels using sorbita nmonopalmitate and sorbitan monostearate: A comparative study, Journal of Applied Polymer Science, **2013**, 129(2), pp. 793-805. (SCI, Impact factor: 1.4)
16. D. Satpathy, **Sagiri S. S.**, B. Behera, K. Pal* and K. Pramanik, Sunflower oil based lecithin organogels as matrices for controlled drug delivery. Journal of Applied Polymer Science, **2013**, 129(2), pp. 585-594. (SCI, Impact factor: 1.4)

17. **Sagiri S. S.**, B. Behera, K. Pal* and P. Basak, Lanolin based organogels as a matrix for topical drug delivery. Journal of Applied Polymer Science, **2013**, 128(6), pp. 3831-3839.
18. B. Behera, **Sagiri S. S.**, K. Pal* and A. Srivastava, Modulating the physical properties of sunflower oil and sorbitan monopalmitate based organogels, Journal of Applied Polymer Science, **2012**, 127(6), pp.4910-4917. (SCI, Impact factor: 1.4)
19. **Sagiri S. S.**, B. Behera, T. Sudheep and K. Pal* Effect of composition on the properties of the tween 80-span 80 based organogels, Designed Monomers & Polymers, **2012**, 15(3), pp. 253-273.(SCI, Impact factor: 1.34)
20. B. Behera, V. Patil, **Sagiri S. S.**, K. Pal* and S. S. Ray, Span-60 based organogels as probable matrices for transdermal/topical delivery systems, Journal of Applied Polymer Science, **2012**, 125(2), pp. 852-863.(SCI, Impact factor: 1.4)
21. S. Mallick, **Sagiri S. S.**, B. Behera, K. Pal* and S. S. Ray, Gelatin-based emulsion hydrogels as a matrix for controlled delivery system, Materials & Manufacturing Processes, **2012**, 27(11), pp. 1221-1228. (SCI, Impact factor: 1.39)
22. C. Bhattacharya, N. Kumar, **Sagiri S. S.**, K. Pal* and S. S. Ray, Development of span 80–tween 80 based fluid-filled organogels as a matrix for drug delivery, Journal of Pharmacy and Bioallied Sciences, **2012**, 4(2), pp. 155-163.
23. N. Kumar, B. Behera, **Sagiri S. S.**, K. Pal*, S. S. Ray and S. Roy, Bacterial vaginosis: Etiology and modalities of treatment—A brief note, Journal of Pharmacy and Bioallied Sciences, **2011**, 3(4), pp. 496-503.
24. S. Sahoo, N. Kumar, C. Bhattacharya, **Sagiri S.S.**, K. Jain, K. Pal*, S. S. Ray and B. Nayak, Organogels: Properties and applications in drug delivery, Designed Monomers & Polymers, **2011**, 14, pp. 95-108. (SCI, Impact factor: 1.34)

BOOK CHAPTERS

1. **Sagiri S. S.**, P. Pattnaik, K. Pal*, S. S. Ray, Book chapter titled **"Drug Delivery, Iontophoretic"** in "Encyclopedia of Biomedical Polymers and Polymeric Biomaterials", ***In Press***. **To be published by: Taylor and Francis Group, USA.**

2. K. Pal*, **Sagiri S. S.**, V. K. Singh, B. Behera, I. Banerjee, K. Pramanik, Book chapter titled **"Natural Polymers in Tissue Engineering: Methods of scaffold fabrication and Applications"** in "Encyclopedia of Biomedical Polymers and Polymeric Biomaterials", ***In Press***. **To be published by: Taylor and Francis Group, USA.**

3. K. Pal*, **Sagiri S. S.**, B. Behera, S. S. Ray, K. Pramanik, Book chapter titled **"Biopolymeric Microparticles in Medicine and Regenerative Medicine: Design and Applications"** in "Encyclopedia of Biomedical Polymers and Polymeric Biomaterials", ***In Press***. **To be published by: Taylor and Francis Group, USA.**

4. B. Behera, **Sagiri S. S.**, Sudheep, V. Patil, V. Varghese, B. Biswal, K. Pal***,** S. Roy, S. S. Ray and B. Nayak; Book chapter titled **"Drug Delivery Methodologies"** in "Modern Biotechnology and its Applications", 2013, Volume 2, pp. 611-647. **Published by: New India Publishing Agency, India (ISBN: 978-93-81450-83-3).**

COMMUNICATED PAPERS

1. Sagiri, S. S., K. Pal*, I. Banerjee, Krishna Pramanik and Piyali Basak, *Core (cocoa butter and mango butter organogels)-shell (alginate)-type hybrid microparticles: A controlled delivery vehicle*.

CONFERENCES ATTENDED

1. International Conference on Biomaterials Implant Devices and Tissue Engineering - BIDTE 2012, Chennai, during Jan 6-8, 2012.

2. World Congress on Biotechnology, organized by OMICS publishing group during March 21-23, 2011 at Hyderabad, India.

WORKSHOP/ REFRESHER COURSES ATTENDED

1. 2 day workshop on the bioinformatics was attended, held at the Dept. of Biotechnology and Medical engineering, National Institute of Technology-Rourkela in August 2012.

2. Attended the workshop on Trends in the Biotechnology in 2008 organized by VITU, Vellore.